THE UNIVERSITY
of EDINBURGH

THE UNIVERSITY *of* EDINBURGH

Investigating the role of WT1-expressing progenitors and the function of WT1 in visceral adipose tissue angiogenesis

Teodora-Valentina Aldea

Thesis submitted for the degree of Doctor of Philosophy

The University of Edinburgh

2020

Declaration

This thesis is entirely my own work and, apart from where stated, the experiments were performed by me. The work outlined below has not been submitted for any other degree or professional qualification.

Teodora-Valentina Aldea, August 2020

Abstract

Unlike brown or subcutaneous white adipose tissue, visceral white adipose tissue (VWAT) is closely linked to cardiometabolic disease. The Wilms tumour 1 gene (*WT1*), an important developmental transcription factor, has been shown to be expressed in the progenitors of VWAT both in human and mouse. Moreover, adipose tissue expansion requires the formation of blood vessels and WT1 has previously been shown to be involved in angiogenesis during development and tumour formation. We were therefore interested in investigating the role of WT1 in VWAT angiogenesis by characterising the different WT1-expressing microvascular cell populations in VWAT and by focusing on the function of WT1 in angiogenesis.

In order to look into the role of WT1 and WT1-expressing cells *in vitro* and *in vivo*, we used a lineage tracing (*Wt1*^{CreERT2}*; mTmG*) mouse line and a reporter (*Wt1*$^{GFP/+}$) line. Additionally, we used a conditional knock-out (*CAG*^{CreERT2}*; Wt1*$^{loxP/loxP}$) model, obtained by crossing *CAG*^{CreERT2} mice, where CreERT2 is expressed ubiquitously under the synthetic CAG promoter, with floxed *Wt1*$^{loxP/loxP}$ mice. We analysed WT1 expression in several main VWAT depots present in mice (epididymal, omental, mesenteric, perirenal and pericardial) and found that WT1 is expressed by CD31+ endothelial cells and PDGFRβ+ pericytes in several VWAT depots. Moreover, our lineage tracing experiments revealed that WT1-expressing cells give rise to cells which reside in the perivascular space of microvessels and that the contribution of WT1+ cells to the adipocyte population of VWAT is decreased in obesity. In humans, omental fat, which surrounds the intestines, is one of the most studied and easily accessible VWAT depots and our experiments on human omental VWAT showed that WT1-expressing cells are present in the perivascular area of microvessels and WT1 levels are increased during obesity. We further investigated the role of WT1, which we achieved by deleting WT1 *in vitro* in stromal vascular fraction cells and sorted pericytes. RNAi-mediated deletion of *Wt1* did not show significant changes in in vitro angiogenic potential. Finally, we aimed to investigate the differences between WT1+ and WT1- pericytes in visceral adipose tissue, by using RNA sequencing to analyse the transcriptome of the two populations.

Our data suggest that sub-populations of VWAT cells which express microvascular markers are derived from WT1-expressing cells, and also express WT1 in adulthood, which points to a potential role of WT1 in VWAT homeostasis and expansion. However, in our *in vitro* experiments, knocking down *Wt1* in murine adipose-derived

SVF cells and pericytes did not impair angiogenic potential. Nevertheless, the fact that WT1 expression in human omental tissue is increased during obesity may point to a role of WT1 in human adipose remodelling.

Lay summary

According to the World Health Organization (WHO), worldwide obesity has nearly tripled in the past 45 years, and in 2016 close to 2 billion adults were either overweight or obese. The consequences of obesity on overall health are well-known nowadays – high blood pressure, increased risk of type 2 diabetes and heart disease. This makes adipose tissue (or fat) an important subject of research as we try to understand and manage obesity.

Humans and mice have two types of adipose tissue, white and brown, which have very different functions. The role of brown fat is to burn energy as heat. White adipose tissue (WAT), on the other hand, is used by the body to store excess calories. WAT is stored in several parts of the body and is roughly divided into subcutaneous white adipose tissue (SWAT), which is found “under the skin” and visceral white adipose tissue (VWAT), which surrounds several of the main internal organs in distinct ‘pockets’ or *depots.*

Many studies have shown that not all types of adipose tissue are bad, and that VWAT seems to be the main culprit as far as the health risks of obesity go. SWAT, on the other hand, is often described as ‘good fat’. Other studies have focused on the differences between VWAT and SWAT, aiming to pinpoint genetic and molecular differences between the two which might explain their different implications on human health.

One gene in particular, Wilms’ tumour 1 (*WT1*), was recently shown to be activated in VWAT, but not in SWAT. *WT1*, a gene originally discovered in tumour cells, encodes a protein which regulates many genes during development and afterwards, including genes involved in the formation of blood vessels in several organs. Moreover, adipose tissue needs to form new blood vessels in order to support its growth during weight gain. Taking this into account, we were interested to see if the WT1 protein plays a similar role in the blood vessels of VWAT.

In order to look into this, we examined both human and mouse VWAT tissue from several VWAT depots and studied the different types of cells which are used to build blood vessels. We found that WT1 is expressed in some pericytes, cells found on the outside of blood vessels which help maintain the integrity of these vessels and serve as a source of new fat cells. We further isolated and grew pericytes in the laboratory, examining whether these can form vessel-like structures when we delete the *WT1*

gene. Additionally, we compared pericytes expressing *Wt1* with pericytes where *Wt1* is not expressed, and found that these two subsets have different profiles which may mean they serve different functions in VWAT.

Acknowledgements

I think a lot of us start a PhD wholly focused on the subject matter we are about to study and the careers we would like our PhD to build towards. But in the past 4 years I have come to learn that the most valuable lessons have come from the many people I had the opportunity to meet.

A first (and big) ‘thank you!’ goes to my supervisors: You-Ying, who always pushed me to best myself and carefully examine my thought process and Bruno, who always found something exciting even in my negative results. Another one to Bob Hill and Matt Bailey for the career and general wellbeing chats. And a super-massive ‘thank you’ to all the staff and students at Edinburgh University who shared samples (Roland and Lynne, thank you!), reagents, office spaces, cakes and Nespresso pods with me and who taught me a lot on topics such as best research practices, resilience, science communication and craft beers.

I would also like to thank my family (or families, rather). Firstly, my parents and grandma, who always made me believe I can do anything and who will be very happy to know I’ve finally written this thing. Secondly, the old friends who I have grown to see as family – Andreea, Blair, Hris and Andy, I look forward to our next gathering around an unnecessarily large spread of foods.

And a last ‘thank you’ to all the Bucharest and Edinburgh friends who prevented me from losing my marbles and made sure I got fed and taken outside often enough – especially Alina, who always lends a kind ear to my nonsense, and Nat, whose name I wish I could cross-stitch onto this page for extra authenticity.

Table of contents

List of figures

Chapter 1

Chapter 2

Chapter 3

Chapter 4

Chapter 5

List of tables

Chapter 2

Chapter 5

Appendix

List of frequently used abbreviations

αSMA	Alpha-smooth muscle actin
BAT	Brown adipose tissue
EC	Endothelial cell
HIF	Hypoxia-inducible factor
PC	Pericyte
PDGF	Platelet-derived growth factor
PDGFR	Platelet-derived growth factor receptor
RNAi	RNA interference
siRNA	Short interfering RNA
SVF	Stromal vascular fraction
SWAT	Subcutaneous white adipose tissue
VEGF	Vascular endothelial growth factor
VEGFR	Vascular endothelial growth factor receptor
VWAT	Visceral white adipose tissue
WAT	White adipose tissue

Chapter 1

Introduction

1.1 Adipose tissue overview

Over the past decades, obesity has been gaining increased attention in the biomedical community due to its effects on cardiometabolic health. Obesity, defined as excess accumulation of adipose tissue, is a major risk factor for diabetes, cardiovascular disease and cancer (WHO, 2020). Moreover, worldwide obesity has almost tripled in the past 45 years, with close to 2 billion adults being overweight or obese in 2016 (WHO, 2020).

Research has shown that not all adipose tissues are equal. In both mouse and human, there are several types of adipose tissue - white, beige, and brown. White adipose tissue is further divided into subcutaneous white adipose tissue (SWAT) and visceral white adipose tissue (VWAT) and over the past decades it has become obvious that excess VWAT, rather than SWAT, is more closely linked to cardiometabolic disease (Després and Lemieux, 2006; Després et al., 1990; Pouliot et al., 1992).

Several studies have shown that VWAT, which is deposited around internal organs like the heart, kidney, or mesentery is correlated with the presence of cardiovascular disease and the metabolic syndrome, a cluster of conditions including dyslipidaemia, hypertension, insulin resistance and impaired glucose tolerance (reviewed in Tchernof and Després, 2013). Moreover, visceral obesity can also be seen in otherwise normal-weight individuals with diagnosed metabolic syndrome (Ruderman *et al*., 1998).

It is now becoming increasingly clear that, in both human and mouse, VWAT differs from other types of adipose tissue in several ways. VWAT has a more pro-inflammatory phenotype arising from dysfunctional lipid storage (Cartier et al., 2009). Moreover, failure of VWAT to store excess triglycerides appropriately can eventually lead to ectopic fat deposition at remote sites such as skeletal muscle, the liver, the kidney or the heart, which increases the risk of cardiovascular and metabolic complications (Figure 1.1; Tchernof and Després, 2013).

The development of obesity involves complex interactions between the many cell types making up adipose tissue, and the crosstalk between adipocytes, vascular cells, immune cells, adipose progenitors and other stromal cells is central to understanding adipose homeostasis and expansion.

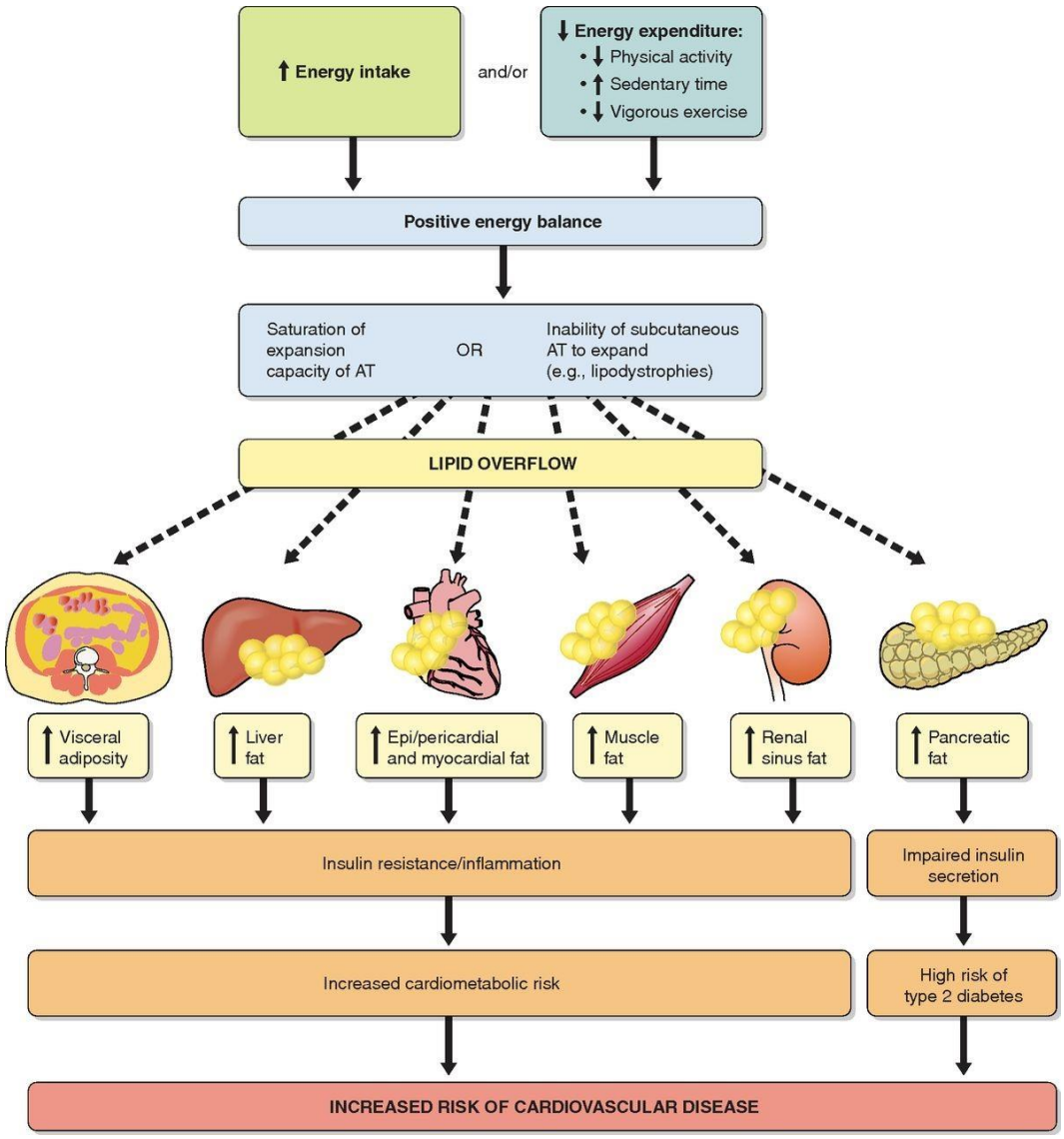

Figure 1.1. The saturation of SWAT expansion capacity leads to ectopic fat deposition. *This figure illustrates how the inability of adipose tissue to store excess lipids can lead to their deposition in the liver, kidney, pancreas or muscle, leading to cardiovascular disease (Tchernof and Després, 2013)*

1.1.1 Adipose tissue types and depots

The correlation between increased body fat and metabolic or cardiovascular disorders has been investigated for a long time, but only recently has it become clear that not all types of fat function or affect overall health in the same way. Adipose tissue, which serves as a natural energy store, is located in the body in several depots with different properties.

Firstly, based on morphology and function, adipose tissue is divided into brown adipose tissue (BAT) and white adipose tissue (WAT). White adipocytes, which are

unilocular, can store and release higher numbers of fatty acids, while brown adipocytes, which are multilocular and contain more mitochondria, are better equipped to produce heat and expend energy through the process of adaptive thermogenesis, with the aid of uncoupling protein 1 (UCP1) (Cinti, 2005). More recently, beige adipocytes have also been discovered. Although they are found in WAT depots, beige adipocytes express UCP1, which is normally expressed by brown adipocytes (Wu et al., 2012).

Secondly, WAT can be divided into subcutaneous adipose tissue (SWAT), which is found under the skin, and visceral (VWAT), which surrounds internal organs (Wajchenberg, 2000).

Thirdly, VWAT itself is further divided into several depots, which are similarly distributed in human and mouse. Humans and mice both have omental, retroperitoneal, perirenal, mesenteric and peri/epicardial VWAT, while mice additionally have epididymal adipose depots (Figure 1.2).

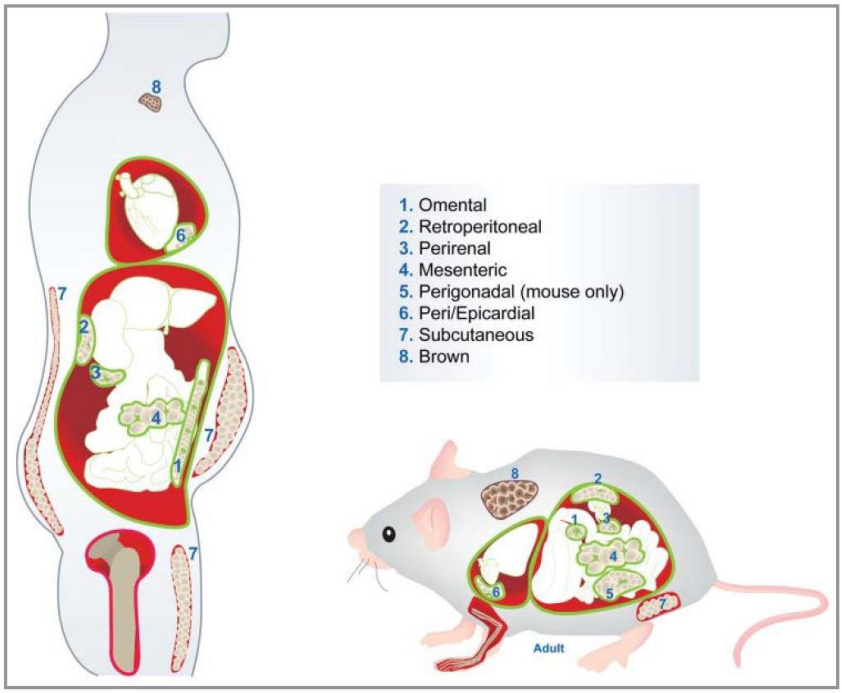

Figure 1.2. Distribution of visceral white (1-6), subcutaneous white (7), and brown (8) adipose tissue in human and mouse *(adapted from Cleal, Aldea, & Chau, 2017).*

VWAT depots can be different in terms of differentiation potential and gene expression profile, especially with regards to genes involved in development, adipogenesis, metabolism, inflammation and angiogenesis (reviewed in Cleal, Aldea, & Chau, 2017). However, building a complete overview of VWAT depots can be challenging

due to differences in methodology across research groups. Human visceral adipose samples can be difficult to source and most studies on human VWAT focus on omental adipose tissue (Arner et al., 2013; Fried et al., 1998; Verboven et al., 2018). In mouse, studies on VWAT often focus on one or two depots at a time, with emphasis on epididymal (perigonadal) VWAT.

1.1.2 Differences between SWAT and VWAT

In terms of the main differences between the two types of white adipose tissue, SWAT has been found to have protective effects, while VWAT fat has been found to be associated with an increased risk of cardiometabolic disease. For several decades, researchers have described a positive correlation between increased visceral adiposity and increased levels of plasma triglycerides, insulin and glucose (Després et al., 1990; Pouliot et al., 1992). Increased visceral adiposity, as measured by waist circumference, is associated with dyslipidemia, a state characterized by high circulating levels of triglycerides and low levels of high-density lipoprotein cholesterol (Pascot et al., 2001). Visceral obesity is also associated with an increased risk of developing type 2 diabetes (Balkau et al., 2007; Wang et al., 2005) and can predict the risk of myocardial infarction and all-cause mortality (Kuk et al., 2006; Yusuf et al., 2005). Moreover, visceral obesity has also been shown to be a predictor of hypertension (Hayashi et al., 2003). Finally, increased visceral adiposity may be a risk factor for certain types of cancer, such as colorectal cancer (Kang et al., 2010; Yamamoto et al., 2010).

SWAT and VWAT are different not just because they have different anatomical locations and implications for morbidity, but also in terms of the intrinsic properties of the depots and their respective adipose precursor cells. For instance, SWAT shows higher expression levels of genes necessary for adipogenesis (Drolet et al., 2008). VWAT, on the other hand, exhibits increased levels of secreted cytokines and higher expression of genes involved in inflammation and angiogenesis (Tchernof and Després, 2013).

Adipose expansion is achieved either through hypertrophy (the increase in adipocyte size) or hyperplasia (the increase in the total number of adipocytes). It has been proposed that hypertrophy is associated with a failure of existing adipocytes to provide storage for excess lipids, which then are trafficked to other locations like the liver or the skeletal muscle (Tchernof and Després, 2013). Moreover, VWAT may expand as a result of SWAT dysfunction, as an intermediate step between general adipose

expansion and ectopic fat deposition (Després and Lemieux, 2006). However, this does not fully explain cases in which large VWAT accumulation is observed without SWAT expansion. SWAT and VWAT also seem to show different endocrine activities. VWAT-specific factors have been described, such as omentin, which is expressed much more highly in omental adipose tissue than in subcutaneous (Yang et al., 2006). Moreover, VWAT and SWAT secrete different levels of the same adipokines, which may provide insight into the pathophysiology of high visceral adiposity. For instance, VWAT explants obtained from obese patients secrete higher levels of VEGF, adiponectin, leptin and IL-6 *in vitro* than SWAT explants (Fain et al., 2004).

The difference in the systemic effects of different adipose depots may be explained by earlier developmental processes, which is why the development of adipose tissue is another area quickly gaining ground. Recently, genetic lineage tracing experiments have revealed different developmental origins of murine SWAT and VWAT, as well as a subset of VWAT adipose progenitors which expresses the Wilms' tumour 1 gene (*Wt1*), while *Wt1* is not expressed in SWAT or BAT (Chau et al., 2014).

Developmental differences between SWAT and VWAT may relate not only to the origins of the depots per se, but also to different patterns of stem cell commitment in early pre-natal and post-natal days. Han et al. have shown that murine epididymal adipose tissue develops in the first 14 days after birth, and that the cells comprising the depot during the first 4 postnatal days are not committed to an adipogenic fate *in vitro* in the absence of other stromal cells. Moreover, the adipogenic capacity of these progenitors seems to be dependent on the presence of the ECM, vascular cells and immune cells (Han et al., 2011).On the other hand, preadipocytes isolated from SWAT have a higher adipogenic potential and show higher expression of adipogenesis-related genes like PPAR-γ (Kim et al., 2016; Tchkonia et al., 2002).

1.1.3 Visceral obesity and its consequences on overall health

As mentioned previously, as many as 20% of adults worldwide suffer from metabolic syndrome, a cluster of conditions encompassing hypertension, visceral obesity, low glucose tolerance, increased cholesterol levels and abnormal levels of circulating triglycerides, which increases the risk of developing cardiovascular disease and type 2 diabetes (O'Neill and O'Driscoll, 2015). While many morphological, molecular and physiological differences have been described between SWAT and VWAT, it is important to first point out that age and sex greatly influence the accumulation of adipose tissue. In both males and females, excess visceral fat tends to amass more

with age and, in females, this is particularly significant after menopause (Lanska et al., 1985; Zamboni et al., 1992). Throughout life, however, males are more likely to accumulate adipose tissue in the abdominal area, whereas female adipose tissue preferentially accumulates around the hips and thighs (Krotkiewski et al., 1983). Although men generally present a higher percentage of visceral adipose tissue, the increase in VWAT in men is also correlated with an increase in total adipose mass, whereas women may have a high percentage of VWAT without overall excess weight (Kvist et al., 1988).

These differences in adipose accumulation between men and women may be explained by sex hormone levels. Menopause, when rapid visceral fat accumulation is observed in women, is also accompanied by oestrogen deficiency (Tchernof and Després, 2000). Moreover, low testosterone levels in males are associated with increased visceral adiposity (Seidell et al., 1990). Plasma levels of sex hormone-binding globulin are also negatively correlated with visceral obesity and an increased risk of metabolic syndrome (Tsai et al., 2004).

Genetic variance can also determine predisposition to VWAT accumulation. For instance, certain variants of genes like *ADIPOQ* (adiponectin) or *RETN* (resistin) have been shown to be more closely linked to visceral obesity (Bouchard et al., 2004; Katsuda et al., 2007). In men, variation of the *SIRT1* gene, which encodes a deacetylase important in cellular regulation, has also been correlated with visceral obesity risk (Peeters et al., 2008). Moreover, in adolescent males, functional variation in the androgen receptor gene was also associated with visceral adiposity, with low numbers of CAG repeats in exon 1 of this gene correlating with increased VWAT and hypertension (Pausova et al., 2010).

As described in the previous section, accumulation of VWAT is linked to dyslipidaemia, predisposition to developing type 2 diabetes and an increased risk of cardiovascular disease (Balkau et al., 2007; Kuk et al., 2006; Pascot et al., 2001). The pathological consequences of increased visceral adiposity are believed to be at least in part due to the accumulation of surplus free fatty acids (FFAs) in ectopic locations when adipose depots are unable to store the excess of lipids and expand accordingly (Tchernof and Després, 2013). However, it is worth noting that different VWAT depots seem to have unique ‘metabolic signatures’. For instance, human mesenteric and omental adipose progenitors differ in the expression of lipid metabolism genes (Tchkonia et al., 2007).

1.1.4 Adipose progenitors and the adipose microenvironment

Adipose tissue contains mature adipocytes, as well as what is commonly known as the stromal vascular fraction, which includes adipose progenitors, vascular cells and immune cells. The microenvironment of mature adipose tissue has been increasingly studied and can be broadly described in terms of the cell making up adipose and the growth and inflammatory factors secreted by these cells (Quail and Dannenberg, 2019).

The cell population most central to adipose research consists of adipose progenitors. Murine adipose progenitors/preadipocytes have been successfully isolated from VWAT or SWAT based on a panel of well-established markers. Rodeheffer *et al*. have described white adipose progenitors (Lin-CD29+CD34+Sca-1+CD24+) (Rodeheffer et al., 2008). Moreover, this population gives rise to a more committed preadipocyte population (Lin-CD29+CD34+Sca-1+CD24-), with loss of CD24 marking the commitment to adipogenesis (Berry and Rodeheffer, 2013). Lastly, lineage tracing experiments showed that white adipocytes in all WAT depots are derived from cells expressing platelet-derived growth factor receptor α (PDGFRα), and that nearly all CD24+ and CD24- adipose progenitors are also traced by PDGFRα lineage tracing (Berry and Rodeheffer, 2013).

Differences also exist between subsets of adipose progenitors within the same VWAT depot. This is illustrated by several recent studies focused on adipose progenitor heterogeneity. For instance, two sub-populations of progenitors, distinguished by different surface marker profiles, have been described in murine epididymal VWAT: adipose precursor cells (LY6C-CD9-PDGFRβ+), which are highly adipogenic, and fibro-inflammatory progenitors (LY6C+PDGFRβ+), which lack adipogenic capacity but have a more pro-inflammatory profile (Hepler et al., 2018a). Similarly, Lee *et al*. revealed distinct subpopulations of murine adipocytes and preadipocytes, marked by different metabolic and transcriptomic profiles (Lee et al., 2019). Moreover, Chau et al. showed that expression of *Wt1*, which is observed in VWAT but not SWAT or BAT, is confined to a subset of adipose progenitors only, with differences between *Wt1*+ and *Wt1*- yet to be investigated (Chau et al., 2014a).

In adulthood, and especially when adipose remodelling is required, the activation of adipose progenitors relies heavily on the microenvironment. Studies investigating the behaviour of progenitors transplanted from VWAT into either subcutaneous or visceral depots have shown that, regardless of origin, the proliferation and differentiation of

progenitors is mostly triggered by high fat diet-induced changes in the microenvironment (Jeffery et al., 2016). Moreover, proliferation of adipose progenitors also seems to be influenced by the presence of sex-dependent hormones like oestrogens (Jeffery et al., 2016).

Alongside stem cells, resident adipose immune cells are an essential component of adipose tissue. Macrophages, eosinophils, regulatory T (T_{reg}) cells and natural killer (NK) cells all contribute to the homeostasis of adipose tissue. Resident macrophages are of particular interest in adipose research. These normally have an anti-inflammatory M2 phenotype, maintaining low levels of inflammatory cytokines and aiding angiogenesis (Caputa et al., 2019). During homeostasis, M2 macrophages secrete anti-inflammatory cytokines such as IL-10, which can prevent adipocyte hypertrophy (Gao et al., 2013). Macrophage infiltration increases with increasing adipose mass and, interestingly, macrophages accumulate more in obese VWAT than in obese SWAT, a phenomenon which is closely linked to the presence of hepatic fibroinflammatory lesions (Cancello et al., 2006). T_{reg} cells are also important in maintaining the anti-inflammatory profile of homeostatic adipose tissue. Moreover, VWAT presents a specific sub-population of T_{reg} cells, which express genes involved in lipid metabolism and which require PPARγ in order to help preserve insulin sensitivity (Cipolletta et al., 2012).

Adipose stromal cells further include fibroblasts, which can be identified by the presence of fibroblast-specific protein 1 (FSP1). However, fibroblasts also express markers of vascular cells such as α-smooth muscle actin (αSMA, a marker of VSMCs) and PDGFRβ, a marker of pericytes (Zhang et al., 2018). Although the role of fibroblasts in adipose tissue homeostasis has been largely unclear, studies have revealed their role in cancer or tissue regeneration (Kalluri, 2016). In adipose tissue, Zhang et al. have shown that fibroblasts expressing FSP1 do not have adipogenic potential but are nevertheless important in tissue homeostasis. Furthermore, activating canonical Wnt signalling in these fibroblasts results in a reduction in adipose tissue (Zhang et al., 2018).

Lastly, the adipose tissue also contains a complex vascular network, composed of large vessels and arteries, as well as smaller microvessels – arterioles, venules and capillaries. All microvessels are primarily composed of a layer of endothelial cells, which is further covered and stabilized by perivascular cells, also known as pericytes. In larger microvessels like arterioles and venules, the endothelial layer is also

surrounded by smooth muscle cells and fibroblasts (Majesky et al., 2011; Zhao and Chappell, 2019).

Initially described in 1873 by Rouget (Rouget, 1873), pericytes attach to the surface of endothelial cells and embed themselves into the basement membrane of small vessels, where they serve several functions. Firstly, they stabilize the newly formed capillaries and restrain the proliferation of ECs, which is necessary for vessel maturation. Moreover, they can attach to the junctions between ECs, which decreases the permeability of the vessel (Armulik et al., 2010; Daneman et al., 2010; De Palma et al., 2017). Outside the adipose microenvironment, adipose-derived pericytes have more recently also shown potential in regenerative medicine, due to their chondrogenic and osteogenic potential (Hindle et al., 2017; Hung et al., 2015).

The adipose microenvironment also includes the numerous factors secreted by the cell populations described above, which have been studied intently since the discovery that adipose tissue actively participates in endocrine signalling. The first advance in this regard was the finding that leptin is an adipose-derived cytokine (or adipokine) important in the regulation of energy balance. More than two decades ago, Zhang et al. identified the *lep* gene in mice and showed that *ob* mutations lead to obesity and associated metabolic disorders like type 2 diabetes (Zhang et al., 1994). This further led to the identification of several adipokines which are important in the homeostasis and growth of adipose tissue. While most of these secreted factors act in a paracrine fashion, two hormones in particular, leptin and adiponectin, have since been widely recognized as endocrine hormones acting on remote organs such as the brain (Scheja and Heeren, 2019; Scott et al., 2011).

Leptin is primarily expressed in adipocytes and leptin-deficient *ob/ob* mice show not only equivalents of human morbid obesity, but also insulin resistance. Leptin levels increase during periods of increased caloric intake and fall during long periods of starvation (Ahlma et al., 1996). Moreover, leptin receptors have been identified in neurons in the hypothalamus, which suggests that leptin signalling is involved in the control of the neural circuits which impact feeding behaviour (Friedman, 2016). However, leptin has also been suggested to play a role in the control of thermoregulation (Kaiyala et al., 2016).

Adiponectin is also expressed primarily in adipocytes and its levels are reduced in obesity. Experiments on adiponectin knockout mice have highlighted several

consequences of adiponectin deficiency, including insulin resistance, low levels of fatty-acid transport protein (FATP-1) and high levels of the pro-inflammatory cytokine TNFα (Maeda et al., 2002). This is believed to be due to the fact that the release of adiponectin is important for the increased activity of PPARγ and AMP kinase (Fang and Judd, 2018).

Many of the other adipokines are, however, secreted by preadipocytes, immune cells and vascular cells as opposed to adipocytes. Other molecules include adipsin, which is thought to modulate the effect of obesity on inflammation and glucose metabolism, fatty acid-binding protein 4 (FABP4), which is released as a result of lipolysis, and Neuregulin 4, which is a member of the epidermal growth factor (EGF) family that has anti-inflammatory properties and is necessary for the maintenance of adipose blood vessels (Cook et al., 1987; Nugroho et al., 2018; Scheja and Heeren, 2019; Villeneuve et al., 2018).

Moreover, microRNAs released by adipose tissue have also been the focus of several studies. For instance, miR-92a can be an indicator of BAT activity in humans, with low levels of miR-92a negatively correlated with BAT activity (Chen et al., 2016). Last but not least, adipocytes and stromal cells also secrete components of the extracellular matrix (ECM), such as collagens, which are essential in the maintenance of the tissue architecture (Mori et al., 2014; Ruiz-Ojeda et al., 2019).

The adipose microenvironment has also been studied in cancer. The obese adipose microenvironment can experience a cascade of changes in adipocytes as well as in vascular and immune cells, which together may promote tumour growth by altering lipid storage or energy expenditure (Brestoff and Artis, 2015). The link between tumour growth and lipid storage is believed to be mediated by immune cells. In lean mice and humans, adipose tissue presents anti-inflammatory cytokines and has a generally anti-inflammatory profile (Quail and Dannenberg, 2019). Weight gain triggers changes not only in adipocytes and preadipocytes, but also in other stromal cell populations, which can cause further changes in the microenvironment. The dysfunctional, hypertrophic growth of adipocytes as a result of a high fat diet is difficult to sustain and eventually leads to adipocyte death. This activates a pro-inflammatory response in adipose tissue, characterized by the release of pro-inflammatory cytokines like TNF, IFNγ and IL-6 (Brestoff and Artis, 2015). The molecules released during adipocyte death also trigger the accumulation of macrophages, which in obese adipose tissue are found in aggregates commonly known as macrophage crowns

(Weisberg et al., 2003). These macrophages are believed to have a pro-inflammatory (M2) phenotype, secreting pro-inflammatory cytokines like IL-6 and TNFα (Howe et al., 2013). In breast adipose tissue, increasing levels of pro-inflammatory cytokines are believed to activate macrophages through the Toll-like receptor 4, which leads to the transcription of further pro-inflammatory genes like IL6. This further leads to the upregulation of CYP19, an important component of the oestrogen signalling pathway, which can increase the likelihood of developing breast cancer (Howe et al., 2013).

1.2 Adipose remodelling and angiogenesis

1.2.1 Angiogenesis

The vasculature, an essential component of all organs and systems, forms primarily during development and expands or regresses afterwards in response to growth, regeneration, disease or changes in muscular or adipose mass. The embryonic vasculature is formed through either *de novo* vessel assembly (vasculogenesis) or sprouting of existing vessels (angiogenesis), whereas adult vascular growth is achieved exclusively through angiogenesis. Vasculogenesis involves the assembly of endothelial precursors known as angioblasts into tube-like structures. Angiogenesis, on the other hand, begins with the migration and re-assembly of existing endothelial cells (Vailhé et al., 2001).

Two distinct types of angiogenesis have been described: capillary sprouting and intussusception. The earliest descriptions of angiogenic growth referred mainly to capillary sprouting (Clark, 1918). Indeed, sprouting is better characterized in the literature than intussusception. During sprouting, specialized endothelial tip cells extend their filopodia in response to the vascular endothelial growth factor A (VEGF-A), while endothelial cells in the stalks of the sprouts proliferate in response to VEGF-A (Gerhardt et al., 2003).

Intussusception, on the other hand, has only been observed and characterized in the last three decades. Studies carried out by Burri et al. in the postnatal rat lung vasculature revealed an alternative angiogenic process through which the existing lumen of a vessel is split by the invasion of a transcapillary tissue pillar, which essentially divides the existing vessel in two (Burri and Tarek, 1990; Caduff et al., 1986). The mechanisms of intussusceptive growth are however less understood than those of sprouting. This is partly because studying it requires scanning electron micrographs of vascular casts, which can be laborious and difficult to obtain. Wilting

et al. showed that VEGF induces intussusceptive growth and endothelial proliferation when applied to chorioallantoic membrane but fails to induce capillary sprouting (Wilting et al., 1996). These conflicting reports on the function of VEGF in sprouting are thought to be due to variability in growth factor concentration and speed of release, emphasising the limitations of culture models and the complexity of the dynamics between growth factors and cell-cell interactions.

Since intussusception is a more recent discovery and more difficult to study, most of the angiogenic mechanisms we are aware of have been discovered in the context of angiogenic sprouting. In both development and adulthood, angiogenesis relies largely on the same molecular and cellular key players, starting with the release of growth factors, followed by the response of the cells and subsequent interactions between cells and their extracellular environment (Reviewed in Carmeliet and Jain, 2011).

Growth factors are essential in the proliferation, assembly and recruitment of all vascular cell types. The main families of growth factors involved in angiogenesis are vascular endothelial growth factors (VEGFs), fibroblast growth factors (FGFs), angiopoietins, the transforming growth factor beta (TGFβ) family and platelet derived growth factors (PDGFs), as well as their respective receptor families, most of which are transmembrane receptor tyrosine kinases (Distler et al., 2003).

The VEGF/VEGFR family is central to angiogenesis. Of the VEGF/VEGFR family, the most studied ligand is VEGF-A, which to date has been found to have six splice variants with different numbers of amino acids – 121, 145, 165, 183, 189 and 206 (Harper and Bates, 2008). Apart from its central role in the vasculature, other roles have been suggested for the VEGF family (Matkar et al., 2017). Of particular interest is the correlation between alterations in the *VEGF* gene and diabetes mellitus and its associated conditions. For instance, certain single nucleotide polymorphisms in the VEGF-C gene have been associated with diabetic retinopathy and diabetic macular oedema (Kaidonis et al., 2015).

Sprouting angiogenesis relies primarily on endothelial cells, which during the process are divided into tip cells and stalk cells (Chen et al., 2019). VEGF receptors on the surface of tip cells initially bind VEGF secreted by neighbouring cells such as pericytes and smooth muscle cells, usually in a dose-dependent manner (Figure 1.3). The tip cell filopodia, which are covered in VEGF receptors, disrupt the extracellular matrix, making way for the tip cell to migrate as another type of ECs, stalk cells, proliferate (Gerhardt, 2008; Ruhrberg et al., 2002).

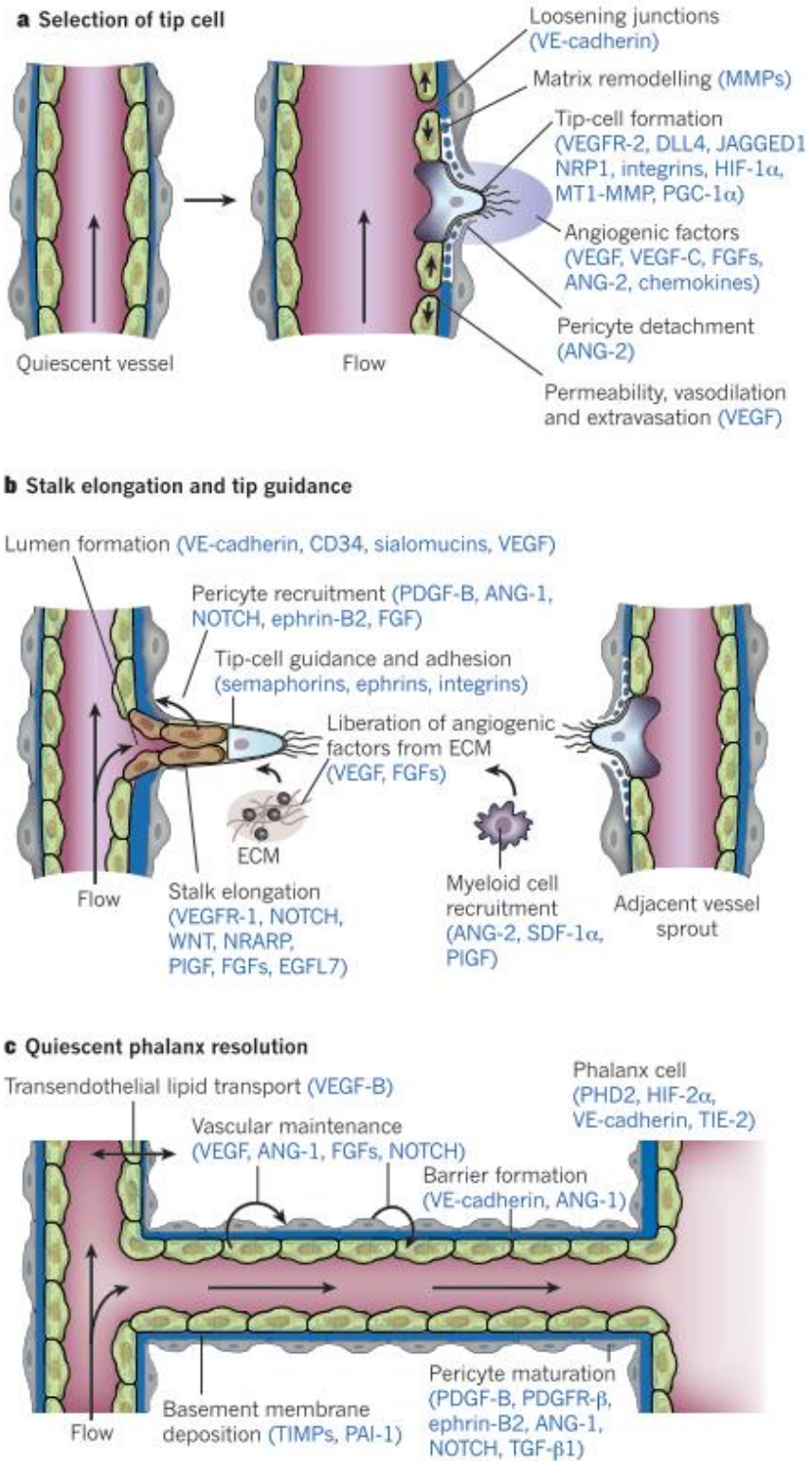

Figure 1.3. The stages of sprouting angiogenesis. *a* ***-*** *Angiogenesis starts with the selection and formation of the endothelial tip cell, followed by the detachment of surrounding pericytes. b -. endothelial stalk cells follow the tip cell and proliferate, leading to the formation of the lumen. c – the newly sprouted capillary fuses with another existing vessel (Carmeliet and Jain, 2011).*

The Delta-Notch pathway is essential for this coordination of tip cells and stalk cells. In response to VEGF-A, endothelial tip cells express DLL4, which binds to Notch1 receptors on the neighbouring endothelial cells. This, in turn, inhibits the expression of VEGFR2 in stalk endothelial cells, ensuring that tip cells are the ones leading the branching (Carmeliet and Jain, 2011). This is supported by the observation that endothelial tip cells express much higher levels of VEGFR2 than stalk cells (Gerhardt et al., 2003).

Another molecule produced by tip cells is PDGFB, which is essential in the recruitment of pericytes (Gerhardt et al., 2003). Pericytes then migrate along the PDGFB gradient in order to reach the tip cells. Capillaries are surrounded by pericytes, which are characterized by antigens like PDGFRβ, NG2, CD146 and RGS5. Although different sub-populations of pericytes show different expression patterns of these markers, PDGFRβ is expressed by all sub-populations, as PDGFB/PDGFRβ signalling is essential in pericyte survival (Craggs et al., 2015).

Interestingly, it has also been suggested that PDGFRβ binding to EC-secreted PDGFB can cause pericytes to detach from the vasculature and promote the proliferation of ECs. Greenberg et al. suggest that VEGF/PDGF signalling not only promotes EC migration and proliferation, but also inhibits the function of vascular smooth muscle cells and pericyte coverage of microvessels. This inhibition involves the formation of a complex between the receptors VEGFR2/PDGFRβ, which prevents PDGFRβ signalling (Greenberg et al., 2008)

The formation of new capillaries is also dependent on the deposition of a basement membrane (BM), which is a type of extracellular matrix (ECM). This relies on the secretion of BM proteins and the adherence of ECs to the BM, which is mediated mainly by integrins. Interactions between microvascular cells are also important here. Stratman et al. have shown that pericyte recruitment during *in vitro* vasculogenesis triggers the production of BM-specific proteins like fibronectin, nidogen-1, perlecan and laminin and that PC-EC co-cultures show an upregulation in integrins and collagen type IV (Stratman et al., 2009).

1.2.2 Adipose remodelling

The remodelling of adipose tissue in response to caloric excess is a complex process, which starts with changes in the size and oxygen requirements of adipocytes. This, in turn, changes the adipose microenvironment into a low-oxygen (hypoxic) one. As

described before, adipose tissue can expand either through hypertrophy (the increase in size of adipocytes) or hyperplasia (the increase in the number of adipocytes), with hyperplasia being considered healthy expansion and hypertrophy being associated with a more pro-inflammatory, unhealthy phenotype (Salans et al., 1968). Patterns of adipose expansion are different between individuals, sexes and depots. For instance, in obese women, SWAT primarily expands through hyperplasia, whereas omental adipose tissue is mostly characterized by hypertrophy (Drolet et al., 2008). Moreover, genes related to adipogenesis and lipid metabolism, such as *PPARγ* and perilipin (*PLIN*), are more highly expressed in the SWAT of obese women (Drolet et al., 2008).

Nevertheless, both SWAT and VWAT show some degree of hypertrophy. High fat feeding triggers adipocyte hypertrophy and mitochondrial uncoupling in mice, which leads to an increase in oxygen consumption and the activation of the hypoxia-inducible factor 1α (HIF-1α) (Lee et al., 2014b). HIFs are heterodimeric transcription factors, composed of an α subunit and a β subunit. There are three alpha subunits (HIF-1α, HIF-2α, HIF-3α), whose expression is dependent on oxygen levels, and one beta subunit (HIF-1β), which is constitutively expressed (Keith et al., 2011).

1.2.3 The adipose tissue vasculature and adipose angiogenesis

1.2.3.1 The adipose tissue vasculature

Adipose tissue is also reliant on its vascular network and vascular cells make up a high proportion of the stromal vascular fraction. Indeed, each adipocyte is surrounded by a capillary, and these capillaries feed into larger microvessels, known as venules and arterioles. Microvessels are primarily composed of endothelial cells (ECs) and adipose ECs are believed to be derived from circulating endothelial progenitor cells (EPCs) which originate in the bone marrow (Cao, 2010). Moreover, the non-fenestrated adipose endothelium has been shown to be important in the transport of fatty acids, which also relies on PPARγ expression in ECs (Briot et al., 2018a). Interestingly, the adipose endothelium has also been found to give rise to adipocytes in both white and brown adipose tissue (Tran et al., 2012).

Capillaries are further surrounded by perivascular cells, or pericytes (PCs). Pericytes are ubiquitously located across the vasculature of all tissues, where they regulate angiogenesis via EC-PC signalling and ensure the stability of vessels (Franco et al., 2011). Moreover, pericytes in various organs have been found to have multipotent potential, express markers of mesenchymal stem cells, and differentiate into mesodermal cells such as adipocytes (Crisan et al., 2008). *In vitro*, these progenitors

have osteogenic, chondrogenic and adipogenic potential. It is thus believed that adipose pericytes are not only essential for the vasculature, but also serve as a source of mesenchymal stem cells (Crisan et al., 2008).

Larger microvessels like arterioles and venules are also surrounded by a layer of vascular smooth muscle cells (VSMCs), which further stabilize vessels and express contractile proteins (Owens, 1995). Adipose stem cells can be differentiated into VSMCs *in vitro* by administering transforming growth factor β1 (TGFβ1) and bone morphogenetic protein-4 (BMP-4) (Wang et al., 2010). *In vitro* experiments have shown that growth media conditioned by human adipocytes induce VSMC proliferation, which relies on VEGF in a dose-dependent manner, and that the presence of adipokines in the media triggers an increase in VSMC expression of VEGFR1, VEGFR2 and VEGF (Schlich et al., 2013)

Interestingly, VEGF is released more by visceral fat of obese patients than subcutaneous fat. Perivascular adipose tissue from patients suffering from type 2 diabetes also releases higher amounts of VEGF than SWAT (Schlich et al., 2013). In obesity, VWAT shows a more pro-inflammatory phenotype than SWAT, and VEGF stimulates not only angiogenesis but also VSMC proliferation, which may contribute to the general increase in VWAT inflammation (Schlich et al., 2013).

The role of the microvasculature in the maintenance and expansion of adipose tissue is increasingly being studied. In adipose tissue, vascular networks serve several functions (Figure 1.4). Firstly, microvessels provide the nutrients and growth factors necessary for the survival and renewal of adipose progenitors and adipocytes. Crucially, they transport fatty acids to adipocytes through the non-fenestrated microvascular endothelium, via fatty acid binding proteins (FABPs) and fatty acid transporters (FATPs). The endothelial cells of the microvasculature are of particular importance here. In ECs, PPARγ regulates the expression of FATPs and FABPs like FATP1, FABP4 and CD36, which in turn regulate fatty acid uptake into the ECs, and loss of this transport mechanisms is believed to lead to direct ECs towards a more pro-inflammatory phenotype. (Briot et al., 2018b; Mehrotra et al., 2014).

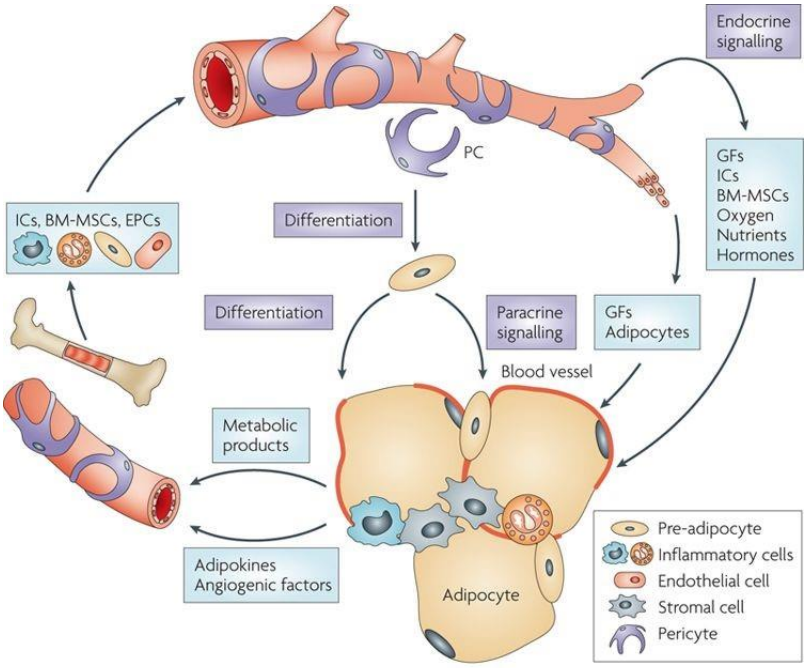

Figure 1.4 The interplay between adipocytes, vascular cells, immune cells and stromal progenitors in adipose tissue. *Blood vessels provide adipose tissue with nutrients, growth factors, oxygen and hormones, as well as immune cells and bone-marrow derived cells necessary for the maintenance and expansion of adipose tissue. Moreover, endothelial cells serve as a source of growth factors and adipokines, whereas pericytes can differentiate into adipocytes when needed* (Cao, 2010)***.***

Secondly, adipose microvessels serve as channels for circulating cells, including adipose progenitors. For example, it has been shown that adipose progenitors originating from transplanted bone marrow differentiate into adipocytes in recipient mice (Gavin et al., 2016).

Thirdly, and perhaps most importantly, the adipose microvasculature serves as a major source of adipose progenitors. Mural cells expressing PDGFRβ differentiate into adipocytes both *in vitro* and *in vivo*; moreover, these progenitors express PPARγ, which is essential for adipogenesis (Tang et al., 2008a). Gupta et al. further showed that the zinc-finger protein 423 (Zfp423) transcription factor is expressed by preadipocytes and essential in adipogenesis, directing adipocyte differentiation by regulating PPARγ expression (Gupta et al., 2010). Moreover, these Zfp423-positive progenitors localize to white adipose tissue vessels, and more specifically to a subset of PDGFRβ-positive pericytes (Gupta et al., 2012). On the other hand, endothelial cells have been less studied in terms of their potential to differentiate into other lineages. However, Tran et al. showed that ECs too can contribute to the adipocyte pool in both white and brown murine adipose tissue. Lineage tracing of cells expressing VE-cadherin, which is an EC marker, demonstrated that ECs can

differentiate into preadipocytes and adipocytes and that these ECs also express Zfp423 (Gupta et al., 2013; Tran et al., 2012). However, PPARγ is also expressed in mural PDGFRβ+ preadipocytes, which have been manipulated *in vivo* to study their role in obesity. Interestingly, it has been demonstrated that overexpressing PPARγ in the mural cells of obese mice can lead to healthy VWAT expansion. This is characterized by an increase in the adipogenic potential of PDGFRβ+ cells, an increase in the number of small adipocytes (suggesting increased hyperplasia), improved insulin sensitivity and an increase in adiponectin levels (Shao et al., 2018). Additionally, knocking out PPARγ in PDGFRβ+ progenitors in perirenal and gonadal adipose tissue results in increased macrophage infiltration and collagen deposition (Vishvanath et al., 2016). However, while this protective role of PPARγ in mural cells is essential during high fat feeding, it is not necessary for adipose tissue homeostasis in lean mice. Other groups have shown that the signalling axis of pericytes, PDGFB/PDGFRβ, is increased in obesity and is essential for the formation of new vessels to support the healthy expansion of adipose tissue. Knocking out PDGFRβ globally in adulthood has been shown to attenuate the detachment of pericytes from the adipose vasculature and reduce vessel formation in high fat diet-fed mice (Onogi et al., 2017). These data point to a complex, multi-faceted role of PDGFRβ-positive perivascular cells in adipose tissue homeostasis and remodelling.

Finally, the signalling pathways involved in the crosstalk between the cell populations making up the microvasculature can influence the self-renewal and differentiation of adipose progenitors, the integrity of the blood vessels and the inflammatory profile of adipose tissue. For example, vascular growth can be influenced by leptin. Cao et al. have shown that leptin, which modulates weight gain by regulating appetite and energy expenditure, also stimulates angiogenesis when co-administered with VEGF and FGF2. Moreover, the vasculature of leptin deficient *ob/ob* mice lacks fenestrations, whereas administering leptin intradermally to these mice increases vascular permeability (Cao et al., 2001). In human chondrosarcoma, adiponectin has also been shown to induce angiogenesis and VEGFA expression in tumours by activating HIF-1α (Lee et al., 2015).

1.2.3.2 Adipose angiogenesis

Adipose angiogenesis is key in the issue of healthy vs. unhealthy adipose remodelling. Once adipocytes increase in size and their demand for oxygen increases, there is a requirement for the vasculature to also expand in order to sustain

this demand. Failure of this can lead to pathological angiogenesis, and obesity is accompanied by a decrease in angiogenesis and associated markers. For instance, subcutaneous tissue from obese patients shows lower levels of VEGF (58% lower compared to lean subjects), as well as a 44% decrease in capillary density (Pasarica et al., 2009).

As described earlier, one of the main functions of the vasculature is to provide the tissue with oxygen, and unhealthy expansion of adipose tissue, particularly through hypertrophy, leads to a hypoxic environment. HIFs regulate genes involved in numerous cellular processes, such as proliferation, stem cell renewal, apoptosis, epithelial-mesenchymal transition (EMT) and, importantly, angiogenesis. *VEGF*, *PDGFB*, *ANGPT1* and *ANGPT2* are just some of the angiogenic genes regulated by these transcription factors (Dengler et al., 2014). It has previously been shown that not only do obese mice have increased levels of HIF-1α and VEGF protein, but, after only one or three days of HFD feeding, HIF-1α protein levels and *VEGF* mRNA levels are increased in epididymal adipose tissue (He et al., 2011; Lee et al., 2014b). Moreover, it has also been demonstrated that HIF-1α binds to the proximal hypoxia response element of the *VEGF* promoter and that this DNA-protein interaction is stronger in adipocytes in response to hypoxia (He et al., 2011).

Despite these findings, other studies have suggested that, under caloric excess and hypoxic stress, HIF-1α upregulation alone cannot sufficiently stimulate local angiogenesis. Instead, constitutive overexpression of *Hif-1α* in mice leads to an increase in local fibrosis and inflammation, as suggested by increased levels of collagens and elastin and expression of inflammatory genes (Halberg et al., 2009). These conflicting reports on the role of hypoxia in adipose angiogenesis might be explained by the fact that the oxygen availability in *in vitro* hypoxia experiments does not accurately reflect the physiological oxygen availability observed *in vivo* (Goossens et al., 2011)

It is also important to distinguish between insufficient and dysfunctional angiogenesis in the context of obesity. While vascular growth in obesity generally fails to cope with the needs of the expanding tissue, it has also been suggested that the growth which does occur is mainly intussusceptive, which may lead to more permeable vessels that eventually lead to the fibrotic and inflammatory phenotype of obese adipose tissue (Crewe et al., 2017). This is also supported by evidence that, in the VWAT of HFD

and *ob/ob* mice, there are more interactions between leukocytes, endothelial cells and platelets (Nishimura et al., 2008).

VWAT and SWAT have different consequences on metabolic health, and one of the questions in the field is whether these depots show different angiogenic profiles. However, studies focused on angiogenesis have shown conflicting reports, which may be due to significant differences in methodology and the aspects of the vasculature which are being investigated. For instance, Ledoux et al. analysed the *in vitro* angiogenic effect of VWAT and SWAT obtained from obese patients on chick chorioallantoïc membrane (CAM) and found not only that both types of adipose tissue stimulate angiogenesis, but that VWAT and SWAT have the same effect on CAM and also express similar levels of VEGF (Ledoux et al., 2008). However, Gealekman et al. found that, when human visceral and subcutaneous explants are embedded in Matrigel® basement membrane matrix, SWAT shows greater angiogenic capacity and an increase in the expression of ANGPTL4, which is pro-angiogenic; however, this capacity decreased in obese subjects (Gealekman et al., 2011). In mice, VWAT of HFD-fed obese mice was found to have increased angiogenic capacity and higher expression levels of genes involved in angiogenesis and inflammation (Song et al., 2016).

The adipose vasculature has attracted much interest as a therapeutic target. However, this area of research has also produced conflicting results and conclusions. Early research suggested, for instance, that blocking angiogenesis with the well-known inhibitor TNP-470 leads to a dose-dependent reduction in weight and adipose tissue, with associated metabolic changes (Rupnick et al., 2002). Further research showed that TNP-470 blocks both VEGF and FGF-2 induced angiogenesis (Bråkenhielm et al., 2004). Although blocking adipose angiogenesis leads to weight loss and associated improvements in overall metabolic health, it is disputed whether these changes can be sustained in the long term and whether any important side effects need to be taken into account. Indeed, anti-angiogenic agents used in cancer treatment have been shown to have side effects like hypertension (Cao, 2010).

Conversely, VEGF-A overexpression in adipocytes has been found to not only activate angiogenic processes, but also induce beiging in subcutaneous adipose tissue. Furthermore, transplantation of adipose tissue which overexpresses VEGFA appears to improve the overall metabolic health of the mice receiving the transplant (Park et al., 2017). Similarly, another group has shown that overexpression of VEGF

leads to a reduction in the hypoxia and obesity induced by a high fat diet, while not having any effect on food intake (Elias et al., 2012).

Stimulation of angiogenesis has also been achieved by targeting other key molecular players of adipose tissue. Interestingly, activation of PPARγ in mice by treatment with the PPARγ agonist Rosiglitazone leads to an increase in capillary formation in VWAT and an upregulation of the angiogenic factors VEGF-A, VEGF-B and angiopoietin-like factor 4 (ANGPTL4), which stimulate EC growth (Gealekman et al., 2008). This highlights yet another role of PPARγ in endothelial cells. Similarly, treating primary human ECs and EC cell lines with the PPARδ agonist GW501516 has been shown to increase EC proliferation and angiogenic sprouting both *in vitro* and *in vivo* (Piqueras et al., 2007).

1.3 Overview of WT1

In 1990, two groups identified the Wilms' tumour 1 (*Wt1*) gene, describing its location on chromosome 11p13. WT1 was then proposed as a driver of Wilms' tumour, a type of paediatric kidney cancer which arises due to both germline mutations in *Wt1* and due to somatic mutations during development (Call et al., 1990; Gessler et al., 1990). Since then, WT1 has gained much attention not only for its role in cancer, but also for the many roles in development and adult homeostasis, some of which are outlined further (Hohenstein and Hastie, 2006).

1.3.1 WT1 in development

Early studies in development showed that WT1 expression during embryogenesis is similar in human and mouse (Armstrong et al., 1993). E8.5 mouse embryos start expressing WT1 in the intermediate mesoderm and lateral plate mesoderm, the latter further giving rise to the coelomic epithelium, which surrounds the coelomic cavity during development. The coelomic epithelium continues to express WT1 and subsequently gives rise to the mesothelium (Armstrong et al., 1993).

WT1 has been shown to be essential for the development of several organs, as demonstrated by global *Wt1* knockout phenotypes which result in embryonic lethality (Herzer et al.; Kreidberg et al., 1993a). WT1 is required for the development of the kidney and gonads and is further expressed in the pulmonary mesothelium during development, where loss of WT1 leads to abnormal lung development (Bandiera et al., 2015; Cano et al., 2013; Kreidberg et al., 1993; Moore et al., 1999). Recently, it

has also been shown that murine adipose mesothelial cells expressing WT1 during late gestation contribute to the adipocyte population in VWAT (Chau et al., 2014).

As far as its function as a transcription factor is concerned, WT1 contains both repressor and activator regulatory domains and can thus both upregulate and downregulate downstream genes. Alternative splicing of WT1 results in isoforms including or lacking three amino acids (KTS) near exon 9 (Hammes et al., 2001) and different isoforms of WT1 appear to have different functions in development. Interestingly, ChIP-seq studies have revealed that most transcriptional targets of WT1 are bound by -KTS isoforms (Lefebvre et al., 2015).

In the kidney, WT1 may suppress apoptosis through the activation of fibroblast growth factors and the suppression of BMP-pSMAD signalling (Motamedi et al., 2014). In heart development, the role of WT1 is linked to its role in EMT, which is exerted through the Wnt/β-catenin signalling pathway (von Gise et al., 2011).

1.3.1.1 WT1 and heart development

As mentioned above, the role of WT1 in development has been shown to be crucial in the heart. *Wt1*-null mice of a C57Bl/6 background die at E13.5 and show several developmental defects, including heart malformations (Moore et al., 1999). Using a YAC transgenic reporter mouse line, Moore et al. showed that the developing heart starts expressing WT1 at E9, in the mesenchymal villi which constitute the proepicardium; the cells of the proepicardium later migrate towards the myocardium, eventually forming the epicardium (Moore et al., 1999). Later in development, WT1 is involved in epithelial-mesenchymal transition (EMT), which is important in the development of the heart and the diaphragm. Mouse embryos carrying epicardial-specific *Wt1* deletions die between E16.5-E18.5 due to heart defects such as oedema, blood build-up in the systemic veins, and failure to form coronary arteries, which suggests WT1 is necessary for the differentiation of mesenchymal cardiovascular progenitors (Martínez-Estrada et al., 2010). WT1 has also been shown to downregulate the expression of *Ccl5* and *Cxcl10* in epicardial cells, which are essential in epicardial cell migration and cardiomyocyte proliferation during heart development (Velecela et al., 2013). Moreover, WT1 activates the tyrosine kinase type B receptor (TrkB), which is required for myocardial vascularisation, as suggested by the lack of subepicardial blood vessels in E12.5 mouse embryos and the increase in apoptotic cells in the epicardium and subepicardium of *Wt1* knockout mice (Wagner et al., 2005).

Interestingly, the mechanism of action of WT1 in heart development contrasts its role in kidney development. During MET in the kidney, WT1 activates *Wnt4*, whereas during EMT in the epicardium, WT1 represses *Wnt4* (Essafi et al., 2011). This switch in function is due to the recruitment of different co-activators/co-repressors, which together direct a process known as chromatin flip-flop, where WT1 along and its co-factors restrict the accessibility of the *Wnt4* locus (Essafi et al., 2011).

The signalling pathways involved in heart development and regeneration further direct immune responses. In the epicardium, WT1 represses the expression of pro-inflammatory chemokines such as CCL5, CXCL10, which are necessary for cardiomyocyte proliferation and epicardial cell migration (Velecela et al., 2013). This upregulation in WT1 is correlated with the upregulation of pro-inflammatory cytokines such as TNFα, IL-1β and IL-6 (Nian et al., 2004). These, in turn, can activate the transcription factor NF-kB, which upregulates WT1, suggesting an anti-inflammatory role of WT1 (Dehbi et al., 1998). This is supported also by the fact that WT1 regulates the expression of IL-10, an anti-inflammatory cytokine (Sciesielski et al., 2010). Moreover, mesothelial cells, which are normally characterized by the expression of WT1, are themselves important in the regulation of inflammation (Kawanishi, 2016).

1.3.1.2 WT1 and the mesothelium

WT1 is highly expressed in the mesothelium, the layer of cells which line most internal organs, providing stability and preventing tissue adhesion. The phenotype of mesothelial cells presents characteristics of both mesenchymal and epithelial cells – while they present the tight junctions and apical-basal polarity of epithelial cells, they express many of the markers specific to mesenchymal cells (Chau and Hastie, 2012). Interestingly, WT1-positive mesothelium has been proposed as a source of progenitors for several organs, including the heart and liver (Chau and Hastie, 2012).

The hypothesis that WT1+ mesothelial cells are progenitors in various organs is supported by several studies (Chau et al., 2014). For instance, lineage tracing studies have revealed that WT1+ progenitors in the serosal mesothelium give rise to smooth muscle cells which become incorporated in the gut vasculature (Wilm et al., 2005). Mesothelial cells have also been found to give rise to smooth muscle cells positive for αSMA and cells expressing PDGFRβ in the developing lung (Que et al., 2008). Finally, WT1+ mesothelial cells have been suggested to contribute to other cell populations in the developing lung, such as endothelial cells, chondrocytes and fibroblast-like interstitial cells (Cano et al., 2013).

1.3.2 WT1 in adult homeostasis and cancer

In the adult organism (both in mouse and human), WT1 continues to be expressed only in a restricted set of tissues and cells. Although WT1 expression is very limited in adult tissues, inducible ubiquitous WT1 deletion in adult mice shows a range of phenotypes within just a few days, from glomerulosclerosis and spleen atrophy to a loss of bone, fat and erythropoietic potential (Chau et al., 2011). Moreover, an important role of WT1 past development is that of a tumour suppressor and oncogene in several types of cancer (Reviewed in Yang et al., 2007).

1.3.2.1 WT1 in adult homeostasis

Throughout adulthood, WT1 continues to be expressed in select organs, such as the kidney, gonads and the intestine, and in specific cell populations like mesothelial cells.

In the adult kidney, WT1 can only be detected in the podocytes. Here, Wnt/β-catenin signalling (which lies downstream of WT1) has been suggested as an important pathway for podocyte function. Proteinuric kidney diseases such as focal segmental glomerulosclerosis and diabetic nephropathy show an upregulation of Wnt and β-catenin and β-catenin ablation can protect against kidney disease post-injury, and are also characterized by a loss of WT1 (Zhou and Liu, 2015).

WT1 expression is also sustained in the adult ovary. Hsu et al. have demonstrated the presence of WT1 in the granulosa cells in primordial, primary and secondary follicles but that the expression levels become lower as the follicles develop, suggesting a role for WT1 in folliculogenesis and in the repression of ovarian differentiation genes (Hsu et al., 1995). In males, WT1 is also present in Sertoli cells. Cre-LoxP-mediated WT1 deletions in adult murine testes lead to cell death in the seminiferous tubules and, histologically, the mouse testes highly resemble those of patients suffering from non-obstructive azoospermia (Wang et al., 2013). Moreover, Sertoli cells deleted for WT1 present altered morphology and polarity and fail to form tight junctions (Wang et al., 2013). WT1 deletions in the testes have further been shown to cause impaired spermatogenesis, marked by an accumulation of undifferentiated spermatogonia in the testes and thought to be caused, again, through a loss of mesenchymal-epithelial balance due to a downregulation of E-cadherin (Zheng et al., 2014).

Adult mice also express WT1 in the intestine. As shown by Wilm et al., expression is maintained in the serosal mesothelium late into adulthood, suggesting that WT1-

positive cells here are a source of progenitors essential in tissue repair (Wilm et al., 2005). This pattern of adult mesothelial expression is also seen in the lung. Here, the behaviour of pleural mesothelial cells is critical in the homeostasis of the lung and dysfunctions of these cells can result in idiopathic pulmonary fibrosis. WT1 is expressed in a subset of these mesothelial cells and loss of WT1 results in mesothelial-mesenchymal transition (MMT), reduced E-cadherin levels and increased expression of fibrotic markers like fibronectin and αSMA, highlighting once again the protective role of WT1 against disease (Karki et al., 2014).

Other cells expressing WT1 throughout adulthood are mesothelial cells lining internal organs, bone marrow cells and gonadal cells (reviewed in Hastie, 2017). WT1 can additionally be found in some cells of the adrenal cortex, which co-express GATA4 and can differentiate into steroidogenic cells following a gonadectomy (Bandiera et al., 2013). Finally, Chau *et al.* have shown that deleting *Wt1* ubiquitously in adult mice leads, within days, to multiple organ failure and a series of dramatic phenotypes such as spleen and pancreas atrophy, glomerulosclerosis, and loss of adipose tissue (Chau et al., 2011).

1.3.2.2 WT1 in cancer

Perhaps the most widely studied aspect of WT1 post-development is its role in cancer. Initially considered a tumour suppressor gene, *Wt1* mutations can cause predisposition to developing Wilms' tumours, which develop in the kidney during childhood. In some Wilms' tumours, overexpression of the platelet-derived growth factor A (PDGFA) has been observed, and WT1 has subsequently been shown to bind to several sites in the promoter of PDGFA and thus act as a repressor (Gashler et al., 1992). Wang et al. have also suggested that loss of downregulation of PDGFA by WT1 is a factor in the growth of Wilms' tumours (Wang et al., 1992).

However, WT1 is also expressed in several other types of cancer, and WT1-positive tumours are generally associated with poorer prognosis. It has thus been proposed that WT1 may also act as an oncogene. This is supported firstly by studies showing that it is expressed in tumours of tissues that otherwise do not express WT1, such as breast tumours, astrocytic tumours and colon tumours (Dessain et al., 2000; Koesters et al., 2004; Oji et al., 2004).

Many studies have focused on the mechanisms through which WT1 acts in cancer. To mention just a few, WT1 has been shown to regulate the oncogenic activity of

KRAS, a gene whose mutations have been found in numerous cancer types, including pancreatic and lung cancer (Vicent et al., 2010). WT1 also activate the promoter activity of *c-myc*, an oncogene which regulates several cell growth and metabolism pathways (Han et al., 2004). Finally, WT1 may act in breast cancer through its role in EMT and in prostate cancer cells by downregulating E-cadherin (Artibani et al., 2017; Brett et al., 2013).

1.3.3 WT1 in angiogenesis

WT1 has also been described as a regulator of angiogenesis in cancer and during revascularization after events like ischaemia.

1.3.3.1 WT1 in the tumour vasculature

WT1 function and expression has further been examined in the vasculature of different tumours. For instance, Wagner et al. have shown that WT1 is expressed in the vasculature of most ovarian, pancreatic, breast, kidney and lung tumours and is typically found in the nuclei of endothelial cells in these vessels (Wagner et al., 2008a). Studies on Ewing sarcoma have also highlighted the role of WT1 in angiogenesis. Induced expression of *WT1* in a *WT1*-null Ewing sarcoma cell line resulted in increased angiogenesis and WT1-positive tumours showed an upregulation of VEGF, MMP9, Tie-2, and Ang-1 (Katuri et al., 2014).

However, here WT1 seems to act mainly in endothelial cells. WT1 plays a role in the migration, proliferation and assembly of endothelial cells, as suggested by the fact that *WT1*-silenced human umbilical vein endothelial cells (HUVECs) stop proliferating and fail to form tubular networks in Matrigel cultures, without however exhibiting any increased apoptosis (Wagner et al., 2008a). It is believed that the activation of WT1 in endothelial cells in cancer or regeneration-associated neovascularization serves to switch the endothelial cells towards a more multipotent phenotype, which aids the formation of new vessels (Scholz et al., 2009).

With regard to its mechanism of action, WT1 was suggested to be a transcriptional regulator of ETS-1, a transcription factor acting on angiogenesis-associated genes like angiopoietin-2 and VEGFR2, both of which were downregulated in *WT1*-silenced cells (Wagner et al., 2008a). Moreover, the impaired *in vitro* angiogenic potential of *WT1*-null HUVECs described by Wagner *et al.* was also observed in conjunction with a decrease in nestin expression following WT1 knockdown. As nestin is an intermediate filament protein directly regulated by WT1, this suggests that WT1 also

plays a role in the way the cytoskeleton is organized and re-organized depending on physiological needs (Wagner et al., 2006).

WT1 regulates the expression of CD31 and CD117 (cKit) and is expressed in the tumour vasculature and stromal cells of several cancers, independently of its expression in cancer cells (Wagner et al., 2014). Moreover, *Wt1* conditional knockouts in *Tie2-CreERT2;Wt1*$^{lox/lox}$ and VE-CreERT2;Wt1$^{lox/lox}$ mice have shown a significant reduction in tumour growth and tumour vascularisation (Wagner et al., 2014).

1.3.3.2 WT1 in angiogenesis after ischemia

Following an infarction, *Wt1* is upregulated in the endothelium and the epicardium and peaks at day 7 post-infarction (Duim et al., 2016). WT1 is also involved in blood vessel formation following an ischaemic event. This was initially suggested after the observation that, post-ischaemia, the rat myocardial vasculature shows an increase in *Wt1* expression and that WT1 co-localizes with cell proliferation markers and VEGF, the main driver of angiogenesis, as well as with endothelial cell and VSMC markers like CD31 and αSMA (Wagner et al., 2002). This is of interest especially as WT1 had normally only been detected in the epicardium. It has further been suggested that the function of WT1 in this scenario is linked to the oxygen availability in the tissue. Indeed, hypoxia triggers the upregulation of WT1 in the kidney and the heart, but not in the brain or the spleen (Wagner et al., 2003).

The simultaneous increase in WT1 and VEGF expression after ischemia is especially of interest as VEGF has been found to be directly or indirectly under the control of WT1. VEGF has several pro-angiogenic and anti-angiogenic isoforms obtained through alternative splicing (Houck et al., 1991). The alternative splicing of VEGF is dependent on the splicing factor kinase SRPK1, which lies under the control of WT1, and the anti-angiogenic $VEGF_{165}$b isoform is downregulated in *Wt1* mutants (Amin et al., 2011). Moreover, WT1 has been shown to directly suppress SRPK1 in kidney podocytes and the -KTS isoform of WT1 regulates VEGF isoform balance through transcriptional regulation of SRPK1 and the serine/arginine-rich splicing factor 1 (Wagner et al., 2019). Similar results have been obtained from an *in vivo* ovarian cancer model, where lentiviral transfections with -KTS WT1 isoforms lead to shortened overall survival, an increase in VEGF expression and higher microvessel density (Yamanouchi et al., 2014). In Ewing sarcoma, WT1 has similarly been shown to bind directly to the VEGF promoter and direct its expression (McCarty et al., 2011). Moreover, WT1 expression in Ewing sarcoma is upregulated by hypoxia and WT1 is

essential for hypoxia-induced angiogenesis (McCarty et al., 2011). Hanson et al. have additionally demonstrated that the zinc finger DNA binding domain of the WT1 protein is essential for its transcriptional regulation of VEGF (Hanson et al., 2007).

1.4 WT1 and adipose tissue

The observation that ubiquitous *Wt1* deletion in adult mice leads to multiple organ failure within days was surprising, especially considering the limited expression of *Wt1* in adulthood (Chau et al., 2011). Mice deleted for *Wt1* showed a variety of phenotypes, including a surprising loss of adipose tissue (Chau et al., 2011). Chau et al. further showed that WT1 is expressed in all visceral adipose depots analysed, but not in subcutaneous or brown adipose tissue (Chau et al., 2014). Moreover, *WT1* mRNA was detected in human visceral adipose tissue, but not in subcutaneous or brown (Chau et al., 2014).

Unlike SWAT, VWAT depots are surrounded by a mesothelial layer; interestingly, in VWAT, WT1 is expressed in the mesothelium of several visceral adipose tissue depots – such as epididymal, perirenal and pericardial adipose tissue. Moreover, the mesothelium has been demonstrated to be a source of progenitors that continue to differentiate into adipocytes or other cell types after birth, depending on the requirements of the tissue (Chau and Hastie, 2015).

Chau *et al.* also showed that WT1 is not detected in mature visceral adipocytes, but is present in a subset of adipose progenitors (Lin−CD31−CD29+CD34+Sca1+CD24− cells), which retain WT1 expression throughout adulthood (Chau et al., 2014). However, it must also be noted that not all adipose progenitors are WT1+, with current data suggesting that WT1+ and WT1- progenitors give rise to adipocytes with different properties (Chau et al., 2014). The percentage of progenitors expressing WT1 is also different across VWAT depots. This has sparked further questions regarding the developmental origins of different adipose depots, with the lateral plate mesoderm being currently suggested as the origin of VWAT (Chau et al., 2014).

Other recent work has been focused on subsets of adipocytes and adipose in murine depots. Lee et al. have revealed three white adipocyte sub-populations, derived from three adipose progenitor populations (Lee et al., 2019). These progenitor populations are characterized by the expression of WT1, transgelin, and myxovirus 1 respectively and exhibit different transcriptional and metabolic signatures. WT1-positive progenitors and the adipocytes derived from these show high glycolytic metabolism,

reduced triglyceride accumulation *in vitro* and responsiveness to TNFα (Lee et al., 2019). This highlights the issue of adipose heterogeneity, both inter-depot and intra-depot, even though the exact function of WT1 in VWAT is currently unknown. Considering the well-documented role of WT1 in inflammation, as well as in developmental and adult angiogenesis, it is important to know whether WT1 is also expressed in the vascular and immune cells of VWAT and, if so, what its role is in these populations.

1.5 Summary

Several different lines of research are currently focusing on the pathological consequences of obesity, and visceral adipose tissue in particular has gained notoriety due to its correlation with the development of the metabolic syndrome. However, as more data are being published, it is becoming increasingly clear that different visceral depots should be approached as individual 'organs' when studying the development, homeostasis and expansion of VWAT.

In parallel, much research has also been carried out on WT1, a transcription factor with many functions in both development and adulthood, which is illustrated by the lethal effect of embryonic *WT1* deletion (Herzer et al.; Kreidberg et al., 1993b) and the multiple organ failure observed when *WT1* is deleted ubiquitously in adult mice (Chau et al., 2011). The recent findings that WT1 is expressed in adult VWAT progenitors and that progenitors expressing WT1 during development give rise to some visceral adipocytes have revealed new angles from which the difference between VWAT and SWAT can be researched. Additionally, VWAT is, like all adipose tissues, reliant on its vasculature and the roles identified for WT1 in angiogenesis in other organs lead to the question of whether WT1 plays a role in the adipose vasculature as well.

1.5.1 Hypothesis

Although WT1 expression is limited after embryogenesis, a population of VWAT adipose progenitors continues to express WT1 into adulthood, in both humans and mice, and the mesothelium has been demonstrated to be a source for these progenitors. Secondly, VWAT is more closely associated to cardiovascular disease and it has an increased angiogenic profile. Thirdly, WT1-expressing mesothelial cells can incorporate into new blood vessels and there is evidence to suggest that WT1 also regulates the expression of genes associated with angiogenesis, such as VEGF.

With this in mind, the aim of my project is to investigate the role of WT1 and WT1-positive adipose progenitors in VWAT angiogenesis. Although certain isoforms of WT1 have been associated with post-transcriptional processes, its best-characterised function remains that of a transcription factor, and this is the function that this project is focused on. Therefore, the main hypothesis of this thesis is:

> *WT1-expressing progenitors are involved in the angiogenic processes associated with adipose tissue formation and homeostasis.*

1.5.2 Aims

In order to address this hypothesis, this project has the following aims:

1. To characterize *in vivo* expression of WT1 in the vasculature of murine and human VWAT
2. To investigate the role of murine WT1 in angiogenesis *in vitro*
3. To investigate the role of WT1 in murine adipose pericytes.

Chapter 2

Materials and methods

2.1 Animal models

An brief overview of the mouse models used for our experiments is outlined in Table 2.1, with further details in the subsections below.

Genotype	Age	Sex	References
Wt1 ^{CreERT2} *;mTmG*	6 MO	M	Chau et al., 2014a; Muzumdar et al., 2007
Wt1 $^{GFP/+}$	>3 MO	M/F	Hosen et al., 2007
CAG ^{CreERT2} *; Wt1* $^{loxP/loxP}$	>3 MO	M/F	Chau et al., 2011; Martínez-Estrada et al., 2010
CAG ^{CreERT2} *; Wt1* $^{loxP/GFP}$	>3 MO	M/F	Chau et al., 2011; Martínez-Estrada et al., 2010
C57Bl/6	>3 MO	M/F	Murray and Little, 1935

Table 2.1. Mouse strains used in experiments.

2.1.1 Animal husbandry

Mice were housed in the animal facilities at the MRC Human Genetics Unit and at Little France, University of Edinburgh. Animals were kept in compliance with Home Office regulations.

2.1.2 *Wt1* lineage tracing model (*Wt1*^{CreERT2}*;mTmG*)

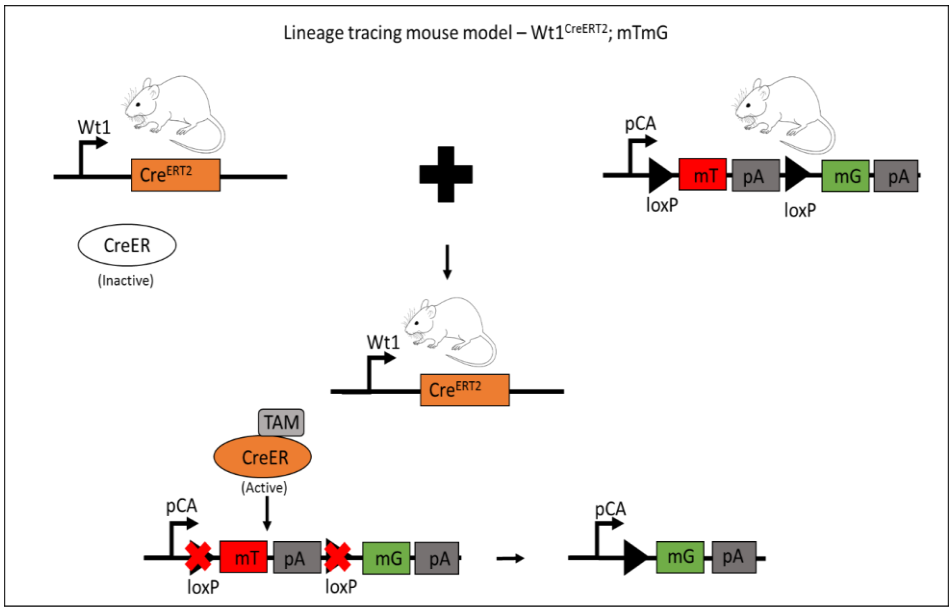

Figure 2.1. Schematic representation of the lineage tracing model Wt1 ^{CreERT2}***;mTmG.*** *This model is obtained by crossing Wt1* ^{CreERT2} *knock-in mice with the reporter mTmG mouse line. In the progeny, CreERT2 is inactive in the absence of tamoxifen and thus no recombination occurs. In the absence of CreERT2-induced recombination, Tomato is expressed ubiquitously in the cell membrane, under the pCA reporter. Tamoxifen activates CreERT2 and the resulting recombination leads to the excision of Tomato and the membranous expression of GFP. Since the expression of Cre is directed by the* Wt1 *promoter, membranous GFP can only be observed in the cells where* Wt1 *is expressed at the time tamoxifen is administered.*

For the lineage tracing *Wt1*^{CreERT2}*;mTmG* model, the tamoxifen-inducible *Wt1*^{CreERT2} (Figure 2.1) mouse line was crossed with a reporter *mTmG* mouse, generating a mouse in which the expression of membranous GFP in a cell indicates *Wt1* expression in its progenitor at the time tamoxifen was administered (Chau et al., 2014a; Muzumdar et al., 2007).

The pups received tamoxifen through the mother's milk. Four doses of tamoxifen (2 doses per week) were given to mothers at beginning of P0. High fat diet mice were fed a HFD since the age of 1 month old and culled at 7.5 months old. Control mice were fed a standard chow diet and culled at 7.5 months old.

2.1.3 *Wt1* reporter model (*Wt1*$^{GFP/+}$)

Wt1$^{GFP/+}$ mice (Figure 2.2) were used to observe the endogenous expression of *Wt1* (Hosen et al., 2007).

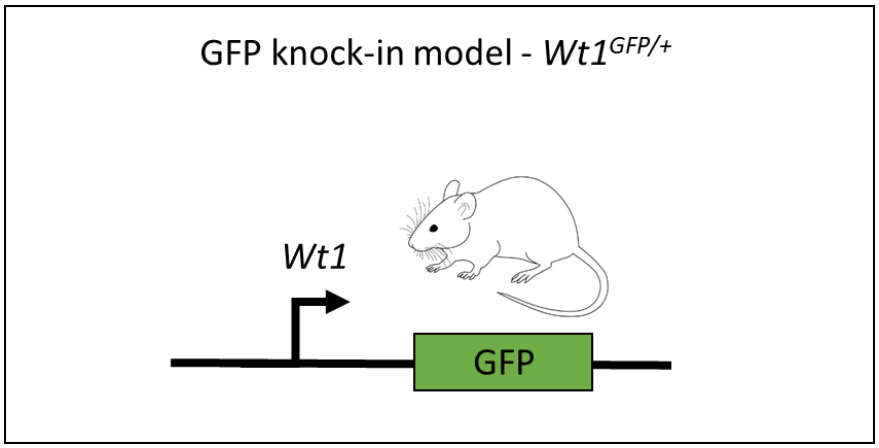

Figure 2.2 Schematic representation of the GFP knock-in mouse model* Wt1$^{GFP/+}$, *where GFP is expressed under the* Wt1 *promoter.

2.1.4 *Wt1* conditional knockout model (*CAG*^{CreERT2}*; Wt1*$^{loxP/loxP}$)

In our conditional knockout model (Figure 2.3), *Wt1* can be deleted by administering 4-hydroxytamoxifen (the active metabolite of tamoxifen). The *CAG*^{CreERT2}*; Wt1*$^{loxP/loxP}$ mouse line was obtained by crossing the CreERT2 line with mice where exon 1 of *Wt1* is flanked by *loxP* sites (*Wt1*$^{loxP/loxP}$), and then further intercrossing the offspring (Chau et al., 2011; Martínez-Estrada et al., 2010).

2.1.5 *Wt1* conditional knockout model (*CAG*^{CreERT2}*; Wt1*$^{loxP/GFP}$)

CAG^{CreERT2}*; Wt1*$^{loxP/GFP}$ (WGER) mice were generated by crossing *Wt1*^{GFP} mice with *CAG*^{CreERT2}*; Wt1*$^{loxP/loxP}$ mice, as described above.

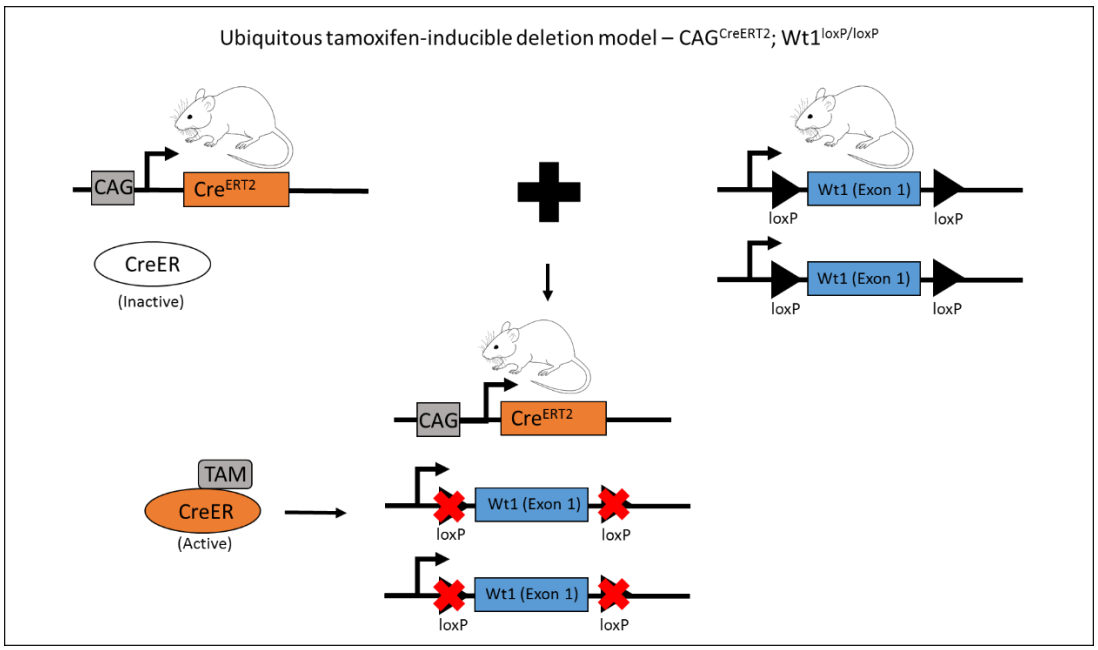

Figure 2.3 Schematic representation of the ubiquitous tamoxifen-inducible Wt1 deletion model – CAG^{CreERT2}; Wt1$^{loxP/loxP}$. *CAG^{CreERT2} male mice, in which CreER is expressed ubiquitously under the synthetic CAG promoter, were crossed with floxed Wt1$^{loxP/loxP}$ females, and the offspring were further intercrossed, resulting in CAG^{CreERT2}; Wt1$^{loxP/loxP}$ progeny. CreER is inactive unless tamoxifen is administered. Tamoxifen was administered to isolated cells in culture*.

2.1.6 CreERT2 control mice (*CAG^{CreERT2}*)

CreERT2 toxicity effects were assessed in cells isolated from *CAG^{CreERT2}* mice.

2.1.7 Wild-type mice

All wild-type mice used were of C57Bl/6 background and housed in the animal facility at Little France, University of Edinburgh.

2.1.8 Genotyping of transgenic mice

DNA extracted from ear clips was used for genotyping. DNA was extracted by placing each ear clip in a 0.5 mL Eppendorf, adding 75 µL Solution 1 (25 mM NaOH and 0.2 mM EDTA in dH_2O), and placing the tube at 95°C for 30 minutes. Then, 75 µL of Solution 2 (40 mM Tris in dH_2O) were added to each tube, and the tubes were vortexed.

Genotyping was performed under the conditions detailed in Table 2.3. For all reaction mixes, we used GoTaq® G2 Hot Start Green Master Mix (M7422, Promega), as well as the primer sequences in Table 2.2.

Gene	Genotyping primer sequences (5' – 3')
Cre	F: GCATTACCGGTCGATGCAACGAGTGATGAG R: GAGTGAACGAACCTGGTCGAAATCAGTGCG
Wt1 co/co	F: TGGGTTCCAACCGTACCAAAGA R: GGGCTTATCTCCTCCCATGT
GFP	F1: GCCTGAAGAACGAGATCAGC F2: GGCAGCTTGAATTCCTCTCA R: AGCCTGAAGCTGCTCACATCC

Table 2.2 Primer sequences used for mouse genotyping.

Gene	PCR reaction mix	PCR conditions
Cre	F primer: 0.5 µL R primer: 0.5 µL GoTaq® Master Mix: 10 µL H_2O: 4 µL DNA: 5 µL	94°C 2 min 94°C 15 s 58°C 30 s 72°C 1 min (35 cycles) 72°C 5 min 4°C 10 min
Wt1 co/co	F primer: 0.5 µL R primer: 0.5 µL GoTaq® Master Mix: 10 µL H_2O: 4 µL DNA: 5 µL	94°C 2 min 94°C 15 s 58°C 30 s 72°C 1 min (35 cycles) 72°C 5 min 4°C 10 min
GFP	F1 primer: 0.5 µL F2 primer: 0.5 µL R primer: 0.5 µL GoTaq® Master Mix: 10 µL H_2O: 3.5 µL DNA: 5 µL	94°C 3 min 94°C 30 s 58°C 30 s 72°C 1 min (35 cycles) 72°C 5 min 4°C 10 min

Table 2.3 Cycling conditions used for mouse genotyping.

2.1.9 Agarose gel electrophoresis

Genotyping of all mice was carried out by agarose gel electrophoresis. 2% agarose gels were made up by dissolving 2 grams agarose powder (UltraPure™ Agarose, 16500500, ThermoFisher) in 100mL of 1X TAE buffer (40mM Tris acetate, 1mM

EDTA) and adding 5 µL of GelRed® Nucleic Acid Gel Stain (#41003, Biotium) per 100 mL of gel. Samples were run in 1X TAE buffer at 120V for one hour.

2.2 Human samples

Humans tissues were obtained courtesy of Prof. Roland Stimson at the University of Edinburgh. Samples were collected from patients aged 18 to 80, due to undergo abdominal surgery within NHS Lothian, Edinburgh. Samples were obtained under the Lothian NRS Human Annotated Bioresource (research ethics committee number 15/ES/0094). Patients were divided into three groups based on BMI: lean (BMI: <25), overweight (BMI: 25.0 - 30.0) and obese (BMI: >30).

2.3 Immunohistochemistry

2.3.1 Human and mouse sample preparation

Samples were fixed in 4% Paraformaldehyde (diluted in PBS) and stored at 4°C overnight. The following day, samples were washed in PBS (3 x 30 min) and then transferred to 70% EtOH. Tissues were embedded in paraffin using a HistoStar™ Embedding Workstation (A81000001, Thermo Fisher).

Paraffin blocks were cut into 5 µm sections using a Leica RM2125 RTS Rotary Manual Microtome. The sections were placed on Thermo Scientific™ SuperFrost Plus™ Adhesion slides (#10149870) slides and dried overnight at 50°C.

2.3.2 Solutions for paraffin immunofluorescence

Tris-EGTA buffer, pH9

For 1 litre ofsolution, 1.211 g Tris base (Tris(hydroxymethyl)aminomethane (TRIS, Trometamol) ≥99%, 443866G, VWR Chemicals) and 0.19 g EGTA (Ethylene glycol-bis(2-aminoethylether)-N,N,N′,N′-tetraacetic acid, E3889, Sigma-Aldrich) were added to 1 L distilled water.

50nM NH_4Cl in PBS

For 1 litre solution, 2.6745g NH_4CL (Ammonium chloride, A9434, Sigma-Aldrich) was dissolved in 1L PBS.

Wash 1 (1X PBS with 1% BSA, 0.2% Gelatin, and 0.05% Saponin)

For 1 litre solution, 2 g gelatin (Gelatin from porcine skin, G1890, Sigma-Aldrich) were added to 200 mL 1X PBS and microwaved until dissolved. This was then added to

10g BSA powder (A3294-50G, Sigma-Aldrich) and 0.5 g Saponin (Saponin from Quillaja Bark Purified, S4521, Sigma-Aldrich), and the volume was made up to 1 L by adding 1X PBS. The solution was prepared fresh for each experiment.

Wash 2 (1X PBS with 0.1% BSA, 0.2% Gelatin, and 0.05% Saponin)

For 1 litre solution, 2g gelatin (Gelatin from porcine skin, G1890, Sigma-Aldrich) were added to 200 mL 1X PBS and microwaved until dissolved. This was then added to 1 g BSA powder (A3294-50G, Sigma-Aldrich) and 0.5 g Saponin (Saponin from Quillaja Bark Purified, S4521, Sigma-Aldrich) and the final volume was made up to 1L by adding 1X PBS. Fresh solution was prepared for each experiment.

Antibody solution (1X PBS with 0.1% BSA and 0.3% Triton X-100)

For 50 mL of antibody solution, 0.05 g BSA were dissolved into 50 mL 1X PBS. 150 µL Triton X-100 were added to the resulting solution.

2.3.3 Immunofluorescence

Sections were dewaxed in xylene (2 x 20 min), washed in 100% EtOH (2 x 10 min), rehydrated in 96%, 85%, and 70% EtOH (1 x 10 min each) and then briefly rinsed in water 3 times. For antigen retrieval, the samples were then immersed in 1.5 L Tris-EGTA buffer, in an InstantPot IP-LUX50 pressure cooker. Antigen retrieval was carried out for 5 minutes, after which samples were left to cool down on a shaker. Slides were then placed in 50nM NH_4Cl solution for 30 minutes and then blocked in Wash 1 (3 x 10 minutes).

Primary antibodies (Table 2.4) were diluted in antibody solution. The sections were encircled on the slide using a PAP Pen (ab2601, Abcam) and were incubated in the primary antibody overnight at 4°C. The next day, slides were washed in Wash 2 (3 x 10 minutes) and incubated with the secondary antibody (Table 2.5, diluted in antibody solution) for 30 min in the dark, at room temperature. The slides were washed again in Wash (3 x 10 minutes), incubated with DAPI diluted in antibody solution (1:5000) for 15 minutes in the dark, at room temperature, and then mounted in VECTASHIELD® Mounting Medium with DAPI (H-1200, Vector Laboratories).

2.3.4 Imaging

Immunofluorescence stained sections were imaged using a Zeiss Axioplan2 epifluorescence microscope and images were acquired and processed using Micro-Manager (μManager, Edelstein et al., 2014).

Primary antibody/stain	Manufacturer	Dilution	Species used on
GFP (goat anti-mouse)	Abcam (ab6673)	1:1000	mouse
WT1 (rabbit anti-mouse)	Abcam (ab89901)	1:1000	mouse, human
CD31 (rabbit anti-mouse)	Abcam (ab28364)	1:50	mouse
CD31 (mouse anti-human)	Dako (M0823)	1:100	human
Perilipin (rabbit anti-mouse)	Sigma (P1998)	1:10,000	mouse
αSMA (mouse anti-mouse)	Sigma (A2547)	1:400	mouse, human
Isolectin-B4	Vector Labs	1:400	mouse
PDGFRb (rabbit anti-mouse)	Abcam (ab32570)	1:100	mouse

Table 2.4. Primary antibodies used for immunofluorescence.

Secondary antibody	Dilution
AlexaFluor 488 donkey anti-rabbit IgG (#A-21206)	1:500
AlexaFluor 488 donkey anti-goat IgG (#A-11055)	1:500
AlexaFluor 594 donkey anti-rabbit IgG (#A-21207)	1:500
AlexaFluor 594 donkey anti-goat IgG (#A-11058)	1:500
AlexaFluor 488 goat anti-mouse IgG (#A-11029)	1:500

Table 2.5 Secondary antibodies used for immunofluorescence.

2.4 Isolation and culture of primary adipose SVF cells, primary adipose pericytes and cell lines

VWAT depots were dissected out of mice using sterile scissors and forceps and were placed in 1X PBS. Fat pads were cut into 1 mm^3 fragments using disposable scalpels and then placed in 5 mL or 10 mL collagenase solution, depending on the size of the fat pad. For the collagenase solution, 0.5 mg/mL Collagenase B (11088815001, Roche) and 4 mg/mL BSA powder (A3294-50G, Sigma-Aldrich) were added to 1X sterile PBS. The solution was then sterile filtered and supplemented with 2% Penicillin/Streptomycin (15070063, Life Technologies).

Samples were incubated at 37% in a shaker for 1 hour and then shaken vigorously and filtered through cell strainers (22363548, Fisher Scientific) into 50 mL falcon tubes. DMEM (10% FCS, 2% Penicillin-Streptomycin and 1% sodium pyruvate) was added to the samples (in volumes equal to the initial volume of the collagenase solution) in order to inactivate the collagenase; the cells were then centrifuged at 300g for 5 minutes. The top lipid layer and supernatant were aspirated and the SVF pellets were re-suspended in growth medium and plated into 6 well plates.

2.4.2 Reagents for tissue culture

All cells were incubated under normoxic conditions (20% O_2, 5% CO_2) in standard tissue culture incubators. bEND3 (ATCC® CRL-2299™) and MCEC cells were obtained from were obtained from Prof. Andrew Baker at the University of Edinburgh.

SVF culture medium

SVF cells were maintained in 1X DMEM (11966025, Life Technologies) supplemented with 10% FCS, 2% Penicillin-Streptomycin (15070063, Life Technologies), and 1% sodium pyruvate (11360070, Life Technologies).

Pericyte culture medium

Freshly isolated pericytes were grown in EGM-2 Endothelial Cell Growth Medium-2 BulletKit (CC-3162, Lonza) until confluent.

bEND3 and MCEC cell culture medium

bEND3 and MCEC cells were cultured in 1X DMEM (11966025, Life Technologies) supplemented with 10% FCS, 2% Penicillin-Streptomycin (15070063, Life Technologies), and 1% sodium pyruvate (11360070, Life Technologies).

2.4.2 Immunofluorescence staining of adherent cells

Cells were isolated following the previously described protocol and seeded in 12 well plates (CLS3512-100EA, Corning). Cells were cultured until confluent (7 days) or treated following the RNAi protocol described later, in section 2.7.2. When ready for staining, all cells were fixed using 400 µL of 4% paraformaldehyde for 10 minutes at 37°C, after which they were washed 3 times with 500 µL 1X PBS. Cells were permeabilised by adding 400 µL 0.1% Triton-X (in 1X PBS) to each well and incubating at room temperature for 15 minutes, followed by 3 washes in 1X PBS. Cells were then blocked by adding 500 µL 2% BSA (in 1X PBS) per well and incubating at

room temperature for 30 minutes. After blocking, primary antibodies were diluted in 500 µL 0.1% BSA and cells were incubated with the antibody dilution for 3 hours at room temperature or overnight at 4°C. After incubation with the primary antibody (antibodies outlined in Table 2.1, used at 1:50 dilution), cells were washed 3 times in 1X PBS and incubated with fluorescent dye-labelled secondary antibodies (Table 2.2) diluted in 0.1% BSA (for 45 minutes at room temperature). Finally, cells were washed again with 1X PBS and incubated for 10 minutes with DAPI in 0.1% BSA.

2.5 Flow cytometry and FACS sorting

Flow cytometry and FACS sorting were carried out by Mari Pattison in the QMRI flow cytometry and cell sorting facility. Flow cytometry was performed using a BD LSRFortessa cell analyser, while FACS sorting was carried out using a BD FACS Aria II cell sorter.

Flow cytometry was performed on freshly isolated SVF cells. After digestion in Collagenase B solution (see Section 2.5.2), SVF cells were resuspended in FACS buffer (PBS supplemented with 5% FCS and penicillin/streptomycin) and further stained with antibodies against surface antigens (Table 2.6), using the protocol described by Cleal & Chau (2016). After each staining step, cells were washed with 3mL FACS buffer and centrifuged for 5 minutes at 300g.

Primary antibody/stain	**Manufacturer**	**Dilution**	**Species used on**
Biotin Mouse Lineage Panel	BD Biosciences (559971)	1:50	mouse
CD31-PeCy7	eBioscience (25-0311-82)	1:500	mouse
cKit-APC-eF780	eBioscience (47-1172-82)	1:100	mouse
PDGFRβ-APC	eBioscience (17-1402-82)	1:100	mouse

Table 2.6 Antibodies used for flow cytometry.

Flow cytometry analysis was carried out with FlowJo™ Software (v10).

2.6 Gene expression analysis

2.6.1 RNA extraction

RNA from freshly dissociated cells, cultured cells and unfixed tissues was extracted using TRIzol® Reagent, following the manufacturer's protocol. Unfixed tissues were homogenized prior to RNA isolation, using an IKA® ULTRA-TURRAX® tissue disperser (Z722359, Sigma).

2.6.2 cDNA synthesis

cDNA synthesis was performed in a 40 µL reaction, using 1 µL 25 mM dNTP mix (10297018, Invitrogen), 1.3 µL Random Hexamers (79236, Qiagen), 8 µL 5x. First Strand Buffer, 0.4 µL 0.1 M DTT, 1 µL SuperScript III Reverse Transcriptase (18080-044, Invitrogen) and1 µL RNaseOUT RNase Inhibitor (10777019, Invitrogen), resulting in a total volume of 12.7 µL. The remaining volume was made up of 1 µg RNA and RNase-free H_2O. The reaction was incubated at 52° for 2.5 hours.

2.6.3 Quantitative real-time polymerase chain reaction (qRT-PCR)

Gene expression was assayed by quantitative real-time polymerase chain reaction (qPCR), using the Roche Universal Probe Library (UPL). 2 µL undiluted cDNA was added to the reaction mix, along with 0.1 µL of each forward and reverse primers (out of a 20µM dilution) (Table 2.7), 0.1 µL of the relevant UPL probe (Table 2.6, 04683633001, Roche), 2.7 µL nuclease-free H_2O, and 5 µL LightCycler® 480 Probes Master (04707494001, Roche).

Gene	**Species**	**Primer sequences (5' – 3')**	**Probe**
Wt1	Mouse	F: ggacgccctacagcagtg R: catctgattccaggtcatgc	#33
WT1	Human	F: agctgtcccacttacagatgc R: ccttgaagtcacactggtatgg	#4
18S	Mouse, human	F: cgattggatggtttagtgagg R: agttcgaccgtcttctcagc	#81
CXCL5	Mouse	F: tgtagagccccaatctccac R: gagctggaggctcattgtg	#25
DCN	Mouse	F: agtgttaattacatcgcagctttg R: agagttgccttcatgattatctca	#92
PTN	Mouse	F: ggacctctgcaagccaaa R: cacagctgccaagatgaaaa	#72
RGS5	Mouse	F: ttcctgcctgaggagtgc R: gtgttcgcaggaatctgactt	#18
IRF7	Mouse	F: cttcagcactttcttccgaga R: tgtagtgtggtgacccttgc	#25
αSMA	Mouse	F: ccagcaccatgaagatcaag R: tggaaggtagacagcgaagc	#58
Vimentin	Mouse	F: ccaacctttttcttccctgaa R: tgagtgggtgtcaaccagag	#109

Table 2.7 DNA primer sequences and UPL probes used for qPCR.

2.7 Gene knockdown

2.7.1 Cre-mediated *Wt1* knockdown in primary adipose SVF cells

Each cell suspension resulting from the collagenase digestion was divided in two, with half of the cells cultured in medium containing 4-hydroxytamoxifen (1 μM) and half serving as a vehicle control (medium containing 1μL/mL 100% EtOH). The cells were harvested when confluent (after approximately 7 days).

2.7.2 siRNA-mediated *Wt1* knockdown in primary adipose SVF cells and primary adipose pericytes

For siRNA-mediated knockdown of *Wt1* in primary adipose SVF, we adapted a previously described protocol (Lee et al., 2014a). SVF cells from C57Bl/6 mice were expanded in culture and, once confluent, plated into 12-well plates at a density of 50,000 cells/well.

24 hours post-plating, cells were transfected with an siRNA against *Wt1* (SI01473108, Qiagen) or with negative control siRNA, both used at a final concentration of 40 nM and diluted in 6 μL HiPerFect Transfection Reagent per well (301704, Qiagen). 24 hours post-transfection, cells were refed with DMEM (10% FCS, 2% penicillin-streptomycin) and left for an additional 24 hours, resulting in a 48-hour knockdown.

2.8 *In vitro* angiogenesis assays

2.8.1 Matrigel-based tube formation assays

Matrigel-based tube formation assays were performed using a modified version of a published protocol (Arnaoutova and Kleinman, 2010). 15,000 cells per well of a 96-well plate were plated on growth factor reduced, phenol red-free Matrigel® (15585729, Corning). Brightfield images were acquired 3, 6, and 24 hours after plating, using an inverted Nikon Eclipse TS100 microscope at 4x magnification. For each experiment, cells were counted using a TC20™ Automated Cell Counter (Bio-Rad).

2.8.2 Network formation image analysis

For network formation quantification, images were analysed using the Angiogenesis Analyzer plugin for ImageJ (Carpentier and Cascone, 2012). Figure 2.4 illustrates the measurements taken by the plugin on a brightfield image of adipose SVF networks.

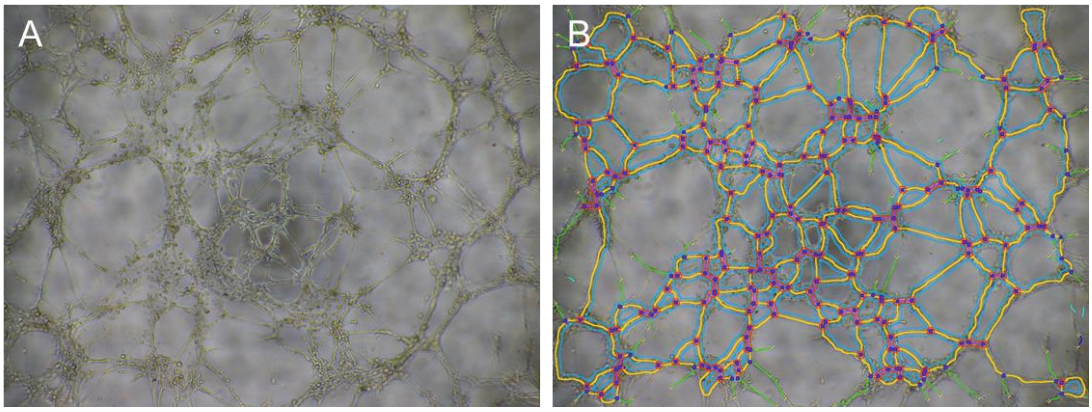

Figure 2.4. A-B: Example of analysis carried out using the Angiogenesis Analyzer plugin for ImageJ. *Green: branches; cyan: twigs; magenta: segments; orange: master segments; blue sky: meshes; red surrounded by blue: nodes surrounded by junctions symbol; junctions surrounded by red: master junctions; blue: isolated elements; cyan: small isolated elements; red surrounded by yellow: extremities. Brightfield images taken at 4X magnification.*

2.9 RNA-sequencing

2.9.1 RNA extraction

For this experiment, epididymal adipose SVF cells were isolated from adult *Wt1*$^{GFP/+}$ mice (n=3). RNA used for sequencing was extracted from FACS-sorted Lin-cKit-CD31-PDGFRb+GFP+ (n=3) and Lin-cKit-CD31-PDGFRb+GFP- cells (n=3) using the RNeasy® Plus Micro Kit (74034, Qiagen). RNA was extracted according to the manufacturer's protocol; the final mass and Q20 quality score of each RNA sample is outlined in Table 2.8. Sequencing and sample quality control were carried out by BGI Genomics (BGI Park, No.21 Hongan 3rd Street, Yantian District, Shenzhen, 518083, China)

Sample	Total mass (µg)	Q20 (%)	GC (%)
GFP- #1	0.0279	99.00%	50.79%
GFP- #2	0.0794	98.96%	51.21%
GFP- #3	0.0211	98.97%	50.77%
GFP+ #1	0.1229	99.06%	50.86%
GFP+ #2	0.4767	99.01%	50.70%
GFP+ #3	0.2406	99.11%	50.79%

Table 2.8. Total mass, Q20 quality score and GC content of all samples used for RNA-sequencing

Analysis was carried out by Matthew Sinton in the Centre for Cardiovascular Science, University of Edinburgh.

2.9.2 RNA-sequencing quality control

Fastq files were first trimmed using Trimmomatic (http://www.usadellab.org/cms/?page=trimmomatic), before performing quality control using FastQC (bioinformatics.babraham.ac.uk/projects/fastqc/).

2.9.3 RNA-sequencing read alignment

RNA-sequencing reads for each sample were mapped using STAR version 2.7.1a (https://academic.oup.com/bioinformatics/article/29/1/15/272537) against the mouse genome build mm10, downloaded via the Ensembl FTP site. Alignment was performed with the following options: --readFilesCommand zcat, --runThreadN 1, --runMode alignReads, quantMode --GeneCounts. The Mus_musculus.GRCm38.98.gtf file contained the coding transcripts in a GTF format.

2.9.4 Differential expression analysis

Gene expression levels were calculated by first running featureCounts (http://subread.sourceforge.net/) on the alignments, to count reads and map to genomic features. Differential expression analysis was then performed using DESeq2 (https://bioconductor.org/packages/release/bioc/html/DESeq2.html), to estimate variance-mean dependence in the generated count data.

2.10 Statistical analysis

Data was expressed as the mean value of the biological replicates (± the standard error of mean). P values were calculated using a two-tailed t-test, with p values smaller than 0.05 defined as statistically significant.

Chapter 3

In vivo expression of WT1 in the vasculature of murine and human VWAT

3.1 Introduction

WT1 is expressed in few tissues and cell types in the adult mouse and human. Previous research has revealed that WT1 is expressed in all VWAT depots in adult mice – epididymal, mesenteric, retroperitoneal, perirenal, omental, and pericardial (Chau et al., 2014). Moreover, a large percentage of WT1+ cells in all depots express adipose progenitor markers (Lin-GFP+CD29+ CD34+ Sca1+CD24-/+), whereas mature adipocytes are not positive for WT1. Similarly, only a subset of VWAT adipose progenitors express WT1, although it is yet unclear what differences there are between WT1+ and WT1- progenitors (Chau and Hastie, 2015b).

In all VWAT depots, most of the Lin-WT1+ cells are positive for adipose progenitor markers, but the identity of the remaining WT1+ cells is presently unknown. As described before, WT1 has been detected in different vascular cell types in adult mouse and human, although mostly in the context of cancer and revascularization post-ischaemia. Endothelial cells (ECs) in tumours express WT1, whereas no WT1 can be detected in healthy adjacent tissue (Wagner et al., 2008a). Moreover, knocking out *Wt1 in vivo* in endothelial cells (Tie2+ and VE-cadherin+) leads to significant tumour regression and a reduction in angiogenesis (Wagner et al., 2014). Moreover, WT1 is expressed in the epicardium of the developing heart but is almost absent from the adult heart, with the exception of local ischaemic events which can trigger *Wt1* expression in vascular ECs and smooth muscle cells (VSMCs) around the infarcted area (Wagner et al., 2002). Interestingly, WT1 is also expressed in ECs in the developing heart at E12.5 (Duim et al., 2015).

However, it is presently not known whether and when WT1 is expressed in microvascular cells in VWAT. The first aim of this chapter is therefore to establish whether WT1 is expressed in murine ECs, VSMCs, and pericytes in various VWAT depots and what the pattern of expression is between different vascular cell types and different depots.

WT1 is also expressed in visceral adipose progenitors and following the fate of these cells can provide insight into the mechanics of adipose expansion. This can be achieved using genetic lineage tracing. Lineage tracing studies have shown that WT1-expressing cells give rise to vascular cells in several tissues. For instance, WT1+ cells in the serosal mesothelium differentiate into VSMCs which then incorporate into the blood vessels in the gut (Wilm, 2005). Epicardial cells expressing WT1 also differentiate into the VSMCs, fibroblasts and myocardial cells necessary for the

development of the heart, mainly through the EMT process (von Gise et al., 2011). Moreover, our group has shown that WT1+ cells give rise to adipocytes in all VWAT depots, although other cell types may also be derived from these progenitors (Chau et al., 2014).

With this in mind, the second aim of this chapter is to map the fate of murine WT1+ cells after birth and investigate potential vascular cell populations derived from these. Genetic lineage tracing has been described in the literature, with inducible Cre-loxP recombination models having the advantage of allowing for temporal control of reporter gene expression. Our model - *Wt1*^{CreERT2}*;mTmG* - has been shown to faithfully trace the fate of WT1+ cells, and has recently been used to trace WT1+ cells in VWAT by Chau et al. (2014). Moreover, we can also use this model to explore differences between lean and obese mice and investigate whether the contribution of WT1+ cells to the VWAT cell populations changes during adipose remodelling.

Finally, *WT1* mRNA has previously been detected in human omental fat, but the location of WT1-positive cells in this tissue is not known. The third aim of this chapter is therefore to investigate the location of WT1+ cells in patient-derived samples obtained from abdominal surgeries and explore differences between lean and obese patients. As detailed before, obesity dramatically changes the microenvironment of adipose tissue and VWAT in particular switches to a hypoxic, pro-inflammatory phenotype marked by changes in adipocyte size, adipogenesis, and vascular remodelling. Moreover, *Wt1* itself is activated in response to hypoxia (Wagner et al., 2003), which suggests that the expression and function of WT1 in VWAT is different between a normoxic lean fat and hypoxic excess fat.

3.1.1 Hypothesis

Considering the role of WT1 and WT1-expressing cells in the vasculature of other adult tissues, the main hypothesis of this chapter is that WT1 is expressed in microvascular cells in VWAT and WT1+ adipose progenitors give rise to microvascular cells in VWAT.

3.1.2 Aims

This chapter therefore has the following aims:

1. Investigate the expression of WT1 in endothelial cells, vascular smooth muscle cells and pericytes in murine VWAT;

2. Trace the fate of WT1-positive progenitors over 6 months in order to establish their contribution to the murine VWAT microvasculature and investigate whether the contribution of WT1+ cells is different between lean and obese mice;
3. Investigate the expression of WT1 in the microvasculature of human VWAT and establish whether there are any differences in WT1 expression between lean, overweight, and obese patients.

3.2 Results

3.2.1 Expression of WT1 in the microvasculature of murine VWAT

WT1 is expressed in VWAT adipose progenitors, which are located in the mesothelium surrounding all VWAT depots, as well as within the rest of the tissue. However, little is known about WT1 expression in microvascular cells in adult murine VWAT. We aimed to look into the expression of WT1 in the visceral vasculature, using the transgenic *Wt1*$^{GFP/+}$ reporter mouse model (Hosen et al., 2007), where GFP is expressed under the *Wt1* promoter.

Paraffin-embedded visceral adipose sections from adult *Wt1*$^{GFP/+}$ mice fed a standard chow diet were co-stained with antibodies against GFP (reflecting endogenous *Wt1* expression) and the microvascular cell markers CD31, αSMA, and PDGFRβ. WT1 is highly expressed in the podocytes of the adult kidney, which means the kidney is an appropriate positive control for WT1 and GFP expression. Figure 3.1 shows a diagram of the *Wt1*$^{GFP/+}$ model (Figure 3.1, A), as well as a representative image of kidney co-stained with antibodies against WT1 and GFP (Figure 3.1, B), where WT1 and GFP are co-expressed in the podocytes and are absent from other cells. Due to the species reactivities of our panel of antibodies, we subsequently used an antibody against GFP to observe WT1 expression.

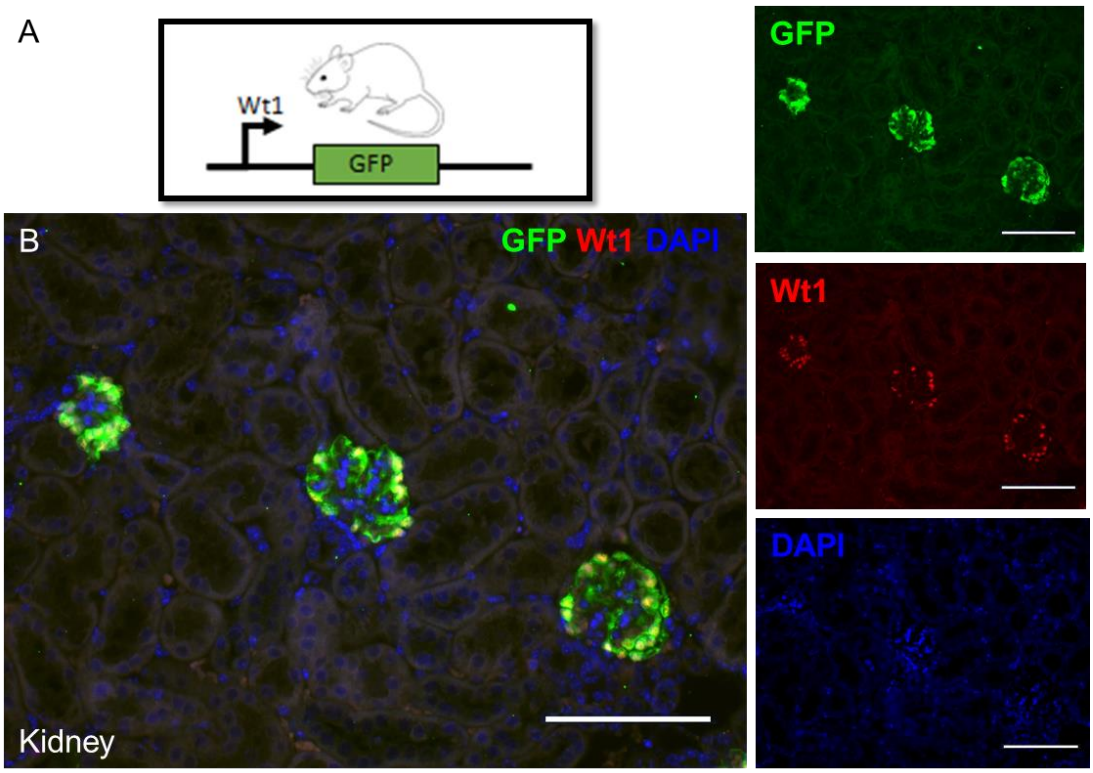

Figure 3.1. Wt1$^{GFP/+}$ reporter model. *A. Diagram of reporter mouse model; GFP is expressed under the Wt1 promoter. B. Paraffin-embedded kidney sections co-stained with antibodies against GFP (green), WT1 (red), and DAPI (blue). GFP and WT1 are co-expressed in the podocytes, which are known to express high levels of WT1 in adulthood. Scale bars: 100 µm*.

Sections from epididymal, omental, pericardial, mesenteric, and perirenal adipose tissue were co-stained with antibodies against GFP and CD31 (Figure 3.2). As expected, some of the GFP+ cells were present in the mesothelia. Moreover, GFP+ cells were detected in the proximity of CD31+ microvessels in all five depots, although we did not see co-expression of GFP and CD31 within the same cells. However, we observed that the prevalence of GFP+ cells throughout the tissue varied between depots. GFP appeared to be more extensively expressed in omental and pericardial VWAT (Figure 3.2, B-C, n=3). Similarly, epididymal, mesenteric and perirenal adipose tissue appeared to express GFP to a lesser extent (Figure 3.2, A, D-E, n=3).

We further co-stained paraffin sections from VWAT depots with antibodies against GFP and αSMA, which marks VSMCs and a subset of pericytes. Similarly, GFP was expressed in cells located next to αSMA+ vessels, and in some cases was co-expressed with αSMA within the same cells (Figure 3.3). Once again, GFP appeared to be expressed more highly and in more cells in omental and pericardial adipose

tissue (Figure 3.3, B-C, n=2 for omental, and n=3 for pericardial). GFP was also detected near αSMA+ vessels and/or in αSMA+ cells in epididymal (Figure 3.3, A, n=2), mesenteric (Figure 3.3, D, n=3), and perirenal (Figure 3.3, E, n=3) adipose tissue.

Lastly, we co-stained paraffin sections from VWAT for GFP and PDGFRβ, which marks pericytes (Figure 3.4). In all five depots, we observed cells positive for both GFP and PDGFRβ, as well as single-positive GFP+ or PDGFRβ+ cells, suggesting the presence of a sub-population of pericytes that express WT1. Figure 3.4 illustrates co-expression of GFP and PDGFRβ in epididymal (panel A, n=2), omental (B, n=2), pericardial (C, n=3), mesenteric (D, n=3), and perirenal (E, n=3). Moreover, some PDGFRβ+ cells were also observed in the mesothelial area (Figure 3.4).

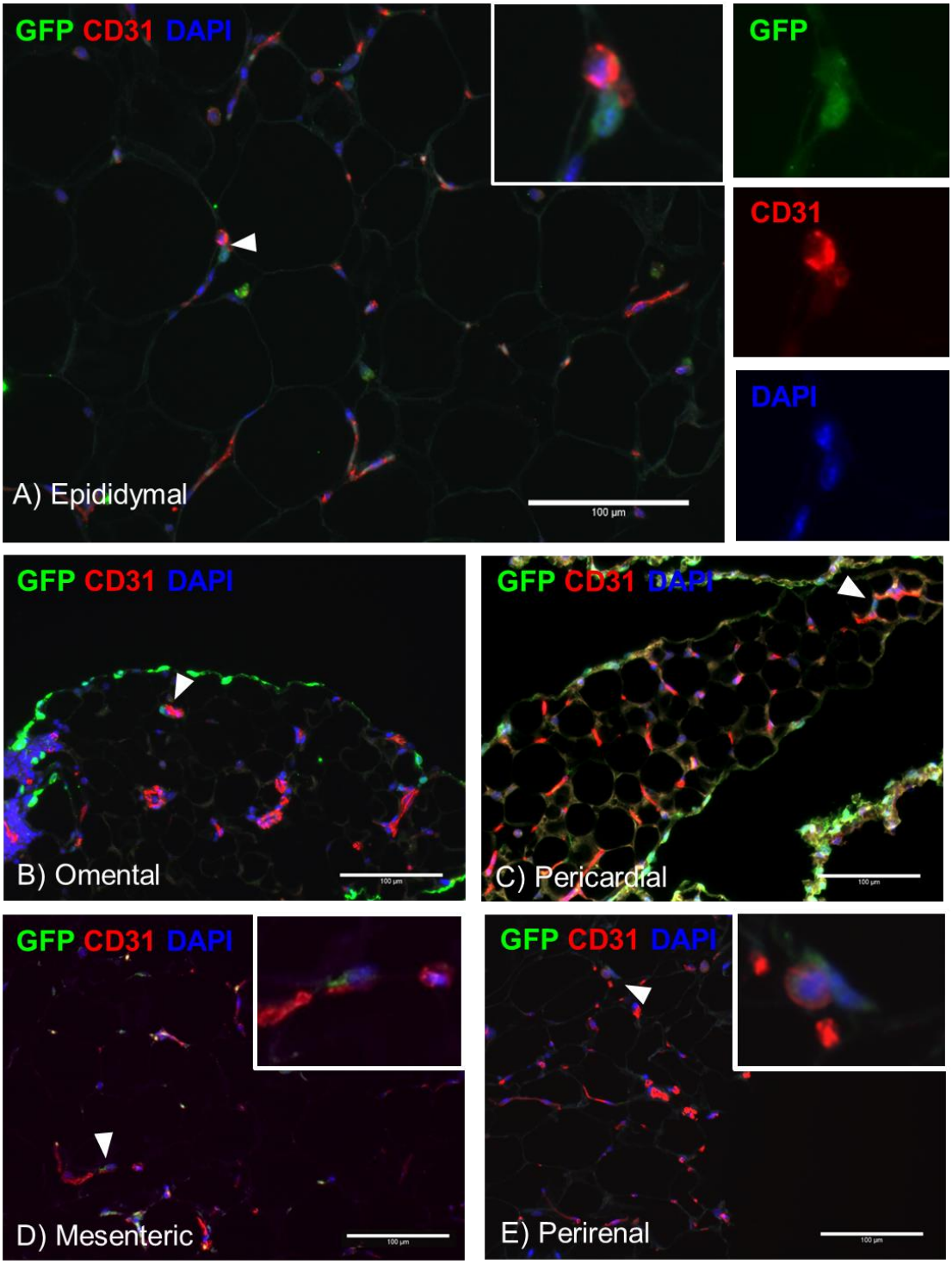

Figure 3.2. WT1-expressing cells are located in the perivascular space of CD31-positive microvessels in VWAT. *Panel A shows paraffin-embedded epididymal adipose tissue stained with GFP (green), CD31 (red) and DAPI (blue), with single-channel images shown to its right (n=3). The remaining panels show omental (B, n=3), pericardial (C, n=3), mesenteric (D, n=3) and perirenal (E, n=3) adipose tissue stained for GFP (green), CD31 (red) and DAPI (blue). White arrows indicate GFP expressed near CD31+ microvessels. Scale bars: 100 µm.*

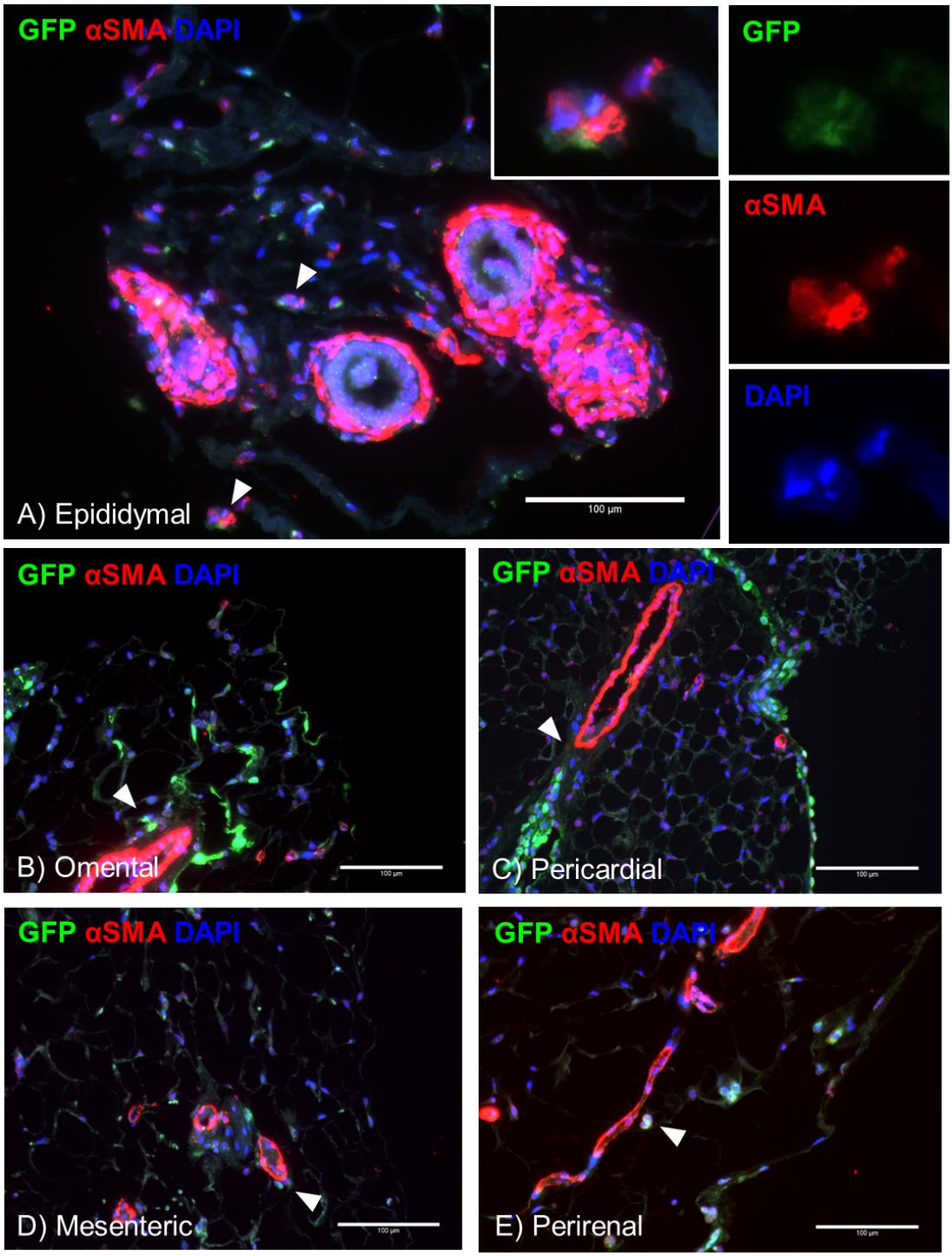

Figure 3.3. WT1-expressing cells are located in the perivascular space of αSMA-positive microvessels in VWAT. *Panel A shows paraffin-embedded epididymal adipose tissue stained with GFP (green), αSMA (red) and DAPI (blue), with single-channel images shown to its right (n=2). The remaining panels show omental (B, n=2), pericardial (C, n=3), mesenteric (D, n=3) and perirenal (E, n=3) adipose tissue stained for GFP (green), αSMA (red) and DAPI (blue). White arrows indicate GFP expressed near αSMA+ microvessels. Scale bars: 100 µm.*

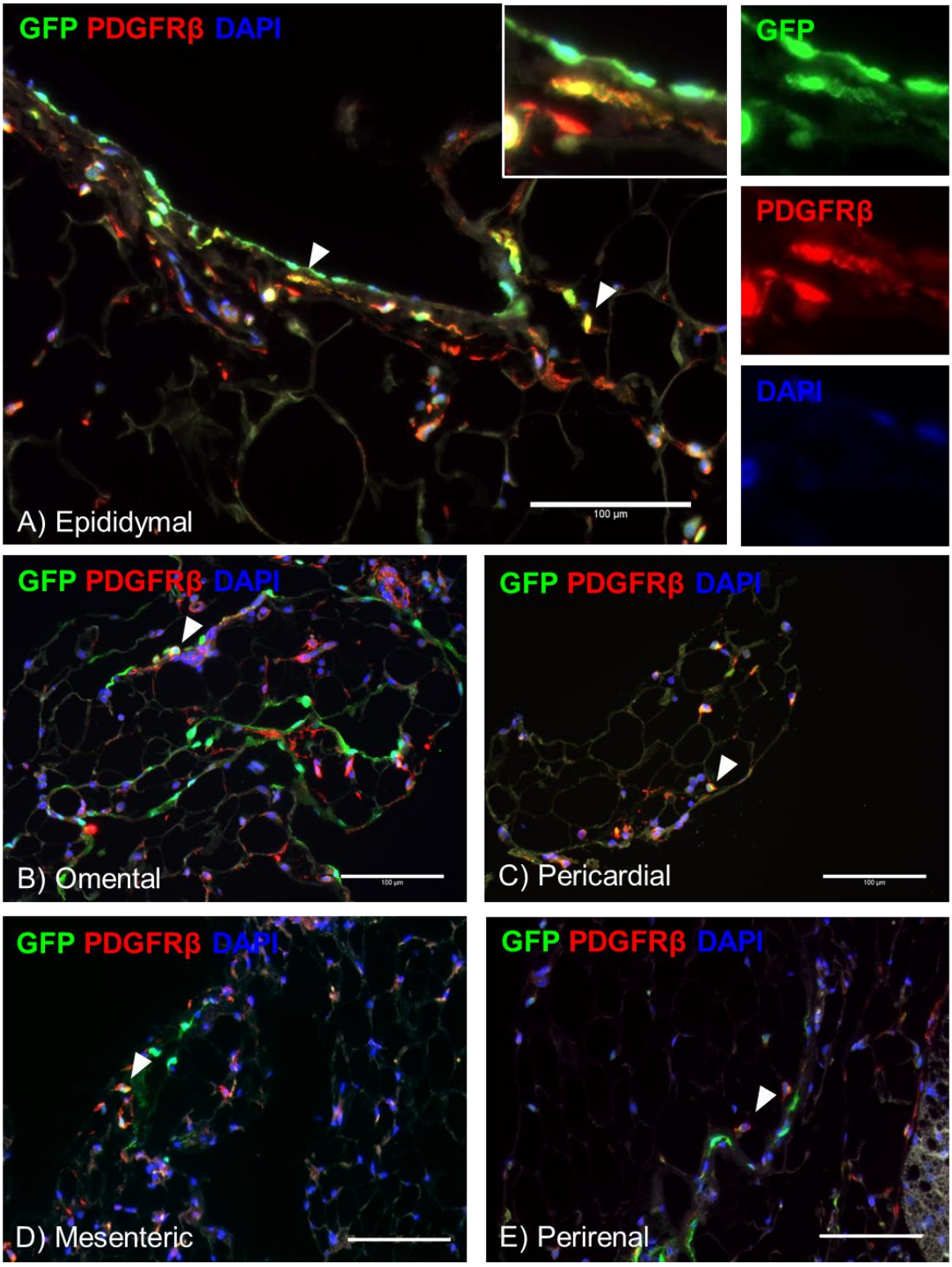

Figure 3.4. WT1 and PDGFRβ are co-expressed in VWAT. *Panel A shows paraffin-embedded epididymal adipose tissue stained with GFP (green), PDGFRβ (red) and DAPI (blue), with single-channel images shown to its right (n=2). The remaining panels show omental (B, n=2), pericardial (C, n=3), mesenteric (D, n=3) and perirenal (E, n=3) adipose tissue stained for GFP (green), PDGFRβ (red) and DAPI (blue). White arrows indicate GFP expressed near PDGFRβ+ microvessels. Scale bars: 100 µm.*

In order to quantify WT1 expression in VWAT vascular cells, we again used the transgenic *Wt1*$^{GFP/+}$ mouse model (Figure 3.5, A). The SVF was isolated from epididymal, omental, pericardial, mesenteric, and perirenal VWAT and cells were used for flow cytometry analysis. As the SVF is a heterogeneous mixture which includes immune cells, preadipocytes and vascular cells, surface markers can be used to isolate or analyse vascular sub-populations. Figure 3.5 illustrates the gating strategy. After gating based on size and granularity (FSC and SSC, Figure 3.5, B), cells were gated based on the expression of the hematopoietic lineage markers CD3e, CD45R, Ly-6G, Ly-6C, CD11b and TER-119 (lineage panel/Lin) and the hematopoietic stem cell marker cKit (CD117, Figure 3.5, C). Double negative cells (Lin-cKit-) were further gated based on the expression of the EC marker CD31 and the expression of the pericyte marker PDGFRβ (Figure 3.5, D). Endothelial cells were defined as Lin-cKit-PDGFRβ-CD31+ and pericytes were defined as Lin-cKit-CD31-PDGFRβ+. As we used freshly dissociated cells for these experiments, αSMA was not included in the marker panel for this experiment.

GFP expression in PDGFRβ+ pericytes was analysed in all five VWAT depots (Figure 3.6, A). While all depots have GFP+ pericytes, the percentage of Lin-cKit-CD31-PDGFRβ+WT1+ cells varies between depots. For instance, 40% of pericytes isolated from epididymal adipose tissue express GFP (Figure 3.6, A, n=4), while in omental and pericardial fat the majority of pericytes are WT1-positive (~75% and 80%, respectively, n=4). Approximately 50% of mesenteric VWAT-derived pericytes express WT1, whereas in perirenal adipose tissue only 30% of Lin-cKit-CD31-PDGFRβ+ cells are GFP+ (n=4). In Figure 3.6, panels B-F show GFP expression in Lin-cKit-CD31-PDGFRβ+ from epididymal (B), omental (C), pericardial (D), mesenteric (E), and perirenal (F) fat. Different depots not only show different percentages of Lin-cKit-CD31-PDGFRβ+GFP- and Lin-cKit-CD31-PDGFRβ+GFP+ cells, but also different levels of GFP signal intensity.

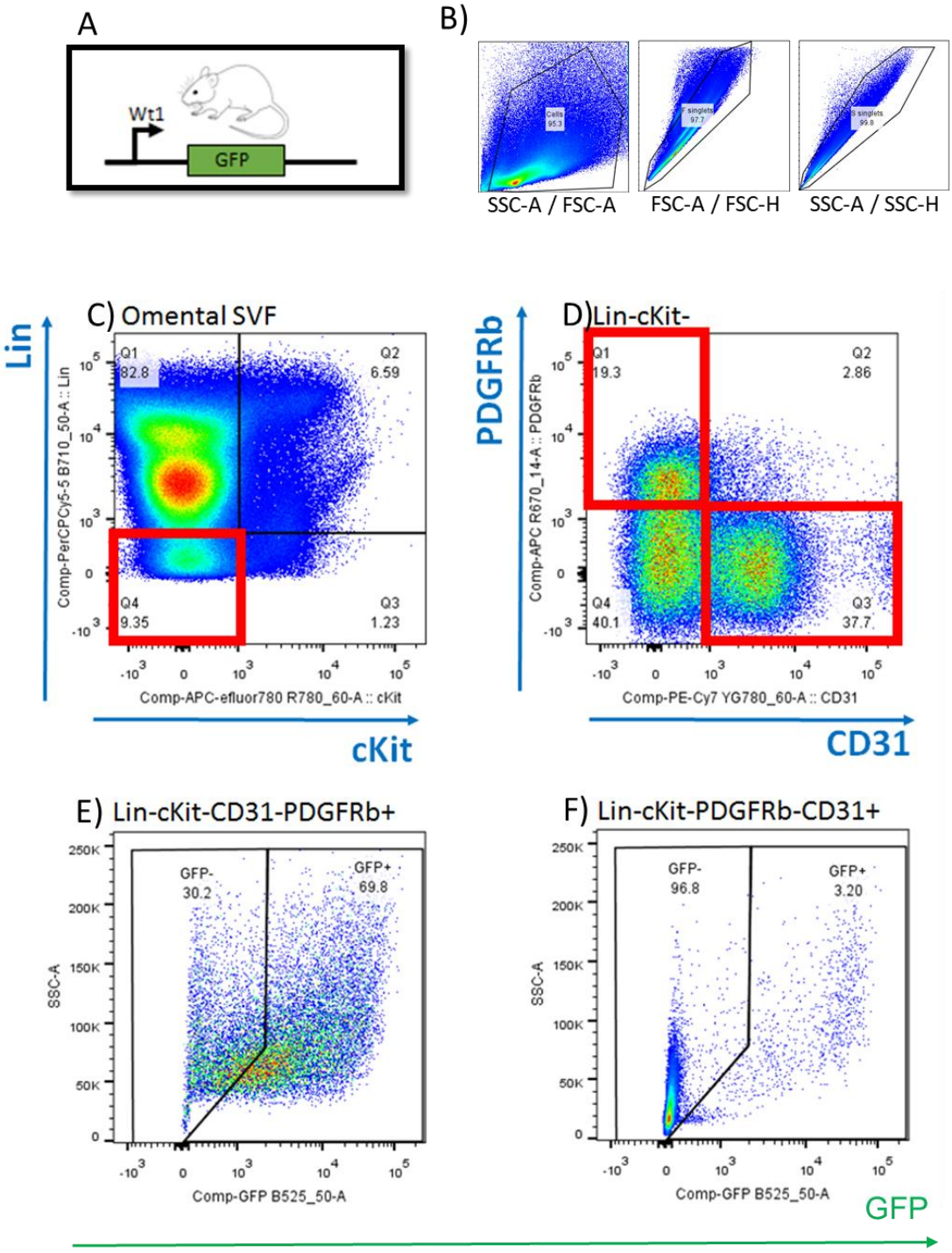

Figure 3.5. Flow cytometry gating strategy for isolating endothelial cells and pericytes from freshly dissociated visceral adipose SVF and analysing GFP expression in these two populations. *Freshly isolated SVF cells from Wt1$^{GFP/+}$ mice (A) were gated based on size and granularity (forward and side scatter, panel B). Next, cells were gated based on the expression of hematopoietic lineage markers (Lin) and the hematopoietic stem cell marker cKit (C). Double negative cells (Lin-cKit-) were further gated based on the expression of EC marker CD31 and pericyte marker PDGFRβ (D). Pericytes (Lin-cKit-CD31-PDGFRβ+, panel E) and ECs (Lin-cKit-PDGFRβ-CD31+, panel F) were finally analysed based on expression of GFP.*

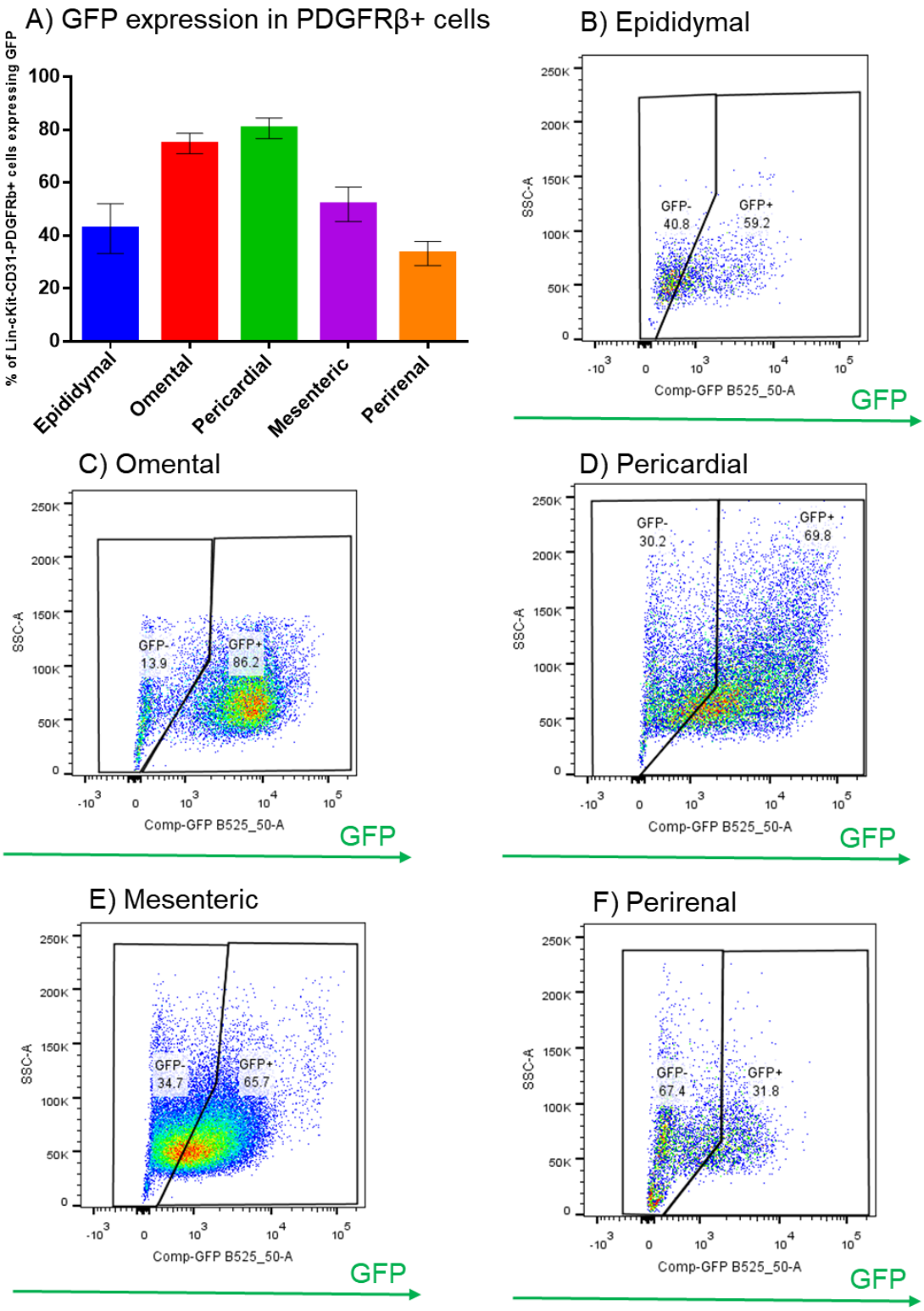

Figure 3.6. GFP is expressed in a subset of VWAT pericytes. *(A) Percentage of pericytes (Lin-cKit-CD31-PDGFRβ+) expressing GFP in five VWAT depots (n=4). Representative dot plots of GFP expression in pericytes from epididymal (B), omental (C), pericardial (D), mesenteric (E), and perirenal (F) adipose tissue. Omental and pericardial show the highest percentage of WT1+ pericytes (75-80%), while perirenal adipose tissue shows the lowest percentage of WT1+ pericytes (35%). Error bars represent the SEM.*

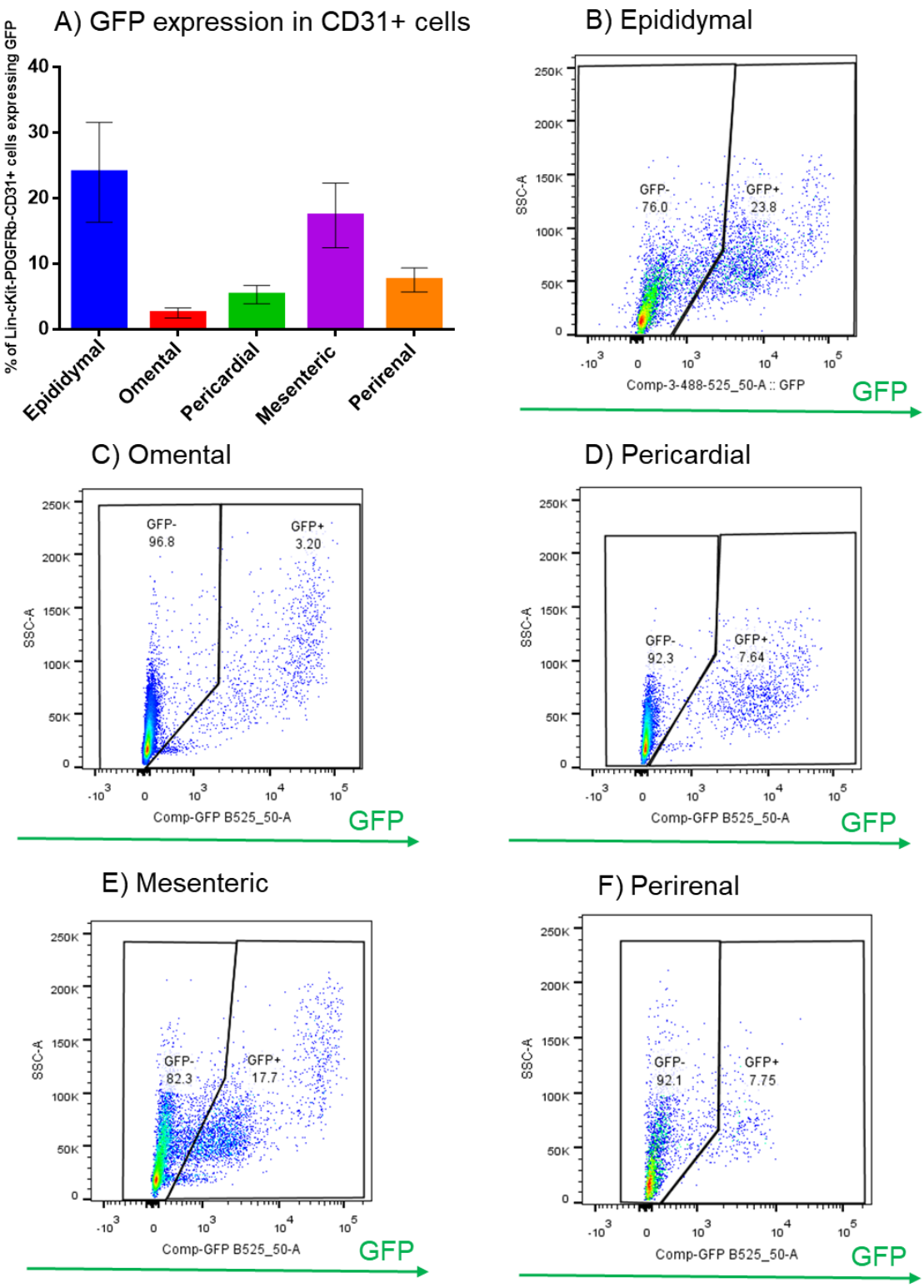

Figure 3.7. GFP is expressed in a subset of VWAT endothelial cells. *(A) Percentage of ECs (Lin-cKit-PDGFRβ-CD31+) expressing GFP in five VWAT depots (n=4). Representative dot plots of GFP expression in ECs from epididymal (B), omental (C), pericardial (D), mesenteric (E), and perirenal (F) adipose tissue. Omental and pericardial show the highgest percentage of WT1+ pericytes (3-5%). Error bars represent the SEM.*

Next, the percentage of endothelial cells expressing WT1 was analysed in the same five VWAT depots (Figure 3.7, n=4). Similarly, all depots present Lin-cKit-PDGFRβ-CD31+GFP+ cells (Figure 3.7, A). In omental and pericardial adipose tissue, less than 5% of endothelial cells are GFP+, whereas in epididymal adipose tissue close to 25% of ECs are GFP+ (n=4). In mesenteric and perirenal fat, ~15% and ~10% of Lin-cKit-PDGFRβ-CD31+ cells respectively were GFP+ (Figure 3.7, A, n=4). In figure 3.7, panels B-F show representative dot plots of GFP expression in Lin-cKit-PDGFRβ-CD31+ from epididymal (B), omental (C), pericardial (D), mesenteric (E), and perirenal (F) fat.

Overall, our findings indicate that WT1 is expressed not only in adipose progenitors, but also microvascular cells in VWAT. Moreover, different VWAT depots might contain different proportions of WT1+ ECs and pericytes.

3.2.2 WT1+ cells in murine VWAT may differentiate into vascular smooth muscle cells and pericytes after birth, but not into endothelial cells

WT1+ cells in the serosal mesothelium have been shown to differentiate into VSMCs making up the vasculature of the gut (Wilm et al., 2005a). We aimed to investigate whether WT1+ cells can give rise to microvascular cells in VWAT as well. For this purpose, we used a previously described lineage tracing model (Chau et al., 2014). *Wt1*^{CreERT2} knock-in mice were crossed with the reporter *mTmG* mouse line. In the absence of CreERT2-induced recombination, Tomato is expressed ubiquitously in the cell membrane, under the pCA reporter. Tamoxifen binds CreERT2, causing it to translocate to the nucleus, and the resulting recombination leads to the excision of Tomato and the membranous expression of GFP. Since the expression of Cre is directed by the *Wt1* promoter, membranous GFP can only be observed in the cells where *Wt1* is expressed at the time tamoxifen is administered. For the following experiment, we analysed tissues from 7.5 month old *Wt1*^{CreERT2}*;mTmG* mice that had received tamoxifen through the mother's milk (four doses of tamoxifen at the beginning of P0) and been fed a standard chow diet.

Figure 3.8 shows a schematic representation of the *Wt1*^{CreERT2}*;mTmG* model (panel A), as well as a representative image of VWAT co-stained with antibodies against GFP and WT1; these images illustrate that GFP+ cells are distinct from WT1+ cels (Figure 3,8, B). CreERT2-negative mice (*Wt1*$^{+/+}$*;mTmG*) were used as negative controls for lineage tracing and samples stained with secondary antibodies only were used as negative controls for immunofluorescence.

We stained epididymal, omental, pericardial, mesenteric, and perirenal adipose tissue with antibodies against GFP and CD31, which is expressed by endothelial cells making up both small capillaries (with a diameter < 10 µm) and larger arterioles and venules (10 – 100 µm) (Figure 3.9). While the staining suggests that some GFP+ cells surround mature microvessels with a diameter of over 10 µm, we did not observe lineage traced cells around small capillaries. Moreover, the location of GFP+ cells suggests these are VSMCs or pericytes (Figure 3.9). This can be observed in all 5 depots analysed (n≥4 in all depots).

To further investigate this, we co-stained VWAT sections from *Wt1*^{CreERT2}*;mTmG* with antibodies against GFP and αSMA. This revealed GFP+ cells located near αSMA+ microvessels in all VWAT depots analysed (epididymal, omental, pericardial, mesenteric, and perirenal, Figure 3.10). Moreover, we also observed cellular co-expression of GFP and αSMA, suggesting that at least part of the lineage traced cells are VSMCs.

Capillaries and microvessels are stabilized by pericytes, which can trigger the proliferation and migration of endothelial cells when angiogenesis is required. Although several markers of pericytes have been described, not all pericytes express all markers; for instance, RGS5 has been described as a marker of brain pericytes, but not in the lung or gut (Bondjers et al., 2003). However, PDGFRβ is recognized as a marker of all pericyte populations. VWAT sections from chow-fed *Wt1*^{CreERT2}*;mTmG* mice were also co-stained for GFP and PDGFRβ (Figure 3.11). All five depots show PDGFRβ+ cells positive for GFP, confirming that WT1+ cells may give rise not only to VSMCs, but also pericytes after birth. Interestingly, we also observed GFP+PDGFRβ+ cells in the mesothelial area.

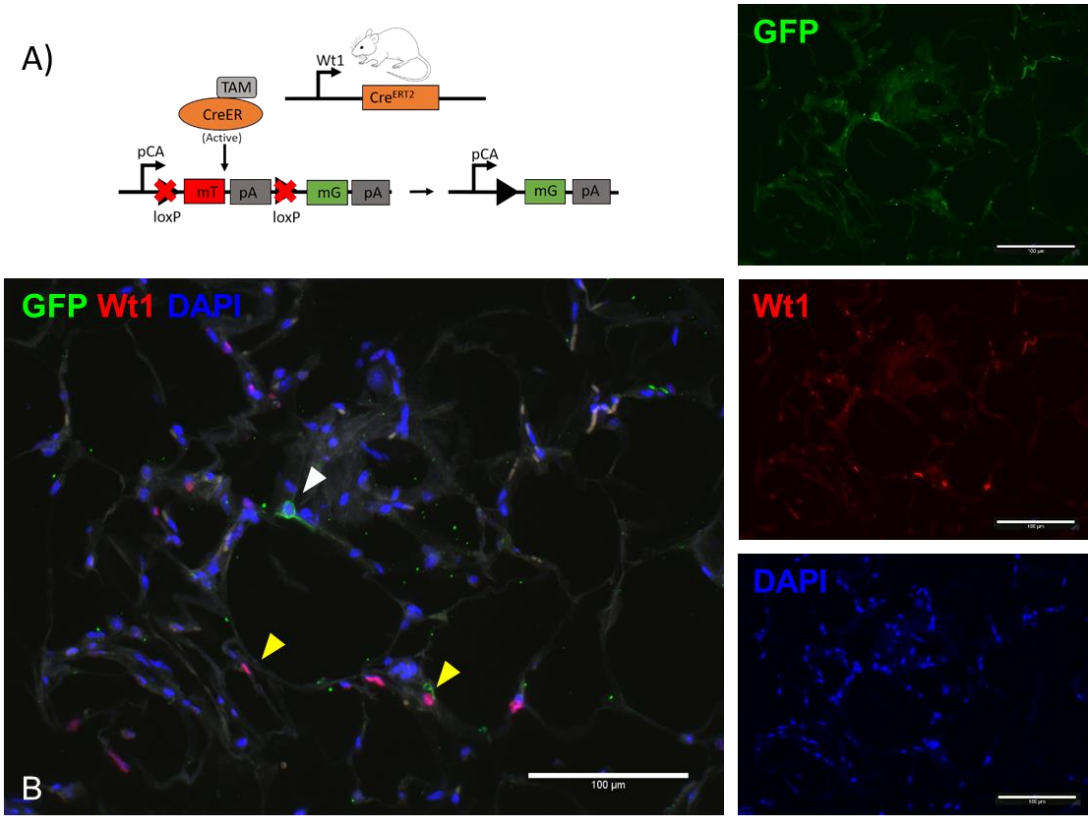

Figure 3.8. Wt1^{CreERT2};mTmG long-term lineage tracing. *A. Wt1^{CreERT2} knock-in mice were crossed with the reporter mTmG mouse line. In the absence of CreERT2-induced recombination, Tomato is expressed ubiquitously in the cell membrane, under the pCA reporter. Tamoxifen binds to CreERT2, causing it to translocate to the nucleus, and the resulting recombination leads to the excision of Tomato and the membranous expression of GFP. Since the expression of Cre is directed by the Wt1 promoter, membranous GFP can only be observed in the cells where Wt1 is active at the time tamoxifen is administered. For these experiments, we used 7.5 month old Wt1^{CreERT2};mTmG mice that had received tamoxifen through the mother's milk (four doses of tamoxifen at the beginning of P0) and been fed a standard chow diet. B. WT1 (red) and GFP (green) expression in murine epididymal VWAT, showing that lineage traced GFP+ cells (white arrow) are WT1-negative. WT1+ cells are indicated by yellow arrows. Scale bars: 100 µm.*

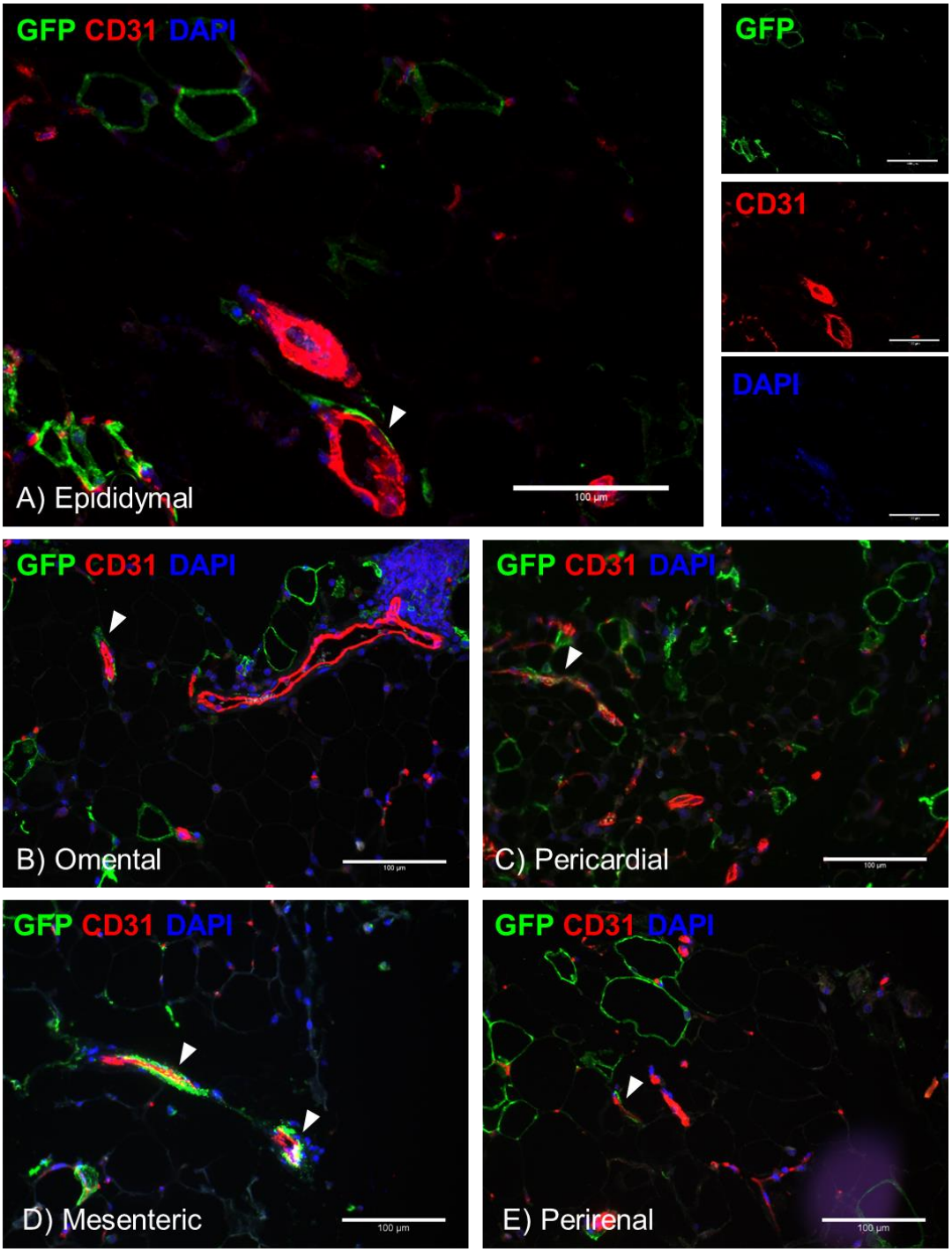

Figure 3.9. Wt1-lineage traced cells are found near CD31+ microvessels. *Panel A shows paraffin-embedded epididymal adipose tissue stained with GFP (green), CD31 (red) and DAPI (blue), with single-channel images shown to its right (n=4). The remaining panels show omental (B, n=5), pericardial (C, n=4), mesenteric (D, n=5) and perirenal (E, n=6) adipose tissue stained for GFP (green), CD31 (red) and DAPI (blue). White arrows indicate GFP expression near CD31+ microvessels. Scale bars: 100 µm.*

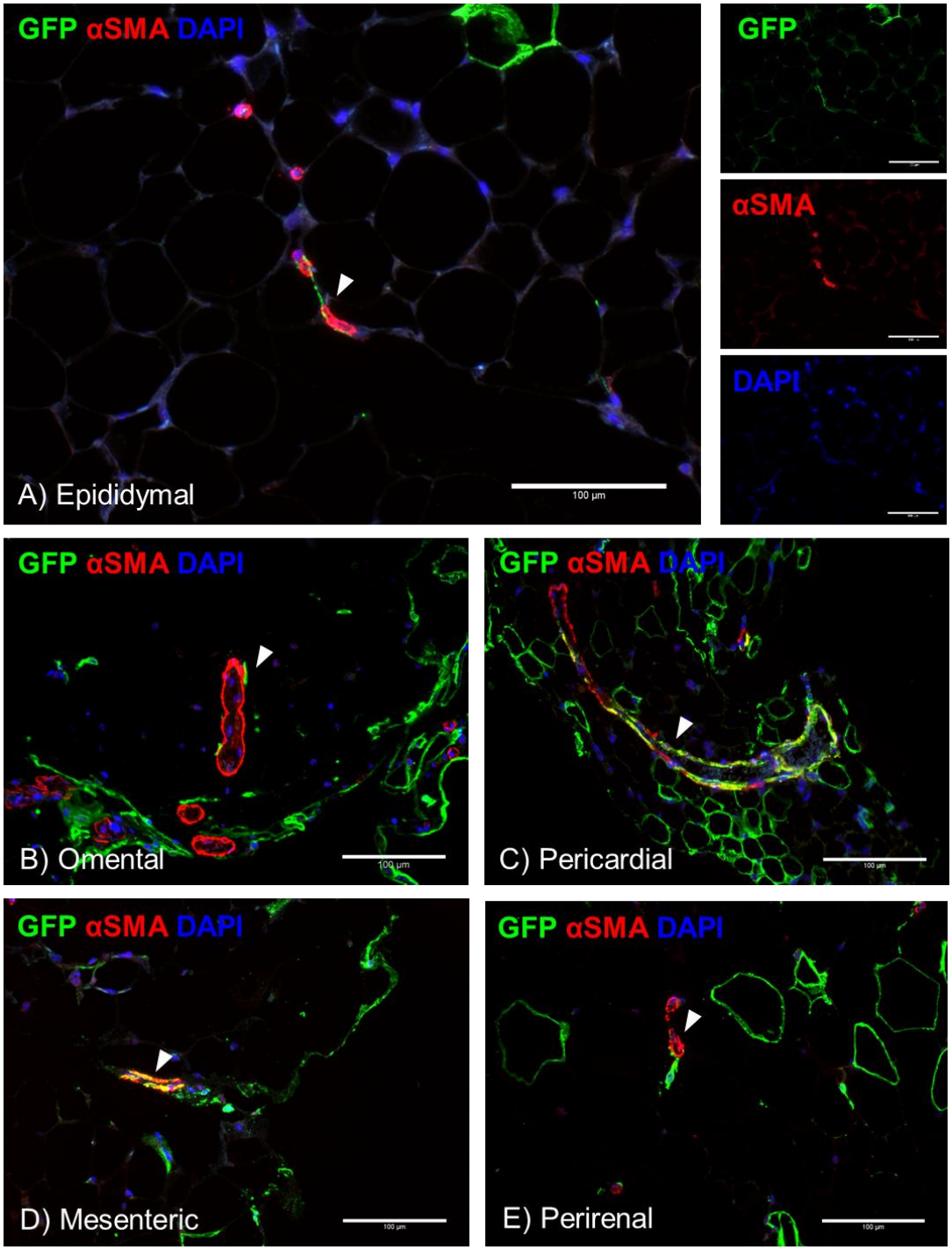

Figure 3.10. Wt1-lineage traced cells are found near αSMA+ microvessels. *Panel A shows paraffin-embedded epididymal adipose tissue stained with GFP (green), αSMA (red) and DAPI (blue), with single-channel images shown to its right (n=5). Panels B-E show omental (B, n=5), pericardial (C, n=4), mesenteric (D, n=5) and perirenal (E, n=6) adipose tissue were stained for GFP (green), αSMA (red) and DAPI (blue). White arrows indicate GFP expression near αSMA+ microvessels. Scale bars: 100 µm.*

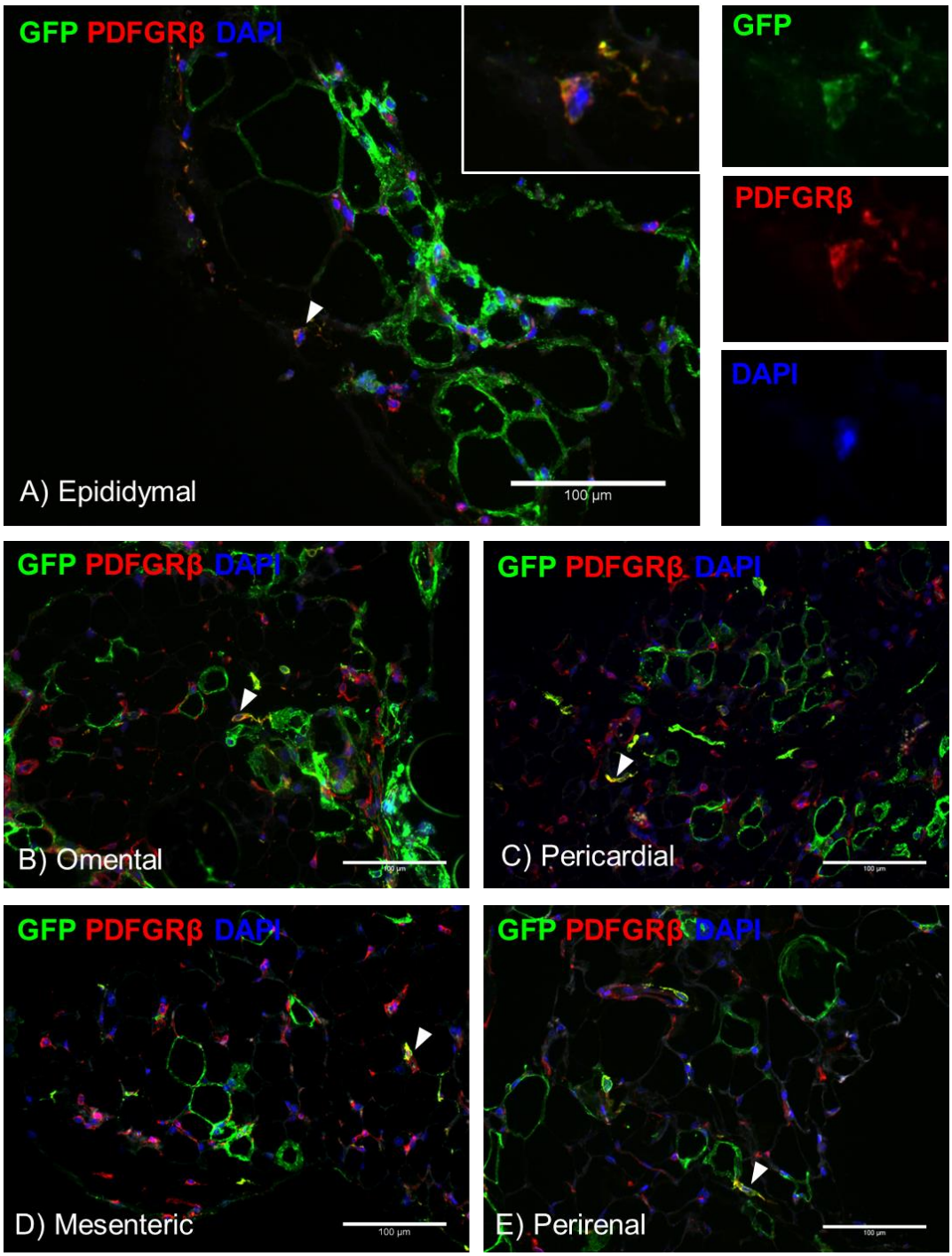

Figure 3.11 A subset of Wt1-lineage traced cells are PDGFRβ-positive. *Panel A shows paraffin-embedded epididymal adipose tissue stained with GFP (green), PDGFRβ (red) and DAPI (blue), with single-channel images shown to its right (n=2). Panels B-E show omental (B, n=4), pericardial (C, n=5), mesenteric (D, n=3) and perirenal (E, n=3) adipose tissue were stained for GFP (green), PDGFRβ (red) and DAPI (blue). White arrows indicate co-expression of PDGFRβ and GFP. Scale bars: 100 µm.*

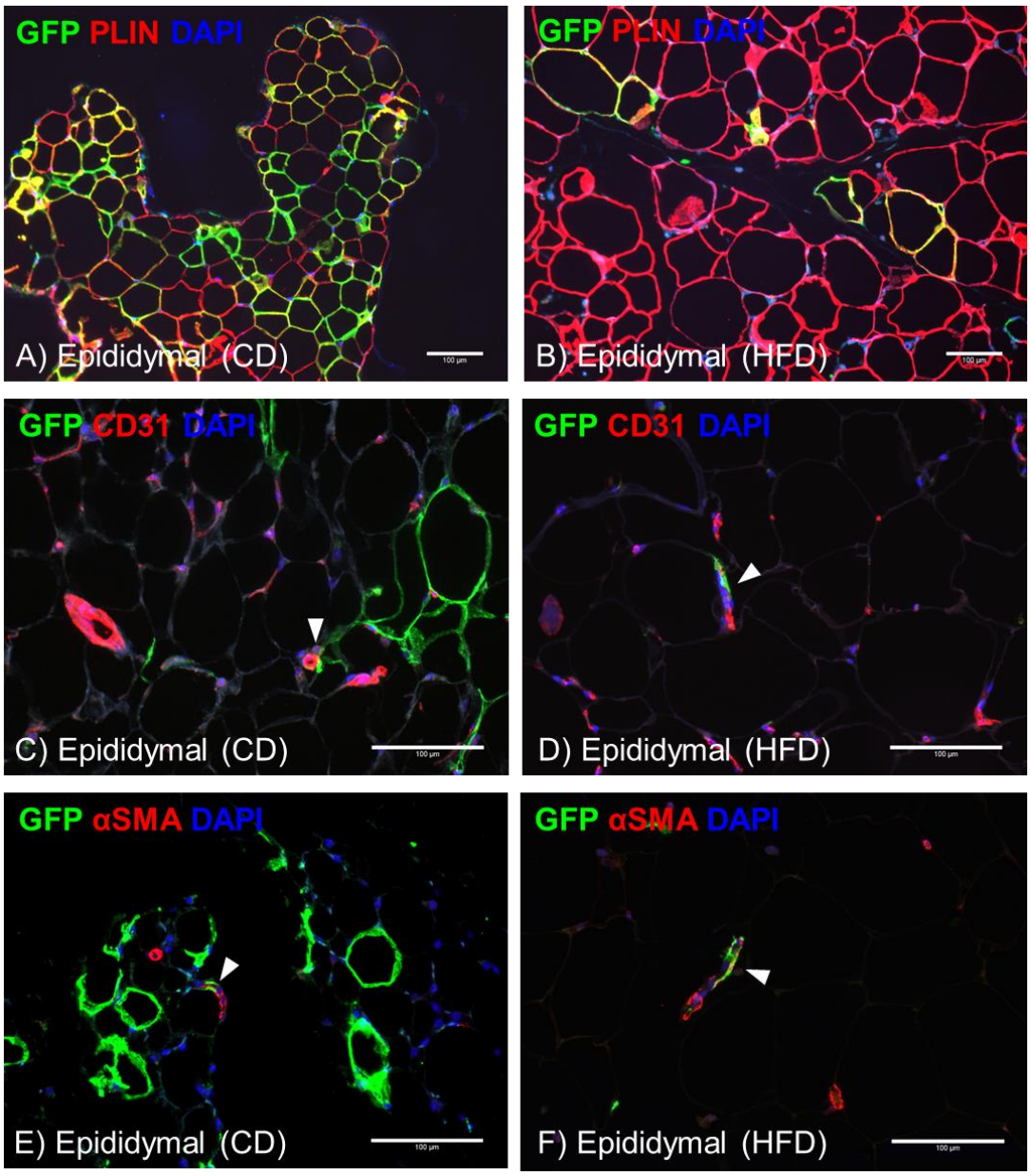

Figure 3.12. Wt1-lineage traced adipocytes and vessels are present in mice fed a standard chow diet (CD) and in mice fed a high fat diet (HFD). *A-B:* ***P****araffin-embedded sections of epididymal fat from CD mice (A) and HFD mice (B) stained for GFP (green), perilipin (PLIN, red) and DAPI (blue). C-D:* ***P****araffin-embedded sections of epididymal fat from CD mice (C) and HFD mice (D) stained for GFP (green), CD31 (red) and DAPI (blue). E-F:* ***P****araffin-embedded sections of epididymal fat from CD mice (E) and HFD mice (F) stained for GFP (green), αSMA (red) and DAPI (blue). Scale bars: 100 µm.*

We also investigated whether *Wt1*-lineage traced vessels are also found in obese mice; we therefore further analysed tissues from 7.5 month old *Wt1*^{CreERT2}*;mTmG* mice dosed with tamoxifen through the mother's milk (four doses of tamoxifen at the beginning of P0) and fed a high fat diet (HFD) from the age of one month.

Figure 3.12 shows representative images of epididymal adipose tissue from CD and HFD mice, co-stained for GFP and CD31 (C-D) and GFP and αSMA (E-F). Our immunofluorescence images show that both CD and HFD samples present lineage traced cells in the perivascular area of CD31+ and αSMA+ vessels. We next aimed to quantify the proportion of vessels where lineage traced cells are found, by counting all microvessels (with a diameter > 10 μm) across several images taken of each depot, and then dividing the number of GFP+ microvessels by the total number of microvessels. Figure 3.13 (A-B) shows the proportion of GFP+ microvessels across five depots – epididymal, omental, pericardial, perirenal and mesenteric. Most depots show that, in HFD-fed mice, there is a trend towards fewer *Wt1*-lineage traced vessels. However, this decrease was not statistically significant.

Perivascular cells have been shown to serve as a pool of adipose progenitors (Tang et al., 2008). Crișan *et al.* also demonstrated that purified perivascular cells show strong adipogenic potential (Crisan et al., 2008). We therefore also co-stained CD and HFD samples from *Wt1*-lineage traced mice for GFP and perilipin (PLIN), which is expressed by mature adipocytes (Figure 3.12, A-B). Both CD and HFD adipose tissue presents *Wt1*-lineage traced adipocytes and this is observed in epididymal fat (Figure 3.12, A), as well as in omental, pericardial, mesenteric and perirenal fat (not pictured). At first glance, we observed fewer GFP+ adipocytes in VWAT from HFD-fed mice. We therefore also quantified the percentage of GFP+ adipocytes in all depots and we found fewer lineage traced adipocytes in the HFD groups (Figure 3.13, C). We observed a statistically significant decrease in the percentage of GFP+ adipocytes in epididymal ($p=0.041$, CD n=6, HFD n=7), omental ($p=0.0012$, CD n=6, HFD n=5), and perirenal ($p=0.0009$, CD n=5, HFD n=6) fat from HFD mice. We also observed a decrease in the percentage of GFP+ adipocytes in pericardial and mesenteric adipose tissue.

Overall, we found that WT1-expressing cells not only give rise to adipocytes but may also differentiate into VSMCs and perivascular cells in five VWAT depots. Quantifying the percentages of lineage traced cells in lean and obese mice indicated that the contribution of WT1+ cells to the adipocyte population is decreased in obesity.

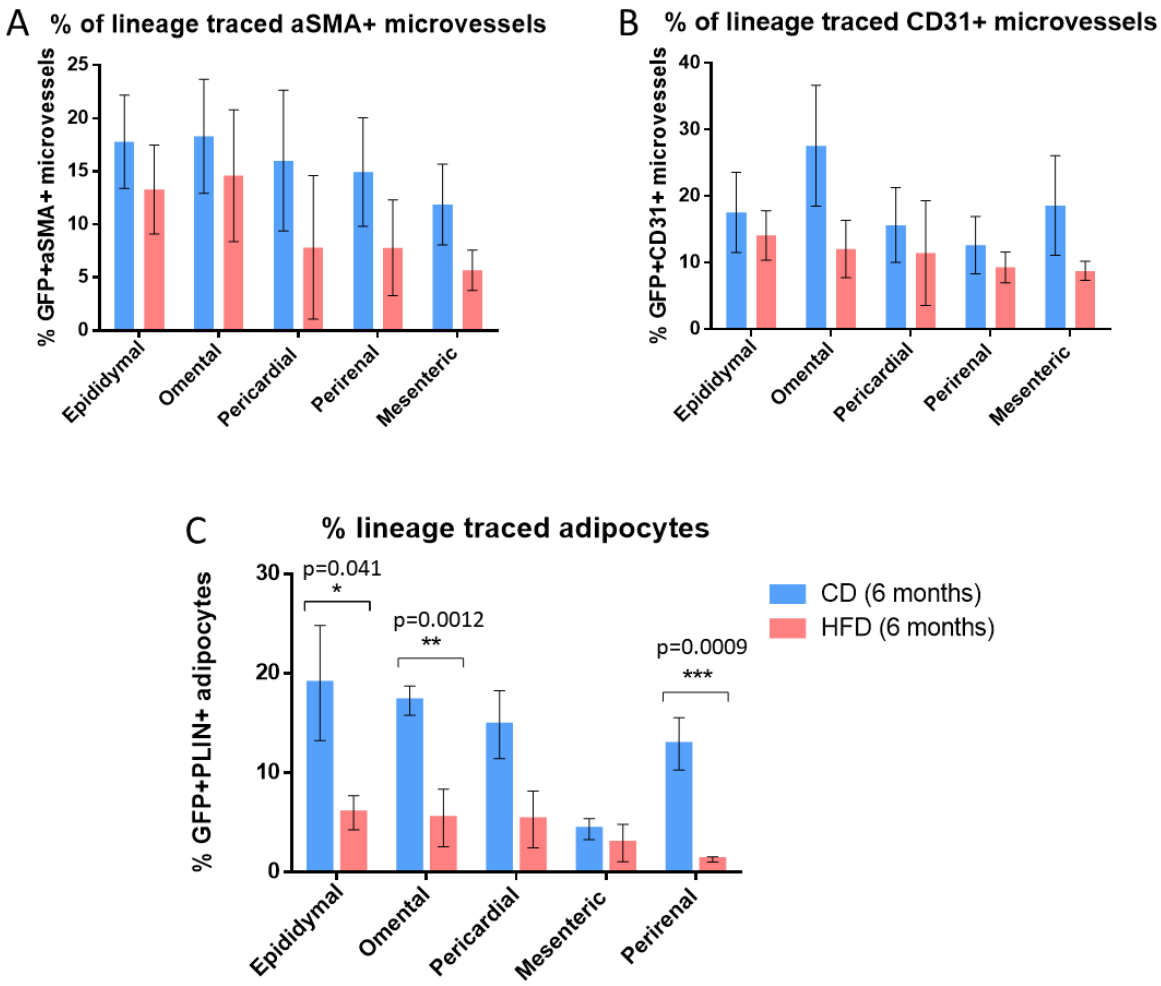

Figure 3.13. The percentage of Wt1-lineage traced microvessels and adipocytes is lower in HFD-fed Wt1^{CreERT2};mTmG mice. A. *VWAT depots from HFD-fed mice show a trend towards reduction in the percentage of αSMA+ vessels presenting GFP+ cells, although not significant (statistical analysis results are outlined in Table A.1).* ***B.*** *VWAT depots from HFD-fed mice show a trend towards reduction in the percentage of CD31+ vessels presenting GFP+ cells, although not significant (statistical analysis results are outlined in Table A.1).* ***C.*** *Epididymal, omental and perirenal adipose tissue from HFD-fed mice shows a significant reduction in the percentage of PLIN+ adipocytes that are GFP + (epididymal: p=0.041; omental: p=0.0012; perirenal: p=0.0009). Pericardial and mesenteric fat also shows a reduction in the percentage of Wt1-lineage traced adipocytes. Error bars indicate the SEM. n≥4 in all groups; n numbers for all conditions are outlined in Table A.1 (Appendix).*

3.2.3 Expression of WT1 in the microvasculature of human VWAT

WT1 mRNA has been detected by qPCR in human omental visceral fat, but not in subcutaneous fat (Chau et al., 2014). We therefore decided to look into the expression and location of WT1 in human VWAT. We collected omental and subcutaneous fat samples from patients undergoing surgery. Based on BMI, we classed the patients as lean (BMI < 25), overweight (BMI = 25-30), and obese (BMI > 30). Paraffin-embedded sections from omental and subcutaneous adipose tissue were stained for WT1 (Figure 3.14). As predicted, no WT1 was detected in subcutaneous fat from the three groups (Figure 3.14, B, D, F). On the other hand, cells positive for nuclear WT1 were present in omental adipose tissue from lean, overweight, and obese individuals (Figure 3.14, A, C, E). Interestingly, as in our murine samples, we observed WT1 expression in the mesothelium of omental adipose tissue (Figure 3.14, A, arrowheads).

In order to find out where the WT1-positive cells are located in relation to the vasculature of omental adipose tissue, we co-stained paraffin-embedded sections for WT1 + CD31 and WT1 + αSMA (Figure 3.15), In Figure 3.15, panels A, C, and E show that WT1+ cells are located in the perivascular area of CD31+ microvessels in lean, overweight, and obese subjects, respectively. Similarly, in all three groups, WT1+ cells are found in the perivascular space of microvessels positive for αSMA (Figure 3.15, B, D, and F). Anthropometric data on all patients included in this analysis can be found in the Appendix (Table A.2)

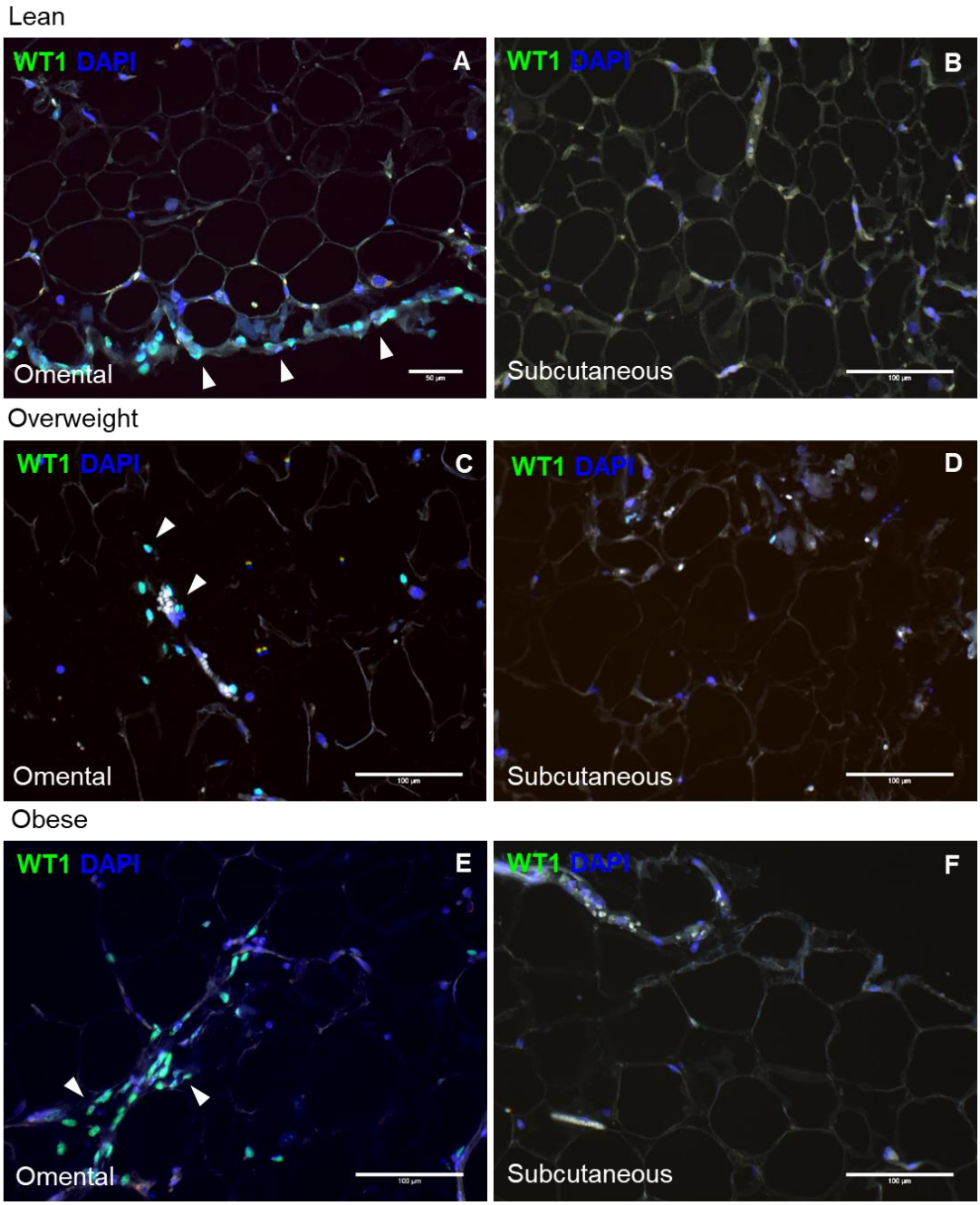

Figure 3.14. WT1 is expressed in omental, but not subcutaneous, adipose tissue from lean, overweight and obese patients. *Paraffin-embedded omental and subcutaneous adipose tissue from lean (A-B, n=4), overweight (C-D, n=4), and obese (E-F, n=6) patients was stained for WT1 (green) and DAPI (blue). Omental adipose tissue is positive for WT1 in all three groups. White arrows indicate WT1+ cells. No WT1 was detected in subcutaneous adipose tissue. Scale bars: 100 µm.*

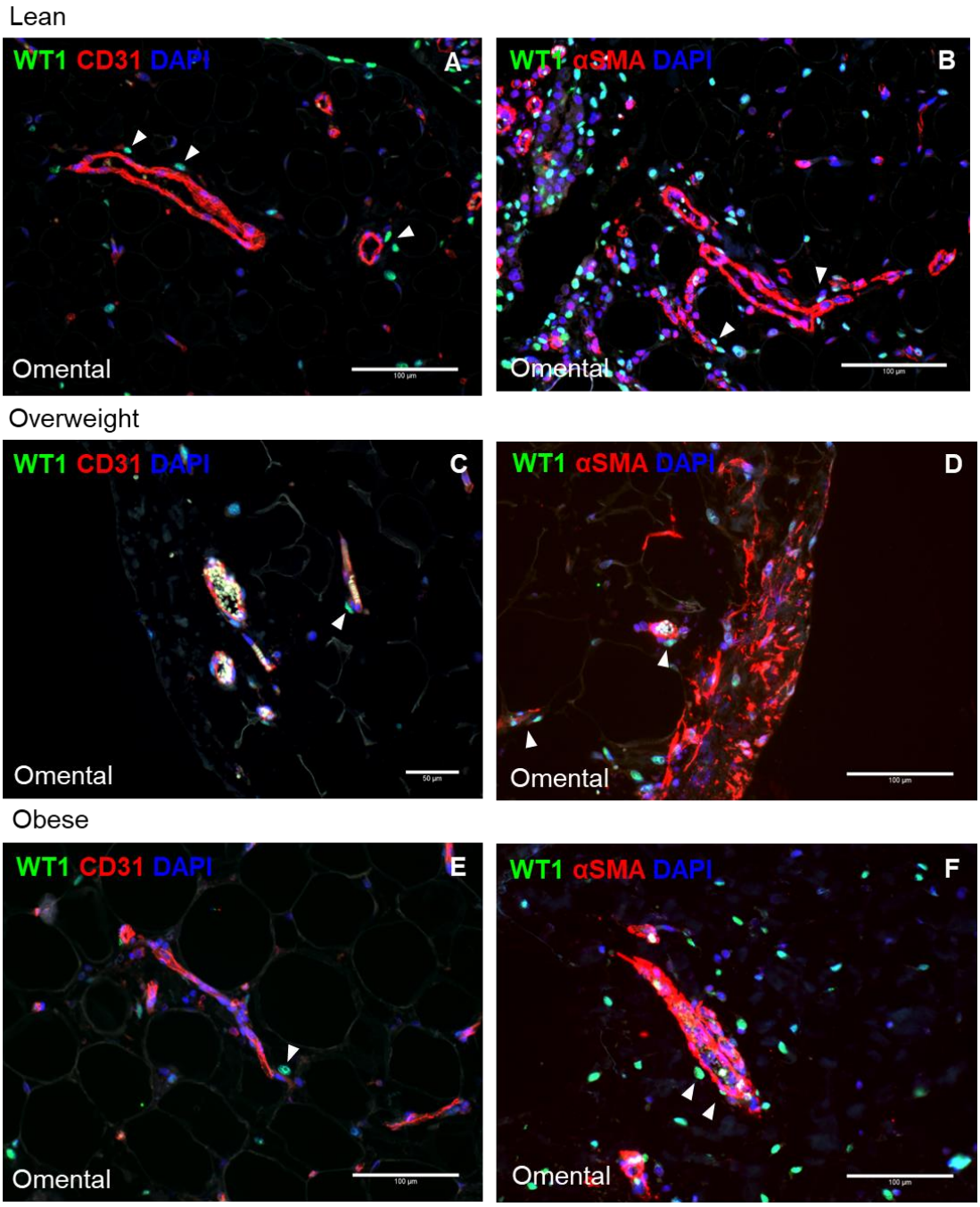

Figure 3.15. WT1-positive cells are found in the perivascular area of vessels in omental fat from lean, overweight and obese patients. *Paraffin-embedded omental adipose tissue from lean (A-B, n=4), overweight (C-D, n=4), and obese (E-F, n=6) patients was co-stained for WT1 + CD31 (A, C, E) and WT1 + αSMA (B, D, F). WT1-positive cells are found in the perivascular area of CD31+ vessels and αSMA+ vessels in all three groups. White arrows indicate WT1+ cells. Scale bars: 100 µm.*

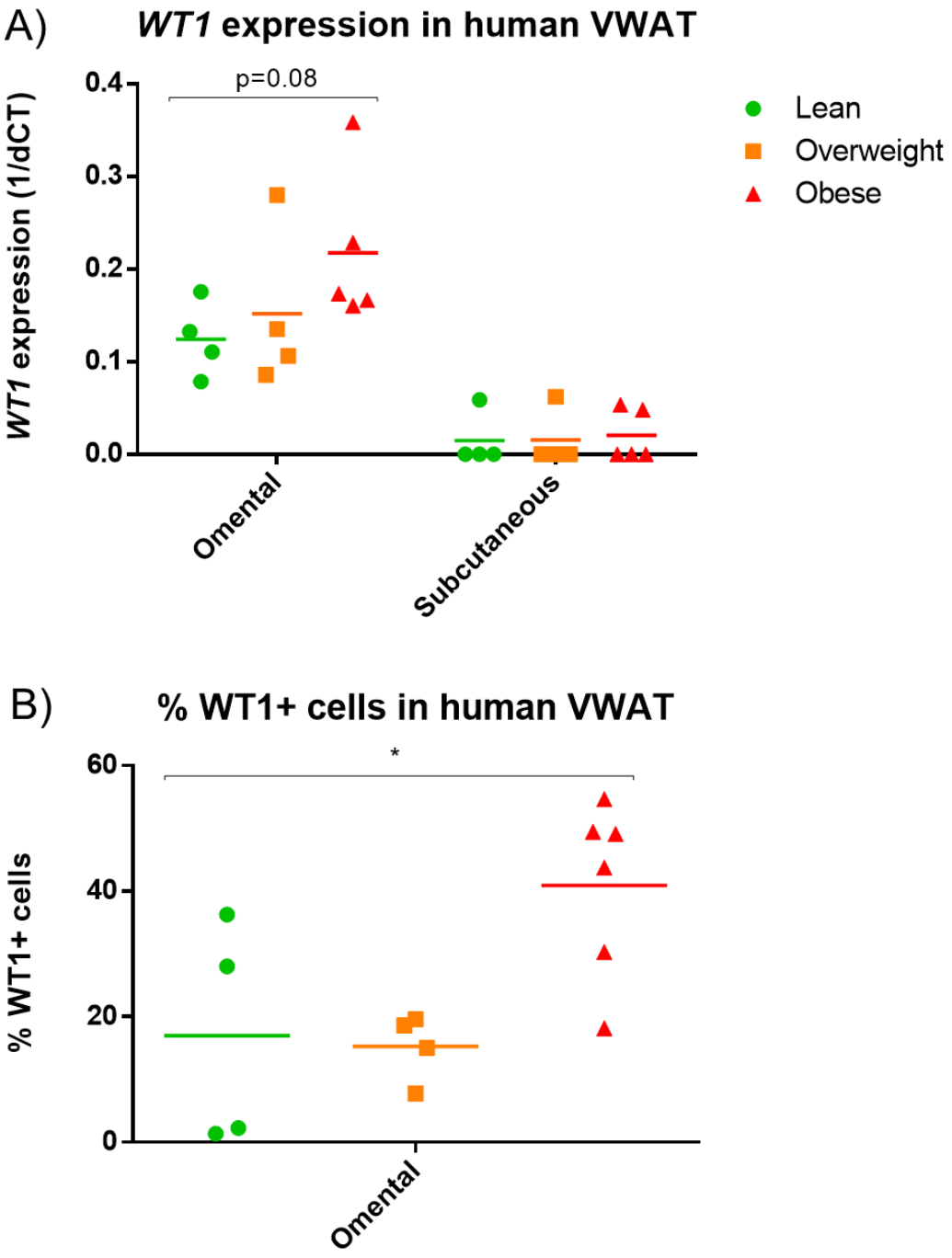

Figure 3.16. WT1 mRNA and the percentage of WT1+ cells are both increased during obesity. *A. WT1 mRNA levels in omental and subcutaneous adipose tissue, extracted from lean (n=4), overweight (n=4), and obese (n=5) patients. Transcript levels are increased in overweight and obese patients (p=0.08 for lean vs. obese). WT1 levels were normalized to 18S mRNA levels in each samples. B. The percentage of WT1+ cells in omental fat from lean (n=4), overweight (n=4), and obese (n=6) patients. Obese patients present a significantly increased percentage of WT1+ cells compared to lean ones (p= 0.043*)

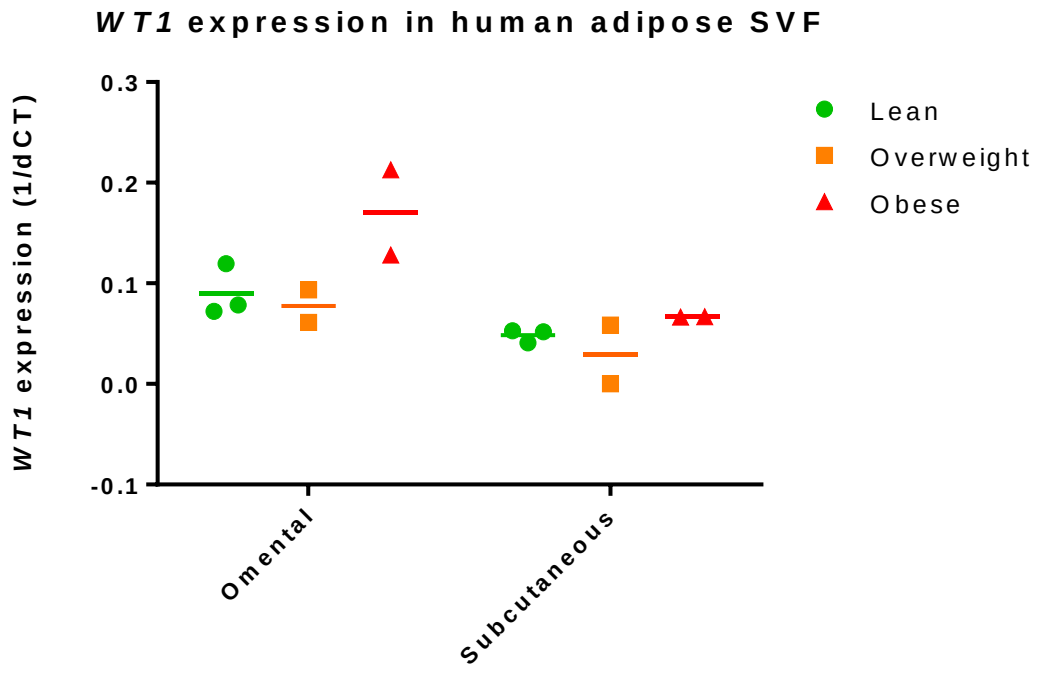

Figure 3.17. WT1 mRNA expression in cultured human omental and subcutaneous SVF cells. *WT1 mRNA levels were measured in SVF cells from lean (n=3), overweight (n=2), and obese (n=2) donors. WT1 levels are expressed as 1/dCT. WT1 levels were normalized to 18S mRNA levels in each samples.*

WT1 signal in human samples was stronger than in murine samples, enabling the quantification of WT1+ cells in human omental adipose tissue, especially since WT1 expression is generally restricted to the nucleus. We quantified the percentage of WT1+ cells in omental adipose tissue from lean (n=4), overweight (n=4), and obese (n=6) patients (Figure 3.16, B). The areas sampled were selected randomly and the percentage of WT1+ cells was calculated by dividing the total number of WT1+ nuclei by the total number of DAPI-stained nuclei (with at least 300 total cells counted overall). Lean and overweight patients showed a similar percentage of WT1+ cells (17% and 15.25%, respectively). However, we observed a much higher percentage of WT1+ cells in samples from obese patients (40.93%). The proportion of WT1+ cells was significantly higher in obese patients compared to lean ones (p=0.043). However, there was no significant difference between lean and overweight samples (Figure 3.16, B).

We also performed qRT-PCR in order to analyse *WT1* transcript levels in whole omental adipose tissue obtained from lean (n=4), overweight (n=4), and obese (n=5) patients (Figure 3.16, A). As expected, *WT1* was undetectable or close to the threshold of detection in subcutaneous adipose tissue from all three groups. In

omental adipose tissue, we observed an increase in *WT1* levels in overweight compared to lean subjects, as well as an increase in obese subjects compared with lean subjects, with the latter showing a trend towards significance (p=0.08).

We further looked into *WT1* expression in SVF cells in culture. We isolated SVF cells from omental and subcutaneous adipose tissue from lean (n=3), overweight (n=2), and obese (n=2) subjects and expanded these in culture for 7 days (until confluent). SVF cells derived from the adipose tissue of obese subjects presented higher levels of *WT1* than SVF cells isolated from lean or overweight subjects (Figure 3.17). However, when we compared only SVF from overweight subjects with SVF cells from lean subjects we did not observe any difference in *WT1* transcript levels (Figure 3.17). Interestingly, subcutaneous SVF cells showed some *WT1* transcripts after being cultured to confluence (Figure 3.17).

Overall, these results indicate that not only is WT1 present in human omental adipose tissue from all three groups, but that *WT1* transcript levels and the number of WT1+ cells both seem to be increased during obesity. These results were most obvious in unfixed adipose tissue, where the *WT1* mRNA levels and percentage of WT1+ cells were analysed. However, this difference was not maintained when adipose-derived SVF cells were kept in culture, suggesting that *WT1* expression is different *in vivo* and *in vitro*.

3.3 Discussion

It has been demonstrated that WT1 is expressed in both murine and human visceral adipose tissue, but absent from subcutaneous adipose tissue (Chau et al., 2014a). While it is known that WT1 is expressed in visceral adipose progenitors, we currently have no information about WT1 expression in other cell populations in VWAT (Chau et al., 2014). As angiogenesis is essential for the homeostasis and remodelling of VWAT, and WT1 is important for angiogenesis in development and cancer, we wanted to firstly look into the expression of WT1 in the VWAT vasculature.

First, the experiments in this chapter aimed to establish whether WT1 is expressed in microvascular cells in murine VWAT. Second, we aimed to trace the fate of WT1-expressing cells after birth, establish whether these cells can differentiate into microvascular cells, and investigate whether the contribution of WT1+ cells to the vasculature is altered under HFD. Third, we aimed to find out whether WT1+ cells are present in human omental VWAT, where WT1+ cells are located in relation to the

omental vasculature, and whether there are any differences in human *WT1* gene expression between lean, overweight, and obese subjects.

3.3.1 WT1 is expressed by microvascular cells in VWAT

In murine VWAT, we used the *Wt1*$^{GFP/+}$ mouse model to identify the location of WT1-expressing cells and the expression of WT1 in microvascular cells in five VWAT depots. We identified WT1-positive cells in the perivascular area of vessels positive for CD31, αSMA, and PDGFRβ and co-expression of GFP and PDGFRβ in the same cells. Our immunofluorescence data did not reveal co-expression of GFP and CD31 in endothelial cells. However, our flow cytometry data show two microvascular cell populations positive for GFP: Lin-cKit-PDGFRβ-CD31+GFP+ and Lin-cKit-CD31-PDGFRβ+GFP+, which may be due to the higher sensitivity of flow cytometry analysis, *in vivo*, CD31 is expressed more highly at the endothelial cell-cell junctions (Lertkiatmongkol et al., 2016), which may make it difficult to detect co-expression of CD31 and WT1 by immunofluorescence alone.

Although different VWAT depots have different sizes, with omental and pericardial adipose tissue being much smaller than, for instance, epididymal, we observed by flow cytometry a higher proportion of PCs expressing GFP, which suggests the varying sizes of distinct VWAT depots does not influence these results.

Both ECs and pericytes in VWAT can be divided into WT1-negative and WT1-positive sub-populations. A role of WT1 in ECs has been previously described in the context of cancer, where it is involved in EC proliferation and migration (Wagner et al., 2008a). Similarly, in tumours, WT1 has been shown to regulate the expression of factors responsible for the alternative splicing of VEGF (Wagner et al., 2019). These and other studies suggest that an increased need for vascularisation is accompanied by upregulation of WT1 and its downstream targets. Our finding that WT1 is expressed in a subset of adipose ECs could mean that WT1 is also involved in EC proliferation and migration during VWAT expansion, although whether its role is likely to be protective or pathological may depend on the complex interactions between several cell populations in the VWAT microenvironment.

However, the proportion of WT1+ cells was much higher in adipose pericytes from all VWAT depots analysed, which suggests a role of WT1 in pericytes rather than in ECs. Pericytes have been thoroughly described in terms of their role in the vasculature, but also as a source of adipocytes, especially during hyperplastic expansion of obese

adipose tissue (Vishvanath et al., 2016). It is thus important to establish whether the function of WT1 in pericytes is related to their role in stabilising the vasculature, to their role as adipose progenitors, or both.

Interestingly, WT1 signal in samples from our *Wt1*$^{GFP/+}$ mice was strongest in mesothelial cells, some of which also expressed PDGFRβ. Elsewhere in the adipose tissue analysed, WT1 signal tended to be weaker, which may be an indication that WT1 is more essential in the mesothelium. This is particularly of interest as, for instance, studies in the liver have revealed that mesothelial cells can differentiate into perivascular mesenchymal cells (Asahina et al., 2011). Our finding of WT1+/- populations of adipose pericytes is, however, also significant because of other studies showing subsets of pericytes with different functions. For instance, Hepler et al. showed that PDGFRβ+ stromal cells in murine visceral fat can be divided into two sub-populations based on LY6C expression, with LY6C-CD9-PDGFRβ+ cells having high adipogenic potential and LY6C+PDGFRβ+ cells presenting a fibro-inflammatory phenotype (Hepler et al., 2018). It is, therefore, possible that WT1+/- pericytes may have different functions in the homeostasis and expansion of adipose tissue.

3.3.2. WT1-positive cells contribute to the VWAT microvasculature differently during homeostasis and during diet-induced obesity

Our lineage tracing experiments show that, after birth, WT1-expressing cells continue to give rise not only to adipocytes, but also to pericytes. We also observed *Wt1*-lineage traced cells surrounding the perivascular area of vessels positive for CD31 and αSMA, although whether the lineage traced cells themselves are ECs or VSMCs is difficult to assess by IHC alone.

Interestingly, we observed a decrease in the contribution of WT1+ cells to adipocytes in diet-induced obesity. We also observed a potential downward trend in the contribution of WT1+ cells to microvascular cell populations. Although we were not able to quantify individual PDGFRβ+ cells or vessels due to the morphology of the tissue and the continuous pattern of PDGFRβ expression along the microvessels, quantifying vessels positive for CD31 and αSMA revealed a decreasing trend in lineage traced vessels in obese mice. Moreover, the proportion of *Wt1*-lineage traced adipocytes was significantly lower in obesity. Considering the fact that PDGFRβ+ pericytes have been proposed as a source of adipocytes, the decrease in the number of vessels presenting perivascular GFP may be correlated with the decrease in WT1-derived adipocytes (Shao et al., 2018). It is, however, important to note that the

perceived decrease in GFP+ adipocytes may also be a result of adipocyte death and vascular dysfunction as a result of diet-induced obesity ye(Strissel et al., 2007; Ye, 2011).

3.3.3 WT1 expression is increased in human omental adipose tissue during obesity

Similarly to murine VWAT, *WT1* mRNA has been previously detected in human visceral fat (Chau et al., 2014). In our experiments, we also identified WT1 in VWAT by immunofluorescence. Moreover, we found that some WT1-positive cells in human omental fat are located in the perivascular area of microvessels positive for CD31 and αSMA. However, while processing our samples we found that WT1 expression can vary throughout the tissue, with clusters of WT1+ cells abundant in some areas, while other parts of the same human sample might present few WT1+ cells. In humans, the omentum is a large, 'apron'-like adipose depot which covers most abdominal organs (Wilkosz et al., 2005). It is therefore likely that small samples obtained from abdominal surgeries are not entirely representative of the whole depot, which may lead to increased variation across biological replicates. Another limitation of these data lies in the heterogeneous patient populations included here, comprising both males and females with ages ranging from 33 to 76 (Appendix, Table A.2).

Although we saw some variability in our human data, we have nevertheless identified an increase in *WT1* transcripts and an increase in the number of WT1+ cells during obesity. At the transcript level, *WT1* mRNA was increased in obese subjects compared to lean counterparts, with a trend towards significance. We further identified a significant increase in the proportion of WT1+ cells in obese subjects, although these cells may be ECs and pericytes, as well as progenitors located elsewhere in the stroma or mesothelium. Nonetheless, the increase in WT1+ cells during obesity suggests a role for WT1 in adipose remodelling. Moreover, considering the role of WT1 in angiogenesis and inflammation, it is possible that WT1+ cells here have a role in the pro-inflammatory, pro-angiogenic microenvironment of obese VWAT (Nian et al., 2004; Scholz et al., 2009; Sontake et al., 2018).

We also observed a large proportion of WT1+ cells in the mesothelium of human VWAT from all groups, which is consistent with murine WT1 expression in the VWAT mesothelium. The mesothelium, which consists of a layer of mesoderm-derived epithelial-like cells, has recently been proposed as a key player in metabolic health and disease. For instance, adipose mesothelial cells have been shown to acquire a pro-inflammatory phenotype in obesity (Darimont et al., 2008). Moreover, mesothelial

cells secrete cytokines such as IL-8 (Gupta and Gupta, 2015). Lastly, the mesothelium has also been proposed as a source of preadipocytes and adipocytes in VWAT (Chau et al., 2014a).

These newly revealed functions of the adipose mesothelium are essential for a better understanding of adipose biology and are also of therapeutic relevance, as cells isolated from adipose tissue are frequently used in clinical settings (Strong et al., 2015; Tremolada et al., 2010; Zuk et al., 2001). Many *in vitro* studies involve isolation and manipulation of the stromal vascular fraction, which will inevitably include mesothelial cells. WT1 is not only a mesothelial marker but also a transcriptional regulator of several angiogenesis and inflammation genes (McCarty et al., 2011; Velecela et al., 2013). Its increased expression in obese subjects suggests that it either modulates inflammation and angiogenesis directly during adipose remodelling, or continues to serve as a source of cells necessary for adipose expansion.

Interestingly, we observed that the differences between patient groups in terms of *WT1* expression are not the same when analysing unfixed tissue and SVF cells after 7 days in culture. While a direct comparison cannot be made between mRNA levels in cultured SVF cells and mRNA levels in whole unfixed tissue, it is still worth pointing out that any differences between groups of lean or obese mice/patients must be assessed in unfixed tissue or freshly isolated cells, as *WT1* expression in these cells may be dependent on their microenvironment.

3.3.4 Conclusions

The results in this chapter indicate that WT1 is expressed in sub-populations of murine microvascular cells such as ECs and pericytes. Moreover, *Wt1*-lineage traced cells are still present in VWAT at the age of 6 months and their location suggests that WT1+ cells differentiate into perivascular cells after birth. Although we observed this in all depots analysed, we also noticed differences in WT1 expression between epididymal, omental, pericardial, mesenteric, and perirenal fat. These different expression profiles suggest that different mechanisms are employed in different VWAT depots, stressing the importance of examining each depot individually when carrying out studies on visceral adipose tissue. Moreover, the fact that the majority of pericytes in omental and pericardial fat express WT1, taken together with the data from Chau et al. showing higher percentages of adipose precursors expressing WT1 and data showing PDGFRb+ populations aiding healthy adipose expansion, suggest these WT1-

positive pericytes play a role in the maintenance of a healthy adipocyte population (Chau et al., 2014; Shao et al., 2018).

On the other hand, our human data show an increase in *WT1* mRNA levels and WT1+ cells in obesity. This may be a consequence of an increasingly hypoxic environment, where WT1 gets activated by HIF-1 (WAGNER et al., 2003), although it is yet to be determined whether WT1 and WT1-expressing cells later modulate the microenvironment of expanding adipose tissue.

Chapter 4

Investigating the role of murine WT1 in *in vitro* angiogenesis

4.1 Introduction

Adipose tissue relies on vascular growth, both during homeostasis and during remodelling. Therefore, studying adipose angiogenesis *in vitro* is useful in order to reveal the cellular and molecular processes governing the adipose vasculature. Vascular cells, such as endothelial cells, pericytes, and smooth muscle cells, can be isolated from the stromal vascular fraction (SVF) of adipose tissue and analysed or further manipulated *in vitro*. However, such specific populations may be difficult to obtain from small adipose depots and often require large numbers of samples to be pooled.

One alternative to this is assessing the *in vitro* angiogenic potential of the heterogenous SVF. Firstly, several studies have shown that SVF has angiogenic potential *in vivo.* For instance, SVF cells isolated from human subcutaneous adipose tissue have been found to aid wound healing in nude mice when delivered together with ECM components to the tail veil (Sun et al., 2017). Similarly, SVF cells isolated from murine epididymal adipose tissue can promote vasomotor relaxation in dysfunctional small arteries (Morris et al., 2015). Secondly, studies have also revealed the *in vitro* angiogenic properties of adipose SVF cells. For instance, human adipose SVF secretes high levels of angiogenic factors, including VEGF (Rehman et al., 2004; Vezzani et al., 2018). Moreover, freshly isolated rat SVF cells plated on Matrigel® ECM form aggregates and later show tip/stalk cell formation and branching (Zakhari et al., 2018).

Considering the above, we aimed to investigate the role of WT1 on the *in vitro* angiogenic potential of epididymal, omental, and pericardial SVF cells. However, due to the small size of depots such as omental and pericardial adipose tissue, SVF cells require expansion in culture, which means only some sub-populations may be selected through standard cell culture methods (Cleal and Chau, 2016). Therefore, the first aim of this chapter was to investigate which vascular cells are selected from the SVF by culture on standard tissue plates, and what proportion of these cells retain WT1 expression *in vitro.*

Several previous studies have looked into the *in vitro* function of WT1 in angiogenesis, both by investigating direct transcriptional targets of WT1 and by performing *Wt1* gene deletions in various models. Several studies in human and mouse cells have revealed an essential role of WT1 in angiogenesis *in vitro* (McCarty et al., 2011; Wagner et al., 2014, 2008).

For instance, Wagner et al. have shown that *WT1*-silenced human umbilical vein endothelial cells (HUVECs) fail to form tubular networks in Matrigel® cultures (Wagner et al., 2008). Moreover, *WT1* silencing in HUVECs inhibits the migratory and proliferative potential of the cells, as well as the expression of nestin, which is a marker of neovascularization (Wagner et al., 2008). Moreover, WT1 is expressed in the vasculature of several tumour types (including lung, skin, and breast) and *WT1* knockouts in endothelial, hematopoietic and myeloid-derived suppressor cells have been shown to reduce tumour angiogenesis and growth (Wagner et al., 2014).

The mechanisms behind the role of WT1 in cancer have also been investigated. For instance, it was shown that in Ewing sarcoma cells WT1 levels are positively correlated with VEGF levels and that WT1 directly binds to the VEGF promoter (McCarty et al., 2011). Moreover, WT1 expression increases during hypoxia in the kidney and heart, as well as in lymphoblasts and osteosarcoma cells, and HIF-1 binds to the promoter region of *Wt1* (Wagner et al., 2003). This is particularly important when investigating the adipose vasculature, firstly because hypoxia characterises obese adipose tissue, and secondly because hypoxia has been shown to modulate angiogenesis in ischemia and cancer (Krock et al., 2011; Pasarica et al., 2009).

Considering the evidence linking WT1 to angiogenesis, the second aim of this chapter was to investigate whether deleting *Wt1 in vitro* using the *Cre/loxP* system may alter the angiogenic potential of visceral adipose SVF cells. However, Cre recombinases have been previously shown to have unwanted toxic effects, such as chromosomal rearrangements and a reduction in cell proliferation (Adams and van der Weyden, 2001; Loonstra et al., 2001). We therefore also aimed to investigate whether the *Cre/loxP* system approach can be used to delete *Wt1* in adipose SVF cells, whether *Wt1* deletion may affect the behaviour of SVF cells *in vitro* and, if so, whether knocking down *Wt1* through alternative methods such as RNA interference can reveal the function of WT1 on *in vitro* angiogenesis.

4.1.1 Hypothesis

Taking into consideration the fact that WT1 has been shown to modulate angiogenic potential *in vitro* and that the adipose SVF contains vascular cells, we hypothesised that knocking down *Wt1* in murine SVF cells may impair the *in vitro* angiogenic potential of SVF from murine VWAT.

4.1.2 Aims

The aims of this chapter are therefore the following:

1. Examine WT1 expression *in vitro*, in cultured visceral SVF cells from epididymal, omental, and pericardial VWAT.
2. Use the *Cre-loxP* system to delete *Wt1* in vitro and examine the effects of Cre recombination and *Wt1* deletion on angiogenic potential and inflammation
3. If Cre toxicity effects are observed, delete *Wt1* through alternative methods such as RNA interference and examine the effect of *Wt1* deletion on the *in vitro* angiogenic potential of visceral adipose SVF cells.

4.2 Results

4.2.1 Characterisation of visceral adipose SVF cells *in vitro*

As adipose SVF cells have been shown to form tubes *in vitro,* we wanted to investigate whether deleting *Wt1* in the SVF of visceral adipose depots might impair the ability of the cells to assemble into tube-like structures. The data described in the previous chapter showed that WT1 is expressed in both ECs and PCs in all VWAT depots. However, as SVF cells must be expanded in culture in order to render sufficient numbers for tube formation experiments, we first aimed to establish how well WT1 expression is retained *in vitro* and, furthermore, whether WT1 expression is retained in vascular sub-populations.

We selected three depots to focus on for subsequent experiments – epididymal adipose tissue, which due to its size is one of the most widely studied murine visceral depots, and omental and pericardial adipose tissue, which we have previously shown to have high numbers of WT1-expressing cells. Flow cytometry was used to analyse the expression of WT1 in total SVF, as well as the expression of PDGFRβ and CD31 in GFP+Lin-cKit- cells isolated from *Wt1*$^{GFP+/-}$ epididymal, omental and pericardial adipose tissue (Figure 4.1). Firstly, the percentage of GFP+ cells in epididymal VWAT is higher than in omental or pericardial VWAT (30% vs. approximately 10%, Figure 4.1, D). Secondly, although GFP+Lin-cKit- cells make up less than 10% of the total pericardial and omental SVF, at least 20% of these GFP+ cells express PDGFRβ, whereas only 5% of epididymal GFP+Lin-cKit- were PDGFRβ+ (Figure 4.1, E). Finally, in all three depots, only 3-6% of GFP+Lin-cKit- cells were CD31+ (Figure 4.1, F).

Figure 4.2 shows preliminary immunofluorescence data on epididymal SVF cells maintained in culture for 7 days (until confluent) and stained with antibodies against CD31, αSMA, PDGFRβ, and WT1 (n=1). After being maintained in culture, SVF cells were positive for αSMA, PDGFRβ, and WT1 (Figure 4.2, B-D), but not for CD31 (Figure 4.2, A). This is supported by the literature describing optimal culture conditions for ECs, which require additional growth factors to be added to the culture medium (Leopold et al., 2019).

We further investigated the co-expression of WT1 and PDGFRβ in epididymal, omental, and pericardial SVF cells after 7 days in culture. Staining SVF cells with antibodies against WT1 and PDGFRβ revealed that both proteins continue to be expressed *in vitro*. Moreover, as expected, WT1 and PDGFRβ are co-expressed in some of the cells (Figure 4.3, A-C). While cultured SVF cells retain expression of WT1, the proportion of WT1+ cells is lower than in freshly isolated SVF cells, with approximately 5% WT1+ cells in omental SVF and approximately 20% WT1+ cells in pericardial and epididymal SVF (Figure 4.3, D). Moreover, PDGFRβ expression was detected in 20% of omental SVF cells, 30% of pericardial SVF cells and close to 50% of epididymal SVF cells (Figure 4.3, E). Finally, we analysed the percentage of PDGFRβ+ cells expressing WT1 (Figure 4.3, F). We found that the percentage of WT1+ pericytes after culture was lower than in our flow cytometry analysis of freshly isolated SVF cells.

We further looked at the co-expression of WT1 and αSMA in SVF cells maintained in culture. We observed WT1 expression in some of the VSMCs present in epididymal, omental, and pericardial SVF (Figure 4.4, A-C). The percentage of SVF cells expressing αSMA was lower than the percentage of PDGFRβ+ cells (Figure 4.4, E). When analysing co-expression of WT1 and αSMA, we found that 10% of omental, 20% of epididymal, and over 30% of pericardial αSMA+ cells expressed WT1 (Figure 4.4, F).

It has been suggested that, in kidney fibrosis, PDGFRβ+ pericytes express αSMA as they differentiate into myofibroblasts (Humphreys et al., 2010a). Moreover, in fibrotic lung disease, WT1 is upregulated and directly binds to the promoter of the *αSMA* gene (Sontake et al., 2018). We were therefore interested in investigating co-expression of PDGFRβ and αSMA in visceral adipose SVF cells maintained in culture. We co-stained SVF cells from epididymal, omental, and pericardial adipose tissue with antibodies against αSMA and PDGFRβ and found the two co-expressed in a

subset of cells (Figure 4.5, A-C). We further quantified the percentage of PDGFRβ+ cells expressing αSMA. We found that, in omental and epididymal adipose tissue, close to 50% of PDGFRβ+ cells are also positive for αSMA, while this percentage is lower in pericardial adipose tissue (20%; Figure 4.5, F). Figures 4.2 – 4.6 thus show that SVF cells maintained in culture retain PDGFRβ, αSMA, and WT1 expression, and that some PDGFRβ express αSMA as well.

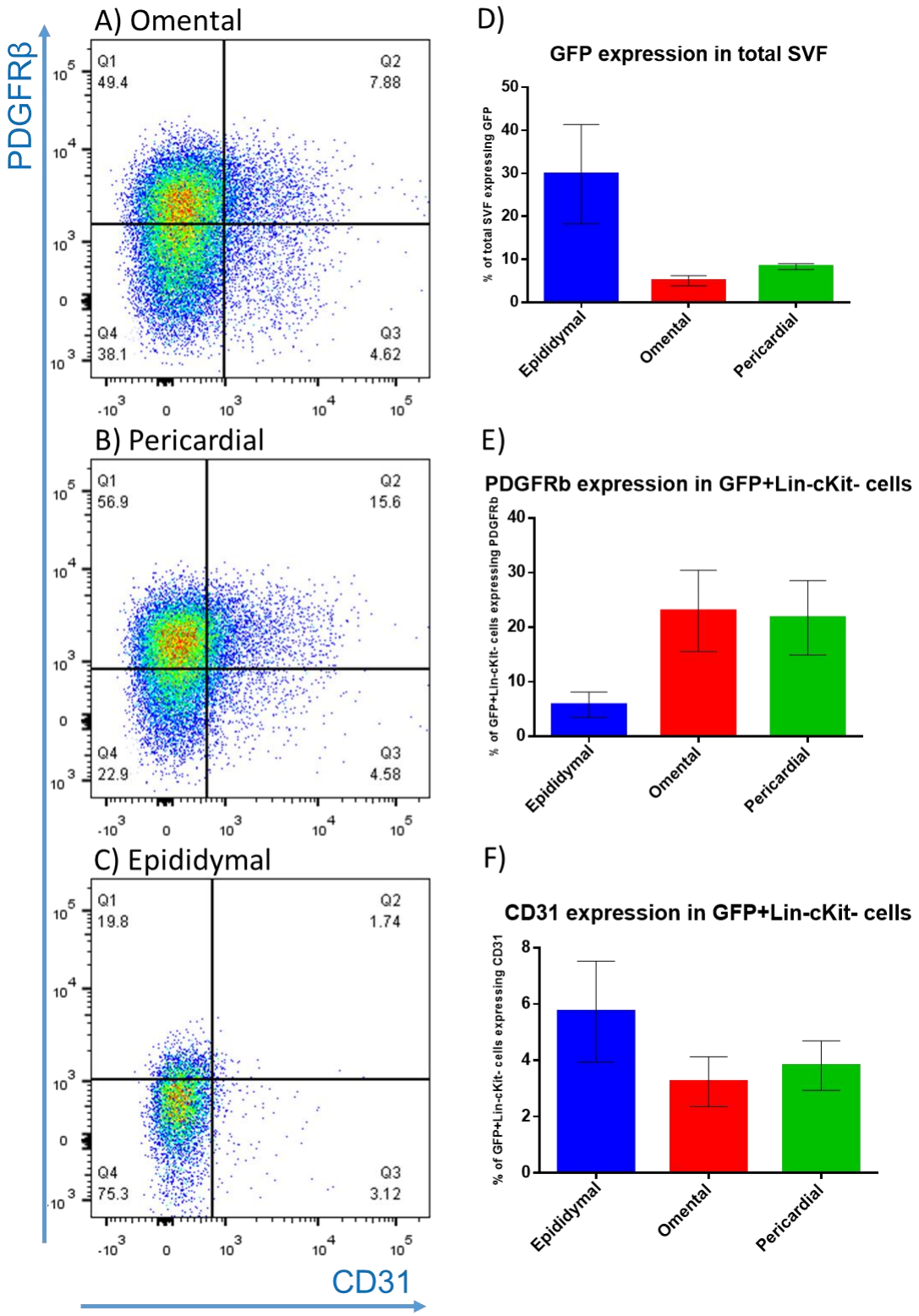

Figure 4.1. WT1 and vascular cell marker expression in freshly isolated VWAT SVF. *Representative plot of PDGFRβ and CD31 expression in omental (A), pericardial (B), and epididymal (C) adipose tissue. D. Expression of GFP in SVF isolated from omental, pericardial, and epididymal adipose tissue. E-F. PDGFRβ and CD31 expression in GFP+Lin-cKit- cells isolated from epididymal, omental, and pericardial adipose tissue. n=4 across all panels.*

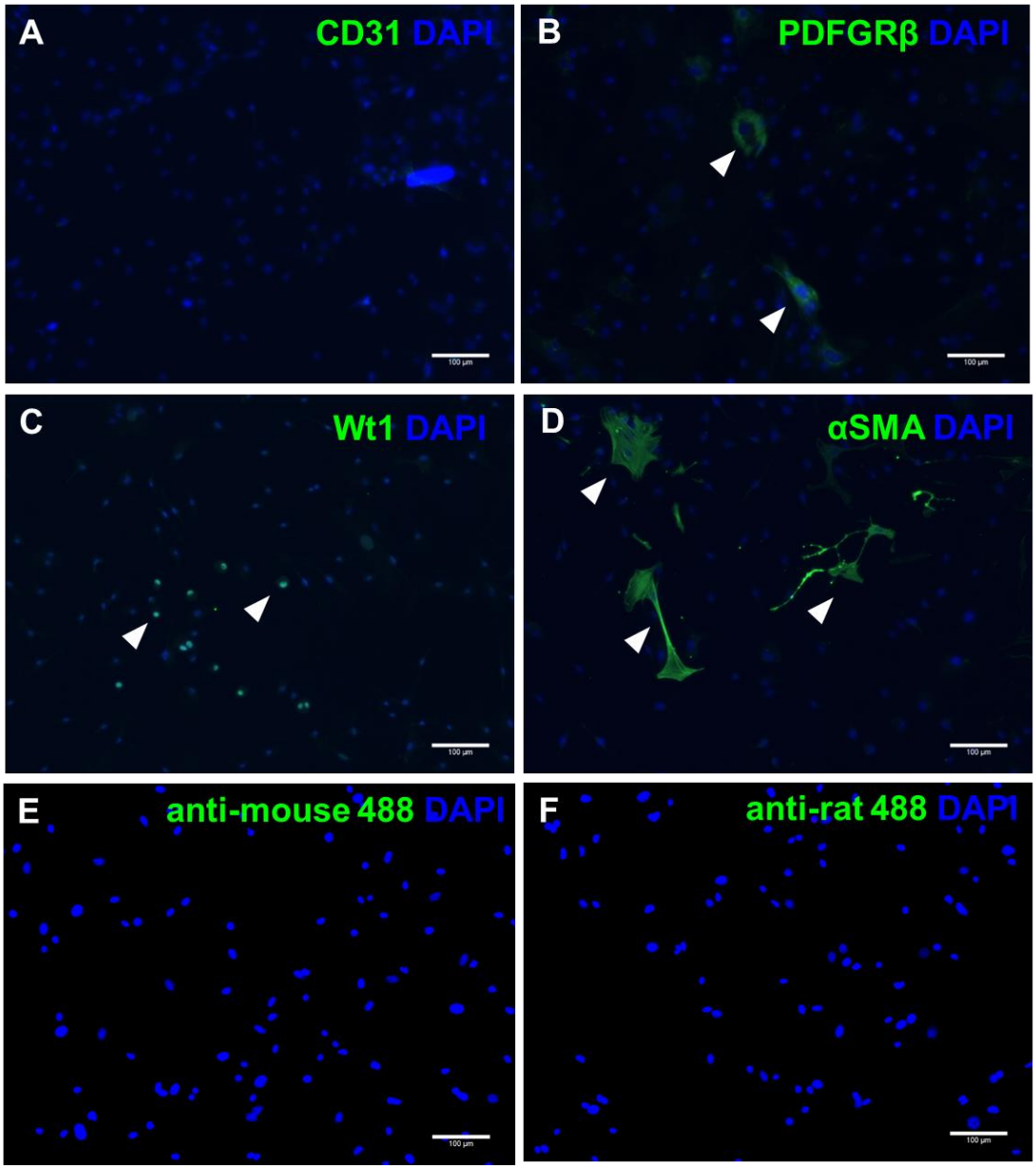

Figure 4.2. Standard method of culturing adipose SVF cells selects for pericytes and VSMCs, but not ECs. *A. Epididymal SVF cells cultured on standard tissue culture plates stained with CD31 antibody (green) and DAPI (blue). No CD31-positive cells are present after 7 days in culture. B Epididymal SVF cells stained with PDGFRβ antibody (green) and DAPI (blue). Arrowheads indicate PDGFRβ+ cells C. Epididymal SVF cells stained with antibodies against WT1 (green) and DAPI (blue). Arrowheads indicate WT1+ cells. D. Epididymal SVF cells stained with αSMA antibody (green) and DAPI (blue). Arrowheads indicate αSMA+ cells. n=1 across all panels. E-F. Secondary antibody controls. Scale bars: 100 μm.*

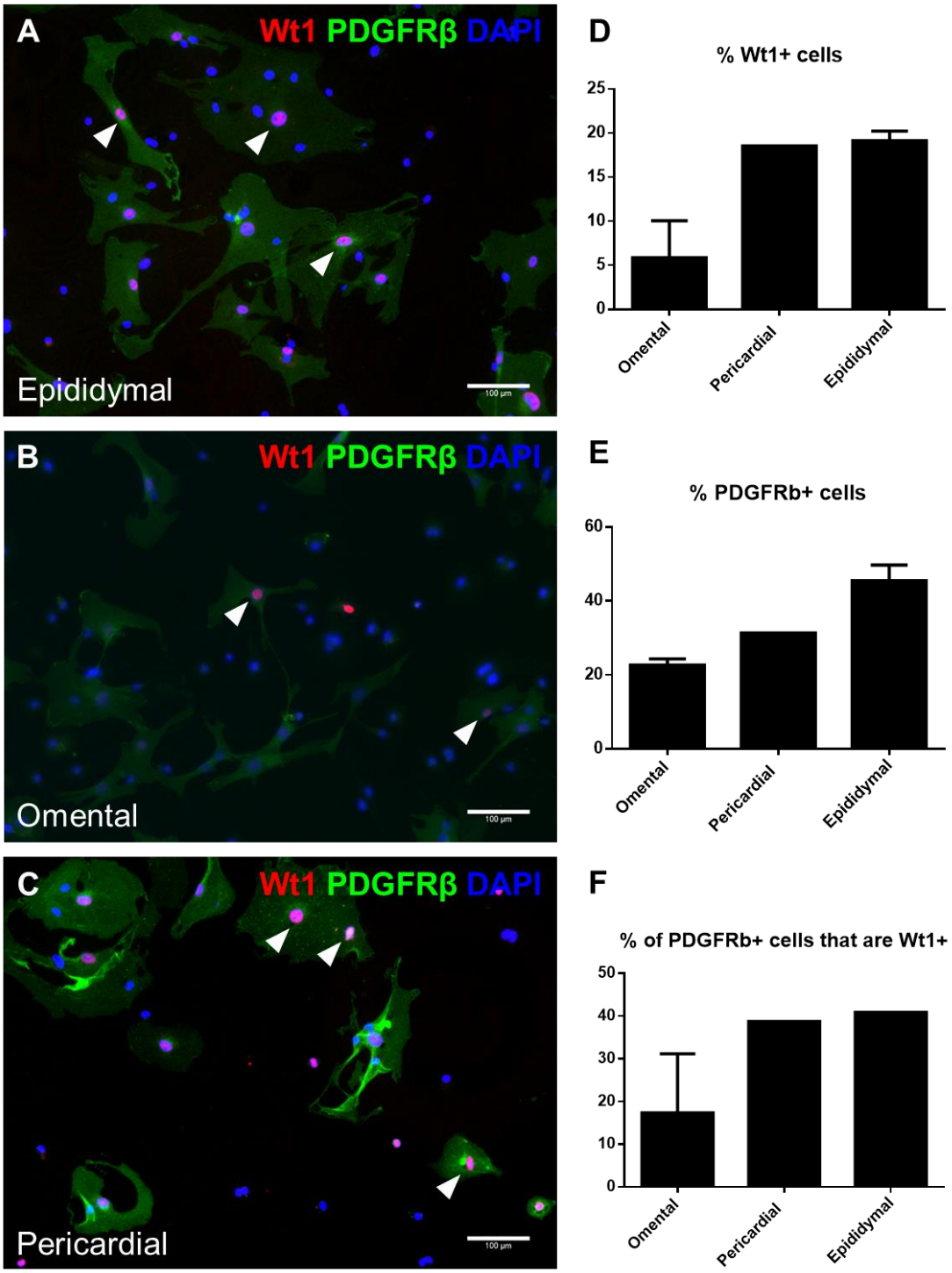

Figure 4.3. SVF cells from epididymal, omental, and pericardial adipose tissue continue to express WT1 and PDGFRβ while being maintained in culture. *Adipose SVF cells isolated from epididymal (A), omental (B), and pericardial (C) adipose tissue stained with WT1 antibody (red), PDFGRβ antibody (green), and DAPI (blue). Arrowheads indicate co-expression of WT1 and PDGFRβ. D: Percentage of omental (n=3), pericardial (n=1), and epididymal (n=2) SVF adipose cells expressing WT1. E: Percentage of omental (n=3), pericardial (n=1), and epididymal (n=2) SVF adipose cells expressing PDGFRβ. F: Percentage of pericytes expressing WT1 in omental (n=3), pericardial (n=1), and epididymal (n=2) SVF. Scale bars: 100 µm.*

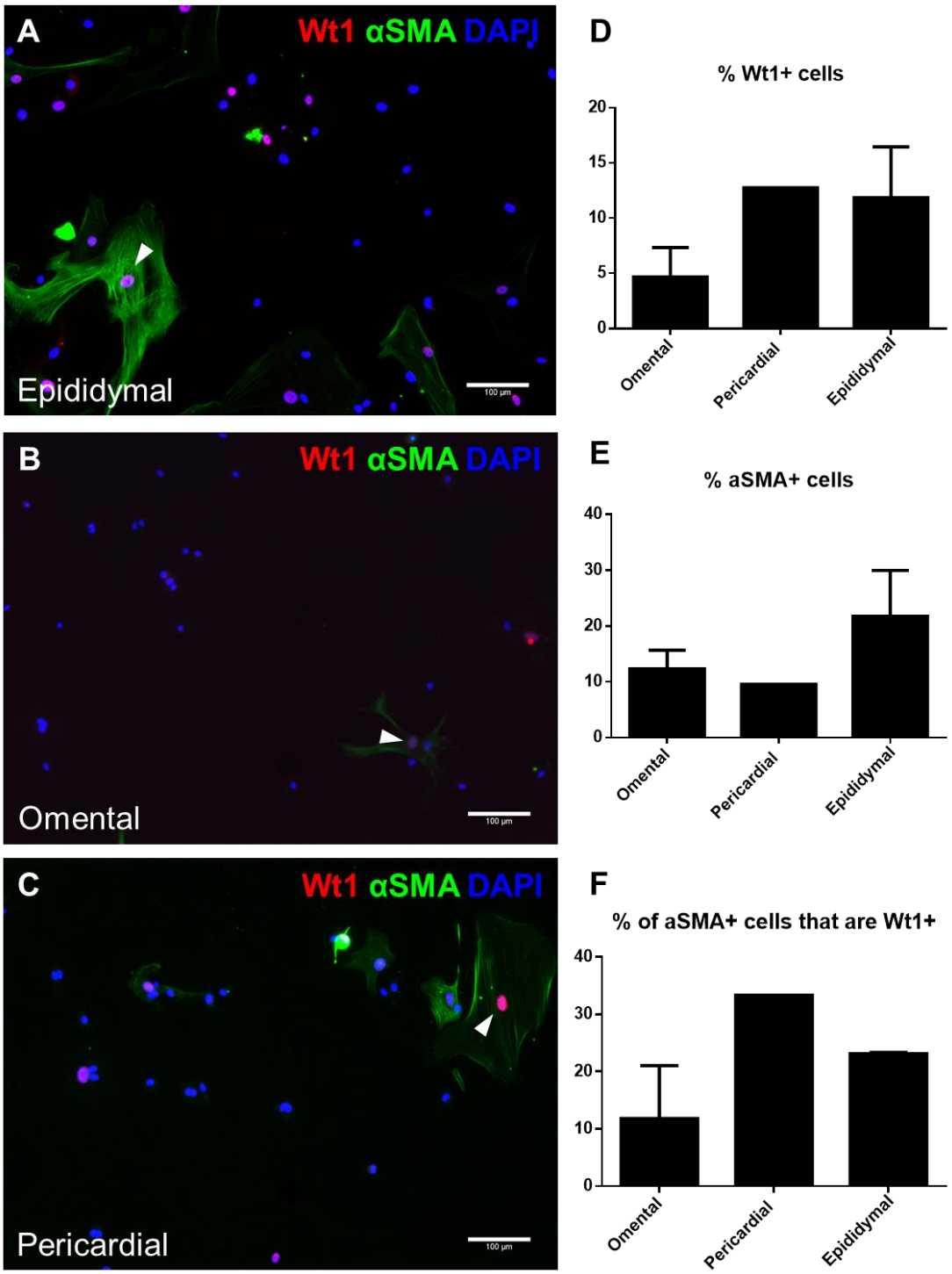

Figure 4.4. SVF cells from epididymal, omental, and pericardial adipose tissue continue to express WT1 and αSMA while being maintained in culture. *Adipose SVF cells isolated from epididymal (A), omental (B), and pericardial (C) adipose tissue stained with WT1 antibody (red), αSMA antibody (green), and DAPI (blue). Arrows indicate co-expression of WT1 and αSMA. D: Percentage of omental (n=3), pericardial (n=1), and epididymal (n=2) SVF adipose cells expressing WT1. E: Percentage of omental (n=3), pericardial (n=1), and epididymal (n=2) SVF adipose cells expressing αSMA. F: Percentage of VSMCs expressing WT1 in omental (n=3), pericardial (n=1), and epididymal (n=2) SVF. Scale bars: 100 µm.*

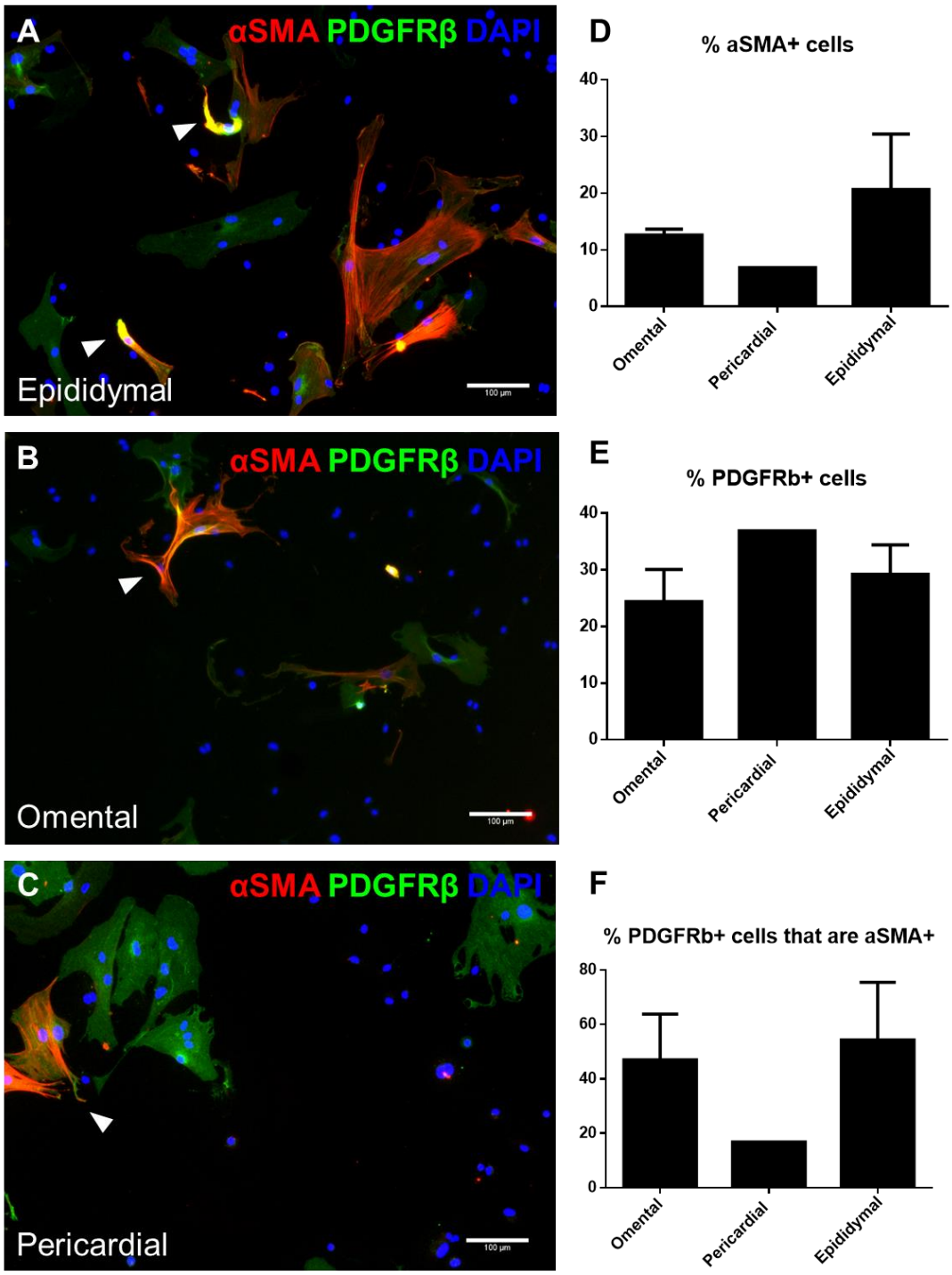

Figure 4.5. Some PDGFRβ+ SVF cells from epididymal, omental, and pericardial adipose tissue express αSMA after being maintained in culture. *Adipose SVF cells isolated from epididymal (A), omental (B), and pericardial (C) adipose tissue stained with αSMA antibody (red), PDFGRβ antibody (green), and DAPI (blue). Arrows indicate co-expression of PDGFRβ and αSMA. D: Percentage of omental (n=2), pericardial (n=1), and epididymal (n=2) SVF adipose cells expressing αSMA. E: Percentage of omental (n=2), pericardial (n=1), and epididymal (n=2) SVF adipose cells expressing PDGFRβ. F: Percentage of PDGFRβ+ cells expressing αSMA in omental (n=2), pericardial (n=1), and epididymal (n=2) adipose tissue. Scale bars: 100 µm.*

4.2.2 The effect of *Cre/loxP*-mediated *Wt1* deletion on tube formation by visceral adipose SVF cells

My next aim was to investigate the effect of *Wt1* deletion on *in vitro* network formation by SVF cells. For this experiment, I selected epididymal and pericardial adipose tissue from $CAG^{CreERT2}$; $Wt1^{loxP/loxP}$ or $CAG^{CreERT2}$; $Wt1^{loxP/GFP}$ mice (further referred to as *Wt1*-deleted cells), as well as an immortalized mouse cardiac endothelial cell (MCEC) line (He et al., 2008). SVF cells were also isolated from CreERT2-negative control mice ($Wt1^{loxP/loxP}$, further referred to as CreERT2- control) and CreERT2-positive control mice ($CAG^{CreERT2}$; $Wt1^{+/+}$, further referred to as CreERT2+ control). As described previously, SVF cells from all three genotypes were maintained in culture until confluent (7 days) and treated with 4-hydroxytamoxifen for 7 days. Cells were subsequently harvested and plated onto wells coated with Matrigel®, in endothelial basal medium (EBM-2), which typically provides the optimal environment for cells to self-assemble into networks of tube-like structures. Images of the assembled networks were acquired 3 hours and 6 hours after seeding.

Figure 4.6 shows images of epididymal SVF-only wells 3 hours (A, C, E) and 6 hours after plating (B, D, F), while figure 4.7 shows epididymal SVF cells co-cultured with MCEC endothelial cells under the same conditions. Pre-quantification, we did not observe any obvious differences between SVF cells deleted for *Wt1* and CreERT2-control cells, as newly formed tube-like structures could be observed in cells isolated from both genotypes (n=3). SVF cells were also co-cultured with MCEC cells in order to investigate whether deleting *Wt1* in SVF cells may have an effect on the signalling between them and endothelial cells. In co-cultures, networks still formed under all three conditions (Figure 4.7). However, we observed that networks formed by epididymal SVF cells isolated from CreERT2+ control mice showed a more disorganized pattern compared to *Wt1*-deleted cells, with more frequent aggregates of cells as opposed to the expected tube-like structures (Figure 4.6, E-F). We observed the same difference between pericardial SVF cells isolated from CreERT2+ control mice and pericardial SVF cells deleted for *Wt1* (Figure 4.8, E-F). However, no obvious differences were present in CreERT2+ control cells co-cultured with MCEC cells (Figure 4.7, E-F; Figure 4.9, E-F).

Having established that SVF can be successfully cultured on Matrigel® membrane both alone and with an endothelial cell line, we sought to quantify the networks formed in order to investigate whether *Wt1* deletion causes a significant difference in

angiogenesis. Before quantifying the effect of *Wt1* deletion on network formation potential, we analysed *Wt1* transcript levels in the knockout and control cells in order to validate our model (Figure 4.10). Both epididymal and pericardial knockout SVF cells showed a reduction in *Wt1* levels compared to the CreERT2- and CreERT2+ control cells. We further quantified the properties of the *in vitro* networks using the Angiogenesis Analyzer plugin for ImageJ (Carpentier and Cascone, 2012). We analysed the number of 'branches' (or tube-like structures), as well as the 'total branching length' (or the total length of the networks) in all conditions (Figures 4.11-4.12). We did not observe any difference between the angiogenic potential of epididymal and pericardial SVF cells deleted for *Wt1* and that of control cells at 3 hours or 6 hours (Figure 4.11). Furthermore, at 3 hours or at 6 hours post-seeding, we did not observe any effect on angiogenesis in co-cultures of MCEC cells and epididymal and pericardial SVF cells deleted for *Wt1* (Figure 4.12).

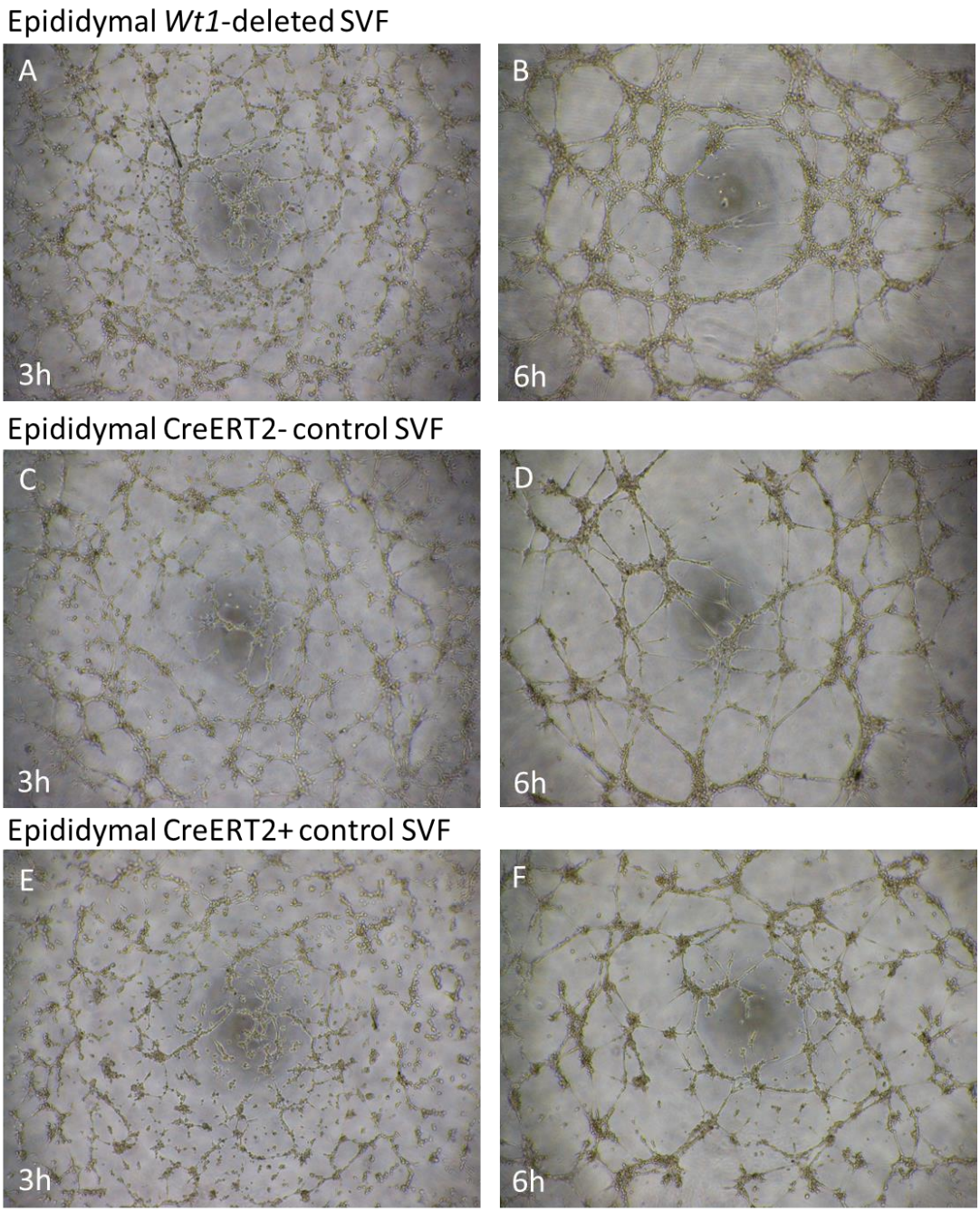

Figure 4.6. The effect of Cre/loxP-mediated Wt1 deletion on tube formation by epididymal SVF cells. *A-B: Tube formation by Wt1-deleted epididymal SVF cells, 3 hours (A) and 6 hours after plating (B). C-D: Tube formation by epididymal SVF cells isolated from CreERT2- control mice, 3 hours (C) and 6 hours after plating (D). E-F: Tube formation by epididymal SVF cells isolated from CreERT2+ control mice, 3 hours (E) and 6 hours after plating (F). n=3 across all conditions. Brightfield images acquired at 4X magnification.*

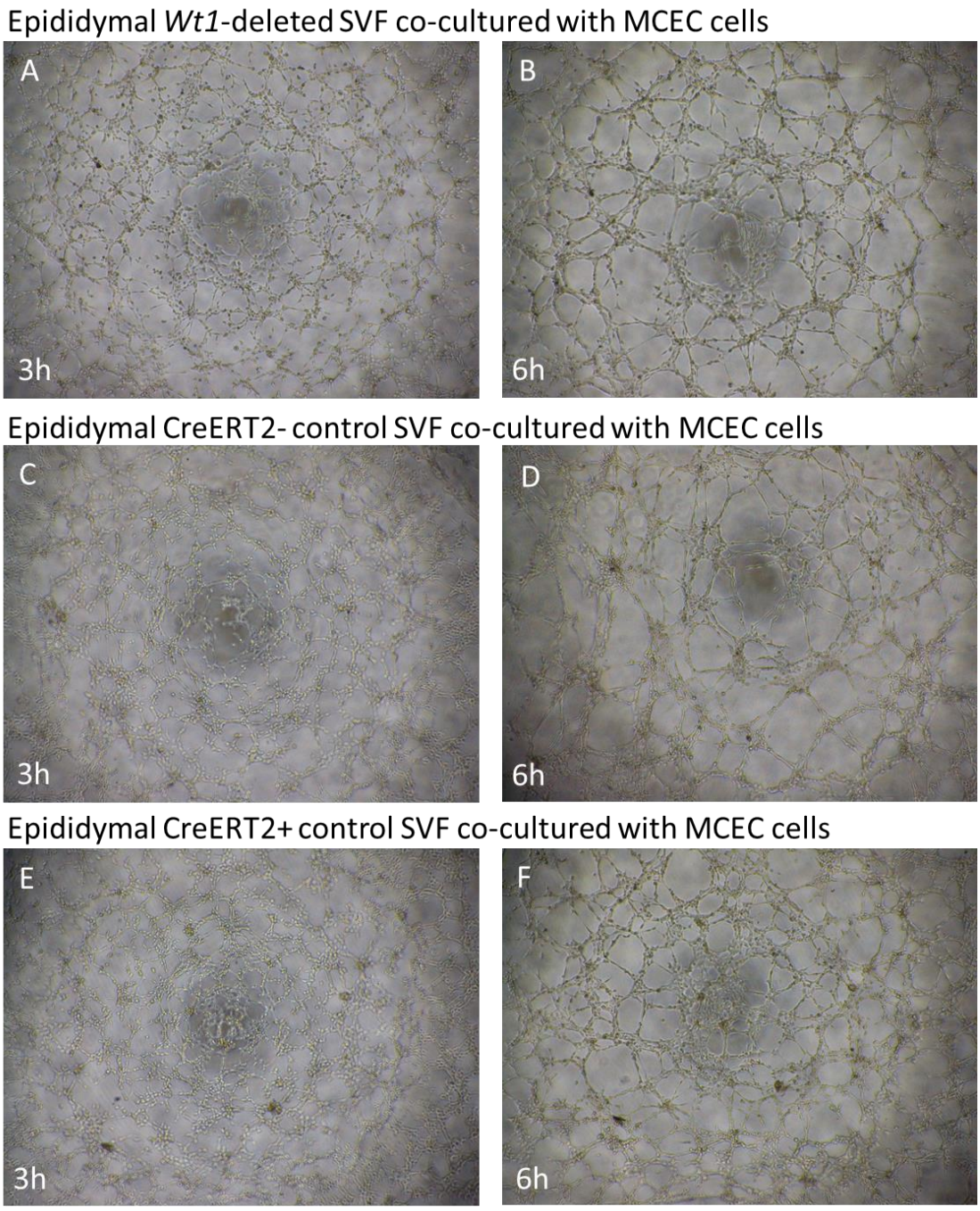

Figure 4.7. The effect of Cre/loxP-mediated Wt1 deletion on tube formation by epididymal SVF cells co-cultured with MCEC cells. *A-B: Tube formation by Wt1-deleted epididymal SVF cells co-cultured with MCEC cells, 3 hours (A) and 6 hours after plating (B). C-D: Tube formation by epididymal SVF cells isolated from CreERT2- control mice co-cultured with MCEC cells, 3 hours (C) and 6 hours after plating (D). E-F: Tube formation by epididymal SVF cells isolated from CreERT2+ control mice co-cultured with MCEC cells, 3 hours (E) and 6 hours after plating (F). n=3 across all conditions. Brightfield images acquired at 4X magnification.*

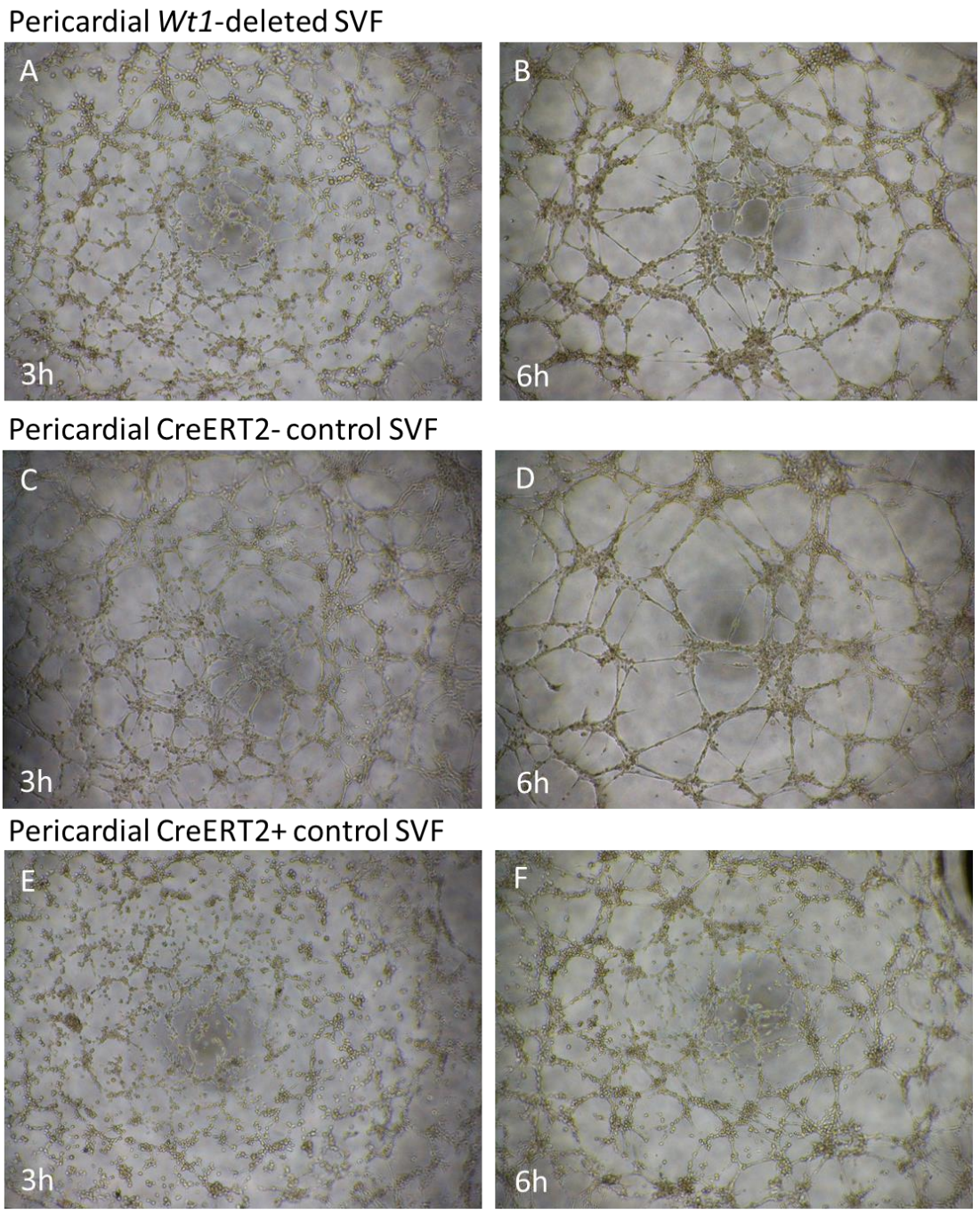

Figure 4.8. The effect of Cre/loxP-mediated Wt1 deletion on tube formation by pericardial SVF cells. *A-B: Tube formation by Wt1-deleted pericardial SVF cells, 3 hours (A) and 6 hours after plating (B). C-D: Tube formation by pericardial SVF cells isolated from CreERT2- control mice, 3 hours (C) and 6 hours after plating (D). E-F: Tube formation by pericardial SVF cells isolated from CreERT2+ control mice, 3 hours (E) and 6 hours after plating (F). n=3 across all conditions. Brightfield images acquired at 4X magnification.*

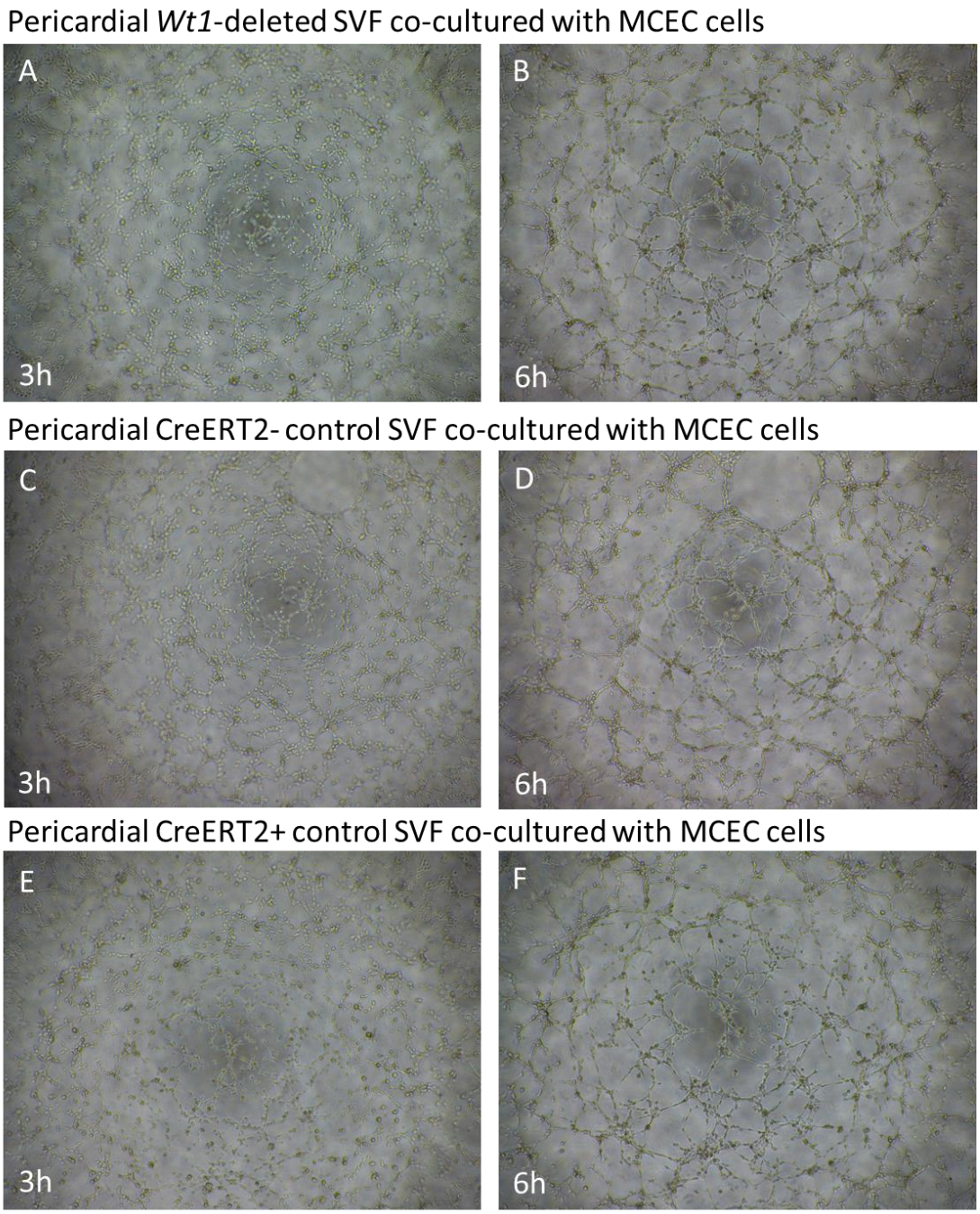

Figure 4.9. The effect of Cre/loxP-mediated Wt1 deletion on tube formation by pericardial SVF cells co-cultured with MCEC cells. *A-B: Tube formation by Wt1-deleted pericardial SVF cells co-cultured with MCEC cells, 3 hours (A) and 6 hours after plating (B). C-D: Tube formation by pericardial SVF cells isolated from CreERT2- control mice co-cultured with MCEC cells, 3 hours (C) and 6 hours after plating (D). E-F: Tube formation by pericardial SVF cells isolated from CreERT2+ control mice co-cultured with MCEC cells, 3 hours (E) and 6 hours after plating (F). n=3 across all conditions. Brightfield images acquired at 4X magnification.*

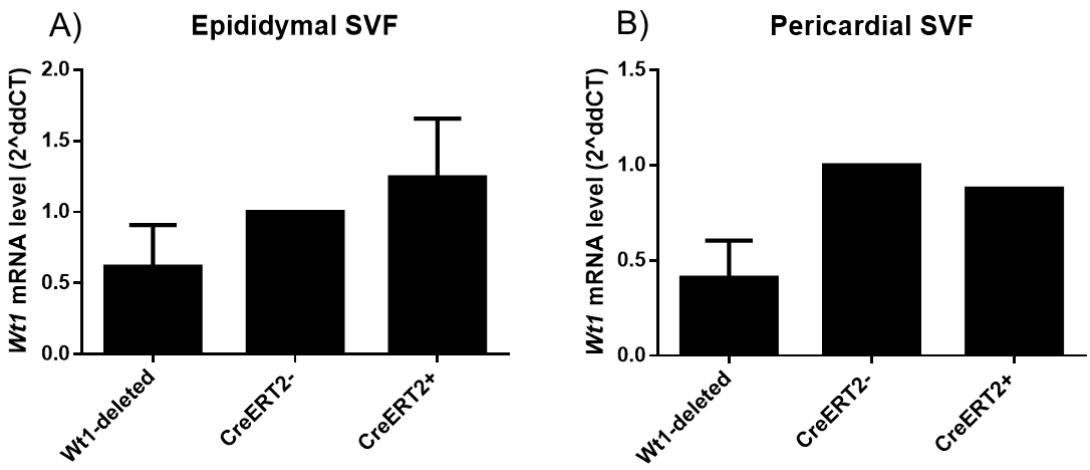

Figure 4.10. qPCR analysis to validate Cre/loxP-mediated Wt1 knockdown in epididymal and pericardial SVF treated with 4-hydroxytamoxifen. *Wt1 mRNA levels in Wt1-deleted and CreERT2+ control cells from epididymal SVF (A) and pericardial SVF (B) were normalized to Wt1 levels in CreERT2- control cells. Wt1 mRNA levels were reduced in Wt1-deleted cells compared to CreERT2- cells in epididymal (p=0.320518559) and pericardial (p=0.09412) samples (n=3; error bars represent the SEM).*

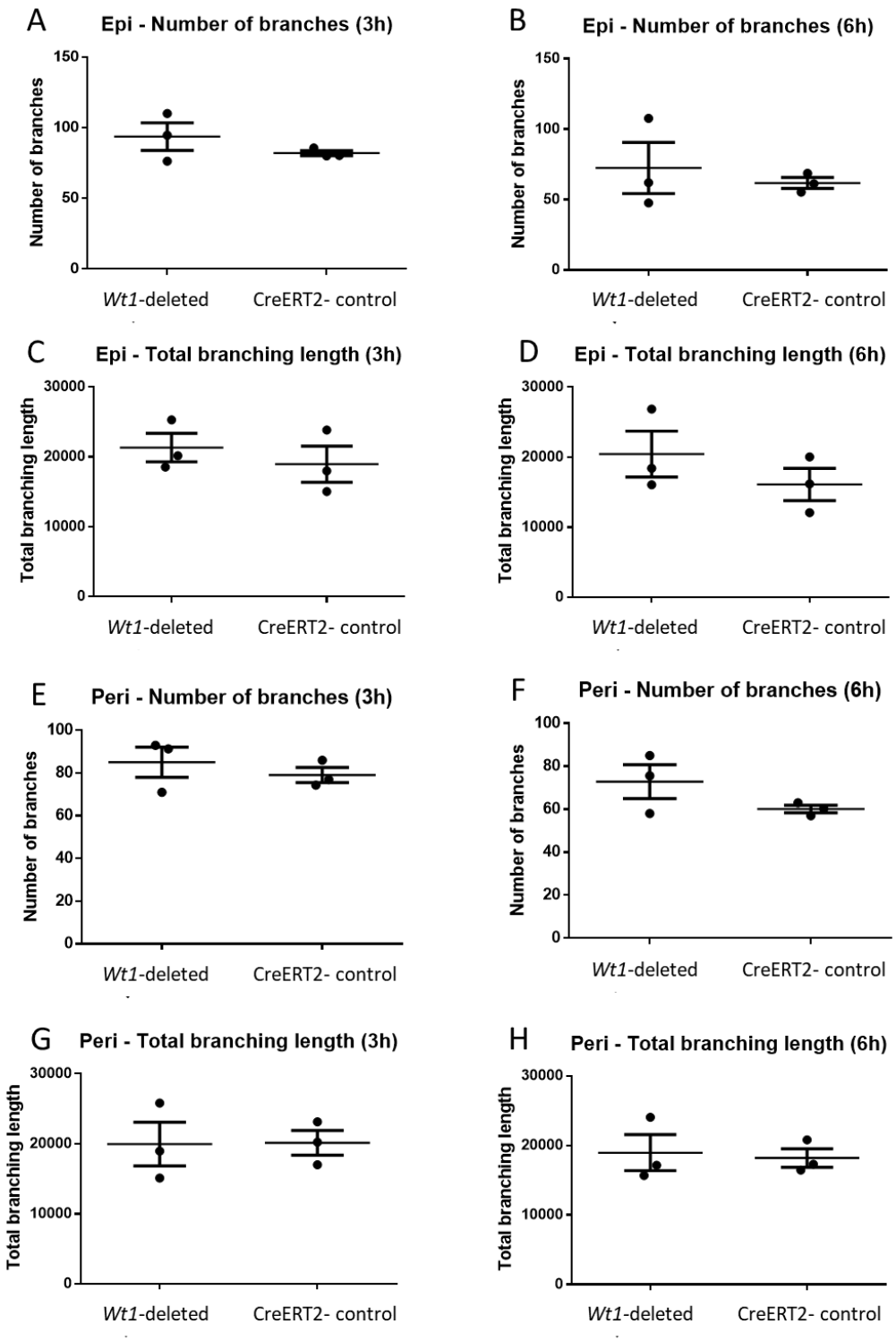

Figure 4.11. Quantification of network formation potential of epididymal and pericardial SVF cells using Angiogenesis Analyzer. *For each condition, the number of 'branches' (or tubes) formed and the length of the network were quantified. A-D: No significant differences were observed in the network formation potential of Wt1-deleted epididymal SVF cells at 3 hours and 6 hours (n=3). E-H: No significant differences were observed in the network formation potential of Wt1-deleted pericardial SVF cells at 3 hours and 6 hours (n=3). Results of statistical analysis are outlined in Table A.3 (Appendix)*

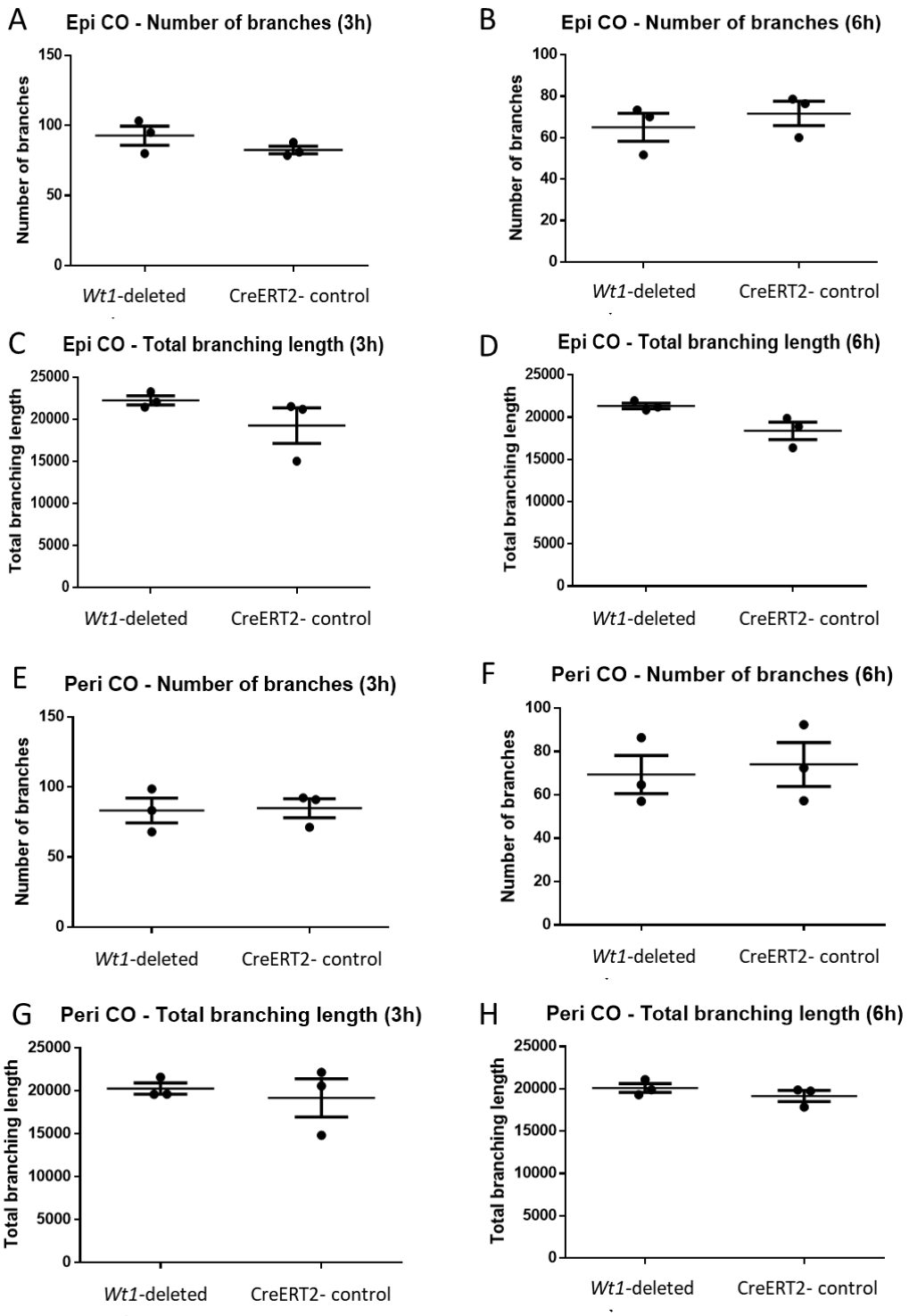

Figure 4.12. Quantification of network formation potential of epididymal and pericardial SVF cells co-cultured with MCEC cells. *For each condition, the number of 'branches' (or tubes) formed and the length of the network were quantified. A-D: No significant differences were observed in the network formation potential of Wt1-deleted epididymal SVF cells co-cultured with MCEC cells at 3 hours and 6 hours (n=3). E-H: No significant differences were observed in the network formation potential of Wt1-deleted pericardial SVF cells co-cultured with MCEC cells at 3 hours and 6 hours (n=3). Results of statistical analysis are outlined in Table A.3 (Appendix)*

4.2.3 CreERT2 toxicity effects on tube formation potential and gene expression of epididymal and pericardial SVF cells

As shown before, assessing the angiogenic potential of SVF cells alone and in co-cultures did not show significant differences between mutant and CreERT2- control cells. However, when observing the behaviour of mutant and control cells, we saw that the networks formed by pericardial CreERT2+ control cells did not seem to be as orderly as those formed by CreERT2- or *Wt1*-deleted cells (Figure 4.8, E-F). Moreover, we noticed slightly lower levels of *Wt1* mRNA in pericardial CreERT2+ control cells treated with 4-hydroxytamoxifen than in Cre- cells (Figure 4.10, B).

We therefore hypothesised that CreERT2 has a deleterious effect on pericardial cells *in vitro*. We first compared network formation in CreERT2- control cells and CreERT2+ control cells. Figure 4.13 shows network formation in pericardial SVF cells 3 hours (A, C) and 6 hours (B, D) after plating, with the overlays generated by the Angiogenesis Analyzer ImageJ plugin. Networks formed by CreERT2+ cells appeared to be less robust and more disorganized compared to our controls. Furthermore, this was mirrored in the number of isolated segments, i.e. segments not connected to larger branches (Figure 4.13, E-F). At both timepoints, networks formed by CreERT2+ cells presented more isolated segments than those formed by CreERT2- control cells (n=3). Similar effects were observed in epididymal SVF cells as well (data not shown).

We also aimed to assess whether CreERT2 has any effects on the expression of other genes in pericardial adipose SVF cells *in vitro*. Pericardial SVF cells isolated from $CAG^{CreERT2}$; $Wt1^{loxP/loxP}$,, $CAG^{CreERT2}$ and wild-type mice were expanded in culture for 7 days (until confluent) and treated with 4-hydroxytamoxifen throughout. Cells were then harvested and total RNA was used for gene expression analysis. Figure 4.14, A shows the expression of *Wt1* in *Wt1*-deleted, CreERT2+ control cells and wild-type cells when treated with 4-hydroxytamoxifen and with 100% EtOH (as vehicle control). As expected, *Wt1*-deleted cells showed a reduction in *Wt1* levels after treatment with 4-hydroxytamoxifen, while in wild-type cells the expression of *Wt1* was not affected by the presence of 4-hydroxytamoxifen (Figure 4.14, A). However, CreERT2+ control cells treated with 4-hydroxytamoxifen also showed a reduction in *Wt1* levels (Figure 4.14, A). We further looked into the expression of several inflammation-related genes previously identified as WT1 targets in our lab (unpublished data). We selected 5 genes: C-X-C Motif Chemokine Ligand 5 (CXCL5), decorin (DCN), interferon regulatory factor 7 (IRF7), pleiotrophin (PTN), and Regulator of G-protein signaling 5

(RGS5). Upon CreERT2 activation in CreERT2+ control cells, we noticed changes in the expression of all 5 genes, with higher levels of *CXCL5, DCN, IRF7* and *RGS5* in 4-hydroxytamoxifen-treated cells than in vehicle controls (Figure 4.14, B, C, D, F) and lower levels of *PTN* after CreER activation (Figure 4.14, E). Moreover, we observed changes in the expression of *DCN* and *PTN* in *Wt1*-deleted cells (Figure 4.14, B-F).

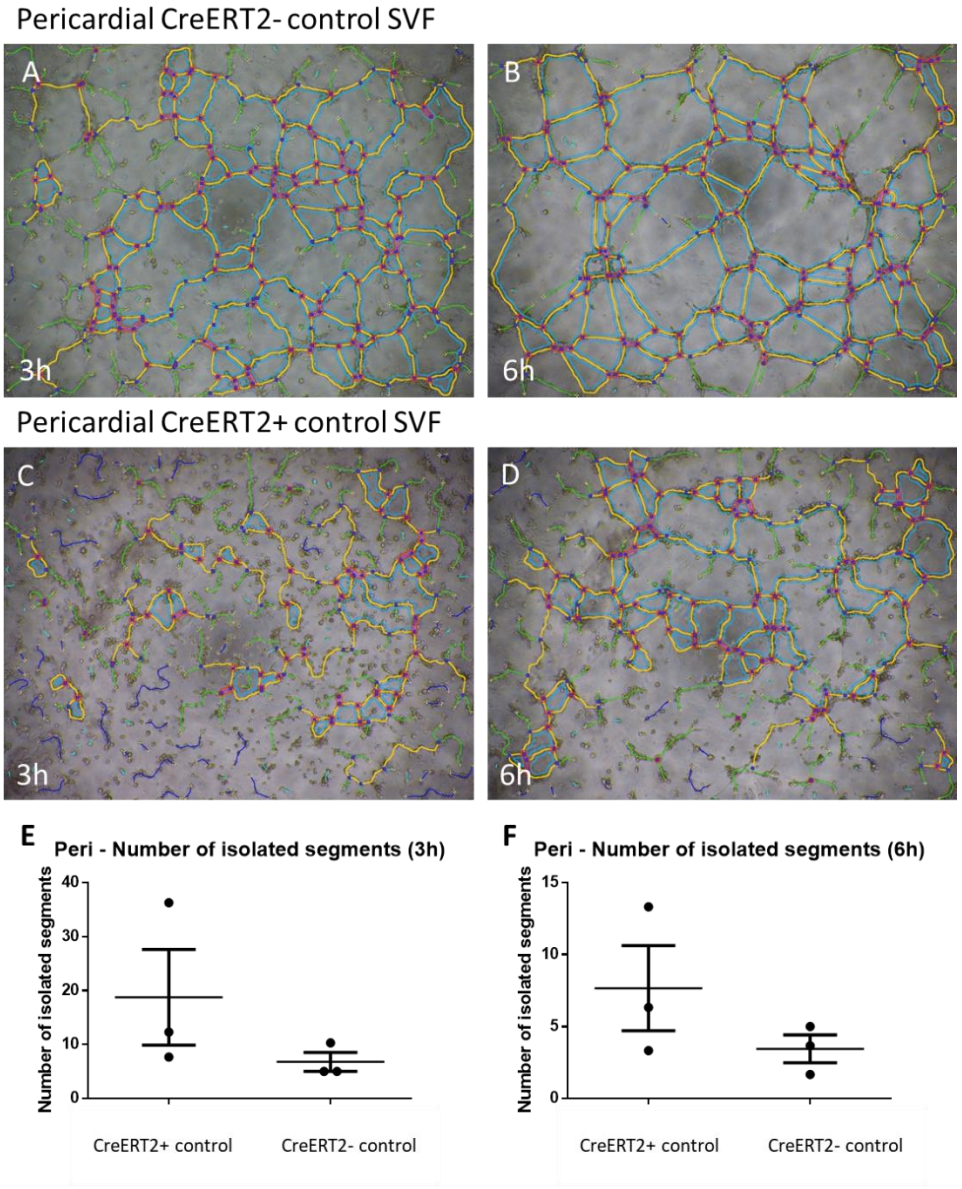

Figure 4.13. The effect of CreERT2 on in vitro tube formation by pericardial SVF cells. *A-B: Networks formed by pericardial CreERT2- control cells 3 hours after plating (A) and 6 hours after plating (B). C-D: Networks formed by pericardial CreERT2+ control cells 3 hours (C) and 6 hours (D) after plating. E-F: Quantification of isolated segments in CreERT2- and CreERT+ control pericardial cells 3 hours (E, p=0.25) and 6 hours (F, p=0.24) after plating (n=3).*

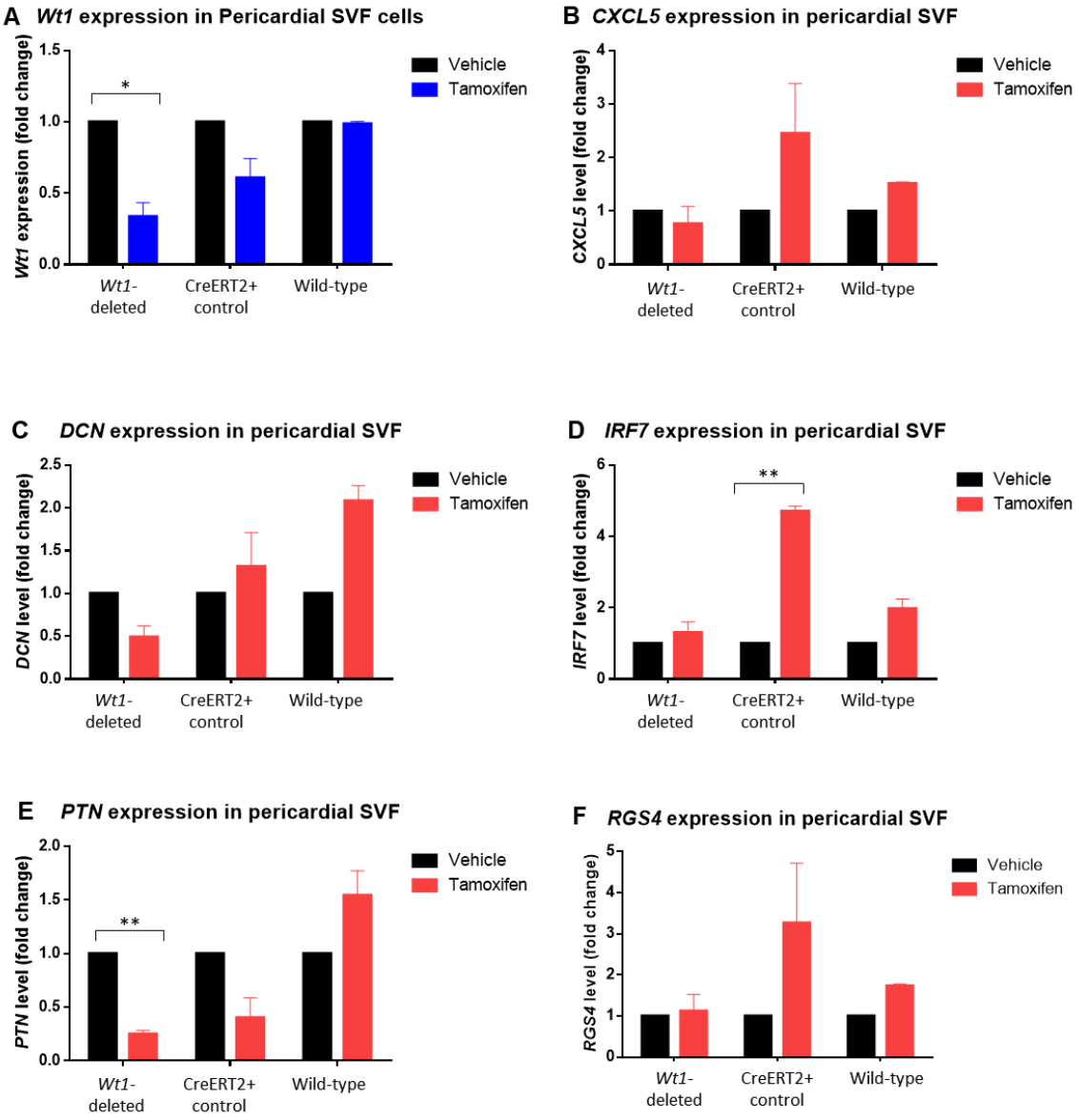

Figure 4.14. The effect of CreERT2 on the expression of inflammation genes in pericardial SVF cells. *A: Wt1 mRNA levels in pericardial adipose Wt1-deleted SVF cells, CreERT2+ control cells, and wild-type mice (n=3). B-F: Gene expression levels of Cxcl5, Dcn, Irf7, Ptn and Rgs5 in Wt1-deleted, CreERT2+ control cells and wild-type cells (n=3). Results of statistical analysis are detailed in Table A.4 (Appendix)*

4.2.4 The effect of RNAi-mediated *Wt1* deletion on tube formation by visceral adipose SVF cells

In light of the *in vitro* data from experiments using the *Cre/loxP* system, we further looked into the effects of *Wt1* deletion using RNA interference. We used a short interfering RNA (siRNA) against *Wt1* in SVF cells isolated from the epididymal, pericardial and omental adipose tissue of wild-type C57BL/6 mice. Figure 4.15 shows *Wt1* levels in cells treated with an anti-*Wt1* siRNA, as well as in cells treated with scramble control siRNA and transfection reagent only. As expected, cells treated with siRNA against *Wt1* showed a reduction in *Wt1* mRNA levels in epididymal (figure 4,15, A), pericardial (Figure 4.15, B) and omental (Figure 4.15, C) SVF cells, with knockdown cells from all 3 depots showing a reduction in *Wt1* expression of at least 75%.

To confirm that the *Wt1* deletion is also reflected at protein level, immunofluorescence was also performed on cells treated with siRNA against *Wt1.* Wild-type epididymal, omental, and pericardial cells cultured *in vitro* were treated with anti-*Wt1* siRNA, scramble control siRNA and HiPerfect transfection reagent and were stained with anti-WT1 and anti-PDGFRβ antibodies (Figure 4.16). In Figure 4.16, panels A-D show representative images of epididymal SVF cells deleted for *Wt1* (A), as well as images of the relevant controls – scramble control (B), mock transfection control (C), and untreated cells (D). All controls showed cells positive for WT1 and/or cells where WT1 and PDGFRβ are co-expressed, whereas knockdown cells showed visibly fewer WT1+ cells. Figure 4,16, E-J further shows the percentage of WT1+ cells in omental (E), pericardial (F), and epididymal SVF cells (G), as well as the percentage of PDGFRβ+ cells expressing WT1 in omental (H), pericardial (I), and epididymal SVF (J). In omental SVF, less than 1% of cells expressed WT1 after knockdown, while this percentage ranged between 2 and 5% in our controls; moreover, only around 2%of PDGFRβ+ cells were positive for WT1 after knockdown, compared to 10–20% in controls (Figure 4.16, E, H). In pericardial SVF cells, only around 2% of cells expressed WT1 after incubation with anti-*Wt1* siRNA, compared to 5-13% in controls, and only around 5% of PDGFRβ+ cells were WT1+ after knockdown, compared to 20-50% in our controls (Figure 4.16, F, I). Similarly, only 2% of knockdown epididymal SVF cells were positive for WT1, compared to 6-8% in controls, whereas under 5% of PDGFRβ+ cells were WT1+, compared to 15-25% in controls (Figure 4.16, G, J).

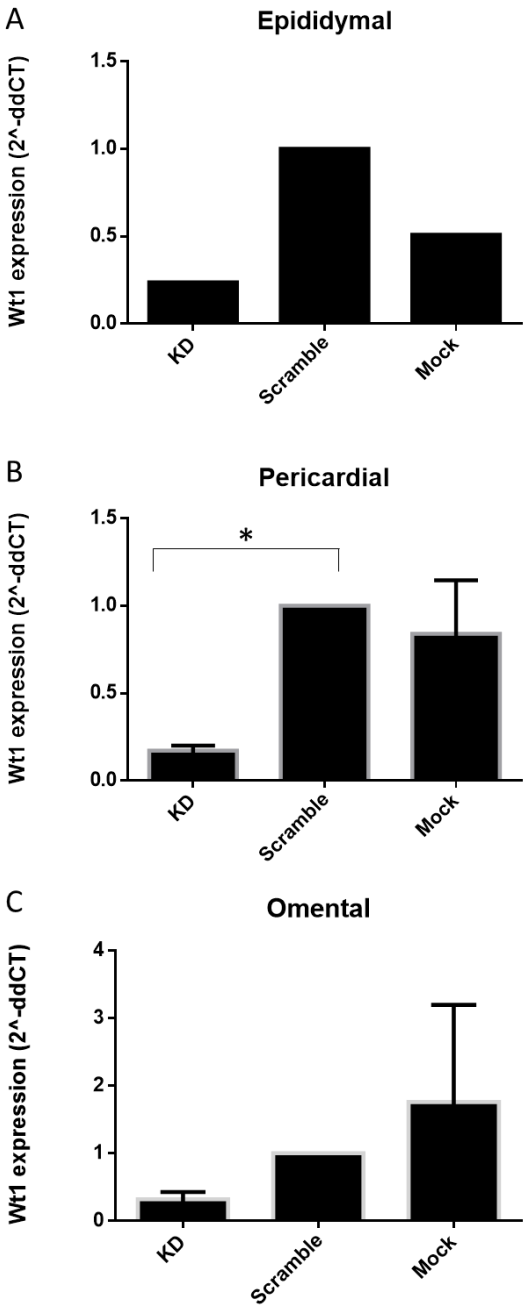

Figure 4.15. Validation of RNAi-mediated Wt1 knockdown in epididymal, pericardial, and omental SVF. *Wt1 mRNA levels in KD (Wt1-deleted) and mock transfection control cells from epididymal SVF (A, n=1), pericardial SVF (B, n=3), and omental SVF (C, n=3) were normalized to Wt1 levels in control cells treated with a scramble siRNA. Wt1 knockdown was significant in pericardial (p=0.011) KD cells compared to scramble control and close to statistical significance in omental KD cells (p=0.05).*

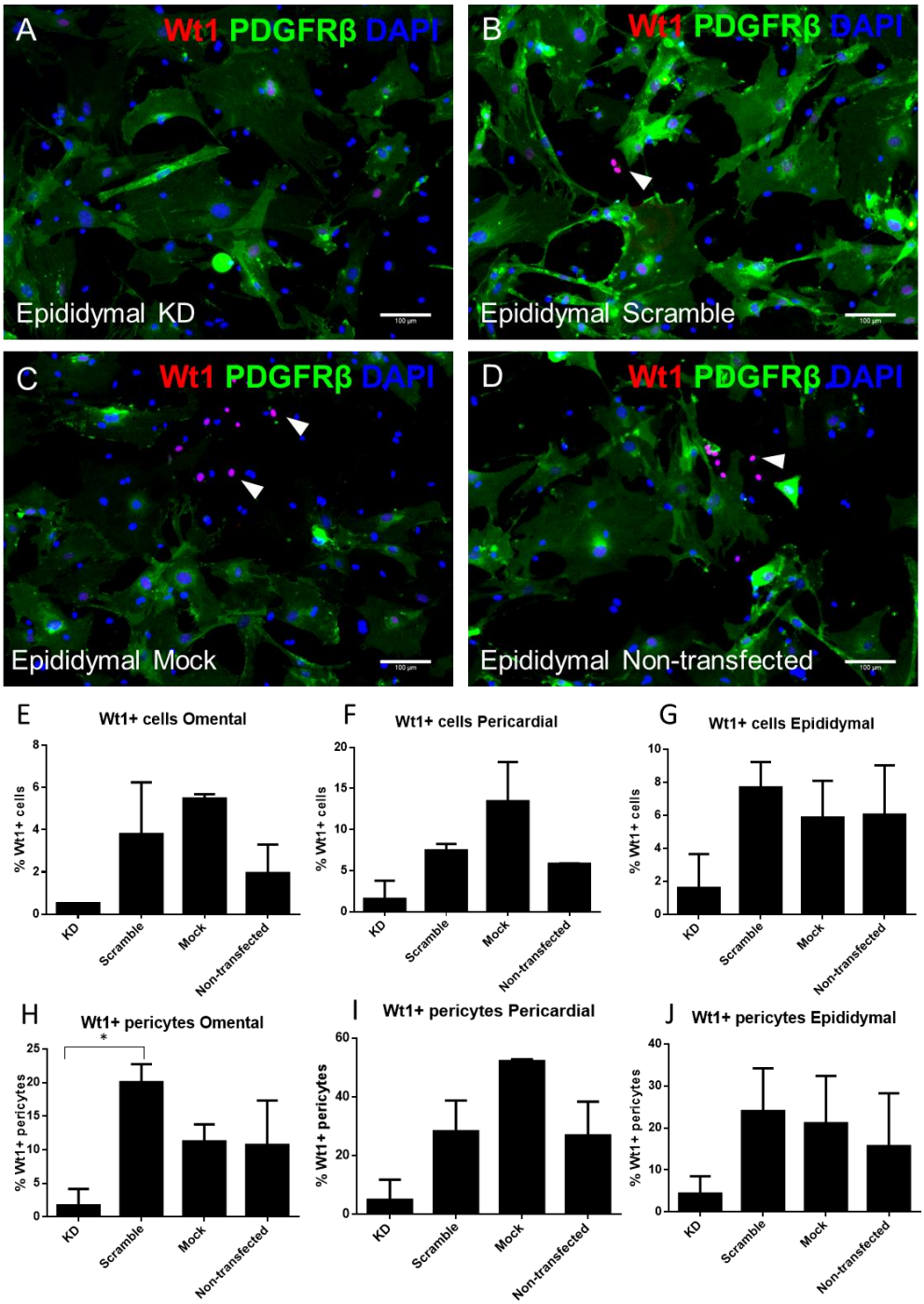

Figure 4.16. Validation of RNAi-mediated Wt1 knockdown in cultured SVF cells from epididymal, pericardial, and omental adipose tissue. *A-D. Representative images of epididymal SVF cells in culture after RNAi-mediated knockdown. WT1+ cells are indicated by white arrows; scale bars: 100 µm. E, H. Percentage of WT1+ cells and WT1+ pericytes in omental adipose tissue in knockdown cells and control cells (n=2). F, I. Percentage of WT1+ cells and WT1+ pericytes in pericardial adipose tissue in knockdown cells and control cells (n=2). G, J. Percentage of WT1+ cells and WT1+ pericytes in epididymal adipose tissue in knockdown cells and control cells (n=3). Results of statistical analysis are detailed in Table A.5 (Appendix)*

Having observed a reduction in *Wt1* transcript in all 3 depots, both at gene expression and protein expression levels, we further looked into the effect of siRNA-mediated *Wt1* knockdown on the *in vitro* angiogenic potential of omental, pericardial and epididymal adipose SVF cells. Cells were isolated and expanded in culture for one passage as before, subsequently transfected with siRNA against *Wt1*, scramble control siRNA or no siRNA, and finally used for tube formation assays on Matrigel®.

Figure 4.17 shows knockdown (A) and control (B-D) epididymal SVF cells 3 hours after plating. No visible difference in angiogenic potential was observed 3 hours after seeding. Moreover, quantification of total branches and branching length using the Angiogenesis Analyzer plugin for ImageJ (Carpentier and Cascone, 2012) revealed no significant differences in network formation by knockdown cells and control cells (n=1, Figure 4.17, E-F). Similarly, 6 hours after plating, epididymal SVF cells deleted for *Wt1* formed networks similar to those assembled by control cells (Figure 4.18, A-D) and the number of branches and total branching length were not significantly altered in knockdown cells (n=1, Figure 4.18, E-F).

We performed the same knockdown protocol and assay on pericardial adipose SVF cells. Figure 4.19 (A-D) shows representative images of networks formed by pericardial cells deleted for *Wt1,* as well as control cells, 3 hours after plating. No visible differences are present between the four cell populations, which is mirrored by the quantification of branches and branching length (Figure 4.19, E-F). Similarly, no significant differences were observed between knockdown and control cells at 6 hours (Figure 4.20).

Finally, we looked into the *in vitro* angiogenic potential of omental adipose SVF cells deleted for *Wt1.* Figure 4.21 (A-D) shows representative images of knockdown cells (A), as well as scramble control cells (B), mock transfection control cells (C), and non-transfected cells (D), 3 hours after plating. Similarly to epididymal and pericardial adipose SVF, no visible differences were observed in the networks formed by knockdown cells compared to control cells (Figure 4.21, E-F). Figure 4.22 (A-D) further shows the same cells 6 hours after plating. Again, no visible differences were observed in the networks formed by cells deleted for *Wt1* (Figure 4.22, E-F).

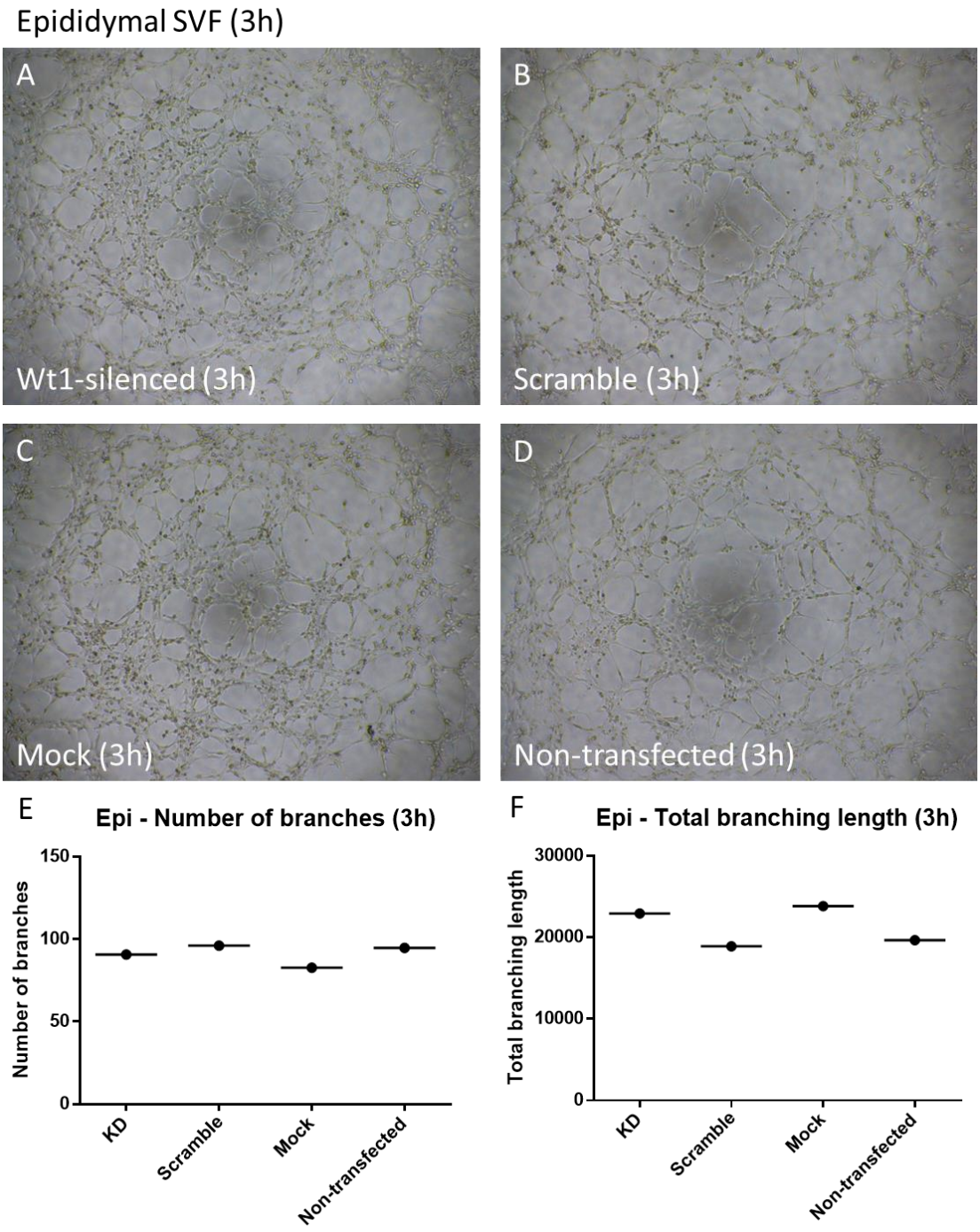

Figure 4.17. The effect of RNAi-mediated Wt1 deletion on tube formation by epididymal SVF cells 3 hours post-seeding. *For each condition, the number of 'branches' (or tubes) formed and the length of the network were quantified. Network formation by epididymal SVF cells deleted for Wt1 (A), treated with scramble control siRNA (B), mock transfection control cells (C), and non-transfected cells (D). No significant differences in network formation were observed 3 hours after plating (E-F, n=1). Brightfield images were acquired at 4X magnification.*

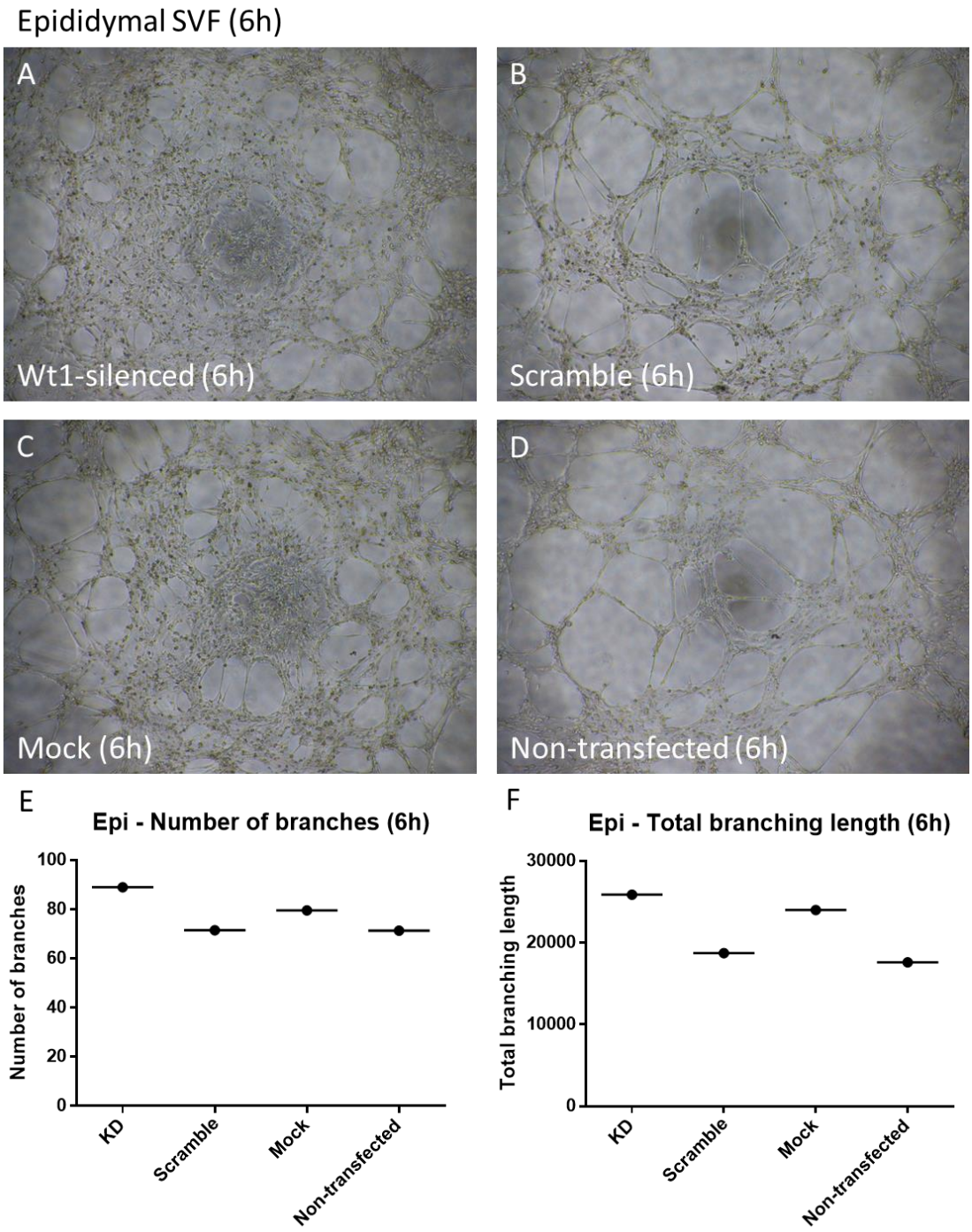

Figure 4.18. The effect of RNAi-mediated Wt1 deletion on tube formation by epididymal SVF cells 6 hours post-seeding. *For each condition, the number of 'branches' (or tubes) formed and the length of the network were quantified. Network formation by epididymal SVF cells deleted for Wt1 (A), treated with scramble control siRNA (B), mock transfection control cells (C), and non-transfected cells (D). No significant differences in network formation were observed 6 hours after plating (E-F, n=1). Brightfield images were acquired at 4X magnification.*

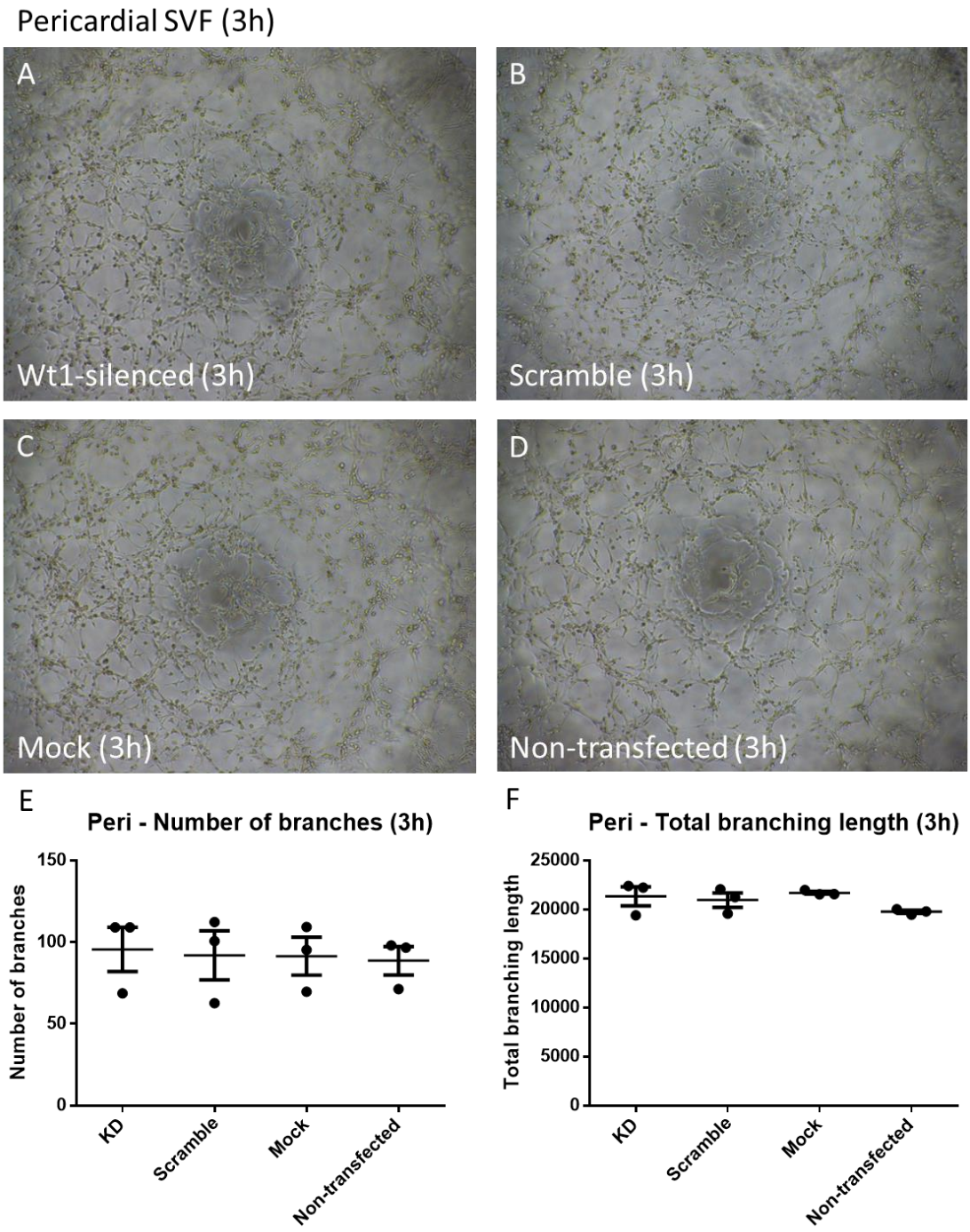

Figure 4.19. The effect of RNAi-mediated Wt1 deletion on tube formation by pericardial SVF cells 3 hours post-seeding. *For each condition, the number of 'branches' (or tubes) formed and the length of the network were quantified. Network formation by pericardial SVF cells deleted for Wt1 (A), treated with scramble control siRNA (B), mock transfection control cells (C), and non-transfected cells (D). No significant differences were observed in the number of branches (p=0.41) or total branching length (p=0.43) between KD and Scramble control cells 3 hours after plating (E-F, n=3). Brightfield images were acquired at 4X magnification.*

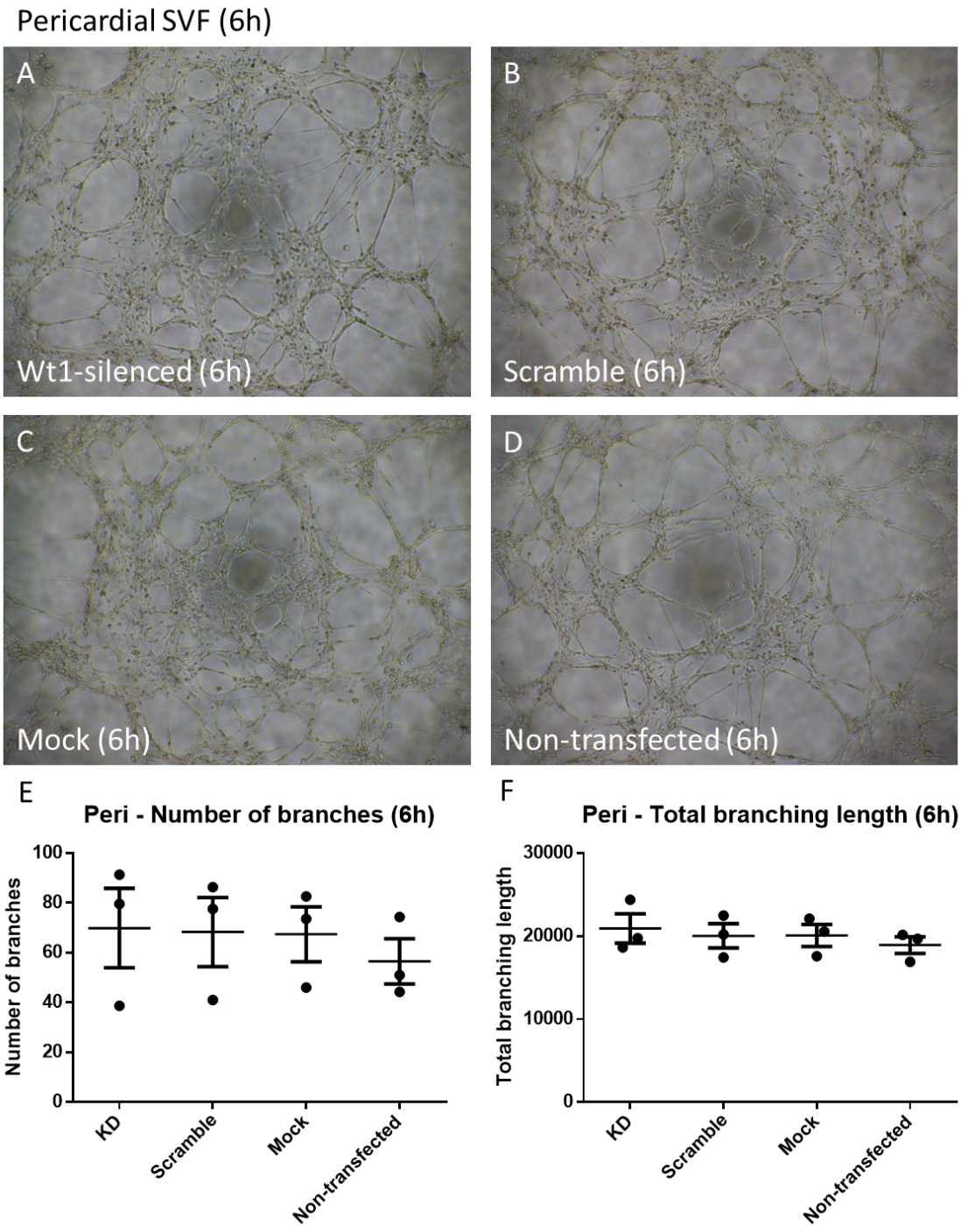

Figure 4.20. The effect of RNAi-mediated Wt1 deletion on tube formation by pericardial SVF cells 6 hours post-seeding. *For each condition, the number of 'branches' (or tubes) formed and the length of the network were quantified. Network formation by pericardial SVF cells deleted for Wt1 (A), treated with scramble control siRNA (B), mock transfection control cells (C), and non-transfected cells (D). No significant differences were observed in the number of branches (p=0.54) or total branching length (p=0.33) between KD and Scramble control cells 6 hours after plating (E-F, n=3). Brightfield images were acquired at 4X magnification.*

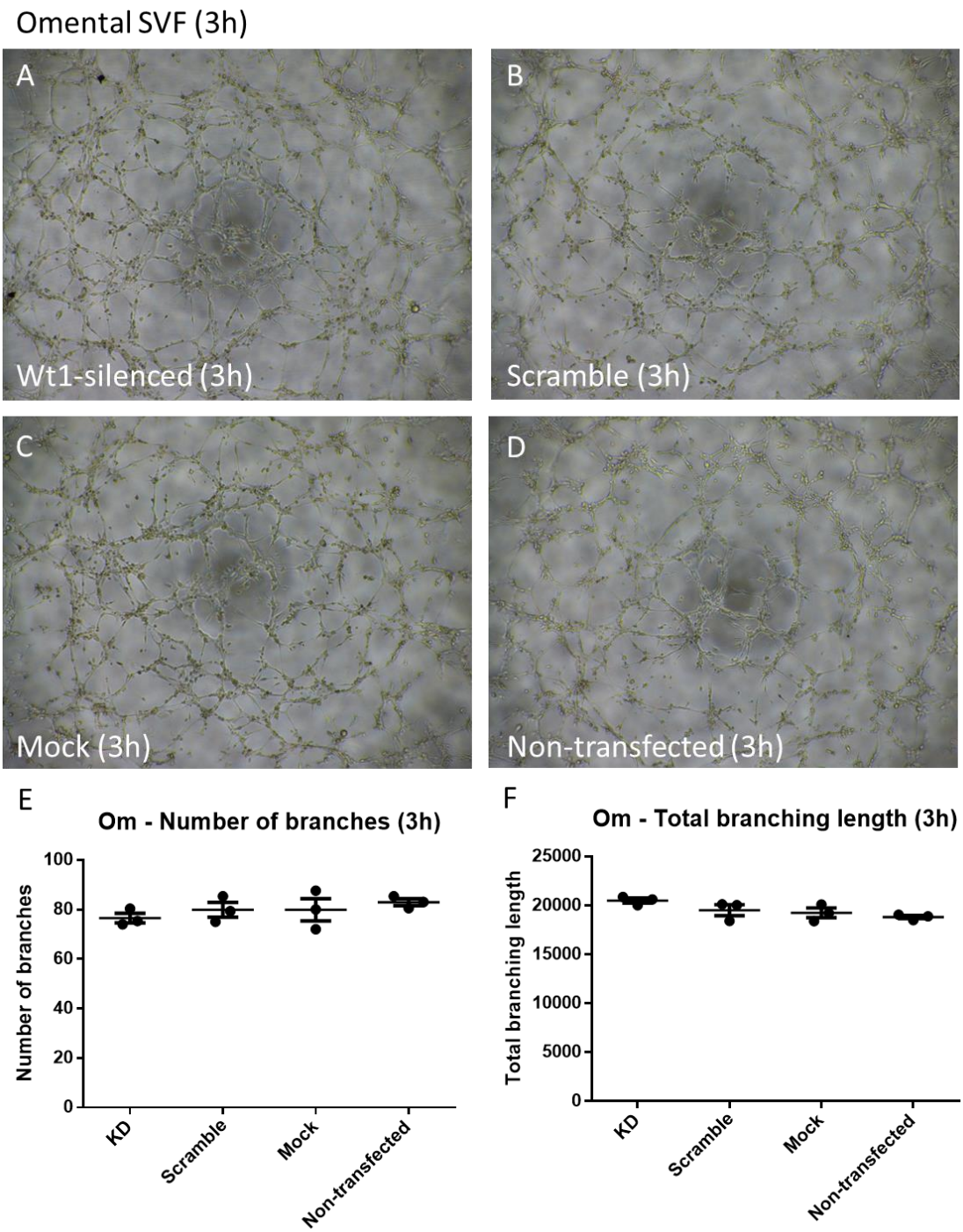

Figure 4.21. The effect of RNAi-mediated Wt1 deletion on tube formation by omental SVF cells 3 hours post-seeding. *For each condition, the number of 'branches' (or tubes) formed and the length of the network were quantified. Network formation by omental SVF cells deleted for Wt1 (A), treated with scramble control siRNA (B), mock transfection control cells (C), and non-transfected cells (D). No significant differences were observed in the number of branches (p=0.56) or total branching length (p=0.09) between KD and Scramble control cells 3 hours after plating (E-F, n=3). Brightfield images were acquired at 4X magnification.*

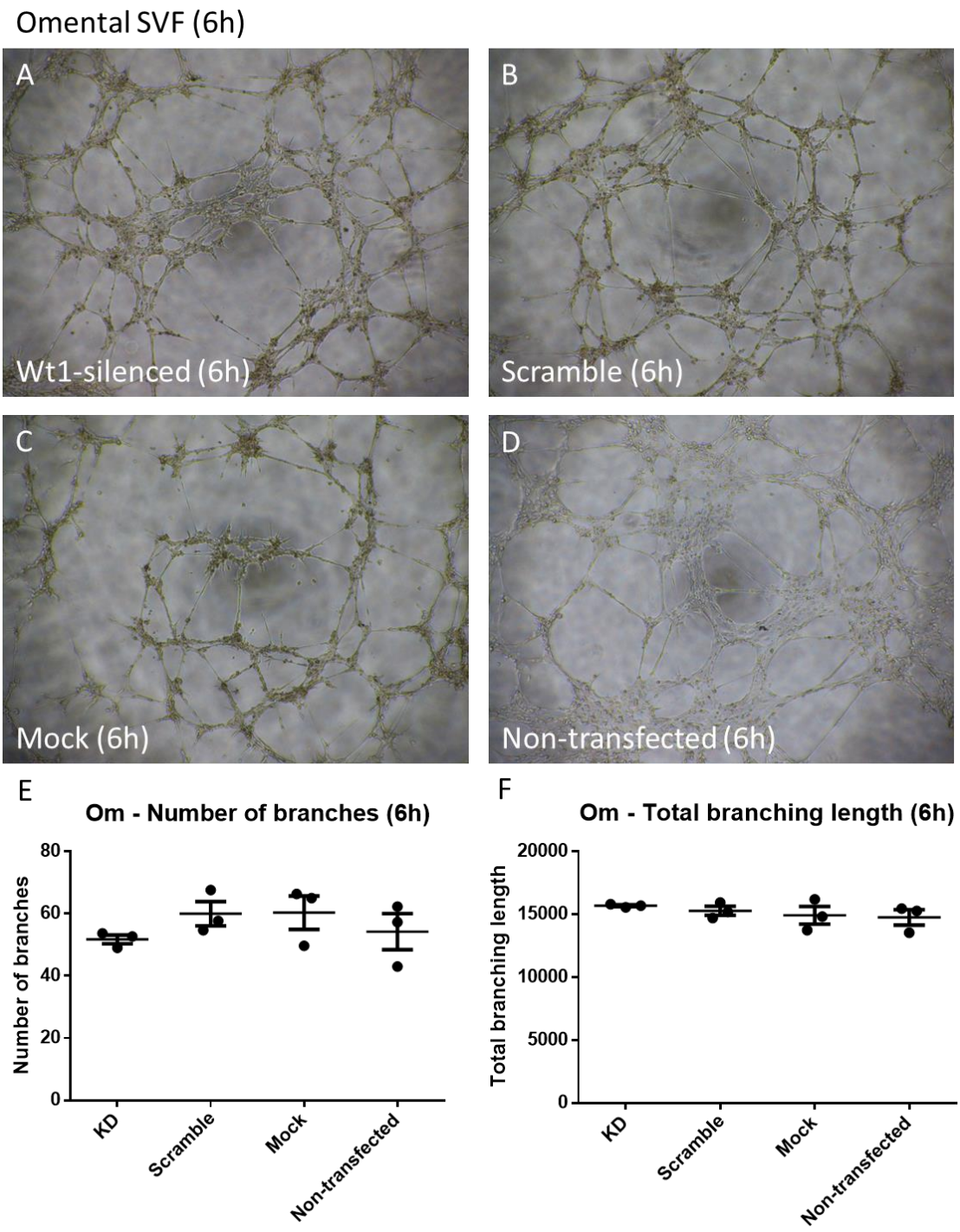

Figure 4.22. The effect of RNAi-mediated Wt1 deletion on tube formation by omental SVF cells 6 hours post-seeding. *For each condition, the number of 'branches' (or tubes) formed and the length of the network were quantified. Network formation by omental SVF cells deleted for Wt1 (A), treated with scramble control siRNA (B), mock transfection control cells (C), and non-transfected cells (D). No significant differences were observed in the number of branches (p=0.25) or total branching length (p=0.29) 6 hours after plating (E-F, n=3). Brightfield images were acquired at 4X magnification.*

4.3 Discussion

WT1 has been shown to be expressed in several vascular cell populations, both in humans and in mice. WT1 is not only expressed in cardiac and tumour ECs (Duim et al., 2015), but is actively involved in EC proliferation and migration in the tumour vasculature (Wagner et al., 2008a). WT1 is also expressed in human SMCs, where it is upregulated during the non-proliferative state of the cells (Small et al., 2006). Although WT1 expression in adipose pericytes has not been described before, the results discussed in the previous chapter showed WT1 expression in pericytes isolated from 5 visceral adipose depots. Moreover, *Wt1* knockdowns have shown to impair angiogenesis both *in vitro* and *in vivo* (Wagner et al., 2014, 2008a).

With this in mind, the experiments detailed above aimed to firstly describe WT1 expression in the cell sub-populations selected through standard adipose SVF isolation methods. Second, we performed *Wt1* deletions in epididymal and pericardial adipose SVF cells isolated from *CAG^{CreERT2}; Wt1$^{loxP/loxP}$* mice, and analysed the effect of these deletions on the *in vitro* network formation potential. Given that we observed a potential toxic effect of CreER in these cells, we then assessed the impact of *Wt1* deletions on *in vitro* angiogenesis using an alternative RNAi deletion model. RNAi-mediated knockdowns also showed no significant effect on network formation *in vitro*.

4.3.1 Standard cell culture methods used for adipose SVF select for cells expressing pericyte, VSMC, and myofibroblast markers, but not for endothelial cells

The isolation of SVF cells from murine or human adipose depots has been described previously (Senesi et al., 2019). Moreover, isolating cells based on adherence alone has been shown to select for cells expressing mesenchymal stem cell markers (Bieback et al., 2008). In my experiments, I further stained SVF cells (both freshly isolated and adherent) with antibodies against WT1 and the vascular cell markers CD31 (for endothelial cells), PGDFRβ (pericytes) and αSMA (VSMCs). We found that, in all three depots analysed (epididymal, omental, and pericardial), PGDFRβ+ cells make up a lot more of the freshly isolated GFP+Lin-cKit- population than CD31+ cells do. Moreover, after attachment to cell culture plates, we did not detect any CD31 expression in SVF cells from either depot, but did observe PGDFRβ and αSMA expression, confirming that subsequent experiments may indicate the role of WT1 in pericytes and VSMCs. Studies in ECs have previously shown that *Wt1* deletion can significantly impair angiogenic potential (Wagner et al., 2014, 2008). However, knowledge on the function of WT1 in perivascular cells is limited, except for studies

showing the role of WT1 in the formation of cardiovascular progenitor cells (Martínez-Estrada et al., 2010). While our flow cytometry analysis showed WT1 expression in a large proportion of omental and pericardial pericytes, we nevertheless observed that the percentage of WT1+ cells decreased after expansion in culture.

4.3.2 *Cre/loxP*-mediated *Wt1* deletion does not alter the *in vitro* angiogenic potential of epididymal and pericardial SVF cells

In our two-dimensional assays, we found that *Cre/loxP*-mediated *Wt1* deletion in pericardial and epididymal SVF cells did not significantly alter their *in vitro* network formation potential. A role here may be played by the potential CreER toxicity observed, which is described in more detail below.

4.3.3 Potential CreERT2 toxicity is observed in epididymal and pericardial adipose SVF cells

CreER toxicity has been described previously, where activated CreER cuts pseudo-*loxP* sites, resulting in DNA damage and growth inhibition (Loonstra et al., 2001). In my experiments, I found small, although not statistically significant differences between cells deleted for *Wt1* and control cells. When we compared CreERT2+ and CreERT2- control cells, we however observed differences in network formation; considering the controls included in these experiments, we suggest that this is an effect of CreERT2 and not an effect of 4-hydroxytamoxifen. Although the difference between means was not statistically significant, CreERT2+ control cells showed much greater variability than CreERT2- cells, suggesting that CreRT2 activation in pericardial adipose cells alters the behaviour of these cells.

We found that CreERT2 activation in epididymal, omental and pericardial SVF cells also has an effect on the expression of *Wt1.* Here, *Wt1* expression was lower in CreERT2+ control cells treated with 4-hydroxytamoxifen than in wild-type cells, suggesting an off-target effect of CreERT2 even in the absence of floxed *Wt1* (Figure 4.14). Moreover, this effect extended further onto inflammation genes previously found to be under the control of WT1, such as *CXCL5* and *PTN*.

4.3.4 RNAi-mediated *Wt1* deletion does not affect the *in vitro* angiogenic potential of epididymal, omental, and pericardial SVF cells

In our RNAi experiments, we did not observe any significant changes in angiogenic potential after *Wt1* knockdown. There are several possible reasons for this. Firstly,

SVF cells maintained in culture are still a heterogeneous population including cells other than pericytes and vascular smooth muscle cells. Therefore, knocking down *Wt1* in such a mixed population may not be enough to reveal the *in vivo* role of WT1 in our populations of interest. It has previously been shown that adipose-derived stem cells positive for PGDFRβ aid endothelial cell network formation on Matrigel® and that this effect may be due to the fact that PGDFRβ+ progenitors secrete angiogenic, inflammatory and mobilization factors (Traktuev et al., 2008).

Previous studies focused on the role of WT1 in angiogenesis used mainly endothelial cells (Duim et al., 2015; Wagner et al., 2008). As we observed much lower expression of WT1 in ECs isolated from most visceral depots, our experiments were subsequently focused on vascular cells of mesenchymal origin. Therefore, deleting *Wt1 in* adipose endothelial cells only may show a stronger phenotype. However, in small depots such as omental or pericardial fat, it may be difficult to obtain sufficient material and it may be necessary to either pool high numbers of samples or passage the cells several times to expand the cell population, which may affect *Wt1* expression.

Additionally, 2D network formation assays are generally used to assess angiogenesis in ECs (DeCicco-Skinner et al., 2014; Francescone et al., 2011). It is possible that different assays may be more suitable for evaluating angiogenic potential in PCs/VSMCs. In my experiments, I also attempted to use 3D assays to investigate the effect of *Wt1* deletion, where fragments of adipose tissue are embedded in Matrigel® supplemented with growth factors. Although using this method for adipose tissue has been described before (Rojas-Rodriguez et al., 2014), the data obtained through this assay were highly variable and we were unable to accurately observe the effect of CreERT2-mediated deletion (data not included).

4.3.5 Conclusions

The *in vitro* experiments in this chapter aimed to look into the function of WT1 in adipose vascular cells. Our previous results showed a high percentage of visceral adipose pericytes expressing WT1. Moreover, in this chapter we show that a large percentage of the adipose SVF cells we isolated and expanded in culture express markers of VSMCs and PCs, although the expression on WT1 in these cells decreases after 7 days in culture.

We found that deleting *Wt1* (through either the *Cre/loxP* system or RNAi) in SVF isolated from several visceral depots has no significant effect on *in vitro* network

formation when using 2D Matrigel-based assays. Similarly, *Wt1* deletion did not influence network formation by SVF cells co-cultured with endothelial cells.

One caveat of the experiments detailed above is that all assays were conducted in standard incubator conditions (37°C, 95% relative humidity, and a CO2 concentration of about 5%). However, adipose expansion is often accompanied by hypoxia, and *Wt1* is overexpressed as a result of hypoxia (Wagner et al., 2003). It is, therefore, possible that conducting the same assays under hypoxic conditions will give different results. The lack of a phenotype resulting from our *Wt1* deletions may also be due to the fact that, as described in the beginning of the chapter, WT1 expression in pericytes is reduced after the cells are maintained in culture for several days.

Chapter 5

Investigating the role of WT1 in murine adipose pericytes

5.1 Introduction

As the experiments outlined in the previous chapter showed that knocking down *Wt1* in SVF cells does not lead to an impairment in angiogenic potential *in vitro*, we further aimed to narrow down the focus of our experiments by isolating and performing experiments on VWAT-derived pericytes alone. Pericytes (PCs), are found surrounding the blood vessels of all tissues, regulating angiogenesis through interactions with ECs and the microenvironment or supporting the integrity of vessels (Birbrair et al., 2014). Our previous experiments showed that some VWAT-derived pericytes express WT1 (Chapter 3, Section 3.2.1) and, as the current literature suggests, there is significant overlap between those angiogenesis genes expressed in pericytes and those regulated by WT1 in other organs or systems d(Birbrair et al., 2014; Darland et al., 2003; Katuri et al., 2014).

Several angiogenesis genes have been shown to be regulated by WT1. WT1 may regulate the expression of nestin in the developing heart (Wagner et al., 2006). Similarly, it has been shown that WT1 binds to the promoter of *α4integrin* (Kirschner et al., 2006). In adulthood, and specifically after cardiac ischemia, WT1 has been shown to potentially regulate ETS-1, a transcription factor which regulates ANG-2 and VEGFR2 (Wagner et al., 2008a). The role of WT1 in angiogenesis has, as previously detailed, also been described in cancer. In Ewing sarcoma, WT1 appears to upregulate *VEGF*, *MMP9*, *Tie-2* and *Ang-1* (Katuri et al., 2014). Furthermore, WT1 regulates the expression of the splicing factor kinase SRPK1, which directs the alternative splicing of the different VEGF isoforms (Amin et al., 2011).

When looking into the literature describing how PCs may regulate the vasculature at molecular level, we noticed that some of the genes involved in this process are genes regulated by WT1. For instance, VEGF, a classic marker of endothelial cells, is also produced by pericytes, and several functions of PC-derived VEGF have been suggested. VEGF secreted by pericytes has been shown to have profound effects on neighbouring ECs, promoting EC survival and stability (Darland et al., 2003). The wider implications of this PC-EC crosstalk have also been investigated. For instance, studies in the brain show that PC-derived VEGF contributes to an increased permeability of the blood-brain barrier during a stroke (Bai et al., 2015). Similarly, nestin is expressed by both ECs and PCs and is considered a marker of a subset of pericytes, with nestin + PCs suggested to play a more important role in tumour vessel stabilisation than nestin- PCs (Klein et al., 2014).

However, other properties of PCs have been described beyond their primary role as angiogenic regulators. For instance, pericytes and their mesenchymal stem cell descendants have been thoroughly characterised for their role in regenerative medicine (reviewed in Gomez-Salazar et al., 2020; James and Péault, 2019; Pittenger et al., 2019). In the kidney, pericytes regulate blood pressure (Shaw et al., 2018) and can be involved in fibrosis, through production of collagens such as collagen-1α1 and/or differentiation into myofibroblasts (Humphreys et al., 2010b; Lin et al., 2008). Moreover, this differentiation into myofibroblasts also leads to detachment and subsequent shortage of pericytes from the kidney vasculature, which can lead to nephron ischemia (Schrimpf and Duffield, 2011). In the lung, the role of pericytes in supplying fibroblasts has also been described in conjunction with their role as source of vascular smooth muscle cells. Lineage tracing of lung mesothelial cells has shown, that they differentiate into VSMCs in the developing lung (Que et al., 2008). A role of WT1 in myofibroblast transformation has further been described in pulmonary fibrosis, where WT1 upregulates αSMA, leading to mesothelial-to-myofibroblast and fibroblast-to-myofibroblast transition (Sontake et al., 2018).

As there seems to be a high degree of overlap between pericyte genes involved in angiogenesis and known WT1 targets, we were interested in finding out whether deleting *Wt1* in pericytes can affect their *in vitro* angiogenic potential. Finally, we aimed to explore other potential differences between WT1+ and WT1- PCs which may not be reflected in our *in vitro* assays.

5.1.2 Hypothesis

Considering the high percentage of WT1+ cells in a subset of VWAT-derived pericytes and the previous evidence regarding the effect of pericytes on EC angiogenesis, we hypothesised that deleting *Wt1* in VWAT-derived pericytes impairs the ability of these pericytes to form *in vitro* vascular networks when co-cultured with ECs that don't express *Wt1*. Moreover, we wanted to investigate whether the transcriptome of WT1+ PCs found in VWAT differs from that of WT1- PCs.

5.1.3 Aims

The aims of this chapter are therefore the following:

1. Delete *Wt1* in VWAT-derived pericytes and observe the effect of this deletion on the angiogenic potential of co-cultured PCs and ECs.

2. Explore the transcriptomic differences between WT1+ and WT1- pericytes isolated from murine VWAT.

5.2 Results

5.2.1 The effect of RNAi-mediated *Wt1* deletion on tube formation by visceral adipose pericytes

In our previous experiments (Chapter 4, Section 4.2.4), SVF cells deleted for *Wt1* via RNAi did not show an altered angiogenic phenotype when cultured in a 2D model. However, the SVF is a heterogeneous cell population and our experiments outlined in Chapter 3 suggested that a significant proportion of PDGFRβ+ cells expressed WT1. We therefore aimed to investigate the effect of *Wt1* deletion in pericytes isolated by FACS sorting from VWAT depots based on PDGFRβ expression.

Lin-cKit-CD31-PDGFRβ+ cells were isolated from wild-type murine epididymal, omental, and pericardial adipose tissue by FACS according to the protocol described in Chapter 3. Sorted cells were then maintained in culture until confluent (for 7 days) and subsequently stained with antibodies against PDGFRβ and αSMA (Figure 5.1). Figure 5.1 shows that PDGFRβ expression is maintained in a significant proportion of the epididymal, omental, and pericardial cells isolated (panels A, C, and E), while αSMA is only expressed sporadically (panels B, D, and F). Moreover, maintaining the sorted cells in culture (over a period of 7 days) did not lead to a loss of WT1 expression (Figure 5.1, arrowheads).

Although we successfully sorted Lin-cKit-CD31-PDGFRβ+ cells from epididymal, omental, and pericardial VWAT, omental and pericardial adipose depots did not yield enough cells to carry out subsequent experiments. We therefore focused only on epididymal cells for our following experiments.

Sorted Lin-cKit-CD31-PDGFRβ+ cells were expanded in culture and either transfected with a short interfering RNA (siRNA) against *Wt1*, following the protocol used in the experiments outlined in Chapter 4, transfected with a scramble control siRNA or transection reagent only, or not transfected at all. Figure 5.2 shows the *Wt1* mRNA levels in non-transfected epididymal pericytes and in bEND3 endothelial cells, a brain-derived endothelial cell line selected based on its lack of *Wt1* expression (Montesano et al., 1990). No *Wt1* mRNA was detected in bEND3 cells. Pericytes isolated from epididymal fat pads transfected with anti-*Wt1* siRNA showed lower

levels of *Wt1* mRNA, with silenced cells showing a 75% reduction in *Wt1* expression overall (Figure 5.3).

We then looked into whether *Wt1* silencing affects the angiogenic potential of epididymal pericytes when they are co-cultured with endothelial cells. We then performed tube formation assays on Matrigel® membrane, including the relevant controls.

Figures 5.4 shows knockdown (A) and control (B-D) epididymal PCs co-cultured with bEND3 cells, 3 and 6 hours after plating. After 3 hours, we did not observe any visible differences in angiogenic potential between the different conditions. We again used the Angiogenesis Analyzer plugin for ImageJ (Carpentier and Cascone, 2012) in order to quantify the total number of branches (Figure 5.4, E) and the branching length of the networks (Figure 5.4, F). This revealed no significant differences between the conditions.

Similarly, we examined the *in vitro* effect of *Wt1* deletions in epididymal VWAT-derived pericytes 6 hours after plating. Figure 5.5. (A-D) shows the networks formed by *Wt1*-silenced cells and control cells co-cultured with bEND3 cells. We again quantified the number of branches present in the networks (Figure 5.5, E) and the total length of the networks formed under each condition (Figure 5.5, F) and observed no significant differences in tube formation.

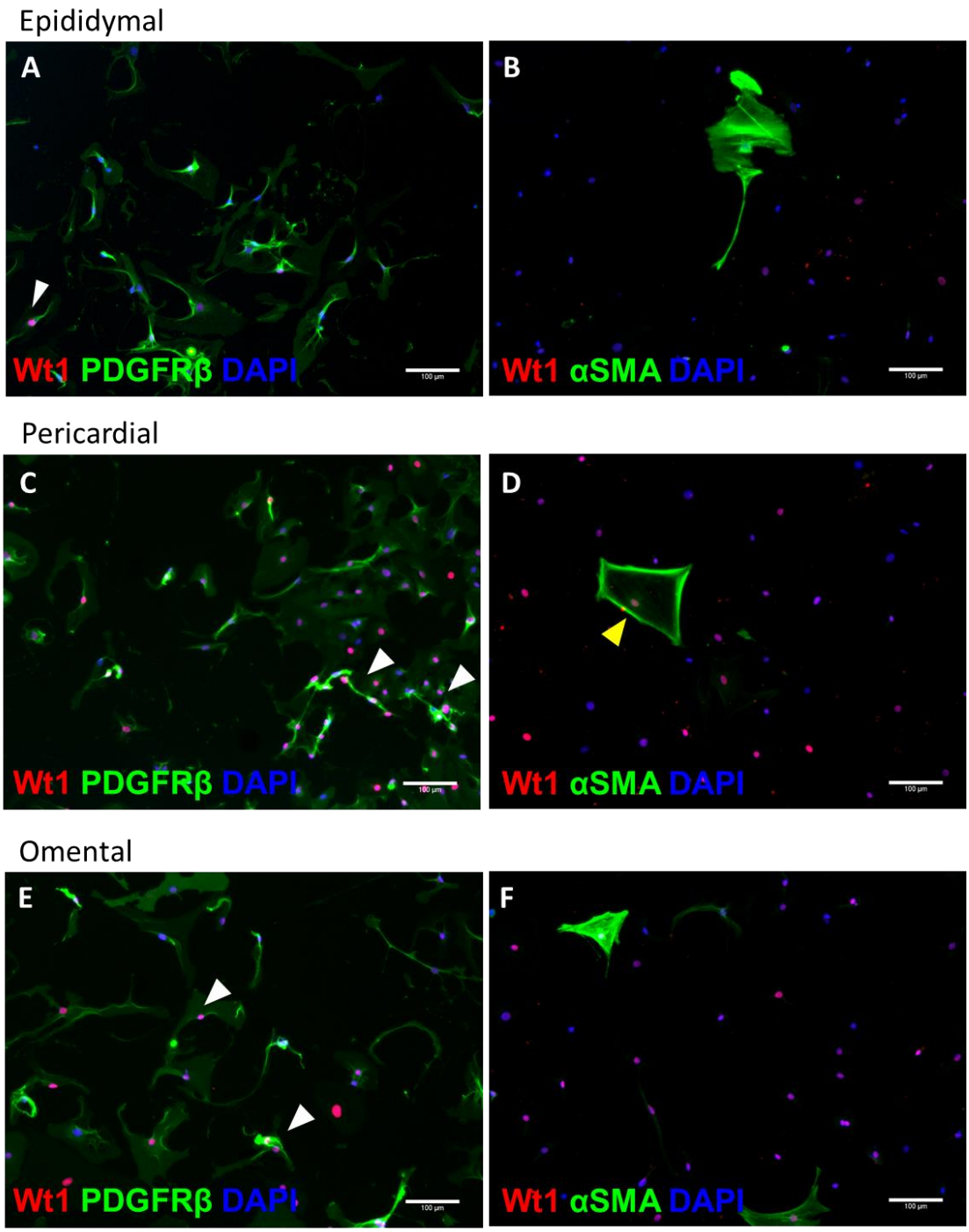

Figure 5.1. Pericytes isolated from epididymal, pericardial, and omental adipose tissue continue to express WT1 while being maintained in culture. *A, C, E: FACS-sorted Lin-cKit-CD31-PDGFRβ+ pericytes isolated from epididymal (A), pericardial (C), and omental (E) adipose tissue stained with DAPI (blue) and antibodies against WT1 (red) and PDFGRβ (green). B, D, F: FACS-sorted Lin-cKit-CD31-PDGFRβ+ pericytes isolated from epididymal (B), pericardial (D), and omental (F) adipose tissue stained with DAPI (blue) and antibodies against WT1 (red) and αSMA (green). White arrowheads indicate co-expression of WT1 and PDFGRβ. Yellow arrowhead indicates co-expression of WT1 and αSMA. N=1 across all panels. Scale bars: 100 µm.*

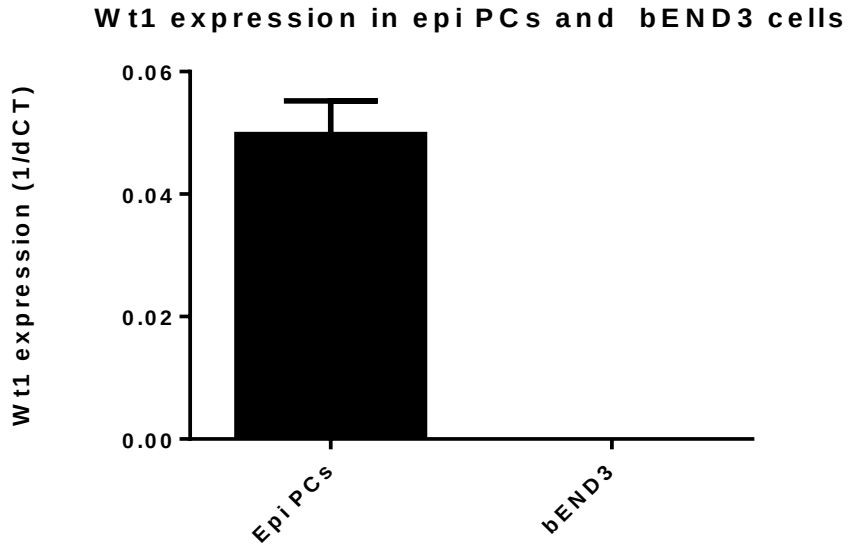

Figure 5.2. Wt1 mRNA expression in cultured epididymal pericytes and bEND3 cells. *Wt1 mRNA levels were quantified using qPCRs and normalized to 18S mRNA levels in all samples. Epididymal PCs – n=3. bEND3 – n=1. Error bars represent the standard error of the mean*.

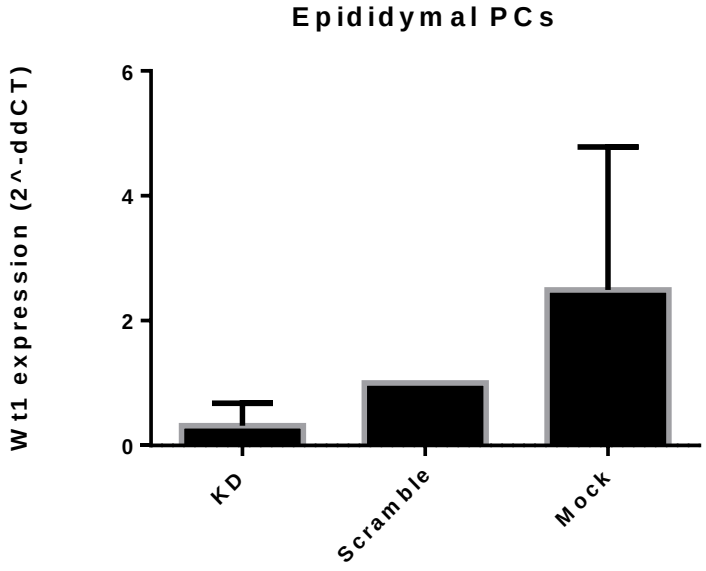

Figure 5.3. Validation of RNAi-mediated Wt1 knockdown in epididymal FACS-sorted Lin-cKit-CD31-PDGFRβ+ pericytes. *Wt1 mRNA levels in KD (Wt1-silenced) and mock transfection control cells from epididymal PCs were assessed by qPCR and normalized to Wt1 levels in control cells treated with a scramble siRNA. Wt1 levels in KD cells were lower than in scramble control cells, showing a trend towards significance (p=0.08)..Error bars represent the standard error of the* mean; n=3.

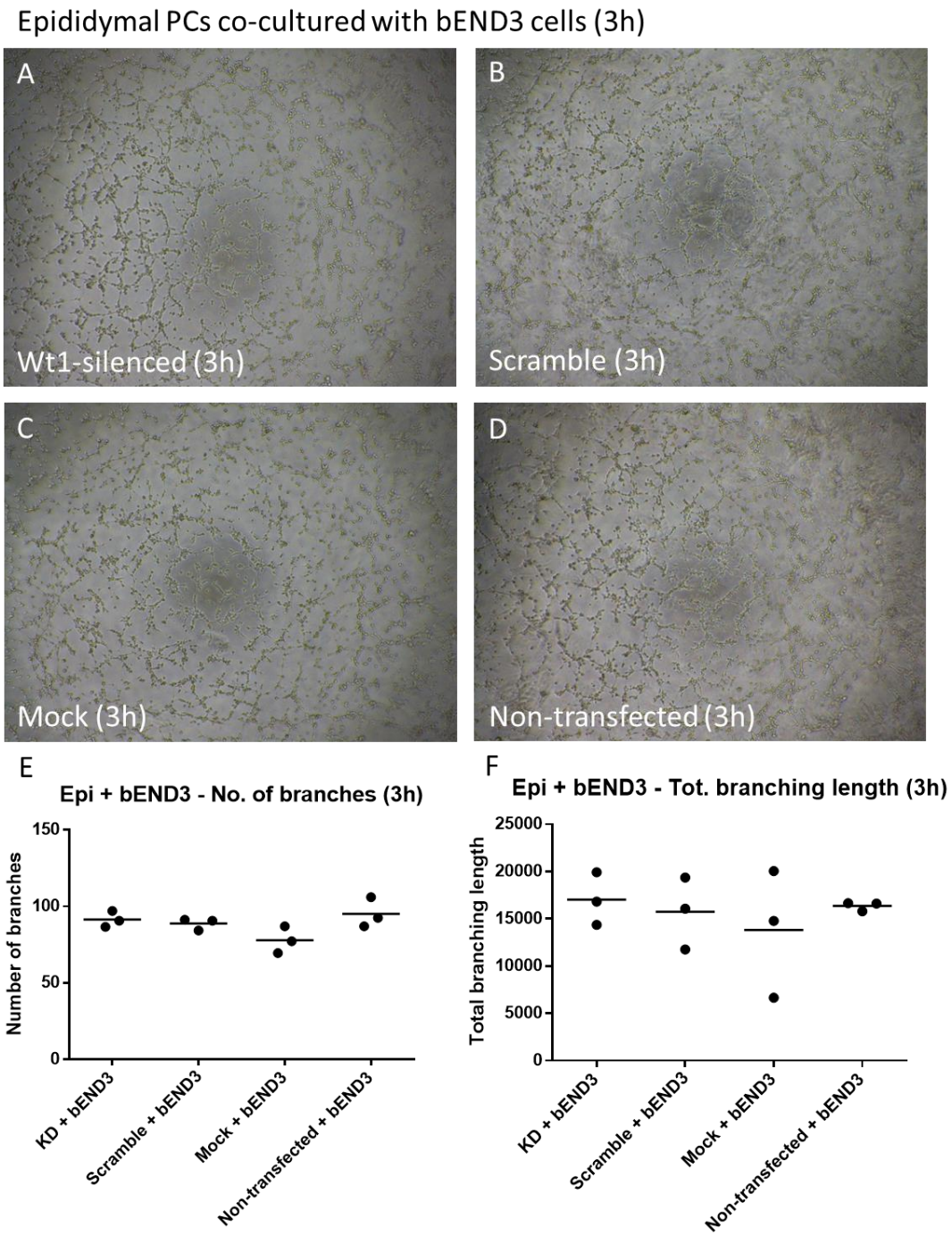

Figure 5.4. The effect of RNAi-mediated Wt1 deletion on tube formation in co-cultures of epididymal-derived PCs and bEND3 cells, 3 hours after seeding. *For each condition, the number of 'branches' (or tubes) formed and the length of the network were quantified. Network formation by co-cultures with epididymal PCs deleted for Wt1 (A), treated with scramble control siRNA (B), mock transfection control PCs (C), and non-transfected PCs (D). No significant differences between KD cells and Scramble control cells were observed in the number of branches (p=0.31) or the total branching length (p=0.18) 3 hours after plating (E-F, n=3). Brightfield images were acquired at 4X magnification.*

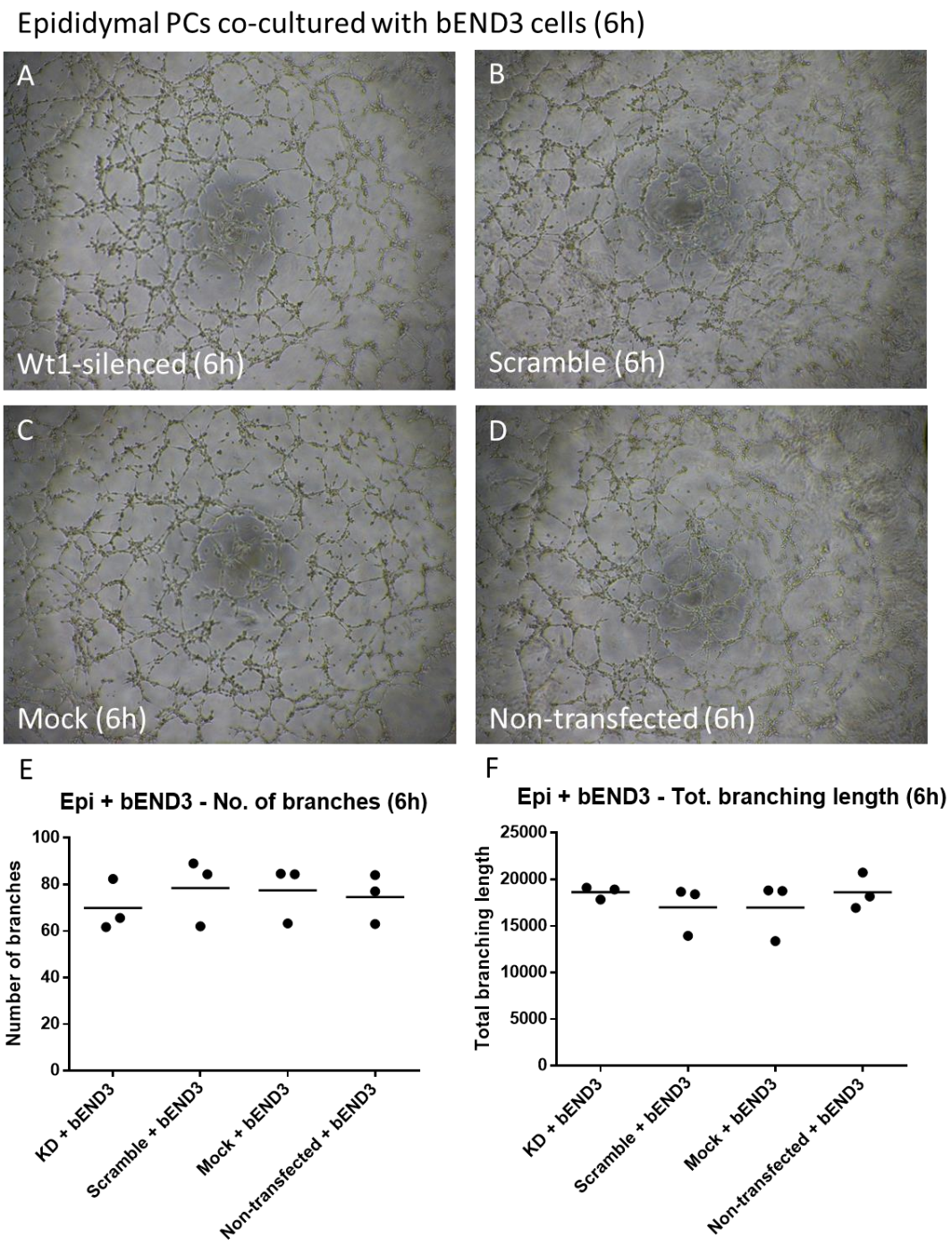

Figure 5.5. The effect of RNAi-mediated Wt1 deletion on tube formation in co-cultures of epididymal-derived PCs and bEND3 cells, 6 hours after seeding. *For each condition, the number of 'branches' (or tubes) formed and the length of the network were quantified. Network formation by co-cultures with epididymal PCs deleted for Wt1 (A), treated with scramble control siRNA (B), mock transfection control PCs (C), and non-transfected PCs (D). No significant differences were observed between KD cells and scramble control cells n the number of branches (p=0.25) and total branching length (p=0.44) 6 hours after plating (E-F, n=3). Brightfield images were acquired at 4X magnification.*

5.2.2 RNA-sequencing and transcriptomic analysis of WT1+ and WT1- pericytes isolated from epididiymal VWAT

In order to identify genes and pathways enriched in WT1+ adipose-derived pericytes, we isolated SVF cells from the epididymal adipose tissue of *Wt1*$^{GFP/+}$ mice and FACS sorted Lin-cKit-CD31-PDGFRβ+ pericytes based on GFP expression. This resulted in two distinct populations, Lin-cKit-CD31-PDGFRβ+GFP+ (further referred to as WT1+ PCs) and Lin-cKit-CD31-PDGFRβ+GFP- (further referred to as WT1- PCs), which were further used for RNA sequencing. Sequencing data rendered 14,793 transcripts expressed in both WT1+ and WT1- adipose pericytes. In order to identify genes that are differentially expressed, we used the Paolo Shiny application for R (https://paolo.shinyapps.io/ShinyVolcanoPlot/). We applied a log2fold cut-off of ±1.5 and an adjusted p value cut-off of 0.05. 414 genes were further identified as significantly up- or downregulated in WT1+ pericytes (Figure 5.6). 201 of these genes were downregulated in WT1+ PCs, whereas 213 genes were upregulated in WT1+ PCs.

In order to identify pathways differentially expressed between WT1+ and WT1- epididymal PCs, I first carried out gene ontology analysis using GOrilla (http://cbl-gorilla.cs.technion.ac.il/). GOrilla analysis can be performed by either inputting a single list of ranked genes or two unranked lists (including a target list and a background list). In order to identify just the pathways upregulated in WT1+ PCs, we analysed a single ranked list of the 213 upregulated genes, ordered by log fold change. Although 213 is too small a number of genes for a meaningful GO term enrichment analysis, we nevertheless identified one enriched biological process GO term related to the regulation of muscle contraction (Figure 5.7).

Six genes related to the regulation of muscle contraction GO term were significantly upregulated in WT1+ epididymal pericytes - endothelin 1 (*Edn1*), desmoplakin (*Dsp*), adrenergic receptor, alpha 1b (*Adra1b*), prostaglandin-endoperoxide synthase 1 (*Ptgs1*), atpase, na+/k+ transporting, beta 1 polypeptide (*Atp1b1*), and potassium inwardly-rectifying channel, subfamily j, member 2 (*Kcnj2*) (Table 5.1). The log2 fold change values and adjusted p values of these 6 genes are outlined in Table 5.2.

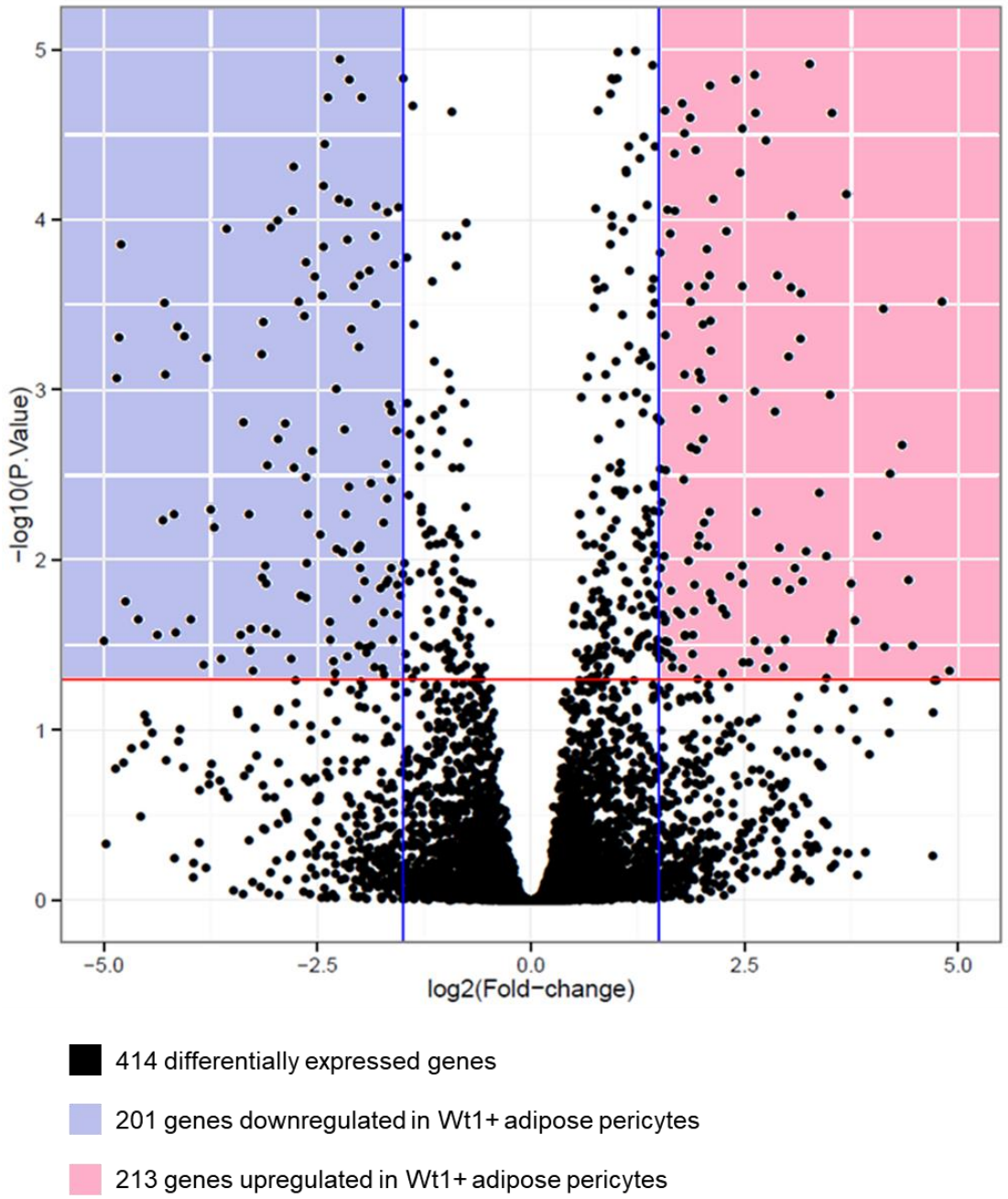

Figure 5.6. Summary of RNA sequencing results. *Volcano plot representation of differentially expressed genes in WT1+ and WT1- adipose pericytes. 14,793 genes were expressed in both WT1+ and WT1- adipose pericytes. In order to identify significantly under- or overexpressed genes, we applied a log2fold cut-off of +/- 1.5 and an adjusted p value cut-off of 0.05 (-log10 = 1.3). 414 genes were differentially expressed. The points enclosed in the light blue rectangle represent genes downregulated in WT1+ adipose pericytes, whereas the points in the pink rectangle represent genes overexpressed in WT1+ pericytes.*

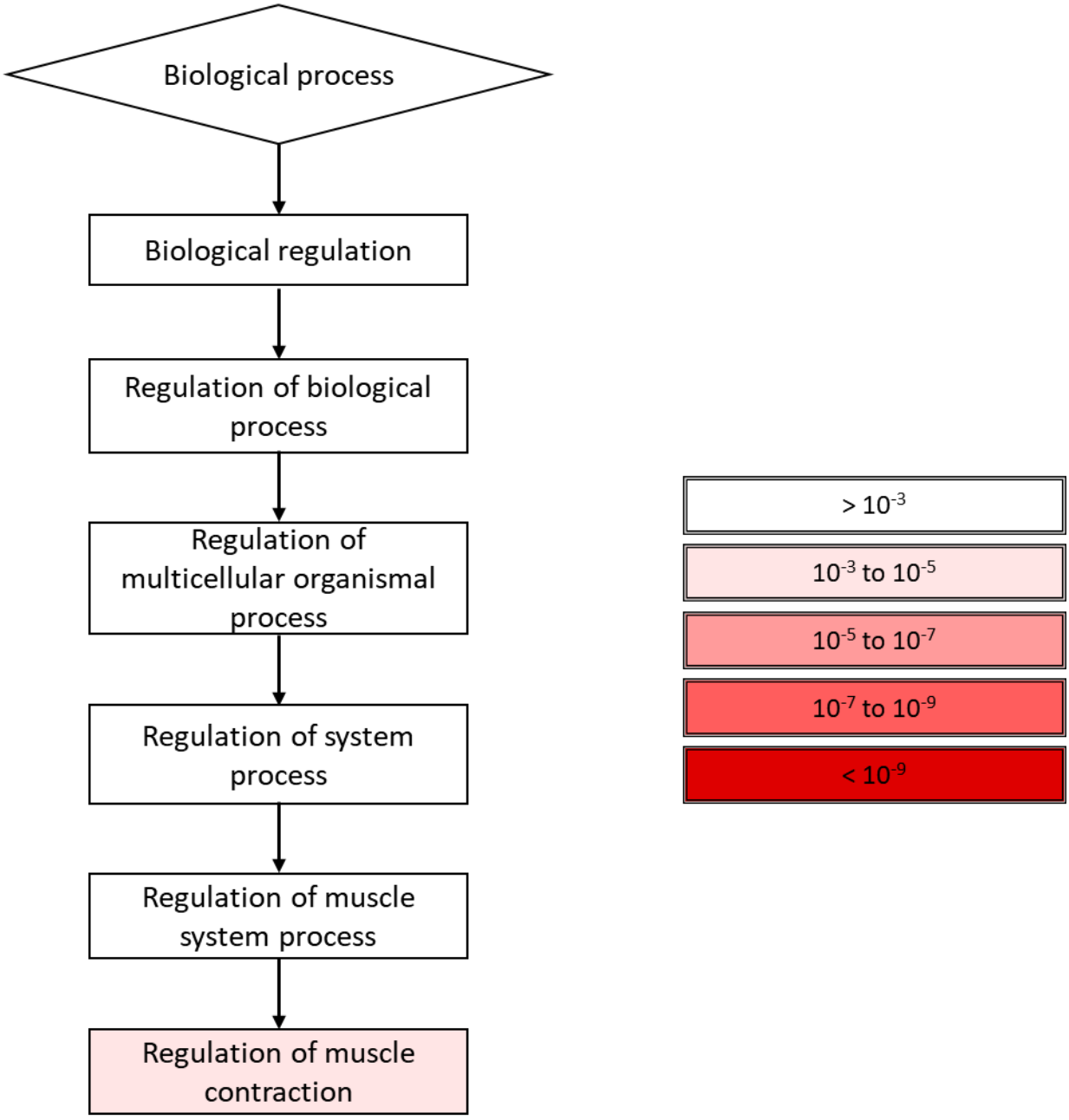

Figure 5.7. GO term enriched in WT1+ epididymal pericytes, as identified by the GOrilla visualisation tool. *GO analysis was performed on the genes that are significantly upregulated in WT1+ pericytes. GO analysis identified one enriched GO term (regulation of muscle contraction).*

GO term	Description	P value	FDR q value	Enrichment	Genes
GO:0006937	Regulation of muscle contraction	8.01E-4	1E0	3.80	***Edn1*** – endothelin 1 ***Dsp*** – desmoplakin ***Adra1b*** – adrenergic receptor, alpha 1b ***Ptgs1*** – prostaglandin-endoperoxide synthase 1 ***Atp1b1*** – atpase, na+/k+ transporting, beta 1 polypeptide ***Kcnj2*** – potassium inwardly-rectifying channel, subfamily j, member 2

Table 5.1 Upregulated genes associated with the regulation of muscle contraction, as identified by the GOrilla visualisation tool. *GO analysis identified 6 genes related to the regulation of muscle contraction- Edn1, Dsp, Adra1b, Ptgs1, Ato1b1 and Kcnj2.*

Gene name	Log2 fold change	Adjusted p value
Edn1	4.74	8.04E-19
Dsp	3.79	0.022589824
Adra1b	3.69	7.07E-05
Ptgs1	3.32	3.57E-11
Atp1b1	3.50	4.48E-10
Kcnj2	5.47	0.006073031

Table 5.2 Log2 fold change values and adjusted p values of regulation of muscle contraction genes significantly upregulated in WT1+ PCs.

We also carried out functional enrichment analysis using DAVID: Database for Annotation, Visualization, and Integrated Discovery v6.8 (https://david.ncifcrf.gov/). Analysis of the 213 transcripts significantly upregulated in W1+ epididymal pericytes revealed associations with several pathways from the KEGG database.

25 pathways were found to be associated with the 213 genes upregulated in WT1+ adipose pericytes (Table 5.3). Out of these, 20 pathways were significantly upregulated ($p<0.05$); after correcting the p values using the Benjamini method (Benjamini and Hochberg, 1995), we identified two pathways containing genes significantly upregulated in WT1+ PCs: proteoglycans in cancer and melanoma (Table 5.3).

10 genes upregulated in WT1+ PCs were associated with the proteoglycans in cancer KEGG pathway: erb-b2 receptor tyrosine kinase 3 (Erbb3), fibroblast growth factor 2 (Fgf2), fibronectin 1 (Fn1), filamin, beta (Flnb), inositol 1,4,5-triphosphate receptor 3 (Itpr3), met proto-oncogene(Met), related RAS viral (r-ras) oncogene 2 (Rras2), and three members of the Wnt gene family: wingless-type MMTV integration site family member 1 (Wnt1), wingless-type MMTV integration site family, member 10B (Wnt10b), wingless-type MMTV integration site family, member 2 (Wnt2). These 10 genes are outlined in Table 5.4, along with their respective log2 fold changes and adjusted p values.

Moreover, 6 genes upregulated in WT1+ PCs were associated with the melanoma KEGG pathway: three members of the fibroblast growth factor (Fgf) family - fibroblast growth factor 1 (Fgf1), fibroblast growth factor 2 (Fgf2), and fibroblast growth factor 9 (Fgf9), as well as met proto-oncogene (Met), microphthalmia-associated transcription factor (Mitf) and platelet-derived growth factor, C polypeptide (Pdgfc). These 6 genes are outlined in Table 5.5, along with their respective log2 fold changes and adjusted p values.

Interestingly, one of the KEGG pathways upregulated in WT1+ PCs was the insulin secretion pathway (Table 5.3; p value = 0.048). The four upregulated genes which are associated with this pathway are outlined in Table 5.6, along with their log2 fold changes and adjusted p values calculated in the primary analysis. The following genes were associated with this KEGG pathway: ATPase, Na+/K+ transporting, beta 1 polypeptide (Atp1b1), adenylate cyclase 2 (Adcy2), cAMP responsive element binding protein 5 (Creb5), inositol 1,4,5-triphosphate receptor 3 (Itpr3).

We also looked at associations between known KEGG pathways and genes significantly downregulated in WT1+ adipose PCs (Table 5.7). Several pathways were identified by DAVID, including the vascular smooth muscle contraction KEGG pathway. The genes in this pathway which are downregulated in WT1+ adipose PCs are outlined in Table 5.8; these include actin, alpha 2, smooth muscle, aorta (*Acta2*), adenosine A2a receptor (*Adora2a*), adrenergic receptor, alpha 1a (*Adra1a*), arginine vasopressin receptor 1A (*Avpr1a*), myosin, light polypeptide 9, regulatory (*Myl9*), protein phosphatase 1, regulatory (inhibitor) subunit 14A (*Ppp1r14a*).

KEGG pathway	No of genes	P value	Benjamini (adjusted p value)
Proteoglycans in cancer	10	1,2E-4	1,8E-2
Melanoma	6	5,4E-4	4,1E-2
Pathways in cancer	12	1,1E-3	5,8E-2
Axon guidance	7	1,3E-3	5,1E-2
Wnt signalling pathway	7	2,1E-3	6,4E-2
Melanogenesis	6	2,4E-3	6,1E-2
PI3K-Akt signalling pathway	10	5,7E-3	1,2E-1
Ras signalling pathway	8	5,8E-3	1,1E-1
Gap junction	5	8,8E-3	1,4E-1
Protein digestion and absorption	5	9,6E-3	1,4E-1
Hippo signalling pathway	6	1,4E-2	1,8E-1
Regulation of actin cytoskeleton	7	1,5E-2	1,8E-1
Rap1 signalling pathway	7	1,6E-2	1,7E-1
Thyroid hormone synthesis	4	2,9E-2	2,8E-1
Gastric acid secretion	4	3,1E-2	2,8E-1
Salivary secretion	4	3,6E-2	3,1E-1
Adrenergic signalling in cardiomyocytes	5	4,6E-2	3,5E-1
Focal adhesion	6	4,6E-2	3,4E-1
Insulin secretion	4	4,8E-2	3,3E-1
Aldosterone synthesis and secretion	4	4,8E-2	3,3E-1
cGMP-PKG signalling pathway	5	6,9E-2	4,3E-1
Retrograde endocannabinoid signalling	4	7,4E-2	4,4E-1
MAPK signalling pathway	6	8,9E-2	4,9E-1
Cholinergic synapse	4	9,2E-2	4,8E-1
Basal cell carcinoma	3	9,3E-2	4,7E-1

Table 5.3. KEGG pathways upregulated in WT1+ epididymal adipose pericytes. *25 pathways were identified to be associated with genes significantly upregulated in WT1+ pericytes compared to WT1- pericytes. Rows in light green are pathways with a p value of <0.05; rows in dark green contain the pathways with a Benjamini corrected p value of <0.05. n=3*

Proteoglycans in cancer		
Gene name	**Log2 fold change**	**Adjusted p value**
erb-b2 receptor tyrosine kinase 3 (*Erbb3*)	2.91	0.008
fibroblast growth factor 2 (*Fgf2*)	1.80	1.24E-06
fibronectin 1(*Fn1*)	2.47	0.000245
filamin, beta (*Flnb*)	1.74	8.39E-09
inositol 1,4,5-triphosphate receptor 3(*Itpr3*)	1.91	0.02
met proto-oncogene (*Met*)	2.10	0.016
related RAS viral (r-ras) oncogene 2 (*Rras2*)	2.30	1.09E-14
wingless-type MMTV integration site family, member 1 (*Wnt1*)	6.54	0.003041
wingless-type MMTV integration site family, member 10B (*Wnt10b*)	4.24	7.54E-08
wingless-type MMTV integration site family, member 2 (*Wnt2*)	2.24	0.019

Table 5.4. Genes upregulated in WT1+ adipose pericytes which are associated with the proteoglycans in cancer KEGG pathway. *10 genes upregulated in WT1+ adipose PCs were associated with this KEGG pathway. N=3.*

Melanoma		
Gene name	**Log2 fold change**	**Adjusted p value**
fibroblast growth factor 1(*Fgf1*)	2.13	7.56E-05
fibroblast growth factor 2(*Fgf2*)	1.79	1.24E-06
fibroblast growth factor 9(*Fgf9*)	2.88	0.00021
met proto-oncogene (*Met*)	2.10	0.016
microphthalmia-associated transcription factor (*Mitf*)	1.51	0.00016
platelet-derived growth factor, C polypeptide (*Pdgfc*)	4.49	8.84E-15

Table 5.5. Genes upregulated in WT1+ adipose pericytes that are associated with the melanoma KEGG pathway. *6 genes upregulated in WT1+ adipose PCs were associated with this KEGG pathway. N=3*

Insulin secretion		
Gene name	**Log2 fold change**	**Adjusted p value**
ATPase, Na+/K+ transporting, beta 1 polypeptide (*Atp1b1*)	3.49	4.48E-10
adenylate cyclase 2 (*Adcy2*)	2.62	1.41E-05
cAMP responsive element binding protein 5 (*Creb5*)	1.97	0.00079
inositol 1,4,5-triphosphate receptor 3 (*Itpr3*)	1.91	0.020

Table 5.6. Genes upregulated in WT1+ adipose pericytes that are associated with the insulin secretion KEGG pathway. *4 genes upregulated in WT1+ adipose PCs were associated with this KEGG pathway. N=3*

KEGG pathway	No of genes	P value	Benjamini (adjusted p value)
cAMP signaling pathway	10	5,9E-4	7,3E-2
Neuroactive ligand-receptor interaction	11	2,2E-3	1,3E-1
Cell adhesion molecules (CAMs)	8	3,4E-3	1,3E-1
ECM-receptor interaction	6	4,1E-3	1,2E-1
Calcium signaling pathway	8	6,0E-3	1,4E-1
Arrhythmogenic right ventricular cardiomyopathy (ARVC)	5	8,6E-3	1,7E-1
cGMP-PKG signaling pathway	7	1,4E-2	2,2E-1
Vascular smooth muscle contraction	6	1,9E-2	2,6E-1
Hematopoietic cell lineage	5	1,9E-2	2,4E-1
Axon guidance	6	2,0E-2	2,3E-1
Insulin resistance	5	4,4E-2	4,1E-1
PI3K-Akt signaling pathway	9	6,1E-2	4,9E-1
AMPK signaling pathway	5	6,9E-2	5,1E-1
Protein digestion and absorption	4	9,0E-2	5,8E-1

Table 5.7. KEGG pathways downregulated in WT1+ epididymal adipose pericytes. *14 pathways were identified to be associated with genes significantly downregulated in WT1+ pericytes compared to WT1- pericytes. Rows in light orange contain the pathways with a p value of <0.05. n=3.*

Vascular smooth muscle contraction		
Gene name	**Log2 fold change**	**Adjusted p value**
actin, alpha 2, smooth muscle, aorta (*Acta2*)	-2.14	5.08E-06
adenosine A2a receptor (*Adora2a*)	-2.37	1.91E-05
adrenergic receptor, alpha 1a (*Adra1a*)	-3.51	5.02E-16
arginine vasopressin receptor 1A (*Avpr1a*)	-2.21	0.0091
myosin, light polypeptide 9, regulatory (*Myl9*)	-1.52	1.84E-12
protein phosphatase 1, regulatory (inhibitor) subunit 14A (*Ppp1r14a*)	-3.43	1.48E-12

Table 5.8. Genes downregulated in WT1+ adipose pericytes that are associated with the vascular smooth muscle contraction KEGG pathway. *6 genes downregulated in WT1+ adipose PCs were associated with this KEGG pathway. N=3.*

5.3 Discussion

Previously, I had not observed changes in the *in vitro* angiogenic potential of SVF cells where *Wt1* had been deleted (Chapter 4, section 4.2.4). I hypothesised that this may be because the heterogeneity of the adipose SVF may have been masking the effect of *Wt1* deletion in what is, in fact, a small population of Wt1+ pericytes. In this chapter, I aimed to look into VWAT-derived pericytes in particular, firstly by deleting *Wt1* in these cells only and examining the effect of this deletion on their angiogenic potential and the angiogenic potential of endothelial cells, and secondly by looking into the transcriptomic differences between WT1+ and WT1- adipose pericytes.

5.3.1 RNAi-mediated *Wt1* deletion in epididymal PCs does not alter their *in vitro* angiogenic potential

In order to investigate the behaviour of VWAT pericytes and their effect on endothelial cells in angiogenesis *in vitro*, we isolated and sorted Lin-cKit-CD31-PDGFRβ+ pericytes from epididymal adipose tissue and co-cultured these in Matrigel-coated wells with bEND3 cells, an endothelial cell line which does not express *Wt1*. No significant differences in tube formation were observed between *Wt1*-silenced and control cells co-cultured with ECs, suggesting that *Wt1* deletion in epididymal PCs does not affect angiogenesis of bEND3 in a co-cultured tube formation assay.

5.3.2 RNA-sequencing and transcriptomic analysis of WT1+ and WT1- perivascular cells isolated from epididiymal VWAT

Seeing as previous work has shown the presence of distinct pericyte subsets in adipose tissue (Hepler et al., 2018), we were curious to explore whether these WT1+ and WT1- pericytes might belong to different subsets. Comparing the transcriptome of WT1+ and WT1- epididymal derived PCs, we found 213 genes significantly overexpressed in WT1+ PCs compared to the WT1- PCs, out of 14,793 transcripts expressed in both sub-populations of PCs derived from epididymal adipose tissue. However, whether these altered pathways play a functional role in the expansion of VWAT and obesity overall remains to be investigated.

Some of our pathway analysis results do point to some interesting trends in the transcriptome of WT1+ cells. Firstly, the two most prominent pathways associated with genes upregulated in WT1+ cells were the proteoglycans in cancer and melanoma KEGG pathways. Together, these pathways include not only members of the *Wnt* family or the well-described proto-oncogene Met, but also genes involved in

angiogenesis, such as 3 of the fibroblast growth factors (*Fgf1*, *Fgf2* and *Fgf9*) and *Pdgfc*. The role of proteoglycans has been described not only in the tumour microenvironment and vascular expansion, but also in angiogenesis in general (Iozzo and Sanderson, 2011).

Although the upregulation of genes belonging to the Wnt family is not a surprise, seeing as the interplay between WT1 and the Wnt pathway is well documented (Paris et al., 2015), it is interesting to observe several angiogenesis genes upregulated in WT1+ PCs. We previously discussed angiogenesis genes such as VEGFR2 and Ang-2 being indirectly under the control of WT1 (Wagner et al., 2008b) and ChIP-seq experiments have also shown FGF to be a transcriptional target of WT1 in renal progenitors (Motamedi et al., 2014). Here, we observed 3 members of the FGF family (Fgf1, Fgf2 and Fgf9) significantly upregulated in WT1+ PCs compared to WT1- PCs.

The upregulation of *Pdgfc* in WT1+ cells is also interesting. While all the growth factors and receptors in the PDGF(R) family have been shown to be involved in angiogenesis, the PDGFC ligand in particular has been shown to promote tumour growth through its role in the recruitment of cancer-associated fibroblasts (Anderberg et al., 2009).

We also found that four of the genes upregulated in WT1+ PCs are associated with the insulin secretion KEGG pathway, which is supported by many studies which have documented the role of the vasculature in insulin secretion and type 2 diabetes (reviewed in Richards et al., 2010). Moreover, there is evidence suggesting pericytes play an important role in central insulin signalling, as the regulation of blood vessels in the pancreas is essential for adequate insulin release (Almaç et al., 2018). Interestingly, one of the pathways downregulated in WT1+ PCs relates to vascular smooth muscle contraction and includes the genes *Adra1a*, which is part of the adrenergic receptor gene family and *Acta2*, encoding αSMA, a marker of VSCMs (Wang et al., 2006). Interestingly, Hepler et al. also showed one subset of pericytes expressing a different adrenergic receptor gene, *Adrb3,* and suggested this subset may mark more committed adipocyte precursors (Hepler et al., 2018a).

5.3.3 Conclusions

The results outlined in this chapter revealed that deleting *Wt1* in VWAT PCs does not significantly change their potential to form vascular-like structures *in vitro,* although one way to further test this would be to co-culture VWAT-derived PCs with VWAT-derived ECs rather than immortalized endothelial cells. Furthermore, we looked at

transcriptomic differences between epididymal adipose PCs which express WT1 and those which are WT1-negative. We identified several pathways which are differentially expressed between the two populations in lean mice. However, in order to confirm that these indeed mark two sub-populations of PCs, the differentially expressed genes would need to be validated. Furthermore, it would also be interesting to explore differences between VWAT WT1+ and WT1- PCs isolated from obese mice, and to investigate whether the differences we observed above are more pronounced or whether entirely different pathways are upregulated in WT1+ PCs during obesity.

Chapter 6

Discussion and conclusions

Visceral white adipose tissue (VWAT) is increasingly being studied in a worldwide effort to reveal the mechanisms of pathological obesity. VWAT accumulation is associated with increased risk of developing type 2 diabetes (Wang et al., 2005), hypertension and other cardiovascular disease (Hayashi et al., 2003; Yusuf et al., 2005), as well as cancer (Kang et al., 2010).

Although the correlation between excess VWAT and increased risk of cardiometabolic disease is well documented, the mechanisms through which VWAT affects overall health remain elusive due to the heterogeneity of this type of adipose tissue. Firstly, VWAT is composed of several depots with different metabolic profiles. Secondly, each VWAT depots contains multiple populations of adipocytes, pre-adipocytes, vascular cells and immune cells. Recent data have also shown that some VWAT adipocytes have a different developmental origin from subcutaneous adipocytes (Chau et al., 2014b), originating from WT1+ progenitors.

One of the main research questions arising based on this knowledge is whether WT1, which also marks distinct populations of adipose progenitors during adulthood, is expressed in other cell types and, if so, what its role in these cell types is in adipose tissue. Some studies have shown that WT1 plays a role in angiogenesis (Katuri et al., 2014; Wagner et al., 2014, 2008a), and even more lines of research have highlighted the importance of angiogenesis in obesity (Lemoine et al., 2012). Our experiments were therefore focused on the role of WT1 in VWAT angiogenesis. Moreover, as WT1 has been shown previously to mark VWAT progenitors in both humans and mice, the experiments in this thesis were carried out on tissues obtained from both organisms. Lastly, we wanted to address the fact that many studies on adipose tissue often focus on one or two VWAT depots, whereas it is yet unclear whether distinct VWAT depots have different metabolic profiles, origins and implications for cardiometabolic health. We therefore included several VWAT depots in some of the experiments we carried out on mouse tissues.

6.1 *In vivo* expression of WT1 in the vasculature of murine and human VWAT

Our first experiments looked at the expression of WT1 and the location of WT1+ cells *in vivo,* in both mouse and human. Firstly, we saw by immunofluorescence that WT1+ cells are located near vessels expressing CD31, αSMA and PDGFRβ in five murine VWAT depots - epididymal, pericardial, omental, perirenal and mesenteric. Moreover, immunofluorescence images also showed that WT1 is co-expressed with PDGFRβ in some cells (some of which are found in the mesothelium of VWAT). Further flow

cytometry experiments showed expression of WT1 in both endothelial cells and pericytes isolated from the 5 VWAT depots. Secondly, we used *Wt1*-lineage tracing to show that cells expressing WT1 post-natally not only give rise to adipocytes, but also other cells found in near CD31+ and αSMA+ microvessels. Additionally, the contribution of WT1+ cells to the adipocyte population is decreased in obesity and WT1+ cells may also contribute less to other cell populations (such as microvascular cells) in adult obese mice. Finally, our immunofluorescence data from human samples also showed an abundance of WT1+ cells in omental adipose tissue isolated from lean, overweight, and obese patients alike. Moreover, we saw that tissues collected from obese patients present an increase in *Wt1* mRNA and in the total percentage of WT1+ cells compared with tissues from lean donors. However, when analysing human visceral SVF after 7 days in culture we did not observe any significant differences between lean, overweight and obese samples.

These findings firstly add to previous literature describing the expression of WT1 in vascular cells. With regard to the role of pericytes in obesity, it has been previously suggested that PDGFRβ+ cells play a role in maintaining metabolically healthy adipose tissue (Shao et al., 2018) and that mesothelial cells can differentiate into perivascular mesenchymal cells (Asahina et al., 2011). Moreover, previous research has identified distinct adipose pericyte subsets and a contribution of pericytes to the adipose pool (Hepler et al., 2018a; Tang et al., 2008b). In this context, our finding that a subset of PDGFRβ+ visceral pericytes express WT1 raises the question of whether WT1+ and WT1- pericytes have different functions in angiogenesis and/or adipogenesis, a question which is addressed in chapter 5.

Several studies have shown the presence and role of WT1 in ECs in the tumour vasculature and in cardiac ECs (Duim et al., 2015; Timar et al., 2005; Wagner et al., 2014), here we were only able to confirm WT1 expression in VWAT ECs by flow cytometry but not by immunofluorescence. Co-staining VWAT samples from *Wt1*$^{GFP/+}$ reporter mice with antibodies against WT1 and CD31 did not reveal co-expression of the two proteins, and I hypothesise that this may be either due to low WT1 expression in these cells or due to the fact that, *in vivo*, CD31 is mainly expressed at cell-cell junctions (Lertkiatmongkol et al., 2016). It is also worth keeping in mind the fact that, to date, the literature describing the role of WT1 in ECs during adult angiogenesis is mainly confined to the tumour microenvironment (Katuri et al., 2014; Wagner et al., 2014, 2008b). Furthermore, the role of WT1 in ECs in the cardiovascular setting has

mainly been described in the context of development (Duim et al., 2016), with transient expression in ECs also linked to a role in cardiac regeneration (Ogley R., 2018).

This also leads us to our next research question – the expression and role of WT1 in lean vs. obese VWAT. In our lineage tracing experiments we saw a significant decrease in *Wt1*-lineage traced adipocytes in three VWAT depots from obese mice (epididymal, omental, and perirenal). We additionally also observed a potential decrease in *Wt1*-lineage traced microvessels during obesity. These data, along with the fact that we observed PDGFRβ+ in WT1+ mesothelial cells, raises another interesting question – whether there is a role of WT1+ pericytes in VWAT homeostasis and expansion and whether this role changes during obesity.

Finally, we showed the presence and location of WT1+ cells in human omental VWAT. This is notable as, previously, only the presence of *WT1* transcript had been demonstrated in VWAT (Chau et al., 2014). Interestingly, our data also showed a difference in WT1 expression and WT1+ cell numbers between lean, overweight, and obese patients. This is particularly interesting considering that obese adipose tissue (and VWAT in particularly) tends to be a pro-inflammatory, hypoxic environment and the knowledge that WT1 is activated in response to hypoxia (WAGNER et al., 2003). Moreover, this finding is also interesting in the context of the trends we observed in lean vs obese *Wt1*-lineage traced mice. Finally, our insight into these differences between lean and obese patients are also limited by the relatively small sample size, by the fact that our patient population includes both males and females and by the wide age range (33 to 76 years).

The data described in Chapter 3 show several trends worthy of further *in vivo* investigation. However, other essential pieces of the puzzle need to be collected in order to draw more definitive conclusions. Although our human data showed differences in WT1 expression between lean and obese subjects, we are much more limited when it comes to exploring the *in vivo* fate of human adipose progenitors.

6.2 The *in vitro* role of murine WT1 in visceral adipose tissue angiogenesis

Following the *in vivo* data described above, we carried out subsequent *in vitro* experiments in order to investigate the function of WT1 (Chapter 4). We showed by flow cytometry that WT1 expression (as indicated by our use of the $Wt1^{GFP/+}$ mouse model) varies between depots - 30% of epididymal SVF cells are GFP+, whereas only

around 10% of the total omental and pericardial SVF cells are GFP+. Conversely, around 20% of GFP+Lin-cKit- cells in omental and pericardial VWAT are PDGFRβ+, whereas only around 5% of epididymal GFP+Lin-cKit- are PDGFRβ+, further highlighting inter-depot differences. I also aimed to find out whether isolating SVF cells based on adherence alone retains WT1 expression in perivascular cells. I found that no CD31+ ECs were selected for through this culture method; we also found that PGDFRβ+ and αSMA+ cells made up a significant proportion of SVF cells cultured this way, although the percentage of PGDFRβ+ positive for WT1+ was lower in cultured cells compared to the freshly dissociated cells analysed previously by flow cytometry waned in culture. Some PGDFRβ+ cells also expressed αSMA in culture.

When culturing SVF cells from *CAG^{CreERT2}; Wt1$^{loxP/loxP}$* mice and adding 4-hydroxytamoxifen in order to delete *Wt1,* we observed a decrease in *Wt1* transcript levels but nevertheless did not observe any effect on tube formation *in vitro.* However, we did observe potential effects of activated Cre in these cells, with both *in vitro* tube formation and cytokine gene expression altered in Cre control cells. Using an alternative, RNAi-based approach also showed a decrease in *Wt1* expression in SVF cells treated with anti-*Wt1* siRNA but no effect of the *Wt1* knockdown on tube formation.

Although the results above showed that *Wt1* deletion in VWAT SVF cells does not impair their *in vitro* angiogenic potential, they nevertheless open several other questions in the field. Firstly, the experiments summarised above showed that culturing SVF cells based on adherence alone selects for pericytes and VSCMs but no ECs. However, a smaller percentage of PDGFRβ+ cells were WT1+ than we had previously seen in freshly dissociated cells used for flow cytometry. This is an interesting finding, especially as it has been shown that cell culture conditions can significantly alter the transcriptional profile of primary cells - using a high-throughput microfluidics approach, Januszyk et al. showed that adipose-derived stem cells maintained in culture showed significant differences in their transcriptional profile between passage numbers P0, P1 and P2 (Januszyk et al., 2015). Interestingly, the pathways upregulated at higher passages are thought to shift the cells towards a more proliferative transcriptional profile (Januszyk et al., 2015).

Secondly, we observed a potentially toxic effect of CreERT2. The deleterious effect of Cre recombinase has been previously described. CreERT activation in mouse embryonic stem cells leads to a reduction in growth and proliferation, an effect which

seems to be dose-dependent (Loonstra et al., 2001). In a cardiovascular Cre mouse model, Cre activation has also been shown to induce cardiomyocyte apoptosis and cardiac fibrosis, and this effect was found to be dependent on the amount of Tamoxifen injected and the subsequent level of Cre activity (Bersell et al., 2013). The *in vitro* effects of Cre-loxP recombination have further been demonstrated in bone marrow cells used in CFU assays, highlighting that such genetic deletion models are not ideal for this assay (McHaffie et al., 2016). CreER was also shown to induce DNA damage and cryptic *loxP* site cleavage in an intestine-specific Villin-CreER^{T2} mouse model, again highlighting the caveats of employing this model, particularly in stem cells (Bohin et al., 2018). Another factor to consider when discussing the effects of inducible CreER is the effect of tamoxifen itself. During development, tamoxifen has been shown to modulate apoptosis (Takebayashi et al., 2008). However, most of the deleterious effects of tamoxifen have been described in relation to its role as a selective estrogen receptor modulator and its subsequent effect on bone homeostasis in mice (Zhong et al., 2015). As Cre toxicity has been described in cell cultures before, our results may confirm previous reports. Importantly, to our knowledge CreERT2 toxicity has not been shown in tube-formation assays.

Thirdly, we found that while VWAT SVF form robust networks in tube formation assays, this potential is not affected when *Wt1* is knocked down. The SVF has been thoroughly described and shown to contain not only mesenchymal-type stem cells but also preadipocytes, vascular cells, immune cells, and fibroblasts. Moreover, several groups have demonstrated the angiogenic properties and behaviour of SVF cells; mouse and rat adipose-derived SVF cells have been shown to promote vasomotor relaxation of arteries *in vivo*, secrete angiogenic factors *in vitro* and form networks when plated on Matrigel® ECM (Morris et al., 2015; Rehman et al., 2004; Sun et al., 2017). In parallel, *WT1* deletions in endothelial cells have been shown impair *in vitro* angiogenic potential in Matrigel® tube formation assays (Wagner et al., 2008). However, we did not observe an effect of *Wt1* knockdown when carrying out own Matrigel®-based assays. This may be due to several reasons. For instance, WT1 may not actively involved in VWAT angiogenesis. This would contrast the effect of *WT1* deletions observed in other tissues and cell types, such as HUVECs and tumours (Wagner et al., 2008). Another reason might be that the assay we selected for this experiment does not accurately reflect the *in vivo* role of WT1 in angiogenesis and that a more complex 3D assay may be more suitable for reflecting the adipose microenvironment.

The data outlined in Chapter 4 suggest that deleting *Wt1* in VWAT SVF cells does not affect their angiogenic potential *in vitro*. However, these data also point to several important questions related to the methodologies used in *in vitro* angiogenesis research. Firstly, conditional gene knockout models may present caveats that might skew results, so appropriate controls are essential. Secondly, data resulting from primary cells must be analysed carefully, bearing in mind the tendency of cells to change their gene expression profile after being extracted from their microenvironment.

6.3 Investigating the role of WT1 in murine adipose pericytes

In our 2D angiogenesis assays, we did not observe that *Wt1* deletion had any significant effect on tube formation by SVF cells (Chapter 4, Section 2.4.2). As the SVF is a heterogeneous population, including not only vascular cells but also adipose progenitors or immune cells, we wanted to exclude the possibility that the presence of a high proportion of other cell types might downplay the effect of *Wt1* deletion on the angiogenic potential of VWAT SVF cells. We therefore used an RNAi to knock down *Wt1* in VWAT-derived pericytes only and examined the effect of this knockdown on a *Wt1*-null endothelial cell line, bEND3. RNAi-mediated *Wt1* knockdown in sorted Lin-cKit-CD31-PDGFRβ+ co-cultured with bEND3 cells did not show any effect on tube formation *in vitro*. We then sought to examine differences between WT1- and WT1+ adipose pericytes by looking at the whole transcriptome of these cells. We found that 1.43% of the genes expressed were significantly upregulated in WT1+ PCs. Moreover, we used two analysis tools, GOrilla and DAVID, to identify pathways upregulated in the two VWAT PC populations. We identified several pathways upregulated and downregulated in WT1+ PCs. Genes upregulated in WT1+ PCs were most often associated with KEGG cancer pathways and included genes active in tumour angiogenesis, such as *Fgf1*, *Fgf2* and *Fgf9* and *Pdgfc*.

The results outlined in this section primarily show that, while *Wt1* knockdown did not affect the *in vitro* behaviour of VWAT PCs in two-dimensional tube formation assays, WT1+ and WT1- PCs nevertheless have different transcriptomic signatures, with several interesting genes and pathways upregulated in the WT1-expressing population. Publications from other groups support the hypothesis that subsets of pericytes are characterised by different surface marker expression patterns, different functions, and even different origins (Zhang et al., 2020). For instance, during CNS development, one subset of cerebrovascular pericytes differentiates from mature

macrophages (Yamamoto et al., 2017). In adipose research, Hepler *et al*. have shown that murine PDGFRβ+ cells found in visceral fat can be classed into two subsets based on LY6C expression (Hepler et al., 2018b). In our experiments, out of all genes expressed in epididymal PCs, 1.43% were significantly upregulated in WT1+ PCs.

However, only a small number of pathways were enriched in WT1+ PCs, and further experiments are necessary in order to establish whether these pathways are physiologically relevant. The main limitation of our RNA sequencing data is the fact that, due to time constrains, we were not able to validate the genes upregulated in the two subsets of PCs. Moreover, we had previously identified a larger percentage of omental and pericardial PCs positive for WT1 but, as these depots are smaller, we were not able to collect sufficient amounts of good quality RNA for sequencing. Future work would therefore also be focused on the other VWAT depots and their respective WT1+/- PC populations.

Interestingly, our GO analysis identified that some genes upregulated in WT1+ PCs are associated with the regulation of muscle contraction, suggesting a potential role of WT1 in the vasculature. DAVID functional enrichment analysis conversely identified several genes downregulated in WT1+ PCs which are associated with the vascular smooth muscle contraction KEGG pathway. Several genes associated with the insulin secretion KEGG pathway were, on the other hand, upregulated in WT1+ PCs. These results are interesting as is has been shown that insulin inhibits the contraction of vascular smooth muscle (Kahn et al., 1993, 1998). It is therefore possible that the role of WT1 in the adipose vasculature is not necessarily linked to novel angiogenesis, but to how the mature vasculature plays into the homeostasis of adipose tissue.

The experiments described in Chapter 5 show that, although WT1 does not appear to direct sprouting angiogenesis *in vitro*, WT1+ and WT1- PCs nevertheless have different transcriptomic profiles. Interestingly, genes associated with cancer are upregulated in WT1+ PCs; these include genes associated with the *Wnt* pathway, which have previously been shown to be downstream of WT1 in epicardial cells (von Gise et al., 2011). In the future, validation of these genes and pathways and similar analysis on other VWAT depots may shed more light on the physiological implications of our findings.

6.4 Future work

While our experiments generated several interesting results, further data would be needed in order to put these in context and reveal the larger picture of WT1 and VWAT angiogenesis.

In our lineage tracing experiments, we found that microvascular cells in five VWAT depots not only express WT1 in adulthood but may also be derived from WT1+ cells. Moreover, our immunofluorescence data showed that the contribution of WT1+ cells to the vasculature seems to differ between lean and obese mice. However, further flow cytometry data, particularly from *Wt1*^{CreERT2}*;mTmG* lineage tracing mice, would be key to confirming that the *Wt1*-lineage traced cells we observed in our immunofluorescence experiments are indeed VSCMs and PCs. Most importantly, this experiment would also allow us to quantify the percentage of PCs and VSMCs derived from WT1+ progenitors, which was not possible with immunofluorescence images alone. One limitation of our lineage tracing data is also the fact that, at the time of tamoxifen dosing, it is not known whether all WT1+ cells would be adipose progenitors, and some of the labelled cells might be committed pericytes themselves. In order to overcome this limitation and better assess whether WT1+ progenitors differentiate into microvascular cells, future experiments could involve transplanting WT1+ adipose progenitors *in vivo* and observing whether they incorporate into microvessels.

In our data from human tissues, we observed increased levels of *WT1* mRNA in samples collected from obese patients. In order to connect with the lineage tracing data we obtained from our *Wt1*^{CreERT2}*;mTmG* model, similar data from mouse adipose tissue would have to be collected as well, for instance by comparing whole-tissue *Wt1* mRNA and protein levels from lean and obese wild-type mice. While whole-tissue mRNA can be informative, it is also important to zoom in on the percentages of cells expressing WT1 in these tissues, especially since we have observed that different murine VWAT depots vary in their proportion of WT1+ cells.

Although it would also be necessary to have information on the percentages of WT1+ cells in humans, mirroring these experiments in human tissue is challenging not only because of the difficulties in obtaining adipose tissue from pericardial, perirenal or mesenteric adipose tissue, but also because subsequent experiments on cells isolated from these depots must be suitable for small numbers of cells. Furthermore, performing flow cytometry analysis experiments on WT1, a nuclear protein which may

be expressed at relatively lower levels compared to tumour cells, comes with its own set of challenges. Although successful WT1 flow cytometry has been shown in human cells, the experiments in question involved cancer cell lines (Kerst et al., 2008). Here, we were not able to successfully sort human SVF cells based on WT1+ expression.

Although we thoroughly examined the effect of *Wt1* deletions in a 2D *in vitro* angiogenesis model, we are also aware that other *in vitro* angiogenesis models might be better at reflecting the adipose microenvironment. In our experiments, we also attempted to culture 3D adipose explants along with growth factors, following a previously published protocol (Rojas-Rodriguez et al., 2014). However, although we observed sprouting in some wells, we were not able to obtain results that were consistent across replicates. It is probable that other 3D adipose constructs, such as gels formed from suspensions of co-cultured cells or similar scaffolds populated with adipocytes and other cells found in the SVF may be more revealing when studying the complex interactions between adipose tissue cells (Cai et al., 2017; Murphy et al., 2019).

In addition to the vasculature, it is worth noting the importance of studying the wider impact of any factors active in the blood vessels of adipose tissue. Looking into transcriptomic differences between WT1+ and WT1- PCs is informative on the pathways which may be involved in metabolic disease. However, the differences we observed between WT1+ and WT1- PCs are only relevant to lean adult mice. It would undoubtedly be interesting to explore the differences between WT1+ and WT1- PCs isolate from obese mice. Considering the effect of hypoxia on WT1 (Wagner et al., 2003) and the multitude of transcriptional targets of WT1, such an experiment may reveal not only more significant differences in the pathways we have already identified, but also additional up/downregulated pathways.

Extrapolating from the pathways we identified in our transcriptomic analysis, other aspects of the adipose tissue microenvironment are also important. Inflammation in VWAT is a particularly important issue as VWAT has been shown to have a pro-inflammatory phenotype and thus wider implications for metabolic health and the risk of developing insulin resistance and type 2 diabetes (Burhans et al., 2019). The link between adipose and vascular health is even more pronounced when we focus on perivascular tissue; here, adipose-derived factors such as leptin, IL-6, TNF-a, CCL5 or CCL2 can lead to a dysfunction of vascular cells, including endothelial cells, smooth

muscle cells and adventitial fibroblasts, and eventually to vascular disease (Nosalski and Guzik, 2017).

Another issue worth pointing out is the ubiquity of mouse models in adipose research, which is also found in the experiments outlined in this thesis. Although mechanisms observed in murine models are often extrapolated to the human biology, recent studies have shown that some pathways can be species-specific. For instance, it has recently been shown that acute glucocorticoid excess promotes BAT thermogenesis in humans by increasing UCP-1 but leads to a decrease in BAT activity and UCP-1 in mice (Ramage et al., 2016). Differences between mice and humans have also been described in terms of immunological response, where different isoforms of the interleukin 1 receptor-associated kinase (IRAK) protein are essential in TLR pathways between humans and mice (Sun et al., 2016).

6.5 Conclusions

Research on adipose tissue, and VWAT in particular is certainly an exciting area at the moment, with many groups working on all different aspects of this complex tissue, from development to metabolic health and inflammation. Our own experiments were focused on just one of the potential factors regulating VWAT – WT1. The data described in this thesis suggest that WT1 might have a complex role in VWAT, but that this role should be further studied in the context of: 1) the cell populations expressing *Wt1*; and 2) the pathways WT1 is known to be involved in. Although our *Wt1* knockdowns did not show a significant phenotype *in vitro*, this is only indicative of new sprouting angiogenesis. However, the expression patterns of WT1 and the different contributions of WT1+ cells to the adipocyte population in lean vs obese subjects does suggest a role for it in the regulation of VWAT and its vasculature. Assuming that WT1 expression in VWAT may be regulated by hypoxia and considering all the known transcriptional targets of WT1, these data raise new questions regarding whether this expression is increased in vascular cells from obese VWAT and, if so, what the consequences of this increase are on blood vessels and their integrity.

References

Adams, D.J., and van der Weyden, L. (2001). Are weCreating problems? Negative effects of Cre recombinase. Genesis *29*, 115–115.

Ahlma, R.S., Prabakaran, D., Mantzoros, C., Qu, D., Lowell, B., Maratos-Flier, E., and Flier, J.S. (1996). Role of leptin in the neuroendocrine response to fasting. Nature *382*, 250–252.

Almaç, J., Weitz, J., Rodriguez-Diaz, R., Pereira, E., and Caicedo, A. (2018). The Pericyte of the Pancreatic Islet Regulates Capillary Diameter and Local Blood Flow. Cell Metab. *27*, 1–15.

Amin, E.M., Oltean, S., Hua, J., Gammons, M.V., Hamdollah-Zadeh, M., Welsh, G.I., Cheung, M.-K., Ni, L., Kase, S., Rennel, E.S., et al. (2011). WT1 mutants reveal SRPK1 to be a downstream angiogenesis target by altering VEGF splicing. Cancer Cell *20*, 768.

Anderberg, C., Li, H., Fredriksson, L., Andrae, J., Betsholtz, C., Li, X., Eriksson, U., and Pietras, K. (2009). Paracrine signaling by platelet-derived growth factor-CC promotes tumor growth by recruitment of cancer-associated fibroblasts. Cancer Res. *69*, 369–378.

Armstrong, J.F., Pritchard-Jones, K., Bickmore, W.A., Hastie, N.D., and Bard, J.B. (1993). The expression of the Wilms' tumour gene, WT1, in the developing mammalian embryo. Mech. Dev. *40*, 85–97.

Armulik, A., Genové, G., Mäe, M., Nisancioglu, M.H., Wallgard, E., Niaudet, C., He, L., Norlin, J., Lindblom, P., Strittmatter, K., et al. (2010). Pericytes regulate the blood-brain barrier. Nature *468*, 557–561.

Arnaoutova, I., and Kleinman, H.K. (2010). In vitro angiogenesis: endothelial cell tube formation on gelled basement membrane extract. Nat. Protoc. *5*, 628–635.

Arner, P., Andersson, D.P., Thörne, A., Wirén, M., Hoffstedt, J., Näslund, E., Thorell, A., and Rydén, M. (2013). Variations in the size of the major omentum are primarily determined by fat cell number. J. Clin. Endocrinol. Metab. *98*.

Artibani, M., Sims, A.H., Slight, J., Aitken, S., Thornburn, A., Muir, M., Brunton, V.G., Del-Pozo, J., Morrison, L.R., Katz, E., et al. (2017). WT1 expression in breast cancer disrupts the epithelial/mesenchymal balance of tumour cells and correlates with the metabolic response to docetaxel. Sci. Rep. *7*, 45255.

Asahina, K., Zhou, B., Pu, W.T., and Tsukamoto, H. (2011). Septum Transversum-Derived Mesothelium Gives Rise to Hepatic Stellate Cells and Perivascular Mesenchymal Cells in Developing Mouse Liver. Hepatology *53*, 983.

Bai, Y., Zhu, X., Chao, J., Zhang, Y., Qian, C., Li, P., Liu, D., Han, B., Zhao, L., Zhang, J., et al. (2015). Pericytes Contribute to the Disruption of the Cerebral Endothelial Barrier via Increasing VEGF Expression: Implications for Stroke. PLoS One *10*, e0124362.

Balkau, B., Deanfield, J.E., Després, J.-P., Bassand, J.-P., Fox, K.A.A., Smith, S.C., Barter, P., Tan, C.-E., Van Gaal, L., Wittchen, H.-U., et al. (2007). International Day for the Evaluation of Abdominal Obesity (IDEA): a study of waist circumference, cardiovascular disease, and diabetes mellitus in 168,000 primary care patients in 63 countries. Circulation *116*, 1942–1951.

Bandiera, R., Vidal, V.P.I., Motamedi, F.J., Clarkson, M., Sahut-Barnola, I., von Gise, A., Pu, W.T., Hohenstein, P., Martinez, A., and Schedl, A. (2013). WT1 Maintains Adrenal-Gonadal Primordium Identity and Marks a Population of AGP-like Progenitors within the Adrenal Gland. Dev. Cell *27*, 5–18.

Bandiera, R., Sacco, S., Vidal, V.P.I., Chaboissier, M.-C., and Schedl, A. (2015). Steroidogenic organ development and homeostasis: A WT1-centric view. Mol. Cell. Endocrinol. *408*, 145–155.

Benjamini, Y., and Hochberg, Y. (1995). Controlling the False Discovery Rate: A Practical and Powerful Approach to Multiple Testing. J. R. Stat. Soc. Ser. B *57*, 289–300.

Berry, R., and Rodeheffer, M.S. (2013). Characterization of the adipocyte cellular lineage in vivo. Nat. Cell Biol. *15*, 302–308.

Bersell, K., Choudhury, S., Mollova, M., Polizzotti, B.D., Ganapathy, B., Walsh, S., Wadugu, B., Arab, S., and Kühn, B. (2013). Moderate and high amounts of tamoxifen in αmHC-MerCreMer mice induce a DNA damage response, leading to heart failure and death. DMM Dis. Model. Mech. *6*, 1459–1469.

Bieback, K., Schallmoser, K., Klüter, H., and Strunk, D. (2008). Clinical protocols for the isolation and expansion of mesenchymal stromal cells. Transfus. Med. Hemotherapy *35*, 286–294.

Birbrair, A., Zhang, T., Wang, Z.-M., Messi, M.L., Mintz, A., and Delbono, O. (2014). Pericytes at the intersection between tissue regeneration and pathology: Figure 1. Clin. Sci. *128*, 81–93.

Bohin, N., Carlson, E.A., and Samuelson, L.C. (2018). Stem Cell Reports Report Genome Toxicity and Impaired Stem Cell Function after Conditional Activation of CreER T2 in the Intestine. Stem Cell Reports *11*, 1337–1346.

Bondjers, C., Kalé, M., Hellströ, M., Scheidl, S.J., Abramsson, A., Renner, O., Lindahl, P., Cho, H., Kehrl, J., and Betsholtz, C. (2003). Transcription Profiling of Platelet-Derived Growth Factor-B-Deficient Mouse Embryos Identifies RGS5 as a Novel Marker for Pericytes and Vascular Smooth Muscle Cells.

Bouchard, L., Weisnagel, S.J., Engert, J.C., Hudson, T.J., Bouchard, C., Vohl, M.-C., and Pérusse, L. (2004). Human resistin gene polymorphism is associated with visceral obesity and fasting and oral glucose stimulated C-peptide in the Québec Family Study. J. Endocrinol. Invest. *27*, 1003–1009.

Bråkenhielm, E., Cao, R., Gao, B., Angelin, B., Cannon, B., Parini, P., and Cao, Y. (2004). Angiogenesis Inhibitor, TNP-470, Prevents Diet-Induced and Genetic Obesity in Mice. Circ. Res. *94*, 1579–1588.

Brestoff, J.R., and Artis, D. (2015). Immune regulation of metabolic homeostasis in health and disease. Cell *161*, 146–160.

Brett, A., Pandey, S., and Fraizer, G. (2013). The Wilms' tumor gene (WT1) regulates E-cadherin expression and migration of prostate cancer cells. Mol. Cancer *12*, 3.

Briot, A., Decaunes, P., Volat, F., Belles, C., Coupaye, M., Ledoux, S., Bouloumié, A., Manuscript, A., Briot, A., Decaunes, P., et al. (2018a). Senescence alters PPARγ (peroxisome proliferator-activated receptor gamma)-dependent fatty acid handling in human adipose tissue microvascular endothelial cells and favors inflammation. Arterioscler. Thromb. Vasc. Biol. *38*, 1134–1146.

Briot, A., Decaunes, P., Volat, F., Belles, C., Coupaye, M., Ledoux, S., and Bouloumié, A. (2018b). Senescence alters PPARγ (peroxisome proliferator-activated receptor gamma)-dependent fatty acid handling in human adipose tissue microvascular endothelial cells and favors inflammation. Arterioscler. Thromb. Vasc. Biol. *38*, 1134–1146.

Burhans, M.S., Hagman, D.K., Kuzma, J.N., Schmidt, K.A., and Kratz, M. (2019). Contribution of adipose tissue inflammation to the development of type 2 diabetes mellitus. Compr. Physiol. *9*, 1–58.

Burri, P.H., and Tarek, M.R. (1990). A Novel Mechanism of Capillary Growth in the Rat Pulmonary Microcirculation.

Caduff, J.H., Fischer, L.C., and Burri, P.H. (1986). Scanning Electron Microscope Study of the Developing Microvasculature in the Postnatal Rat Lung.

Cai, X., Xie, J., Yao, Y., Cun, X., Lin, S., Tian, T., Zhu, B., and Lin, Y. (2017). Angiogenesis in a 3D model containing adipose tissue stem cells and endothelial cells is mediated by canonical Wnt signaling. Bone Res. *5*, 1–13.

Call, K.M., Glaser, T., Ito, C.Y., Buckler, A.J., Pelletier, J., Haber, D.A., Rose, E.A., Kral, A., Yeger, H., and Lewis, W.H. (1990). Isolation and characterization of a zinc finger polypeptide gene at the human chromosome 11 Wilms' tumor locus. Cell *60*, 509–520.

Cancello, R., Tordjman, J., Poitou, C., Guilhem, G., Bouillot, J.L., Hugol, D., Coussieu, C., Basdevant, A., Bar Hen, A., Bedossa, P., et al. (2006). Increased infiltration of macrophages in omental adipose tissue is associated with marked hepatic lesions in morbid human obesity. Diabetes *55*, 1554–1561.

Cano, E., Carmona, R., and Muñoz-Chápuli, R. (2013a). Wt1-expressing progenitors contribute to multiple tissues in the developing lung. Am. J. Physiol. Cell. Mol. Physiol. *305*, L322–L332.

Cano, E., Carmona, R., and Muñoz-Chápuli, R. (2013b). Wt1-expressing progenitors contribute to multiple tissues in the developing lung. Am. J. Physiol. Cell. Mol. Physiol. *305*, L322–L332.

Cao, Y. (2010). Adipose tissue angiogenesis as a therapeutic target for obesity and metabolic diseases. Nat. Rev. Drug Discov. *9*, 107–115.

Cao, R., Brakenhielm, E., Wahlestedt, C., Thyberg, J., and Cao, Y. (2001). Leptin induces vascular permeability and synergistically stimulates angiogenesis with FGF-2 and VEGF. Proc. Natl. Acad. Sci. U. S. A. *98*, 6390–6395.

Caputa, G., Castoldi, A., and Pearce, E.J. (2019). Metabolic adaptations of tissue-resident immune cells. Nat. Immunol. *20*, 793–801.

Carmeliet, P., and Jain, R.K. (2011a). Molecular mechanisms and clinical applications of angiogenesis. Nature *473*, 298–307.

Carmeliet, P., and Jain, R.K. (2011b). Molecular mechanisms and clinical applications of angiogenesis. Nature *473*, 298–307.

Carpentier, G., and Cascone, I. (2012). Angiogenesis Analyzer for ImageJ. In ImageJ User and Developer Conference 2012, p.

Cartier, A., Côté, M., Lemieux, I., Pérusse, L., Tremblay, A., Bouchard, C., and Després, J.-P. (2009). Sex differences in inflammatory markers: what is the contribution of visceral adiposity? Am. J. Clin. Nutr. *89*, 1307–1314.

Chau, Y.-Y., and Hastie, N. (2015a). Wt1, the mesothelium and the origins and heterogeneity of visceral fat progenitors. Adipocyte *4*, 217–221.

Chau, Y.-Y., and Hastie, N.D. (2012). The role of Wt1 in regulating mesenchyme in cancer, development, and tissue homeostasis. Trends Genet. *28*, 515–524.

Chau, Y.Y., and Hastie, N. (2015b). Wt1, the mesothelium and the origins and heterogeneity of visceral fat progenitors. Adipocyte *4*, 217–221.

Chau, Y.-Y., Brownstein, D., Mjoseng, H., Lee, W.-C., Buza-Vidas, N., Nerlov, C., Jacobsen, S.E., Perry, P., Berry, R., Thornburn, A., et al. (2011). Acute Multiple Organ Failure in Adult Mice Deleted for the Developmental Regulator Wt1. PLoS Genet. *7*, e1002404.

Chau, Y.-Y., Bandiera, R., Serrels, A., Martínez-Estrada, O.M., Qing, W., Lee, M., Slight, J., Thornburn, A., Berry, R., McHaffie, S., et al. (2014a). Visceral and subcutaneous fat have different origins and evidence supports a mesothelial source. Nat. Cell Biol. *16*, 367–375.

Chau, Y.Y., Bandiera, R., Serrels, A., Martínez-Estrada, O.M., Qing, W., Lee, M., Slight, J., Thornburn, A., Berry, R., Mchaffie, S., et al. (2014b). Visceral and subcutaneous fat have different origins and evidence supports a mesothelial source. Nat. Cell Biol. *16*, 367–375.

Chen, W., Xia, P., Wang, H., Tu, J., Liang, X., Zhang, X., and Li, L. (2019). The endothelial tip-stalk cell selection and shuffling during angiogenesis. J. Cell Commun. Signal. *13*, 291–301.

Chen, Y., Buyel, J.J., Hanssen, M.J.W., Siegel, F., Pan, R., Naumann, J., Schell, M.,

van der Lans, A., Schlein, C., Froehlich, H., et al. (2016). Exosomal microRNA miR-92a concentration in serum reflects human brown fat activity. Nat. Commun. *7*, 11420.

Cinti, S. (2005). The adipose organ. In Prostaglandins Leukotrienes and Essential Fatty Acids, (Churchill Livingstone), pp. 9–15.

Cipolletta, D., Feuerer, M., Li, A., Kamei, N., Lee, J., Shoelson, S.E., Benoist, C., and Mathis, D. (2012). PPAR-γ is a major driver of the accumulation and phenotype of adipose tissue Treg cells. Nature *486*, 549–553.

Clark, E.R. (1918). Studies on the growth of blood-vessels in the tail of the frog larva?by observation and experiment on the living animal. Am. J. Anat. *23*, 37–88.

Cleal, L., and Chau, Y.-Y. (2016). Isolation and Fluorescence-Activated Cell Sorting of Murine WT1-Expressing Adipocyte Precursor Cells. In Methods in Molecular Biology (Clifton, N.J.), pp. 81–91.

Cleal, L., Aldea, T., and Chau, Y.-Y. (2017). Fifty shades of white: Understanding heterogeneity in white adipose stem cells. Adipocyte *6*.

Cook, K.S., Min, H.Y., Johnson, D., Chaplinsky, R.J., Flier, J.S., Hunt, C.R., and Spiegelman, B.M. (1987). Adipsin: A circulating serine protease homolog secreted by adipose tissue and sciatic nerve. Science (80-.). *237*, 402–405.

Craggs, L.J.L., Fenwick, R., Oakley, A.E., Ihara, M., and Kalaria, R.N. (2015). Immunolocalization of platelet-derived growth factor receptor-β (PDGFR-β) and pericytes in cerebral autosomal dominant arteriopathy with subcortical infarcts and leukoencephalopathy (CADASIL). Neuropathol. Appl. Neurobiol. *41*, 557–570.

Crewe, C., An, Y.A., and Scherer, P.E. (2017). The ominous triad of adipose tissue dysfunction: inflammation, fibrosis, and impaired angiogenesis. J. Clin. Invest. *127*, 74–82.

Crisan, M., Yap, S., Casteilla, L., Chen, C.-W., Corselli, M., Park, T.S., Andriolo, G., Sun, B., Zheng, B., Zhang, L., et al. (2008). A Perivascular Origin for Mesenchymal Stem Cells in Multiple Human Organs. Cell Stem Cell *3*, 301–313.

Daneman, R., Zhou, L., Kebede, A.A., and Barres, B.A. (2010). Pericytes are required for bloodĝ€"brain barrier integrity during embryogenesis. Nature *468*, 562–566.

Darimont, C., Avanti, O., Blancher, F., Wagniere, S., Mansourian, R., Zbinden, I., Leone-Vautravers, P., Fuerholz, A., Giusti, V., and Macé, K. (2008). Contribution of mesothelial cells in the expression of inflammatory-related factors in omental adipose tissue of obese subjects. Int. J. Obes. *32*, 112–120.

Darland, D.C., Massingham, L.J., Smith, S.R., Piek, E., Saint-Geniez, M., and D'Amore, P.A. (2003). Pericyte production of cell-associated VEGF is differentiation-dependent and is associated with endothelial survival. Dev. Biol. *264*, 275–288.

DeCicco-Skinner, K.L., Henry, G.H., Cataisson, C., Tabib, T., Curtis Gwilliam, J., Watson, N.J., Bullwinkle, E.M., Falkenburg, L., O'Neill, R.C., Morin, A., et al. (2014). Endothelial cell tube formation assay for the in vitro study of angiogenesis. J. Vis. Exp.

Dehbi, M., Hiscott, J., and Pelletier, J. (1998). Activation of the wt1 Wilms' tumor suppressor gene by NF-κB. Oncogene *16*, 2033–2039.

Dengler, V.L., Galbraith, M., and Espinosa, J.M. (2014). Transcriptional Regulation by Hypoxia Inducible Factors. Crit. Rev. Biochem. Mol. Biol. *49*, 1.

Després, J.-P., and Lemieux, I. (2006). Abdominal obesity and metabolic syndrome. Nature *444*, 881–887.

Després, J.P., Moorjani, S., Lupien, P.J., Tremblay, A., Nadeau, A., and Bouchard, C. (1990). Regional distribution of body fat, plasma lipoproteins, and cardiovascular disease. Arteriosclerosis *10*, 497–511.

Dessain, S.K., Yu, H., Reddel, R.R., Beijersbergen, R.L., Weinberg, R.A., Buluwela, L., Weitzman, S.A., Korz, D., and Sukumar, S. (2000). Methylation of the human telomerase gene CpG island. Cancer Res. *60*, 537–541.

Distler, J.H.W., Hirth, A., Kurowska-Stolarska, M., Gay, R.E., Gay, S., and Distler, O. (2003). Angiogenic and angiostatic factors in the molecular control of angiogenesis. Q. J. Nucl. Med. *47*, 149–161.

Drolet, R., Richard, C., Sniderman, A.D., Mailloux, J., Fortier, M., Huot, C., Rhéaume, C., and Tchernof, A. (2008). Hypertrophy and hyperplasia of abdominal adipose tissues in women. Int. J. Obes. *32*, 283–291.

Duim, S.N., Kurakula, K., Goumans, M.J., and Kruithof, B.P.T. (2015). Cardiac endothelial cells express Wilms' tumor-1. Wt1 expression in the developing, adult

and infarcted heart. J. Mol. Cell. Cardiol. *81*, 127–135.

Duim, S.N., Goumans, M.-J., and Kruithof, B.P.T. (2016). WT1 in Cardiac Development and Disease (Codon Publications).

Edelstein, A.D., Tsuchida, M.A., Amodaj, N., Pinkard, H., Vale, R.D., and Stuurman, N. (2014). Advanced methods of microscope control using μManager software. J. Biol. Methods *1*, 10.

Elias, I., Franckhauser, S., Ferré, T., Vilà, L., Tafuro, S., Muñoz, S., Roca, C., Ramos, D., Pujol, A., Riu, E., et al. (2012). Adipose tissue overexpression of vascular endothelial growth factor protects against diet-induced obesity and insulin resistance. Diabetes *61*, 1801–1813.

Essafi, A., Webb, A., Berry, R.L., Slight, J., Burn, S.F., Spraggon, L., Velecela, V., Martinez-Estrada, O.M., Wiltshire, J.H., Roberts, S.G.E., et al. (2011). A wt1-controlled chromatin switching mechanism underpins tissue-specific wnt4 activation and repression. Dev. Cell *21*, 559–574.

Fain, J.N., Madan, A.K., Hiler, M.L., Cheema, P., and Bahouth, S.W. (2004). Comparison of the Release of Adipokines by Adipose Tissue, Adipose Tissue Matrix, and Adipocytes from Visceral and Subcutaneous Abdominal Adipose Tissues of Obese Humans. Endocrinology *145*, 2273–2282.

Fang, H., and Judd, R.L. (2018). Adiponectin Regulation and Function. In Comprehensive Physiology, (Hoboken, NJ, USA: John Wiley & Sons, Inc.), pp. 1031–1063.

Francescone, R.A., Faibish, M., and Shao, R. (2011). A matrigel-based tube formation assay to assess the vasculogenic activity of tumor cells. J. Vis. Exp.

Franco, M., Roswall, P., Cortez, E., Hanahan, D., and Pietras, K. (2011). Pericytes promote endothelial cell survival through induction of autocrine VEGF-A signaling and Bcl-w expression. Blood *118*, 2906–2917.

Fried, S.K., Bunkin, D.A., and Greenberg, A.S. (1998). Omental and Subcutaneous Adipose Tissues of Obese Subjects Release Interleukin-6: Depot Difference and Regulation by Glucocorticoid [1]. J. Clin. Endocrinol. Metab. *83*, 847–850.

Friedman, J. (2016). The long road to leptin. J. Clin. Invest. *126*, 4727–4734.

Gao, M., Zhang, C., Ma, Y., Bu, L., Yan, L., and Liu, D. (2013). Hydrodynamic

delivery of mIL10 gene protects mice from high-fat diet-induced obesity and glucose intolerance. Mol. Ther. *21*, 1852–1861.

Gashler, A.L., Bonthron, D.T., Madden, S.L., Rauscher, F.J., Collins, T., and Sukhatme, V.P. (1992). Human platelet-derived growth factor A chain is transcriptionally repressed by the Wilms tumor suppressor WT1. Proc. Natl. Acad. Sci. U. S. A. *89*, 10984–10988.

Gavin, K.M., Gutman, J.A., Kohrt, W.M., Wei, Q., Shea, K.L., Miller, H.L., Sullivan, T.M., Erickson, P.F., Helm, K.M., Acosta, A.S., et al. (2016). *De novo* generation of adipocytes from circulating progenitor cells in mouse and human adipose tissue. FASEB J. *30*, 1096–1108.

Gealekman, O., Burkart, A., Chouinard, M., Nicoloro, S.M., Straubhaar, J., and Corvera, S. (2008). Enhanced angiogenesis in obesity and in response to PPARgamma activators through adipocyte VEGF and ANGPTL4 production. Am. J. Physiol. Endocrinol. Metab. *295*, E1056-64.

Gealekman, O., Guseva, N., Hartigan, C., Apotheker, S., Gorgoglione, M., Gurav, K., Tran, K.-V., Straubhaar, J., Nicoloro, S., Czech, M.P., et al. (2011). Depot-Specific Differences and Insufficient Subcutaneous Adipose Tissue Angiogenesis in Human Obesity. Circulation *123*, 186–194.

Gerhardt, H. (2008). VEGF and endothelial guidance in angiogenic sprouting. Organogenesis *4*, 241–246.

Gerhardt, H., Golding, M., Fruttiger, M., Ruhrberg, C., Lundkvist, A., Abramsson, A., Jeltsch, M., Mitchell, C., Alitalo, K., Shima, D., et al. (2003). VEGF guides angiogenic sprouting utilizing endothelial tip cell filopodia. J. Cell Biol. *161*, 1163–1177.

Gessler, M., Poustka, A., Cavenee, W., Neve, R.L., Orkin, S.H., and Bruns, G.A.P. (1990). Homozygous deletion in Wilms tumours of a zinc-finger gene identified by chromosome jumping. Nature *343*, 774–778.

von Gise, A., Zhou, B., Honor, L.B., Ma, Q., Petryk, A., and Pu, W.T. (2011). WT1 regulates epicardial epithelial to mesenchymal transition through β-catenin and retinoic acid signaling pathways. Dev. Biol. *356*, 421–431.

Gomez-Salazar, M., Gonzalez-Galofre, Z.N., Casamitjana, J., Crisan, M., James,

A.W., and Péault, B. (2020). Five Decades Later, Are Mesenchymal Stem Cells Still Relevant? Front. Bioeng. Biotechnol. *8*, 148.

Goossens, G.H., Bizzarri, A., Venteclef, N., Essers, Y., Cleutjens, J.P., Konings, E., Jocken, J.W.E., Cajlakovic, M., Ribitsch, V., Clément, K., et al. (2011). Increased adipose tissue oxygen tension in obese compared with lean men is accompanied by insulin resistance, impaired adipose tissue capillarization, and inflammation. Circulation *124*, 67–76.

Greenberg, J.I., Shields, D.J., Barillas, S.G., Acevedo, L.M., Murphy, E., Huang, J., Scheppke, L., Stockmann, C., Johnson, R.S., Angle, N., et al. (2008). A role for VEGF as a negative regulator of pericyte function and vessel maturation. Nature *456*, 809–813.

Gupta, O.T., and Gupta, R.K. (2015). Visceral Adipose Tissue Mesothelial Cells: Living on the Edge or Just Taking Up Space? Trends Endocrinol. Metab.

Gupta, R.K., Arany, Z., Seale, P., Mepani, R.J., Ye, L., Conroe, H.M., Roby, Y.A., Kulaga, H., Reed, R.R., and Spiegelman, B.M. (2010). Transcriptional control of preadipocyte determination by Zfp423. Nature *464*, 619–623.

Gupta, R.K., Mepani, R.J., Kleiner, S., Lo, J.C., Khandekar, M.J., Frontini, A., Bhowmick, D.C., Ye, L., Cinti, S., and Bruce, M. (2013). Zfp423 Expression Identifies Committed Preadipocytes. *15*, 617–632.

Gupta, R.K.K., Mepani, R.J.J., Kleiner, S., Lo, J.C.C., Khandekar, M.J.J., Cohen, P., Frontini, A., Bhowmick, D.C.C., Ye, L., Cinti, S., et al. (2012). Zfp423 expression identifies committed preadipocytes and localizes to adipose endothelial and perivascular cells. Cell Metab. *15*, 230–239.

Halberg, N., Khan, T., Trujillo, M.E., Wernstedt-Asterholm, I., Attie, A.D., Sherwani, S., Wang, Z. V, Landskroner-Eiger, S., Dineen, S., Magalang, U.J., et al. (2009). Hypoxia-inducible factor 1alpha induces fibrosis and insulin resistance in white adipose tissue. Mol. Cell. Biol. *29*, 4467–4483.

Hammes, A., Guo, J.-K., Lutsch, G., Leheste, J.-R., Landrock, D., Ziegler, U., Gubler, M.-C., and Schedl, A. (2001). Two Splice Variants of the Wilms' Tumor 1 Gene Have Distinct Functions during Sex Determination and Nephron Formation. Cell *106*, 319–329.

Han, J., Lee, J.-E., Jin, J., Lim, J.S., Oh, N., Kim, K., Chang, S.-I., Shibuya, M., Kim, H., and Koh, G.Y. (2011). The spatiotemporal development of adipose tissue. Development *138*, 5027–5037.

Han, Y., San-Marina, S., Liu, J., and Minden, M.D. (2004). Transcriptional activation of c-myc proto-oncogene by WT1 protein. Oncogene *23*, 6933–6941.

Hanson, J., Gorman, J., Reese, J., and Fraizer, G. (2007). Regulation of vascular endothelial growth factor, VEGF, gene promoter by the tumor suppressor, WT1. Front. Biosci. *12*, 2279–2290.

Harper, S.J., and Bates, D.O. (2008). VEGF-A splicing: the key to anti-angiogenic therapeutics? Nat. Rev. Cancer *8*, 880–887.

Hastie, N.D. (2017). Wilms' tumour 1 (WT1) in development, homeostasis and disease. Development *144*, 2862–2872.

Hayashi, T., Boyko, E.J., Leonetti, D.L., McNeely, M.J., Newell-Morris, L., Kahn, S.E., and Fujimoto, W.Y. (2003). Visceral adiposity and the prevalence of hypertension in Japanese Americans. Circulation *108*, 1718–1723.

He, K.L., Deora, A.B., Xiong, H., Ling, Q., Weksler, B.B., Niesvizky, R., and Hajjar, K.A. (2008). Endothelial cell annexin A2 regulates polyubiquitination and degradation of its binding partner S100A10/p11. J. Biol. Chem. *283*, 19192–19200.

He, Q., Gao, Z., Yin, J., Zhang, J., Yun, Z., and Ye, J. (2011). Regulation of HIF-1{alpha} activity in adipose tissue by obesity-associated factors: adipogenesis, insulin, and hypoxia. Am. J. Physiol. Endocrinol. Metab. *300*, E877-85.

Hepler, C., Shan, B., Zhang, Q., Henry, G.H., Shao, M., Vishvanath, L., Ghaben, A.L., Mobley, A.B., Strand, D., Hon, G.C., et al. (2018a). Identification of functionally distinct fibro-inflammatory and adipogenic stromal subpopulations in visceral adipose tissue of adult mice. Elife *7*, 1–36.

Hepler, C., Shan, B., Zhang, Q., Henry, G.H., Shao, M., Vishvanath, L., Ghaben, A.L., Mobley, A.B., Strand, D., Hon, G.C., et al. (2018b). Identification of functionally distinct fibro-inflammatory and adipogenic stromal subpopulations in visceral adipose tissue of adult mice. Elife *7*.

Herzer, U., Crocoll, A., Barton, D., Howells, N., and Englert, C. The Wilms tumor suppressor gene wt1 is required for development of the spleen. Curr. Biol. *9*, 837–

840.

Hindle, P., Khan, N., Biant, L., and Péault, B. (2017). The Infrapatellar Fat Pad as a Source of Perivascular Stem Cells with Increased Chondrogenic Potential for Regenerative Medicine. Stem Cells Transl. Med. *6*, 77–87.

Hohenstein, P., and Hastie, N.D. (2006). The many facets of the Wilms' tumour gene, WT1. Hum. Mol. Genet. *15*, 196–201.

Hosen, N., Shirakata, T., Nishida, S., Yanagihara, M., Tsuboi, A., Kawakami, M., Oji, Y., Oka, Y., Okabe, M., Tan, B., et al. (2007). The Wilms' tumor gene WT1-GFP knock-in mouse reveals the dynamic regulation of WT1 expression in normal and leukemic hematopoiesis. Leukemia *21*, 1783–1791.

Houck, K.A., Ferrara, N., Winer, J., Cachianes, G., Li, B., and Leung, D.W. (1991). The Vascular Endothelial Growth Factor Family: Identification of a Fourth Molecular Species and Characterization of Alternative Splicing of RNA. Mol. Endocrinol. *5*, 1806–1814.

Howe, L.R., Subbaramaiah, K., Hudis, C.A., and Dannenberg, A.J. (2013). Molecular pathways: adipose inflammation as a mediator of obesity-associated cancer. Clin. Cancer Res. *19*, 6074–6083.

Hsu, S.Y., Kubo, M., Chun, S.Y., Haluska, F.G., Housman, D.E., and Hsueh, A.J. (1995). Wilms' tumor protein WT1 as an ovarian transcription factor: decreases in expression during follicle development and repression of inhibin-alpha gene promoter. Mol. Endocrinol. *9*, 1356–1366.

Humphreys, B.D., Lin, S.-L., Kobayashi, A., Hudson, T.E., Nowlin, B.T., Bonventre, J. V, Valerius, M.T., McMahon, A.P., and Duffield, J.S. (2010a). Fate tracing reveals the pericyte and not epithelial origin of myofibroblasts in kidney fibrosis. Am. J. Pathol. *176*, 85–97.

Humphreys, B.D., Lin, S.L., Kobayashi, A., Hudson, T.E., Nowlin, B.T., Bonventre, J. V., Valerius, M.T., McMahon, A.P., and Duffield, J.S. (2010b). Fate tracing reveals the pericyte and not epithelial origin of myofibroblasts in kidney fibrosis. Am. J. Pathol. *176*, 85–97.

Hung, B.P., Hutton, D.L., Kozielski, K.L., Bishop, C.J., Naved, B., Green, J.J., Caplan, A.I., Gimble, J.M., Dorafshar, A.H., and Grayson, W.L. (2015). Platelet-

Derived Growth Factor BB Enhances Osteogenesis of Adipose-Derived but Not Bone Marrow-Derived Mesenchymal Stromal/Stem Cells. Stem Cells *33*, 2773–2784.

Iozzo, R. V., and Sanderson, R.D. (2011). Proteoglycans in cancer biology, tumour microenvironment and angiogenesis. J. Cell. Mol. Med. *15*, 1013–1031.

James, A.W., and Péault, B. (2019). Perivascular Mesenchymal Progenitors for Bone Regeneration. J. Orthop. Res. *37*, 1221–1228.

Januszyk, M., Rennert, R., Sorkin, M., Maan, Z., Wong, L., Whittam, A., Whitmore, A., Duscher, D., and Gurtner, G. (2015). Evaluating the Effect of Cell Culture on Gene Expression in Primary Tissue Samples Using Microfluidic-Based Single Cell Transcriptional Analysis. Microarrays *4*, 540–550.

Jeffery, E., Wing, A., Holtrup, B., Sebo, Z., Kaplan, J.L., Saavedra-Peña, R., Church, C.D., Colman, L., Berry, R., and Rodeheffer, M.S. (2016). The Adipose Tissue Microenvironment Regulates Depot-Specific Adipogenesis in Obesity. Cell Metab. *24*, 142–150.

Kahn, A.M., Seidel, C.L., Allen, J.C., O'Neil, R.G., Shelat, H., and Song, T. (1993). Insulin reduces contraction and intracellular calcium concentration in vascular smooth muscle. Hypertension *22*, 735–742.

Kahn, A.M., Husid, A., Odebunmi, T., Allen, J.C., Seidel, C.L., and Song, T. (1998). Insulin inhibits vascular smooth muscle contraction at a site distal to intracellular Ca2+ concentration. Am. J. Physiol. - Endocrinol. Metab. *274*.

Kaidonis, G., Burdon, K.P., Gillies, M.C., Abhary, S., Essex, R.W., Chang, J.H., Pal, B., Pefkianaki, M., Daniell, M., Lake, S., et al. (2015). Common Sequence Variation in the VEGFC Gene Is Associated with Diabetic Retinopathy and Diabetic Macular Edema. Ophthalmology *122*, 1828–1836.

Kaiyala, K.J., Ogimoto, K., Nelson, J.T., Muta, K., and Morton, G.J. (2016). Physiological role for leptin in the control of thermal conductance. Mol. Metab. *5*, 892–902.

Kalluri, R. (2016). The biology and function of fibroblasts in cancer. Nat. Rev. Cancer 2016 169 *16*, 582.

Kang, H.W., Kim, D., Kim, H.J., Kim, C.H., Kim, Y.S., Park, M.J., Kim, J.S., Cho, S.-

H., Sung, M.-W., Jung, H.C., et al. (2010). Visceral obesity and insulin resistance as risk factors for colorectal adenoma: a cross-sectional, case-control study. Am. J. Gastroenterol. *105*, 178–187.

Karki, S., Surolia, R., Hock, T.D., Guroji, P., Zolak, J.S., Duggal, R., Ye, T., Thannickal, V.J., and Antony, V.B. (2014). Wilms' tumor 1 (Wt1) regulates pleural mesothelial cell plasticity and transition into myofibroblasts in idiopathic pulmonary fibrosis. FASEB J. *28*, 1122–1131.

Katsuda, Y., Asano, A., Murase, Y., Chujo, D., Yagi, K., Kobayashi, J., Mabuchi, H., and Yamagishi, M. (2007). Association of Genetic Variation of the Adiponectin gene with Body Fat Distribution and Carotid Atherosclerosis in Japanese Obese Subjects. J. Atheroscler. Thromb. *14*, 19–26.

Katuri, V., Gerber, S., Qiu, X., McCarty, G., Goldstein, S.D., Hammers, H., Montgomery, E., Chen, A.R., and Loeb, D.M. (2014). WT1 regulates angiogenesis in Ewing Sarcoma. Oncotarget *5*, 2436–2449.

Kawanishi, K. (2016). Diverse properties of the mesothelial cells in health and disease. Pleura and Peritoneum *1*, 79–89.

Keith, B., Johnson, R.S., and Simon, M.C. (2011). HIF1α and HIF2α: sibling rivalry in hypoxic tumour growth and progression. Nat. Rev. Cancer *12*, 9–22.

Kerst, G., Bergold, N., Viebahn, S., Gieseke, F., Kalinova, M., Trka, J., Handgretinger, R., and Müller, I. (2008). WT1 protein expression in slowly proliferating myeloid leukemic cell lines is scarce throughout the cell cycle with a minimum in G0/G1 phase. Leuk. Res. *32*, 1393–1399.

Kim, B., Lee, B., Kim, M.-K., Gong, S.P., Park, N.H., Chung, H.H., Kim, H.S., No, J.H., Park, W.Y., Park, A.K., et al. (2016). Gene expression profiles of human subcutaneous and visceral adipose-derived stem cells. Cell Biochem. Funct. *34*, 563–571.

Kirschner, K.M., Wagner, N., Wagner, K.-D., Wellmann, S., and Scholz, H. (2006). The Wilms tumor suppressor Wt1 promotes cell adhesion through transcriptional activation of the alpha4integrin gene. J. Biol. Chem. *281*, 31930–31939.

Klein, D., Meissner, N., Kleff, V., Jastrow, H., Yamaguchi, M., Süleyman Ergün, and Jendrossek, V. (2014). Nestin(+) tissue-resident multipotent stem cells contribute to

tumor progression by differentiating into pericytes and smooth muscle cells resulting in blood vessel remodeling. Front. Oncol. *4 JUN*.

Koesters, R., Linnebacher, M., Coy, J.F., Germann, A., Schwitalle, Y., Findeisen, P., and von Knebel Doeberitz, M. (2004). WT1 is a tumor-associated antigen in colon cancer that can be recognized byin vitro stimulated cytotoxic T cells. Int. J. Cancer *109*, 385–392.

Kreidberg, J.A., Sariola, H., Loring, J.M., Maeda, M., Pelletier, J., Housman, D., and Jaenisch, R. (1993a). WT-1 is required for early kidney development. Cell *74*, 679–691.

Kreidberg, J.A., Sariola, H., Loring, J.M., Maeda, M., Pelletier, J., Housman, D., and Jaenisch, R. (1993b). WT-1 is required for early kidney development. Cell *74*, 679–691.

Krock, B.L., Skuli, N., and Simon, M.C. (2011). Hypoxia-induced angiogenesis: good and evil. Genes Cancer *2*, 1117–1133.

Krotkiewski, M., Björntorp, P., Sjöström, L., and Smith, U. (1983). Impact of obesity on metabolism in men and women. Importance of regional adipose tissue distribution. J. Clin. Invest. *72*, 1150–1162.

Kuk, J.L., Katzmarzyk, P.T., Nichaman, M.Z., Church, T.S., Blair, S.N., and Ross, R. (2006). Visceral Fat Is an Independent Predictor of All-cause Mortality in Men*. Obesity *14*, 336–341.

Kvist, H., Chowdhury, B., Grangård, U., Tylén, U., and Sjöström, L. (1988). Total and visceral adipose-tissue volumes derived from measurements with computed tomography in adult men and women: predictive equations. Am. J. Clin. Nutr. *48*, 1351–1361.

Lanska, D.J., Lanska, M.J., Hartz, A.J., and Rimm, A.A. (1985). Factors influencing anatomic location of fat tissue in 52,953 women. Int. J. Obes. *9*, 29–38.

Ledoux, S., Queguiner, I., Msika, S., Calderari, S., Rufat, P., Gasc, J.-M., Corvol, P., and Larger, E. (2008). Angiogenesis associated with visceral and subcutaneous adipose tissue in severe human obesity. Diabetes *57*, 3247–3257.

Lee, H.-P., Lin, C.-Y., Shih, J.-S., Fong, Y.-C., Wang, S.-W., Li, T.-M., and Tang, C.-H. (2015). Adiponectin promotes VEGF-A-dependent angiogenesis in human

chondrosarcoma through PI3K, Akt, mTOR, and HIF-α pathway. Oncotarget *6*, 36746–36761.

Lee, K.Y., Luong, Q., Sharma, R., Dreyfuss, J.M., Ussar, S., and Kahn, C.R. (2019). Developmental and functional heterogeneity of white adipocytes within a single fat depot. EMBO J. *38*, e99291.

Lee, M.J., Pickering, R.T., and Puri, V. (2014a). Prolonged efficiency of siRNA-mediated gene silencing in primary cultures of human preadipocytes and adipocytes. Obesity *22*, 1064–1069.

Lee, Y.S., Kim, J., Osborne, O., Oh, D.Y., Sasik, R., Schenk, S., Chen, A., Chung, H., Murphy, A., Watkins, S.M., et al. (2014b). Increased adipocyte O2 consumption triggers HIF-1α, causing inflammation and insulin resistance in obesity. Cell *157*, 1339–1352.

Lefebvre, J., Clarkson, M., Massa, F., Bradford, S.T., Charlet, A., Buske, F., Lacas-Gervais, S., Schulz, H., Gimpel, C., Hata, Y., et al. (2015). Alternatively spliced isoforms of WT1 control podocyte-specific gene expression. Kidney Int. *88*, 321–331.

Lemoine, A.Y., Ledoux, S., Quéguiner, I., Caldérari, S., Mechler, C., Msika, S., Corvol, P., and Larger, E. (2012). Link between Adipose Tissue Angiogenesis and Fat Accumulation in Severely Obese Subjects. J. Clin. Endocrinol. Metab. *97*, E775–E780.

Leopold, B., Strutz, J., Weiß, E., Gindlhuber, J., Birner-Gruenberger, R., Hackl, H., Appel, H.M., Cvitic, S., and Hiden, U. (2019). Outgrowth, proliferation, viability, angiogenesis and phenotype of primary human endothelial cells in different purchasable endothelial culture media: feed wisely. Histochem. Cell Biol. *152*, 377–390.

Lertkiatmongkol, P., Liao, D., Mei, H., Hu, Y., and Newman, P.J. (2016). Endothelial functions of platelet/endothelial cell adhesion molecule-1 (CD31). Curr. Opin. Hematol. *23*, 253–259.

Lin, S.L., Kisseleva, T., Brenner, D.A., and Duffield, J.S. (2008). Pericytes and perivascular fibroblasts are the primary source of collagen-producing cells in obstructive fibrosis of the kidney. Am. J. Pathol. *173*, 1617–1627.

Loonstra, A., Vooijs, M., Beverloo, H.B., Allak, B.A., van Drunen, E., Kanaar, R., Berns, A., and Jonkers, J. (2001). Growth inhibition and DNA damage induced by Cre recombinase in mammalian cells. Proc. Natl. Acad. Sci. U. S. A. *98*, 9209–9214.

Maeda, N., Shimomura, I., Kishida, K., Nishizawa, H., Matsuda, M., Nagaretani, H., Furuyama, N., Kondo, H., Takahashi, M., Arita, Y., et al. (2002). Diet-induced insulin resistance in mice lacking adiponectin/ACRP30. Nat. Med. *8*, 731–737.

Majesky, M.W., Dong, X.R., Regan, J.N., and Hoglund, V.J. (2011). Vascular smooth muscle progenitor cells: Building and repairing blood vessels. Circ. Res. *108*, 365–377.

Martínez-Estrada, O.M., Lettice, L.A., Essafi, A., Guadix, J.A., Slight, J., Velecela, V., Hall, E., Reichmann, J., Devenney, P.S., Hohenstein, P., et al. (2010). Wt1 is required for cardiovascular progenitor cell formation through transcriptional control of Snail and E-cadherin. Nat. Genet. *42*, 89–93.

Matkar, P., Ariyagunarajah, R., Leong-Poi, H., Singh, K., Matkar, P.N., Ariyagunarajah, R., Leong-Poi, H., and Singh, K.K. (2017). Friends Turned Foes: Angiogenic Growth Factors beyond Angiogenesis. Biomolecules *7*, 74.

McCarty, G., Awad, O., and Loeb, D.M. (2011). WT1 protein directly regulates expression of vascular endothelial growth factor and is a mediator of tumor response to hypoxia. J. Biol. Chem. *286*, 43634–43643.

McHaffie, S.L., Hastie, N.D., and Chau, Y.-Y. (2016). Effects of CreERT2, 4-OH Tamoxifen, and Gender on CFU-F Assays. PLoS One *11*, e0148105.

Mehrotra, D., Wu, J., Papangeli, I., and Chun, H.J. (2014). Endothelium as a gatekeeper of fatty acid transport. Trends Endocrinol. Metab. *25*, 99–106.

Montesano, R., Pepper, M.S., Möhle-Steinlein, U., Risau, W., Wagner, E.F., and Orci, L. (1990). Increased proteolytic activity is responsible for the aberrant morphogenetic behavior of endothelial cells expressing the middle T oncogene. Cell *62*, 435–445.

Moore, A.W., McInnes, L., Kreidberg, J., Hastie, N.D., and Schedl, A. (1999). YAC complementation shows a requirement for Wt1 in the development of epicardium, adrenal gland and throughout nephrogenesis. Development.

Mori, S., Kiuchi, S., Ouchi, A., Hase, T., and Murase, T. (2014). Characteristic

expression of extracellular matrix in subcutaneous adipose tissue development and adipogenesis; Comparison with visceral adipose tissue. Int. J. Biol. Sci. *10*, 825–833.

Morris, M.E., Beare, J.E., Reed, R.M., Dale, J.R., LeBlanc, A.J., Kaufman, C.L., Zheng, H., Ng, C.K., Williams, S.K., and Hoying, J.B. (2015). Systemically delivered adipose stromal vascular fraction cells disseminate to peripheral artery walls and reduce vasomotor tone through a CD11b+ cell-dependent mechanism. Stem Cells Transl. Med. *4*, 369–380.

Motamedi, F.J., Badro, D.A., Clarkson, M., Lecca, M.R., Bradford, S.T., Buske, F.A., Saar, K., Hübner, N., Brändli, A.W., and Schedl, A. (2014). WT1 controls antagonistic FGF and BMP-pSMAD pathways in early renal progenitors. Nat. Commun. *5*.

Murphy, C.S., Liaw, L., and Reagan, M.R. (2019). In vitro tissue-engineered adipose constructs for modeling disease. BMC Biomed. Eng. *1*.

Muzumdar, M.D., Tasic, B., Miyamichi, K., Li, N., and Luo, L. (2007). A global double-fluorescent cre reporter mouse. Genesis *45*, 593–605.

Nian, M., Lee, P., Khaper, N., and Liu, P. (2004). Inflammatory cytokines and postmyocardial infarction remodeling. Circ. Res. *94*, 1543–1553.

Nishimura, S., Manabe, I., Nagasaki, M., Seo, K., Yamashita, H., Hosoya, Y., Ohsugi, M., Tobe, K., Kadowaki, T., Nagai, R., et al. (2008). In vivo imaging in mice reveals local cell dynamics and inflammation in obese adipose tissue. J. Clin. Invest. *118*, 710–721.

Nosalski, R., and Guzik, T.J. (2017). Perivascular adipose tissue inflammation in vascular disease. Br. J. Pharmacol. *174*, 3496–3513.

Nugroho, D.B., Ikeda, K., Barinda, A.J., Wardhana, D.A., Yagi, K., Miyata, K., Oike, Y., Hirata, K. ichi, and Emoto, N. (2018). Neuregulin-4 is an angiogenic factor that is critically involved in the maintenance of adipose tissue vasculature. Biochem. Biophys. Res. Commun. *503*, 378–384.

O'Neill, S., and O'Driscoll, L. (2015). Metabolic syndrome: a closer look at the growing epidemic and its associated pathologies. Obes. Rev. *16*, 1–12.

Oji, Y., Suzuki, T., Nakano, Y., Maruno, M., Nakatsuka, S., Jomgeow, T., Abeno, S.,

Tatsumi, N., Yokota, A., Aoyagi, S., et al. (2004). Overexpression of the Wilms' tumor gene WT1 in primary astrocytic tumors. Cancer Sci. *95*, 822–827.

Onogi, Y., Wada, T., Kamiya, C., Inata, K., Matsuzawa, T., Inaba, Y., Kimura, K., Inoue, H., Yamamoto, S., Ishii, Y., et al. (2017). PDGFRβ Regulates Adipose Tissue Expansion and Glucose Metabolism via Vascular Remodeling in Diet-Induced Obesity. Diabetes *66*, 1008–1021.

Owens, G.K. (1995). Regulation of differentiation of vascular smooth muscle cells. Physiol. Rev. *75*, 487–517.

De Palma, M., Biziato, D., and Petrova, T. V. (2017). Microenvironmental regulation of tumour angiogenesis. Nat. Rev. Cancer *17*, 457–474.

Paris, N.D., Coles, G.L., and Ackerman, K.G. (2015). Wt1 and β-catenin cooperatively regulate diaphragm development in the mouse. Dev. Biol. *407*, 40–56.

Park, J., Kim, M., Sun, K., An, Y.A., Gu, X., and Scherer, P.E. (2017). VEGF-A-Expressing Adipose Tissue Shows Rapid Beiging and Enhanced Survival After Transplantation and Confers IL-4-Independent Metabolic Improvements. Diabetes *66*, 1479–1490.

Pasarica, M., Sereda, O.R., Redman, L.M., Albarado, D.C., Hymel, D.T., Roan, L.E., Rood, J.C., Burk, D.H., and Smith, S.R. (2009). Reduced Adipose Tissue Oxygenation in Human Obesity: Evidence for Rarefaction, Macrophage Chemotaxis, and Inflammation Without an Angiogenic Response. Diabetes *58*, 718.

Pascot, A., Lemieux, I., Prud'homme, D., Tremblay, A., Nadeau, A., Couillard, C., Bergeron, J., Lamarche, B., and Després, J.P. (2001). Reduced HDL particle size as an additional feature of the atherogenic dyslipidemia of abdominal obesity. J. Lipid Res. *42*, 2007–2014.

Pausova, Z., Abrahamowicz, M., Mahboubi, A., Syme, C., Leonard, G.T., Perron, M., Richer, L., Veillette, S., Gaudet, D., and Paus, T. (2010). Functional Variation in the Androgen-Receptor Gene Is Associated With Visceral Adiposity and Blood Pressure in Male Adolescents. Hypertension *55*, 706–714.

Peeters, A. V., Beckers, S., Verrijken, A., Mertens, I., Roevens, P., Peeters, P.J., Van Hul, W., and Van Gaal, L.F. (2008). Association of SIRT1 gene variation with visceral obesity. Hum. Genet. *124*, 431–436.

Piqueras, L., Reynolds, A.R., Hodivala-Dilke, K.M., Alfranca, A., Redondo, J.M., Hatae, T., Tanabe, T., Warner, T.D., and Bishop-Bailey, D. (2007). Activation of PPARbeta/delta induces endothelial cell proliferation and angiogenesis. Arterioscler. Thromb. Vasc. Biol. *27*, 63–69.

Pittenger, M.F., Discher, D.E., Péault, B.M., Phinney, D.G., Hare, J.M., and Caplan, A.I. (2019). Mesenchymal stem cell perspective: cell biology to clinical progress. Npj Regen. Med. *4*, 1–15.

Pouliot, M.C., Després, J.P., Nadeau, A., Moorjani, S., Prud'Homme, D., Lupien, P.J., Tremblay, A., and Bouchard, C. (1992). Visceral obesity in men. Associations with glucose tolerance, plasma insulin, and lipoprotein levels. Diabetes *41*, 826–834.

Quail, D.F., and Dannenberg, A.J. (2019). The obese adipose tissue microenvironment in cancer development and progression. Nat. Rev. Endocrinol. *15*, 139–154.

Que, J., Wilm, B., Hasegawa, H., Wang, F., Bader, D., and Hogan, B.L.M. (2008). Mesothelium contributes to vascular smooth muscle and mesenchyme during lung development. Proc. Natl. Acad. Sci. U. S. A. *105*, 16626–16630.

Ramage, L.E., Akyol, M., Fletcher, A.M., Forsythe, J., Nixon, M., Carter, R.N., van Beek, E.J.R., Morton, N.M., Walker, B.R., and Stimson, R.H. (2016). Glucocorticoids Acutely Increase Brown Adipose Tissue Activity in Humans, Revealing Species-Specific Differences in UCP-1 Regulation. Cell Metab. *24*, 130–141.

Rehman, J., Traktuev, D., Li, J., Merfeld-Clauss, S., Temm-Grove, C.J., Bovenkerk, J.E., Pell, C.L., Johnstone, B.H., Considine, R. V, and March, K.L. (2004). Secretion of angiogenic and antiapoptotic factors by human adipose stromal cells. Circulation *109*, 1292–1298.

Richards, O.C., Raines, S.M., and Attie, A.D. (2010). The role of blood vessels, endothelial cells, and vascular pericytes in insulin secretion and peripheral insulin action. Endocr. Rev. *31*, 343–363.

Rodeheffer, M.S., Birsoy, K., and Friedman, J.M. (2008). Identification of White Adipocyte Progenitor Cells In Vivo. Cell *135*, 240–249.

Rojas-Rodriguez, R., Gealekman, O., Kruse, M.E., Rosenthal, B., Rao, K., Min, S., Bellve, K.D., Lifshitz, L.M., and Corvera, S. (2014). Adipose tissue angiogenesis

assay (Elsevier Inc.).

Rouget, C. (1873). Memoire sur le developpement la structure et les proprietes physiologiques des capillaires sanguins et lymphatiques. Arch Physiol Norm Path *5*, 603–663.

Ruderman, N., Chisholm, D., Pi-Sunyer, X., and Schneider, S. (1998). The metabolically obese, normal-weight individual revisited. Diabetes *47*, 699–713.

Ruhrberg, C., Gerhardt, H., Golding, M., Watson, R., Ioannidou, S., Fujisawa, H., Betsholtz, C., and Shima, D.T. (2002). Spatially restricted patterning cues provided by heparin-binding VEGF-A control blood vessel branching morphogenesis. Genes Dev. *16*, 2684–2698.

Ruiz-Ojeda, F.J., Méndez-Gutiérrez, A., Aguilera, C.M., and Plaza-Díaz, J. (2019). Extracellular matrix remodeling of adipose tissue in obesity and metabolic diseases. Int. J. Mol. Sci. *20*.

Rupnick, M.A., Panigrahy, D., Zhang, C.-Y., Dallabrida, S.M., Lowell, B.B., Langer, R., and Folkman, M.J. (2002). Adipose tissue mass can be regulated through the vasculature. Proc. Natl. Acad. Sci. U. S. A. *99*, 10730–10735.

Salans, L.B., Knittle, J.L., and Hirsch, J. (1968). The role of adipose cell size and adipose tissue insulin sensitivity in the carbohydrate intolerance of human obesity. J. Clin. Invest. *47*, 153–165.

Scheja, L., and Heeren, J. (2019). The endocrine function of adipose tissues in health and cardiometabolic disease. Nat. Rev. Endocrinol. 1.

Schlich, R., Willems, M., Greulich, S., Ruppe, F., Knoefel, W.T., Ouwens, D.M., Maxhera, B., Lichtenberg, A., Eckel, J., and Sell, H. (2013). VEGF in the crosstalk between human adipocytes and smooth muscle cells: depot-specific release from visceral and perivascular adipose tissue. Mediators Inflamm. *2013*, 982458.

Scholz, H., Wagner, K.D., and Wagner, N. (2009). Role of the Wilms' tumour transcription factor, Wt1, in blood vessel formation. Pflugers Arch. Eur. J. Physiol. *458*, 315–323.

Schrimpf, C., and Duffield, J.S. (2011). Mechanisms of fibrosis: the role of the pericyte. Curr. Opin. Nephrol. Hypertens. *20*, 297–305.

Sciesielski, L.K., Kirschner, K.M., Scholz, H., and Persson, A.B. (2010). Wilms'

tumor protein Wt1 regulates the Interleukin-10 (IL-10) gene. FEBS Lett. *584*, 4665–4671.

Scott, M.M., Williams, K.W., Rossi, J., Lee, C.E., and Elmquist, J.K. (2011). Leptin receptor expression in hindbrain Glp-1 neurons regulates food intake and energy balance in mice. J. Clin. Invest. *121*, 2413–2421.

Seidell, J.C., Björntorp, P., Sjöström, L., Kvist, H., and Sannerstedt, R. (1990). Visceral fat accumulation in men is positively associated with insulin, glucose, and C-peptide levels, but negatively with testosterone levels. Metabolism. *39*, 897–901.

Senesi, L., De Francesco, F., Farinelli, L., Manzotti, S., Gagliardi, G., Papalia, G.F., Riccio, M., and Gigante, A. (2019). Mechanical and enzymatic procedures to isolate the stromal vascular fraction from adipose tissue: Preliminary results. Front. Cell Dev. Biol. *7*.

Shao, M., Vishvanath, L., Busbuso, N.C., Hepler, C., Shan, B., Sharma, A.X., Chen, S., Yu, X., An, Y.A., Zhu, Y., et al. (2018). De novo adipocyte differentiation from Pdgfrβ + preadipocytes protects against pathologic visceral adipose expansion in obesity. Nat. Commun.

Shaw, I., Rider, S., Mullins, J., Hughes, J., and Péault, B. (2018). Pericytes in the renal vasculature: Roles in health and disease. Nat. Rev. Nephrol. *14*, 521–534.

Small, T.W., Bolender, Z., Bueno, C., O'Neil, C., Nong, Z., Rushlow, W., Rajakumar, N., Kandel, C., Strong, J., Madrenas, J., et al. (2006). Wilms' tumor 1-associating protein regulates the proliferation of vascular smooth muscle cells. Circ. Res. *99*, 1338–1346.

Song, M.-G., Lee, H.-J., Jin, B.-Y., Gutierrez-Aguilar, R., Shin, K.-H., Choi, S.-H., Um, S.H., and Kim, D.-H. (2016). Depot-specific differences in angiogenic capacity of adipose tissue in differential susceptibility to diet-induced obesity. Mol. Metab. *5*, 1113–1120.

Sontake, V., Kasam, R.K., Sinner, D., Korfhagen, T.R., Reddy, G.B., White, E.S., Jegga, A.G., and Madala, S.K. (2018). Wilms' tumor 1 drives fibroproliferation and myofibroblast transformation in severe fibrotic lung disease. JCI Insight *3*.

Stratman, A.N., Malotte, K.M., Mahan, R.D., Davis, M.J., and Davis, G.E. (2009). Pericyte recruitment during vasculogenic tube assembly stimulates endothelial

basement membrane matrix formation. Blood *114*, 5091–5101.

Strissel, K.J., Stancheva, Z., Miyoshi, H., Perfield, J.W., DeFuria, J., Jick, Z., Greenberg, A.S., and Obin, M.S. (2007). Adipocyte death, adipose tissue remodeling, and obesity complications. Diabetes *56*, 2910–2918.

Strong, A.L., Cederna, P.S., Rubin, J.P., Coleman, S.R., and Levi, B. (2015). The Current state of fat grafting: A review of harvesting, processing, and injection techniques. Plast. Reconstr. Surg. *136*, 897–912.

Sun, J., Li, N., Oh, K.S., Dutta, B., Vayttaden, S.J., Lin, B., Ebert, T.S., De Nardo, D., Davis, J., Bagirzadeh, R., et al. (2016). Comprehensive RNAi-based screening of human and mouse TLR pathways identifies species-specific preferences in signaling protein use. Sci. Signal. *9*, ra3.

Sun, M., He, Y., Zhou, T., Zhang, P., Gao, J., and Lu, F. (2017). Adipose Extracellular Matrix/Stromal Vascular Fraction Gel Secretes Angiogenic Factors and Enhances Skin Wound Healing in a Murine Model. Biomed Res. Int. *2017*, 3105780.

Takebayashi, H., Usui, N., Ono, K., and Ikenaka, K. (2008). Tamoxifen modulates apoptosis in multiple modes of action in CreER mice. Genesis *46*, 775–781.

Tang, W., Zeve, D., Suh, J.M., Bosnakovski, D., Kyba, M., Hammer, R.E., Tallquist, M.D., and Graff, J.M. (2008a). White fat progenitor cells reside in the adipose vasculature. Science *322*, 583–586.

Tang, W., Zeve, D., Suh, J.M., Bosnakovski, D., Kyba, M., Hammer, R.E., Tallquist, M.D., and Graff, J.M. (2008b). White fat progenitor cells reside in the adipose vasculature. Science (80-.). *322*, 583–586.

Tchernof, A., and Després, J.-P. (2000). Sex Steroid Hormones, Sex Hormone-Binding Globulin, and Obesity in Men and Women. Horm. Metab. Res. *32*, 526–536.

Tchernof, A., and Després, J.-P. (2013). Pathophysiology of Human Visceral Obesity: An Update. Physiol. Rev. *93*, 359–404.

Tchkonia, T., Giorgadze, N., Pirtskhalava, T., Tchoukalova, Y., Karagiannides, I., Armour Forse, R., Deponte, M., Stevenson, M., Guo, W., Han, J., et al. (2002). Fat depot origin affects adipogenesis in primary cultured and cloned human preadipocytes. Am. J. Physiol. - Regul. Integr. Comp. Physiol. *282*.

Tchkonia, T., Lenburg, M., Thomou, T., Giorgadze, N., Frampton, G., Pirtskhalava,

T., Cartwright, A., Cartwright, M., Flanagan, J., Karagiannides, I., et al. (2007). Identification of depot-specific human fat cell progenitors through distinct expression profiles and developmental gene patterns. Am. J. Physiol. Metab. *292*, E298–E307.

Timar, J., Meszaros, L., Orosz, Z., Albini, A., and Raso, E. (2005). WT1 expression in angiogenic tumours of the skin. Histopathology *47*, 67–73.

Traktuev, D.O., Merfeld-Clauss, S., Li, J., Kolonin, M., Arap, W., Pasqualini, R., Johnstone, B.H., and March, K.L. (2008). A population of multipotent CD34-positive adipose stromal cells share pericyte and mesenchymal surface markers, reside in a periendothelial location, and stabilize endothelial networks. Circ. Res. *102*, 77–85.

Tran, K. Van, Gealekman, O., Frontini, A., Zingaretti, M.C., Morroni, M., Giordano, A., Smorlesi, A., Perugini, J., De Matteis, R., Sbarbati, A., et al. (2012). The vascular endothelium of the adipose tissue gives rise to both white and brown fat cells. Cell Metab. *15*, 222–229.

Tremolada, C., Palmieri, G., and Ricordi, C. (2010). Adipocyte transplantation and stem cells: Plastic surgery meets regenerative medicine. Cell Transplant. *19*, 1217–1223.

Tsai, E.C., Matsumoto, A.M., Fujimoto, W.Y., and Boyko, E.J. (2004). Association of bioavailable, free, and total testosterone with insulin resistance: influence of sex hormone-binding globulin and body fat. Diabetes Care *27*, 861–868.

Vailhé, B., Vittet, D., and Feige, J.J. (2001). In vitro models of vasculogenesis and angiogenesis. Lab. Investig. *81*, 439–452.

Velecela, V., Lettice, L.A., Chau, Y.Y., Slight, J., Berry, R.L., Thornburn, A., Gunst, Q.D., Van Den Hoff, M., Reina, M., Martínez, F.O., et al. (2013). WT1 regulates the expression of inhibitory chemokines during heart development. Hum. Mol. Genet. *22*, 5083–5095.

Verboven, K., Wouters, K., Gaens, K., Hansen, D., Bijnen, M., Wetzels, S., Stehouwer, C.D., Goossens, G.H., Schalkwijk, C.G., Blaak, E.E., et al. (2018). Abdominal subcutaneous and visceral adipocyte size, lipolysis and inflammation relate to insulin resistance in male obese humans. Sci. Rep. *8*, 1–8.

Vezzani, B., Shaw, I., Lesme, H., Yong, L., Khan, N., Tremolada, C., and Péault, B. (2018). Higher Pericyte Content and Secretory Activity of Microfragmented Human

Adipose Tissue Compared to Enzymatically Derived Stromal Vascular Fraction. Stem Cells Transl. Med. *7*, 876–886.

Vicent, S., Chen, R., Sayles, L.C., Lin, C., Walker, R.G., Gillespie, A.K., Subramanian, A., Hinkle, G., Yang, X., Saif, S., et al. (2010). Wilms tumor 1 (WT1) regulates KRAS-driven oncogenesis and senescence in mouse and human models. J. Clin. Invest. *120*, 3940–3952.

Villeneuve, J., Bassaganyas, L., Lepreux, S., Chiritoiu, M., Costet, P., Ripoche, J., Malhotra, V., and Schekman, R. (2018). Unconventional secretion of FABP4 by endosomes and secretory lysosomes. J. Cell Biol. *217*, 649–665.

Vishvanath, L., Macpherson, K.A., Hepler, C., Wang, Q.A., Shao, M., Spurgin, S.B., Wang, M.Y., Kusminski, C.M., Morley, T.S., and Gupta, R.K. (2016). Pdgfrβ+ mural preadipocytes contribute to adipocyte hyperplasia induced by high-fat-diet feeding and prolonged cold exposure in adult mice. Cell Metab. *23*, 350–359.

Wagner, K.-D., Cherfils-Vicini, J., Hosen, N., Hohenstein, P., Gilson, E., Hastie, N.D., Michiels, J.-F., and Wagner, N. (2014). The Wilms' tumour suppressor Wt1 is a major regulator of tumour angiogenesis and progression. Nat. Commun. *5*, 5852.

Wagner, K.-D., El Maï, M., Ladomery, M., Belali, T., Leccia, N., Michiels, J.-F., and Wagner, N. (2019). Altered VEGF Splicing Isoform Balance in Tumor Endothelium Involves Activation of Splicing Factors Srpk1 and Srsf1 by the Wilms' Tumor Suppressor Wt1. Cells *8*, 41.

Wagner, K.D., Wagner, N., Bondke, A., Nafz, B., Flemming, B., Theres, H., and Scholz, H. (2002). The Wilms' tumor suppressor Wt1 is expressed in the coronary vasculature after myocardial infarction. FASEB J. *16*, 1117–1119.

Wagner, N., Wagner, K.-D., Theres, H., Englert, C., Schedl, A., and Scholz, H. (2005). Coronary vessel development requires activation of the TrkB neurotrophin receptor by the Wilms' tumor transcription factor Wt1. Genes Dev. *19*, 2631–2642.

Wagner, N., Wagner, K.-D., Scholz, H., Kirschner, K.M., and Schedl, A. (2006). Intermediate filament protein nestin is expressed in developing kidney and heart and might be regulated by the Wilms' tumor suppressor Wt1. Am. J. Physiol. Integr. Comp. Physiol. *291*, R779–R787.

Wagner, N., Michiels, J.F., Schedl, A., and Wagner, K.-D. (2008a). The Wilms'

tumour suppressor WT1 is involved in endothelial cell proliferation and migration: expression in tumour vessels in vivo. Oncogene *27*, 3662–3672.

Wagner, N., Michiels, J.F., Schedl, A., and Wagner, K.D. (2008b). The Wilms' tumour suppressor WT1 is involved in endothelial cell proliferation and migration: Expression in tumour vessels in vivo. Oncogene *27*, 3662–3672.

WAGNER, K.-D., WAGNER, N., WELLMANN, S., SCHLEY, G., BONDKE, A., THERES, H., and SCHOLZ, H. (2003). Oxygen-regulated expression of the Wilms' tumor suppressor *Wt1* involves hypoxia-inducible factor-1 (HIF-1). FASEB J. *17*, 1364–1366.

Wajchenberg, B.L. (2000). Subcutaneous and Visceral Adipose Tissue: Their Relation to the Metabolic Syndrome. Endocr. Rev. *21*, 697–738.

Wang, C., Yin, S., Cen, L., Liu, Q., Liu, W., Cao, Y., and Cui, L. (2010). Differentiation of Adipose-Derived Stem Cells into Contractile Smooth Muscle Cells Induced by Transforming Growth Factor-β1 and Bone Morphogenetic Protein-4. Tissue Eng. Part A *16*, 1201–1213.

Wang, J., Zohar, R., and McCulloch, C.A. (2006). Multiple roles of α-smooth muscle actin in mechanotransduction. Exp. Cell Res. *312*, 205–214.

Wang, X.N., Li, Z.S., Ren, Y., Jiang, T., Wang, Y.Q., Chen, M., Zhang, J., Hao, J.X., Wang, Y.B., Sha, R.N., et al. (2013). The Wilms Tumor Gene, Wt1, Is Critical for Mouse Spermatogenesis via Regulation of Sertoli Cell Polarity and Is Associated with Non-Obstructive Azoospermia in Humans. PLoS Genet. *9*, e1003645.

Wang, Y., Rimm, E.B., Stampfer, M.J., Willett, W.C., and Hu, F.B. (2005). Comparison of abdominal adiposity and overall obesity in predicting risk of type 2 diabetes among men. Am. J. Clin. Nutr. *81*, 555–563.

Wang, Z.Y., Maddenq, S.L., Deuel, T.F., and Rauscher, F.J. (1992). The Wilms' Tumor Gene Product, WT1, Represses Transcription of the Platelet-derived Growth Factor A-chain Gene*.

Weisberg, S.P., McCann, D., Desai, M., Rosenbaum, M., Leibel, R.L., Ferrante, A.W., and Jr. (2003). Obesity is associated with macrophage accumulation in adipose tissue. J. Clin. Invest. *112*, 1796–1808.

WHO (2020). Obesity and overweight.

Wilkosz, S., Ireland, G., Khwaja, N., Walker, M., Butt, R., Giorgio-Miller, A., and Herrick, S.E. (2005). A comparative study of the structure of human and murine greater omentum. Anat. Embryol. (Berl). *209*, 251–261.

Wilm, B. (2005). The serosal mesothelium is a major source of smooth muscle cells of the gut vasculature. Development *132*, 5317–5328.

Wilm, B., Ipenberg, A., Hastie, N.D., Burch, J.B.E., and Bader, D.M. (2005a). The serosal mesothelium is a major source of smooth muscle cells of the gut vasculature. Development *132*, 5317–5328.

Wilm, B., Ipenberg, A., Hastie, N.D., Burch, J.B.E., and Bader, D.M. (2005b). The serosal mesothelium is a major source of smooth muscle cells of the gut vasculature. Development *132*, 5317–5328.

Wilting, J., Birkenhäger, R., Eichmann, A., Kurz, H., Martiny-Baron, G., Marmé, D., McCarthy, J.E., Christ, B., and Weich, H.A. (1996). VEGF121 induces proliferation of vascular endothelial cells and expression of flk-1 without affecting lymphatic vessels of chorioallantoic membrane. Dev. Biol. *176*, 76–85.

Wu, J., Boström, P., Sparks, L.M., Ye, L., Choi, J.H., Giang, A.-H., Khandekar, M., Virtanen, K.A., Nuutila, P., Schaart, G., et al. (2012). Beige Adipocytes Are a Distinct Type of Thermogenic Fat Cell in Mouse and Human. Cell *150*, 366–376.

Yamamoto, S., Nakagawa, T., Matsushita, Y., Kusano, S., Hayashi, T., Irokawa, M., Aoki, T., Korogi, Y., and Mizoue, T. (2010). Visceral fat area and markers of insulin resistance in relation to colorectal neoplasia. Diabetes Care *33*, 184–189.

Yamamoto, S., Muramatsu, M., Azuma, E., Ikutani, M., Nagai, Y., Sagara, H., Koo, B.N., Kita, S., O'Donnell, E., Osawa, T., et al. (2017). A subset of cerebrovascular pericytes originates from mature macrophages in the very early phase of vascular development in CNS. Sci. Rep. *7*, 1–16.

Yamanouchi, K., Ohta, T., Liu, Z., Oji, Y., Sugiyama, H., Shridhar, V., Matsumura, S., Takahashi, T., Takahashi, K., and Kurachi, H. (2014). The Wilms' Tumor Gene WT1 - 17AA/- KTS Splice Variant Increases Tumorigenic Activity Through Up-Regulation of Vascular Endothelial Growth Factor in an In Vivo Ovarian Cancer Model. Transl. Oncol. *7*, 580–589.

Yang, L., Han, Y., Saiz, S., and Minden, M.D. (2007). A tumor suppressor and

oncogene: the WT1 story. Leukemia *21*, 868–876.

Yang, R.-Z., Lee, M.-J., Hu, H., Pray, J., Wu, H.-B., Hansen, B.C., Shuldiner, A.R., Fried, S.K., McLenithan, J.C., and Gong, D.-W. (2006). Identification of omentin as a novel depot-specific adipokine in human adipose tissue: possible role in modulating insulin action. Am. J. Physiol. Metab. *290*, E1253–E1261.

Ye, J. (2011). Adipose tissue vascularization: Its role in chronic inflammation. Curr. Diab. Rep. *11*, 203–210.

Yusuf, S., Hawken, S., Ôunpuu, S., Bautista, L., Franzosi, M.G., Commerford, P., Lang, C.C., Rumboldt, Z., Onen, C.L., Lisheng, L., et al. (2005). Obesity and the risk of myocardial infarction in 27 000 participants from 52 countries: a case-control study. Lancet *366*, 1640–1649.

Zakhari, J.S., Zabonick, J., Gettler, B., and Williams, S.K. (2018). Vasculogenic and angiogenic potential of adipose stromal vascular fraction cell populations in vitro. Vitr. Cell. Dev. Biol. - Anim. *54*, 32–40.

Zamboni, M., Armellini, F., Milani, M.P., De Marchi, M., Todesco, T., Robbi, R., Bergamo-Andreis, I.A., and Bosello, O. (1992). Body fat distribution in pre- and post-menopausal women: metabolic and anthropometric variables and their inter-relationships. Int. J. Obes. Relat. Metab. Disord. *16*, 495–504.

Zhang, R., Gao, Y., Zhao, X., Gao, M., Wu, Y., Han, Y., Qiao, Y., Luo, Z., Yang, L., Chen, J., et al. (2018). FSP1-positive fibroblasts are adipogenic niche and regulate adipose homeostasis. PLOS Biol. *16*, e2001493.

Zhang, Y., Proenca, R., Maffei, M., Barone, M., Leopold, L., and Friedman, J.M. (1994). Positional cloning of the mouse obese gene and its human homologue. Nature *372*, 425–432.

Zhang, Z. Sen, Zhou, H.N., He, S.S., Xue, M.Y., Li, T., and Liu, L.M. (2020). Research advances in pericyte function and their roles in diseases. Chinese J. Traumatol. - English Ed. *23*, 89–95.

Zhao, H., and Chappell, J.C. (2019). Microvascular bioengineering: A focus on pericytes. J. Biol. Eng. *13*.

Zheng, Q.-S., Wang, X.-N., Wen, Q., Zhang, Y., Chen, S.-R., Zhang, J., Li, X.-X., Sha, R.-N., Hu, Z.-Y., Gao, F., et al. (2014). Wt1 deficiency causes undifferentiated

spermatogonia accumulation and meiotic progression disruption in neonatal mice. REPRODUCTION *147*, 45–52.

Zhong, Z.A., Sun, W., Chen, H., Zhang, H., Lay, Y.A.E., Lane, N.E., and Yao, W. (2015). Optimizing tamoxifen-inducible Cre/loxp system to reduce tamoxifen effect on bone turnover in long bones of young mice. Bone *81*, 614–619.

Zhou, L., and Liu, Y. (2015). Wnt/β-catenin signalling and podocyte dysfunction in proteinuric kidney disease. Nat. Rev. Nephrol. *11*, 535–545.

Zuk, P.A., Zhu, M., Mizuno, H., Huang, J., Futrell, J.W., Katz, A.J., Benhaim, P., Lorenz, H.P., and Hedrick, M.H. (2001). Multilineage cells from human adipose tissue: Implications for cell-based therapies. In Tissue Engineering, (Tissue Eng), pp. 211–228.

Appendix

		Epididymal	Omental	Pericardial	Mesenteric	Perirenal
	CD	5	5	4	5	6
αSMA + GFP	HFD	7	4	5	6	6
	p value	0.48	0.66	0.069	0.099	0.32
	CD	4	5	4	5	6
CD31 + GFP	HFD	6	4	5	6	6
	p value	0.62	0.2	0.69	0.19	0.51
	CD	6	6	4	6	5
PLIN + GFP	HFD	7	5	5	5	6
	p value	0.041	0.0012	0.068	0.515	0.00092

Table A.1. Biological replicates used in the quantification of Wt1-lineage traced adipocyte and microvessels and results of statistical analysis

Lean

Subject number	Age	Sex	BMI (kg/m2)	WHR	% Fat	Fat mass (kg)
1176	33	Female	22.38835489	0.824175824	29.3	16.6
1180	43	Female	22.14876033	0.786324786	29.6	17.9
1200	60	Female	22.7189744	0.926315789	35	19.6
1201	51	Male	23.5260771	0.888324873	24.8	16.5

Overweight

Subject number	Age	Sex	BMI (kg/m2)	WHR	% Fat	Fat mass (kg)
1175	52	Male	26.6953328	ND	30.9	27.5
1184	75	Female	29.37239738	0.813559322	42.1	33.3
1199	40	Female	26.3958034	1.037037037	32.5	25.7
1202	62	Male	25.15589569	0.93877551	22.5	16

Obese

Subject number		Sex	BMI (kg/m2)	WHR	% Fat	Fat mass (kg)
1177	56	Female	38.36638101	1.025	45.3	48.5
1178	59	Female	38.29344433	0.837301587	46.1	42.3
1181	60	Female	33.71488033	0.846846847	42.6	34.5
1182	76	Female	33.33187141	0.901709402	43.5	33.4
1186	69	Male	34.47809627	1.043859649	39.1	39.9
1193	59	Male	30.94571162	1.061946903	29.5	29.1

Table A.2. Anthropometry data of patients included in human VWAT experiments.

Quantification	p value
Epi SVF - Number of branches (3h)	0.36
Epi SVF - Number of branches (6h)	0.66
Epi SVF - Total branching length (3h)	0.059
Epi SVF - Total branching length (6h)	0.084
Peri SVF - Number of branches (3h)	0.49
Peri SVF - Number of branches (6h)	0.32
Peri SVF - Total branching legth (3h)	0.92
Peri SVF - Total branching legth (6h)	0.61
Epi CO - Number of branches (3h)	0.15
Epi CO - Number of branches (6h)	0.17
Epi CO - Total branching length (3h)	0.22
Epi CO - Total branching length (6h)	0.06
Peri CO - Number of branches (3h)	0.78
Peri CO - Number of branches (6h)	0.17
Peri CO - Total branching legth (3h)	0.62
Peri CO - Total branching legth (6h)	0.5

Table A.3. Statistical analysis of tube formation assays experiments using epididymal and pericardial SVF cells deleted for Wt1 by CreERT2 activation.

	(Vechicle control vs. Tamoxifen-treated)	
	Wt1- deleted	CreERT2 control
Wt1 expression	*p*= 0.031	*p*= 0.291
CXCL5 expression	*p*= 0.612	*p*= 0.332
DCN expression	*p*= 0.089	*p*= 0.578
IRF7 expression	*p*= 0.495	*p*= 0.0021
PTN expression	*p*= 0.0034	*p*= 0.262
RGS4 expression	*p*= 0.822	*p*= 0.330

Table A.4. Results of statistical analysis - the effect of CreERT2 on the expression of inflammation genes in pericardial SVF cells

	p value
Wt1+ cells OM	0.31
WT1+ cells HF	0.11
Wt1+ cells EPI	0.051
Wt1+ pericytes OM	0.0055
Wt1+ pericytes HF	0.31
Wt1+ pericytes EPI	0.13

Table A.5. Results of statistical analysis - Validation of RNAi-mediated Wt1 knockdown in cultured SVF cells by immunofluorescence